DEPÓSITO LEGAL ppi 201502ZU4666
Esta publicación científica en formato digital
es continuidad de la revista impresa
ISSN 0041-8811
DEPÓSITO LEGAL pp 76-654

Revista de la Universidad del Zulia

Fundada en 1947
por el Dr. Jesús Enrique Lossada

Ciencias Exactas Naturales y de la Salud

Año 10 N° 27
Mayo - Agosto 2019
Tercera Época
Maracaibo-Venezuela

REVISTA DE LA UNIVERSIDAD DEL ZULIA

Tercera Época

Ciencias Exactas, Naturales y de la Salud

AÑO 10 N° 27 MAYO-AGOSTO 2019

Fundada en 1947 por el Dr. Jesús Enrique Lossada
Adscrita a la Cátedra Libre Historia de la Universidad del Zulia

PUBLICACIÓN AUSPICIADA POR LA
UNIVERSIDAD DEL ZULIA

Indizada, registrada y/o catalogada
electrónicamente en las siguientes bases de datos:

REVENCYT	WOS
LATINDEX	EZB- Elektronische Zeitschriftenbibliothek-
Actualidad Iberoamericana	Universität Regensburg
CLASE	Linkovaci Server SFX- Univerzita Karlova
PERIÓDICA	UBL -Universitas Bibliothek Leipzig
Emerging Sources Citation Index (ESCI).	ZDB- Zeitschriften Datenbank
BIBLAT-Bibliografía Latinoamericana	BSZ Bibliotheksservice Zentrum Baden-Wüuttemberg
FLACSO-Argentina	Issuu: http://Issuu.com/revistadelauniversidaddelzulia

REVISTA DE LA UNIVERSIDAD DEL ZULIA

DEPÓSITO LEGAL ppi 201502ZU4666
Esta publicación científica en formato digital es continuidad de la revista impresa
ISSN 0041-8811
DEPÓSITO LEGAL pp 76-654

Portada:
Concepto gráfico: Laura González
Diagramación final: Reyber Parra

REVISTA DE LA UNIVERSIDAD DEL ZULIA
Calle 67 (prolongación Cecilio Acosta) con Avenida 16 (Guajira)
Sede rectoral de la Universidad del Zulia. Edificio Fundadesarrollo
Maracaibo, estado Zulia, Venezuela.
Correo electrónico: revistadeluz@gmail.com

Revista de la Universidad del Zulia
Tercera Época

ISSN 0041-8811

El Dr. Jesús Enrique Lossada, luego de trabajar infatigablemente hasta lograr la reapertura de la Universidad del Zulia, el 01 de octubre de 1946, le aportó a esta institución su primera revista científica: la *Revista de la Universidad del Zulia*, fundada por este insigne zuliano, el 31 de mayo de 1947. En su Tercera Época la revista mantiene la orientación que le asignara su fundador: es un órgano científico de difusión de trabajos parciales o definitivos de investigadores y/o equipos de investigación nacionales y extranjeros. La revista posee un carácter multidiscliplinario, por ello su temática se divide en tres grandes ejes: a. ciencias sociales y arte; b. ciencias del agro, ingeniería y tecnología; c. ciencias exactas, naturales y de la salud. Su publicación es cuatrimestral. Cada número, de los tres del año, se corresponde con uno de los tres ejes temáticos. La *Revista de la Universidad del Zulia*, por su naturaleza histórica y patrimonial, está adscrita a la Cátedra libre Historia de la Universidad del Zulia.

Autoridades

Jorge Palencia
Rector

Judith Aular de Durán
Vice Rectora Académica

María Artigas
Vice Rectora Administrativa

Marlene Primera
Secretaria

Imelda Rincón Finol
Reyber Parra Contreras
Cátedra Libre
Historia de la Universidad del Zulia

REVISTA DE LA UNIVERSIDAD DEL ZULIA
CIENCIAS EXACTAS, NATURALES Y DE LA SALUD///
AÑO 10 N° 27, Mayo-Agosto 2019
ISSN 0041-8811

Contenido

Effects of density dependent migration on the spread of infectious diseases: A Mathematical Model

Presentación

La *Revista de la Universidad del Zulia* arriba a sus 72 años de historia; han sido años de grandes esfuerzos humanos e institucionales para lograr su permanencia en el tiempo. A partir del 2010 dimos inicio a una tercera época en la que hemos procurado darle continuidad a la misión asignada, en mayo de 1947, por nuestro fundador, el Dr. Jesús Enrique Lossada: servir de "vehículo de ideas" y enlace de la Universidad del Zulia con las diversas realidades donde ella logra incidir.

En efecto, una de estas realidades se concentra en la crisis profunda y generalizada que Venezuela vive actualmente, donde las instituciones universitarias están llamadas a iluminar la conciencia de los hombres y mujeres de nuestro pueblo, a fin de promover la concreción de salidas a tan nefasta realidad nacional, caracterizada por un deterioro moral de la población y el resquebrajamiento de las instituciones democráticas.

La Universidad del Zulia, institución que por más de un siglo forma parte de la historia de Venezuela, también se ha visto afectada por esta crisis, al punto de ir perdiendo gradualmente valiosos recursos de su planta profesoral, a la par de experimentar la merma continua del número de sus estudiantes. Muy a pesar de este deterioro, todavía hoy la universidad de Francisco Ochoa, Francisco Eugenio Bustamante, Jesús Enrique Lossada -entre otras figuras señeras- dispone de no pocos académicos, quienes día a día emulan la voluntad de Héctor para mantener con dignidad el Alma Mater zuliana.

En el presente número 27, dedicado a las Ciencias Exactas, Naturales y de la Salud, damos a conocer los resultados de varias investigaciones en el ámbito de la Medicina, Física, Matemática, Química y Computación. Agradecemos a todos los autores de los siguientes artículos por su aporte en la tarea de generar conocimiento.

Dr. Reyber Parra Contreras

Editor-Coordinador de la *Revista de la Universidad del Zulia*

Contaje de células endoteliales pre y post-iridotomía láser en pacientes con cierre angular agudo

Karol Y. Rivas P.*
Diógenes E. Solórzano G.**

RESUMEN

Objetivo: Comparar el contaje de células endoteliales pre y post-iridotomía láser en pacientes con cierre angular agudo. **Metodología:** Investigación experimental, tipo ensayo no controlado. Constituida por 40 ojos con cierre angular agudo evaluados por Oftalmología del Hospital Universitario de Maracaibo, entre octubre 2017- octubre 2018, requirieron iridotomía con láser. Se realizó gonioscopía, microscopía especular antes y después de la cirugía. **Resultados:** Según gonioscopía 20 (50,0%) ojos mostraron estructuras hasta el trabéculo y 20 (50,0%) ángulos totalmente cerrados. La PIO antes y luego 24 horas, 3 días y 3 meses después del procedimiento disminuyo (p= 0,001) en los ojos con cierre angular agudo y los contralaterales. En los ojos con cierre angular agudo el contaje de células/mm^2 del endotelio corneal pre láser fue de 2472±323, a las 24 horas 1994 ±220, tercer día 1895±125 y a los 3 meses 1865±166 (p=0,001) y en los ojos contralaterales; pre laser 2600±245 y luego 2288 ±210, 2024±248 y 1922±204 (p=0,001). **Conclusión**: La iridotomía láser reduce significativamente la presión intraocular, pero conduce a cambios significativos en la microscopía especular corneal.

PALABRAS CLAVE: Cierre angular agudo, iridotomía con láser, microscopía especular

*Servicio de Oftalmología, Hospital Universitario de Maracaibo. Maracaibo – Venezuela, DRAKAROLRIVAS@GMAIL.COM
** División de Estudios para Graduados. Facultad de Medicina. Universidad del Zulia. Maracaibo - Venezuela.

Recibido: 18/03/2019 Aceptado: 20/04/2019

Counting of endothelial cells pre and post-laser iridotomy in patients with acute angular closure

ABSTRACT

Objective: To compare the counting of endothelial cells pre and post-laser iridotomy in patients with acute angular closure. **Methodology:** Experimental research, non-controlled trial type. Consisting of 40 eyes with acute angular closure evaluated by Ophthalmology of the University Hospital of Maracaibo, between October 2017 and October 2018, they required laser iridotomy. Gonosioscopy was performed, specular microscopy before and after surgery. **Results:** According to gonioscopy 20 (50.0%) eyes showed structures to the trabeculum and 20 (50.0%) completely closed angles. IOP before and then 24 hours, 3 days and 3 months after the procedure decreased (p = 0.001) in eyes with acute angular closure and contralateral eyes. In eyes with acute angular closure, the cell count / mm2 of the pre-laser corneal endothelium was 2472 ± 323, at 24 hours 1994 ± 220, third day 1895 ± 125 and at 3 months 1865 ± 166 (p = 0.001) and in the contralateral eyes; pre-laser 2600 ± 245 and then 2288 ± 210, 2024 ± 248 and 1922 ± 204 (p = 0.001). **Conclusion:** Laser iridotomy significantly reduces intraocular pressure, but leads to significant changes in corneal specular microscopy.

KEY WORDS: Acute angular closure, laser iridotomy, specular microscopy

Introducción

El glaucoma constituye una importante causa de ceguera irreversible tanto a nivel mundial como en Venezuela. El glaucoma de ángulo estrecho es menos frecuente que el de ángulo abierto, se presenta en uno de cada 1000 individuos mayores de 40 años, y es de 3 a 4 veces más frecuente en mujeres que en hombres. Las características anatómicas son un factor predisponente importante, la tendencia familiar y la asociación al aumento de la edad y la hipermetropía (Diaz et al. 2010, Alemán et al. 2011). El mecanismo de producción más común del glaucoma primario de ángulo estrecho (GPAE) es el bloqueo pupilar que se

presenta en 90 % de los casos, existe (10 %) otro mecanismo o combinación de mecanismos sumado al bloqueo pupilar; ejemplo, iris en meseta (Kanski, McAllister. 2009).

En el glaucoma de ángulo estrecho con bloqueo pupilar el paso del humor acuoso (HA) de la cámara posterior a la anterior es impedido por un bloqueo entre el cristalino y el iris; este puede ser relativo o absoluto; cuando es relativo o también llamado funcional, el iris no está adherido al cristalino, pero está tan cerca de él que no es posible el paso del HA de la cámara posterior a la anterior. En el bloqueo pupilar absoluto el iris está adherido a la cara anterior del cristalino (Fernández et al. 2012). Su tratamiento suele comenzar con medidas médicas para disminuir la presión intraocular y aliviar el cierre angular, seguido de iridectomía periférica para eliminar el bloqueo pupilar relativo y prevenir futuros ataques (Anderson et al. 2001, Ritch et al. 1998).

De tal manera que el tratamiento de este tipo del glaucoma es siempre quirúrgico, se identifica la iridotomía láser como una actuación quirúrgica (Garcia et al. 1998, González, González. 1997). En la década de los años setenta del siglo XX se comenzó a experimentar en la realización de iridotomías con láser de Argón. Al inicio de los años ochenta la iridotomía con láser de Argón reemplazó a la tradicional iridectomía quirúrgica incisional como procedimiento de elección en la realización de una perforación en el iris en los pacientes con glaucoma de ángulo estrecho. Se mostró como un procedimiento alternativo, seguro y efectivo a la clásica iridectomía quirúrgica incisional (Garcia et al. 1998(), Shields MB. 1987).

Hoy la iridotomía con láser es el procedimiento de elección en todas las formas de glaucoma de cierre angular en las cuales hay un componente de bloqueo pupilar; es también recomendada como tratamiento profiláctico en pacientes con GPAE latente (Kanski J. 2009:199-240).

Sin embargo, para unos autores este procedimiento no está exento de complicaciones, entre estas se describe una brevemente la visión borrosa, por lo general

dura unos 30 minutos. Menos común es la inflamación de la córnea, hemorragias y en algunos casos aumento de la presión en el ojo. Otros riesgos incluyen quemadura en el revestimiento interno del ojo, afectando el epitelio corneal, situación que genera disminución de las células endoteliales, las cuales son imprescindible para mantener la transparencia de la córnea (Kanski J. 2009:199-240, Garcia et al. 2015, Klapper R. 2011).

Las células endoteliales llevan a cabo un bombeo hídrico desde el estroma de la córnea, mecanismo que impide la inhibición acuosa (edema) y mantiene su transparencia. La población de células endoteliales al nacimiento es de 3500-4000 cel/mm^2 y ésta decrece paulatinamente a 2000 a 2500 cel/mm^2. El límite mínimo para mantener la transparencia se estima en 700 cel/mm2 y la regeneración de estas es baja y disminuye con la edad (Sihota et al. 2017, Golan et al. 2013).

Uno de los métodos no invasivos que facilita la observación a gran aumento del endotelio de la córnea in vivo y que permite conocer el número, forma y tamaño de la población celular endotelial, es la microscopía especular (Golan et al. 2013). Los biomicroscopios modernos con sus sistemas de análisis de imágenes contribuyen al examen de los pacientes con patología de la córnea o sospechosos de daño endotelial y, como para algunos autores la iridotomía láser produce daño en el endotelio de la córnea y determina cierta pérdida de células endoteliales, el riesgo de descompensación postoperatoria de la córnea aumenta si la cifra de células preoperatoria es baja (Pescosolido et al. 2011).

Recientemente, un estudio demostró que la iridotomía en ojos con glaucoma crónico de ángulo cerrado no condujo cambios significativos en la microscopía especular corneal en comparación con pacientes que no se sometieron a esta técnica quirúrgica. Los ojos de los pacientes con glaucoma crónico de ángulo cerrado, sin y después de una iridotomía, tenían un recuento especular menor en comparación con los controles de su edad, pero manteniéndose dentro del rango de normalidad (Pérez P. 2017).

Tomando en cuenta tales informaciones y que la iridotomía con láser es una técnica no invasiva, que no requiere de hospitalización, con una efectividad cercana al 100% en la prevención de ataques agudos de glaucoma y detención de ataques instaurados. Además, el procedimiento completo es breve y tras la cirugía el paciente puede volver a su vida y actividades diarias. No obstante, es interesante dilucidar si después del uso de la referida técnica surgen cambios significativos en el recuento celular epitelial, lo cual es importante conocer para poder continuar recomendando su uso en los pacientes que lo ameriten, por los beneficios que produce. Motivos por los cuales se realizó la presente investigación, con el propósito de comparar el contaje de células endoteliales pre y post- iridotomía láser en pacientes con cierre angular agudo en el Servicio de oftalmología del Hospital Universitario de Maracaibo, en el período comprendido desde octubre 2017 a octubre 2018.

1. Materiales y Métodos

Investigación experimental, tipo ensayo no controlado, donde las variables estudiadas se evaluaron en los mismos pacientes, antes y después del procedimiento quirúrgico, actuando cada sujeto como su propio control. Además, fue prospectivo, transversal. La población quedó constituida por pacientes con diagnóstico de cierre angular agudo, a quienes se les realizó iridotomía con láser en el Servicio de Oftalmología del Hospital Universitario de Maracaibo, en el lapso comprendido entre octubre 2017 a octubre de 2018. La muestra fue calculada a través de un programa estadístico computarizado Epinfo, representada por 20 (40 ojos) pacientes.

Se incluyeron pacientes masculinos o femeninos mayores de 18 de edad, con diagnóstico de cierre angular agudo a quienes se les realizó iridotomía con láser. Se excluyeron pacientes con glaucoma de ángulo abierto, neovascular o congénito, con cataratas maduras, cirugía ocular previa, que utilicen medicamentos que afecten la PIO o sensibilidad visual y, los que no desearon participar en la investigación.

A cada paciente seleccionado se les explicó el estudio y se les solicitó autorización para su inclusión, posteriormente se les realizó una historia clínica exhaustiva, basada en la anamnesis y examen físico minucioso. La evaluación oftalmológica integral incluyó agudeza visual, valoración del segmento anterior (superficie ocular, conjuntiva, esclera, córnea, cámara anterior, pupila y cristalino) con lámpara de hendidura y fondo de ojo.

Se efectuó la valoración de la cámara anterior y el sistema de drenaje del humor acuoso a través de la gonioscopía, que es la técnica estándar de referencia para el diagnóstico de cierre angular agudo (Manterola C. 2006).

La medición de la PIO se efectuó en lámpara de hendidura con tonómetro de aplanación (Goldman), previa colocación de anestesia tópica (Alcaine) con fluoresceina 1 gota en ambos ojos antes la medición de la presión intraocular, la cual será expresada en mmHg. La microscopia especular se medió con un aparato MARCA TOMEY (EM-3000). El riesgo de edema se define según la densidad celular (CD= número de células/mm^2 del endotelio corneal) de acuerdo con la siguiente escala (Mergler, Pleyer. 2011):

- Sin riesgo: aquellos ojos con más de 2 000 cél/mm^2 (Normal).

- Con riesgo: a los conteos de 2 000-1 500 cél/mm^2 (Bajo riesgo).

a) 1 500-1 000 cél/mm^2 (Alto riesgo),

b) 1 000-500 cél/mm^2 (Pre-edema) y

c) Menos de 500 cél/mm^2 (Edema)

A todos los pacientes se les realizó un seguimiento a las 24 horas y a los 7 días postoperatorios y luego a los 3 meses postoperatorios.

Para la recolección de los datos se diseñó un instrumento tipo encuesta, validado por dos expertos en la materia y un experto metodológico, estructurado de la siguiente manera: número de historia, edad, género, PIO, agudeza visual, contaje de células endoteliales pre y post-iridotomía Láser y complicaciones.

Los datos fueron analizados a través de medidas de tendencia central, mediante el uso de cifras absolutas y porcentajes. Se emplearon pruebas de significancia estadísticas (t de Student o Chi cuadrado) para conocer las diferencias entre las variables estudiadas antes y después de la técnica aplicada, considerándose $p<0,05$ como significativo. Se empleó el programa estadístico SPSS, versión 23. Posteriormente, se realizó el análisis e interpretación de los resultados que se expresaron en cuadros y figuras.

2. Resultados

Para comparar el contaje de células endoteliales pre y post- iridotomía láser en pacientes con cierre angular agudo en el Servicio de oftalmología del Hospital Universitario de Maracaibo, se seleccionaron 20 pacientes (40 ojos) con cierre angular agudo, quienes cumplieron con los criterios de inclusión y se les realizó iridotomía láser, de los cuales 12 (60) fueron de sexo femenino y 8 (40,0%) masculinos, con una edad promedio total de 46± 7,7 años. Figura 1.

Al evaluar los hallazgos gonioscópicos 20 (50,0%) ojos mostraron las estructuras hasta el trabéculo anterior y 20 (50,0%) presentaron ángulos totalmente cerrados. Tabla 1.

En los ojos con cierre angular agudo, el grosor de la córnea (530,7±12,9) fue significativamente mayor ($p=0,003$) en comparación con 522,8 ±13,8 obtenido en los ojos contralaterales. Tabla 2.

Al evaluar la PIO antes y luego a las 24 horas, a los 3 días y 3 meses después del procedimiento, se observó descenso estadísticamente significativo (p= 0,001) tanto en los ojos con cierre angular agudo, como en los contralaterales. Figura 2 y 3.

Sobre la agudeza visual se evidencia mejoría en todos los pacientes estudiados, con resultado más favorable a los 3 meses posterior a la iridotomía, a excepción de 2 casos con NPL, tal como se presenta en la tabla 3 y 4.

En los ojos con cierre angular agudo el contaje de células/mm^2 del endotelio corneal pre láser fue de 2472±323, y posteriormente a las 24 horas 1994 ±220, al tercer día 1895±125 y a los 3 meses 1865±166, diferencias significativas (p=0,001) y en los ojos contralaterales; pre laser 2600±245 y luego 2288 ±210, 2024±248 y 1922±204 (p=0,001). Tabla 5.

FIGURA 1

DISTRIBUCION DE LOS PACIENTES EN ESTUDIO SEGUN EDAD Y SEXO

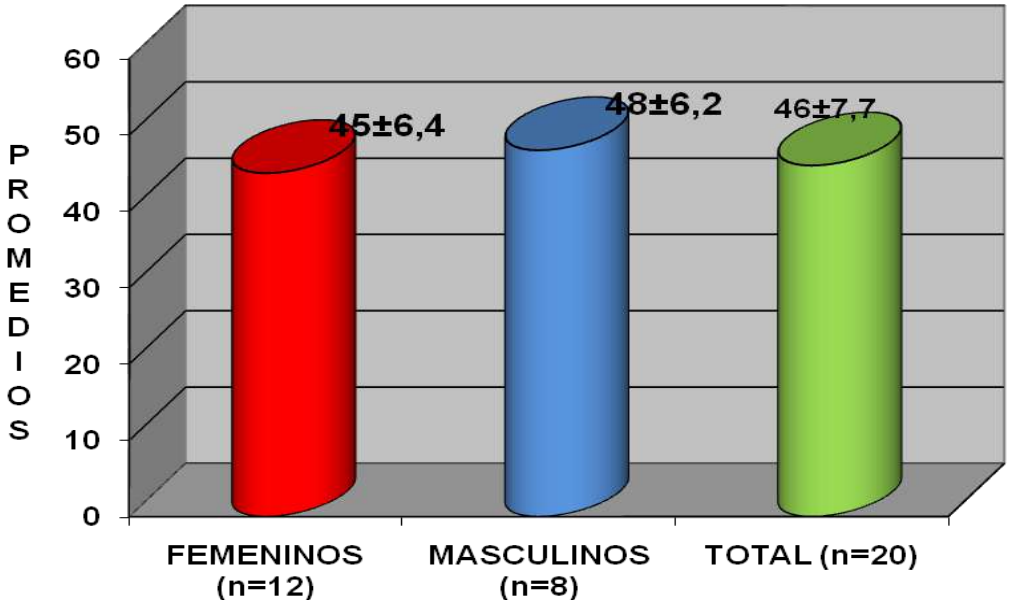

TABLA 1

HALLAZGOS GONIOSCÓPICOS EN LOS PACIENTES ESTUDIADOS

Hallazgos gonioscópicos	Número de ojos
Visualización de las estructuras hasta el trabéculo anterior	20 (50,0%)
ángulos totalmente cerrados	20 (50,0%)
Total	40 (100,0%)

TABLA 2

GROSOR CORNEAL Y PRESIÓN INTRAOCULAR DE LOS PACIENTES ESTUDIADOS

	Ojos con Cierre Angular agudo N=20 ojos	Ojos contralateral sin cierre angular agudo N=20 ojos	*P*
Grosor Corneal (micras)	530,7±12,9	522,8 ±13,8	0,003
PIO (mmHg)	30,35 ±6,5	16,34 ±3,5	0,01

FIGURA 2. PRESION INTRAOCULAR (mmHg)
20 OJOS CON CIERRE ANGULAR AGUDO EN LOS DIFERENTES TIEMPOS EVALUADOS

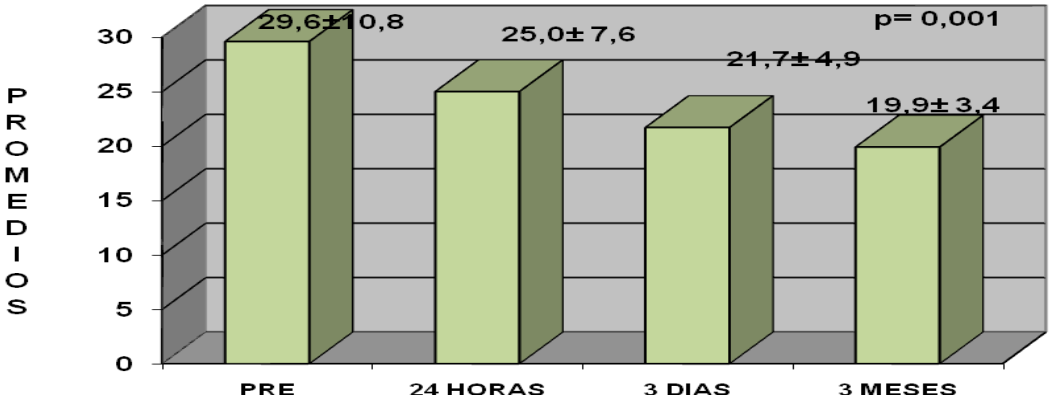

FIGURA 3. PRESION INTRAOCULAR (mmHg)
20 OJOS CONTRALATERAL AL OJO CON CIERRE ANGULAR AGUDO EN LOS DIGERENTES TIEMPOS EVALUADOS

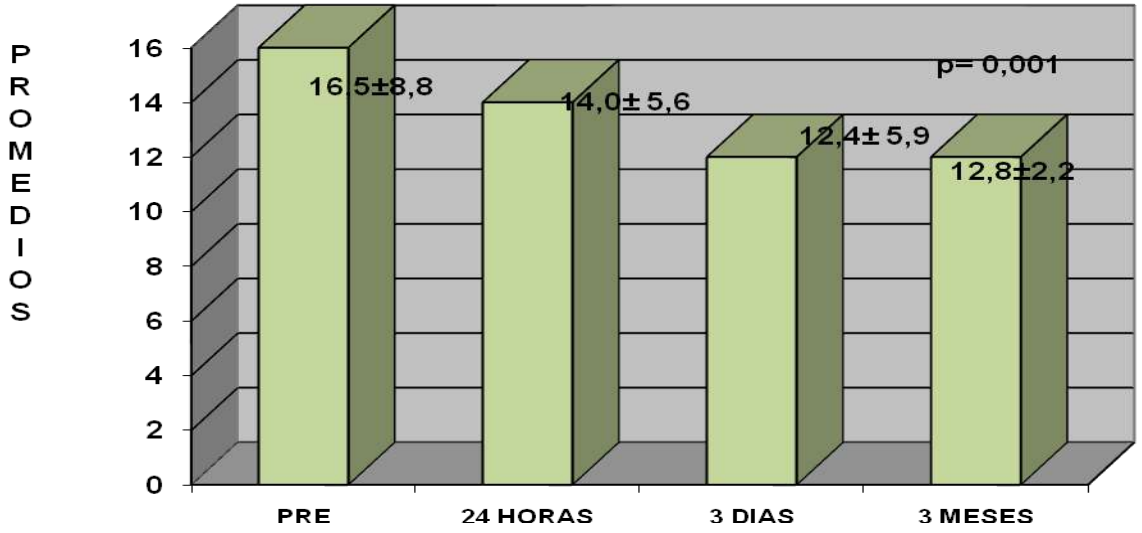

TABLA 3

AGUDEZA VISUAL EN LOS DIFERENTES TIEMPO EVALUADOS EN 20 OJOS CON CIERRE ANGULAR AGUDO

	Pre Laser	24 Horas Post Laser	3 Días Post Laser	3meses Post Laser
20/30	0	0	0	0(0,0%)
20/40	0	0	0	1(5,0%)
20/50	0	0	0	1(5,0%)
20/70	0	0	0	3 (15,0%)
20/80	0	0	0	3(1 5,0%)
20/100	0	0	0	2(10,0%)
20/150	0	0	2 (10,0%)	2(10,0%)
20/200	0	0	2 (10,0%)	2(10,0%)
20/400	0	0	5 (25,0%)	0(0,0%)
Cuenta dedos (CD)	5 (25,0%)	13 (65,0%)	8 (40,0%)	4(20,0%)
Mov de manos(MM)	9(45,0%)	5 (25,0%)	1 (5,0%)	0(0,0%)
Percepción a la luz (PL)	4(20,0%)	0 (0,0%)	0 (0,0%)	0(0,0%)
No percepción a la luz (NPL)	2(10,0%)	2 (10,0%)	2 (10,0%)	2(10,0%)

TABLA 4

AGUDEZA VISUAL EN LOS DIFERENTES TIEMPOS EVALUADOS EN 20 OJOS CONTRALATERAL AL OJO CON CIERRE ANGULAR AGUDO

	Pre Laser	24 Horas Post Laser	3 Días Post Laser	3meses Post Laser
20/30	3 (15,0%)	6 (30,0%)	7 (35,0%)	8(40,0%)
20/40	3 (15,0%)	3 (15,0%)	1 (5,0%)	3(15,0%)
20/50	2 (10,0%)	3 (15,0%)	1(5,0%)	2 (10,0%)
20/70	3 (15,0%)	2 (10,0%)	3 (15,0%)	1 (5,0%)
20/80	6 (30,0%)	3 (15,0%)	0 (0,0%)	3 (15,0%)
20/100	0 (0,0%)	0 (0,0%)	1 (5,0%)	0(0,0%)
20/150	0 (0,0%)	0 (0,0%)	0 (0,0%)	0(0,0%)
20/200	0 (0,0%)	0 (0,0%)	0 (0,0%)	0(0,0%)
20/400	0 (0,0%)	0 (0,0%)	0 (0,0%)	0(0,0%)
Cuenta dedos	0 (0,0%)	0 (0,0%)	0 (0,0%)	1(5,0%)
Mov de manos	1 (5,0%)	1 (5,0%)	1 (5,0%)	0(0,0%)
Percepcion a la luz	0 (0,0%)	0 (0,0%)	0 (0,0%)	0(0,0%)
No percepcion a la luz	2 (1,0%)	2 (10,0%)	2 (10,0%)	2(10,0%)

TABLA 5

NÚMERO DE CÉLULAS/mm² DEL ENDOTELIO CORNEAL EN LOS DIFERENTES TIEMPOS EVALUADOS EN LA POBLACION ESTUDIADA

	Pre Laser	24 Horas Post Laser	3 Días Post Laser	3meses Post Laser	*P*
Ojos con Cierre Angular agudo N=20 ojos	2472±323	1994 ±220	1895±125	1865±166	0,001
Ojos contralateral al ojo con cierre angular agudo N=20 ojos	2600±245	2288 ±210	2024±248	1922±204	0,001

3. Discusión

El manejo del glaucoma incluye la decisión quirúrgica oportuna. La iridotomía láser puede ser una solución quirúrgica, o utilizarse como profilaxis de un evento agudo que puede llevar a la ceguera. En el presente estudio se compara el contaje de células endoteliales pre y post- iridotomía láser en pacientes con cierre angular agudo

En la población estudiada predominó el sexo femenino sobre el masculino en una relación aproximada de 1.5:1, proporción que se corresponde con lo expresado en la literatura sobre una supremacía de las mujeres en el padecimiento del glaucoma primario de ángulo estrecho (González, González. 1997, Golan et al. 2013).

Varios autores concuerdan en que la estrechez del ángulo iridocorneal es un denominador común para el glaucoma por cierre angular en cualquiera de sus variantes (Shields MB. 1987, Pérez P. 2017, Garcia et al. 2008(b), Lee D. 2009, Fernández et al. 2012, Vold, Dustin. 2010, Sihota et al. 2017, Wörner et al. 2011); esto coincide con las

características gonioscópicas del grupo en estudio, la cual que es la técnica estándar de referencia para el diagnóstico de cierre angular agudo, cuando esto ocurre difícilmente se observa la línea de Schwalbe (Wörner et al. 2011).

En el estudio preoperatorio, en la gonioscopía presentaron ángulos totalmente cerrados y un 50% mostraron las estructuras hasta el trabéculo anterior. Los ojos contralaterales sanos, de las estructuras hasta el trabéculo anterior en un paciente con ataque agudo de ángulo cerrado, se consideran como ángulos ocluíbles ya que hasta en 50% de los casos desarrollarán un ataque agudo por oclusión angular. Estos ojos se caracterizan por tener longitudes axiales más cortas, cámaras anteriores más estrechas y cristalinos más gruesos que ojos normales, así como por tener un mayor escalonamiento en el radio de curvatura corneal

El grosor de la córnea también estuvo aumentado en los ojos con cierre angular agudo, como sucede en estos casos, causado por el aumento de la PIO, lo cual constituye un alto factor de riesgo junto a la estrechez del ángulo para el desarrollo de un proceso agudo, lo que ha sido demostrado por otros autores (González, González. 1997, Garcia et al. 2015, Golan et al. 2013).

El descenso de la PIO media post- iridotomía fue estadísticamente significativo al reducirse 4,6 mm Hg a las 24 horas posterior al procedimiento, este descenso se continuo, observándose a los 3 meses una reducción de 9,7 mm Hg, situación que también ocurrió en el contalateral, sin embargo, los cambios no fueron tan acentuados como el ojo con cierre angular agudo. En estudio de García y col, sobre la evolución del glaucoma primario de ángulo estrecho post- iridotomía periférica con Yag láser, la presión intraocular disminuyó 3,1 mm Hg, después de la iridotomía (Garcia et al. 2015). Lo que justifica el valor de la iridotomía periférica con Nd: YAG láser en el cierre angular agudo.

En todos los pacientes después de la iridotomía se observó mejoría de la agudeza visual, a excepción de los casos con NPL. Otros autores reportan que después de la iridotomía la AV se mantuvo igual en 56 ojos (59,6 %), mejoraron 6 ojos (6,4 %) y 32 ojos (34 %)

empeoraron por la profundización o la aparición de nuevos escotomas (Garcia et al. 2015). Lo que contrasta con los hallazgos de la presente investigación.

El endotelio corneal es una estructura delicada y las células disminuyen en cantidad con el transcurso de los años, con un amplio rango de celularidad de 2000 a 4000 cel./mm2. Las densidades celulares endoteliales preoperatorias fue en promedio 2472±323 cel./mm2 en los ojos con cierre angular agudo y 2600±245 cel./mm2, observándose en el postoperatorio un porcentaje de pérdida celular entre 12 %y 15%. Al respecto se describe que la iridotomía láser produce daño en el endotelio de la córnea y determina cierta pérdida de células endoteliales, el riesgo de descompensación postoperatoria de la córnea aumenta si la cifra de células preoperatoria es baja (Pescosolido et al. 2011).

La relación de Láser Yag con alteraciones endoteliales ha sido demostrada por otros autores, por ejemplo; Kozobolis y col., quienes compararon la alteración endotelial que produce la aplicación del Láser Yag en 3 grupos: a) membranas pupilares, b) Iridotomías Láser, c) Capsulotomías, observaron que aparecían algunas áreas oscuras en el endotelio corneal en los grupos a y b. Éstas áreas están totalmente relacionadas con la energía total liberada y concluyen que la alteración endotelial inmediata no es significativa, pero puede acelerar la pérdida celular a largo tiempo, Manterola, C. (2006).

Por su parte, Schwenn y col. (1995), realizaron un estudio prospectivo randomizado comparando la iridotomía Láser Yag y la Iridectomía Quirúrgica y reportaron que los dos métodos, son equivalentes para reducir la presión intraocular y en relación con la agudeza visual, pero tiene el paciente mayor satisfacción con el Láser y el endotelio permanece más estable (no es estadísticamente significativo) (Kozobolis et al. 1998). Así mismo en estudios realizados con Biomicroscopía Ultrasónica, analizan las células endoteliales tras iridotomías por Yag Láser, confirmando que existe una reducción de la densidad celular, siendo esta pérdida celular inversamente proporcional a la distancia de las iridotomías del endotelio Schwenn y col. (1995).

Sin embargo, otros autores como Pérez P. (2017), en su investigación sobre cambios microscópicos especulares tras iridotomía en ojos con glaucoma crónico de ángulo cerrado concluyeron que la iridotomía láser en ojos con glaucoma crónico de ángulo cerrado no condujo a cambios significativos en la microscopía especular corneal central a largo plazo en comparación con pacientes que no se sometieron a iridotomía.

Aunque, se describen complicaciones como; hifema, lesiones corneales (ruptura descemet) sinequias posteriores e iritis (Pescosolido et al. 2011, Lee D. 2009, Vold, Dustin. 2010), en el estudio no se observaron complicaciones, lo que es beneficioso para el paciente y como medida de primera instancia ante el momento en que el paciente nos consulta a la emergencia.

Conclusiones y Recomendaciones

Con base al resultado del estudio se concluye que la iridotomía láser en ojos con cierre angular agudo reduce significativamente la presión intraocular y mejora la agudeza visual, pero conduce a cambios significativos en la microscopía especular corneal.

Tomando en consideración que el conteo de células endoteliales está lejos del umbral de descompensación, así como la efectividad de iridotomía láser en ojos con cierre angular agudo al tratar de resolver el bloqueo pupilar funcional y que está exenta de complicaciones graves, se sugiere tener en cuenta el contaje de células endoteliales previo al procedimiento y un seguimiento a largo plazo de estos pacientes.

Referencias

Alemán Suárez I., Armengol Oramas Y., Suárez Herrera V., Morejón Sanz A. (2011). Evolución y resultados del glaucoma por cierre angular primario. RevMed Electrón [Internet]. 2011 [citado 3 abr 2015]; 33(4). Disponible en: http://www.revmatanzas.sld.cu/revista%20medica/ano%202011/vol4%202011/tema02.htm

Anderson D., Jin J., Wright M. (2001). The Physiologic caracteristic of relative pupilary block, AM J Ophthalmology, 111(1):344.

Díaz Alfonso L., Suárez B., Curbelo M., Soto Serrano Y., Milanés A. (2010). Caracterización epidemiológica del glaucoma primario de ángulo abierto. Medisur [Internet]. [citado 3 abr 2015]; 8(5). Disponible en:http://medisur.sld.cu/index.php/medisur/article/view/896/274

Fernández L., Piloto I, Díaz Y., Obret I., Ferrer M.T., Álvarez G. (2012). Consideraciones terapéuticas en el cierre angular primario. Rev Cubana Oftalmol [Internet]. [citado 23 mar 2015]; 25(3). Disponible en: http://scielo.sld.cu/scielo.php?pid=S0864-21762012000300009&script=sci_arttext

García F., Sedeño I, Novoa E., Pérez D. (2015). Evolución del glaucoma primario de ángulo estrecho postiridotomía periférica con Nd: YAG láser. Rev Cubana Oftalmol [Internet]. Dic [citado 29 Ene 2016]; 19(2). Disponible en: http://scielo.sld.cu/scielo.php?script=sci_arttext&pid=S0864-21762006000200002&lng=es

García J., Arias A., García J. (1998)a. Nueva estrategia terapéutica antiglaucomatosa - Actualización. Universidad Complutense de Madrid: Instituto Castroviejo, pag. 57-74.

García J., Arias A., García J. (2008)b. Nueva estrategia terapéutica antiglaucomatosa. Madrid (España): Merck Sharp Dohme,

Golan S., Levkovitch V., Shemesh G., Kurtz S. (2013) Anterior chamber bleeding after láser peripheral iridotomy. JAMA Ophthalmology, 131(5):626-629.

González J., González M. (1997). Glaucoma por cierre angular primario e Iridotomía preventiva con láser. Archivos Chilenos de Oftalmología, 10(10):115-22.

Kanski J.J., McAllister J.A. (2009). Glaucoma manual a color de diagnóstico y tratamiento. Editorial EDIKA-MED, S.A, pag. 44-50.

Kanski J.J. (2009). Oftalmología Clínica.Glaucoma. 5 ed. Harcourt, Madrid (España): pag. 199-240

Klapper R. (2011). Q-switched neodymiun: YAG láseriridotomy. Ophthalmol. 91 (1):1017.

Kozobolis V.P., Detorakis E.T., Vlachonikolis IG, Paliikaris IG. (1998). Endothelial corneal damage after neodymium:yag laser treatment: pupilar membranectomies, iridotomies, capsulotomies. Ophthalmic Surg. Lasers, Oct; 29(10): 793-802.

Lee D. (2009). Management of Glaucoma. Revophthalmol, 3 (4): 113- 118.

Manterola, C. (2006). Revisión sistemática de literatura con diferentes tipos de diseños. International journal of morphology, 27 (4), 1179-1186.

Mergler S, Pleyer U. (2011). Physiology of the human corneal endothelium--new insights from electrophysiological investigations, KlinMonblAugenheilkd, 228 (20): 520-524

Pérez P. (2017). Cambios microscópicos especulares tras iridotomía en ojos con glaucoma crónico de ángulo cerrado. Revista Journal of glaucoma, 26(9): 750-755.

Pescosolido N., Librando A., Puzzono M., Nebbioso M. (2011). Palmitoylethanolamide effects on intraocular pressure after Nd:YAGláseriridotomy: an experimental clinical study. J OculPharmacolTher, 27(6):629-35.

Ritch R., Shields M.B., Krupin T. (1998). The Glaucomas. 2nd. ed. Mosby Year Book, inc., pag. 1549-1550.

Schwenn O., sell F., Pfeiffer N., Grehn F. (1995). Prophylactic Nd:Yag-laser iridotomy versus surgical iridectomy: a randomized prospective study. Ger J Ophthalmol, Nov; 4(6): 374-379.

Shields M.B. (1987).Glaucoma. 2da. ed. Editorial Médica Panamericana, pag. 432-444.

Sihota R., Agarwal E., James M., Verma M., Kumar L., Gupta V., Kulwant S. (2017). Long-Term Evaluation of Specular Microscopic Changes Following Nd: YAG Iridotomy in Chronic Primary Angle-Closure Glaucoma Eyes Journal of Glaucoma, 26 (9): 762-766

Vold S., Dustin L. (2010). Trabectome Study Group. Impact of lásertrabeculoplasty on Trabectome® outcomes. Ophthalmic SurgLásers Imaging, 41(4):443-51. Citado en PubMed; PMID: 20608613.

Wörner C., Olguín A., Ruiz J. (2011). Cell pattern in adult human corneal endothelium, PLoS One, 6 (11): 19483.

Prevalencia de síndrome pseudoexfoliativo y su asociación con otras enfermedades oculares

Nelson Sanguinetty * **
Mary Oliveros**
Daniela López**
Mayted Mendoza* **
Alexander Rabinovich**
Nairim Sandoval**
Jean Morales* **

RESUMEN

Objetivo: Determinar la prevalencia del síndrome pseudoexfoliativo (SPEX) y su asociación con otras enfermedades oculares. **Metodología:** Estudio descriptivo de corte transversal. Se incluyeron 200 pacientes de ambos sexos, entre 40 y 85 años, de consultas sucesivas del servicio de oftalmología, Hospital Universitario de Maracaibo, desde julio 2017 a julio 2018. La evaluación oftalmológica incluyó: historia clínica, agudeza visual, biomicroscopia con lámpara de hendidura, tonometría de aplanación, gonioscopia y fondo de ojo. Los resultados se expresaron en número y porcentaje. **Resultados:** La prevalencia general del SPEX fue de 31%. Se encontró que 44,64% de los pacientes presento características clínicas compatibles con glaucoma pseudoexfoliativo. La enfermedad ocular más frecuentemente asociada, además del glaucoma fue la catarata con un 25%. **Conclusiones:** El SPEX es una entidad clínica frecuente, presenta asociaciones importantes con patologías como catarata, glaucoma y facodonesis, debe ser estudiada detalladamente ya que al estar presente puede ser fuente de complicaciones quirúrgicas.
PALABRAS CLAVE: catarata, glaucoma, facodonesis, pseudoexfoliación.

* División de Estudios para Graduados, Facultad de Medicina, Universidad del Zulia, Maracaibo – Venezuela, sanguinetty@gmail.com
** Servicio de Oftalmología, Hospital Universitario de Maracaibo. Maracaibo - Venezuela.
Recibido: 15/03/2019 Aceptado: 06/05/2019

Prevalence of pseudoexfoliative syndrome and its association with other eye diseases

ABSTRACT

Objective: To determine the prevalence of pseudoexfoliative syndrome (SPEX) and its association with other eye diseases. **Methodology:** Descriptive cross-sectional study. We included 200 patients of both sexes, between 40 and 85 years, of successive consultations of the ophthalmology service, University Hospital of Maracaibo, from July 2017 to July 2018. The ophthalmological evaluation included: clinical history, visual acuity, biomicroscopy with slit lamp, applanation tonometry, gonioscopy and fundus. The results were expressed in number and percentage. **Results:** The general prevalence of SPEX was 31%. It was found that 44.64% of the patients presented clinical characteristics compatible with pseudoexfoliative glaucoma. The eye disease most frequently associated with glaucoma was cataract with 25%. **Conclusions:** SPEX is a frequent clinical entity, it presents important associations with pathologies such as cataract, glaucoma and phacodonesis, it must be studied in detail since it can be a source of surgical complications when present.
KEY WORDS: cataract, glaucoma, phacodonesis, pseudoexfoliation.

Introducción

El síndrome pseudoexfoliativo (SPEX) es considerado un trastorno sistémico que afecta el globo ocular y se relaciona con la edad, fue descrito por Lindberg en 1917. Se cree que es una manifestación ocular de un síndrome sistémico caracterizado por un trastorno en el que un material fibrilar extracelular se acumula en muchos tejidos oculares y sistémicos. Kanski (2009).

El diagnóstico del SPEX tiene una base clínica. Requiere la presencia de un típico material pseudoexfoliativo en el margen pupilar y la superficie anterior de la cápsula del cristalino, la apariencia característica es un disco central rodeado por una zona clara que, a su vez, está rodeada por un depósito en forma de anillo de caspa. La

atrofia pupilar, presión intraocular elevada (PIO) y el daño del nervio glaucomatoso se ha demostrado en pacientes con SPEX, además de entidades como sublujación de cristalino y obstrucción de la vena central de la retina (OVCR), otros estudios lo han relacionado incluso con accidentes isquémicos transitorios, enfermedad coronaria isquémica. Forsman et al. (2007). La debilidad zonular es mucho más frecuente en pacientes con catarata y PXF, en comparación con la población general. Ritch *et al*. (2007).

El SPEX es el principal factor de riesgo del glaucoma por pseudoexfoliación, cuando el SPEX está asociado a daño glaucomatoso del nervio óptico y del campo visual se denomina glaucoma pseudoexfoliativo (GPEX), un tipo de glaucoma en el que la mayoría de los pacientes presentan un ángulo abierto y crónico que generalmente es unilateral. Benítez *et al* (2015). El glaucoma como tal, es una neuropatía óptica progresiva que constituye la primera causa de ceguera irreversible en el mundo. Actualmente, representa la segunda causa de ceguera en el mundo. La prevalencia del glaucoma primario de ángulo abierto en blancos europeos, estadounidenses y australianos es similar, pero en África, el Caribe y los Estados Unidos es mayor. Se estima que aumente con el crecimiento demográfico y el envejecimiento de la población; así mismo se espera que para el 2020 el número de personas afectadas haya aumentado a 76 millones. Cook *et al*. (2012).

En el año 2010 se estimó que existían 60.5 millones de pacientes afectados con glaucoma primario de ángulo abierto. Un metanálisis de estudios epidemiológicos, estimó la prevalencia de glaucoma primario de ángulo abierto y cerrado, para conocer el número aproximado de personas entre 40 y 80 años de edad que pueden verse afectadas para el año 2020 y 2040. Se considera que para el 2020 se incrementará a 76 millones para finalmente alcanzar 111.8 millones en el 2040 lo que representa el 3.54% de la población. Esta representa la segunda causa de ceguera prevenible en Venezuela.

Tham *et al* (2014). Esto sugiere un incremento desproporcionado, por lo que es necesario realizar estrategias de salud pública para garantizar la detección oportuna y tratamiento temprano con el objetivo de retrasar la pérdida visual.

En base a todos estos argumentos podemos decir que la ceguera, compromete el desenvolvimiento social del individuo, trayendo como consecuencia problemas psicológicos, económicos que repercuten en el bienestar del paciente y se extiende a todos los miembros del grupo familiar y genera un costo económico considerable en los sistemas de salud de todo el mundo. La detección y el tratamiento temprano del daño glaucomatoso representan un punto crucial en el pronóstico y manejo de la enfermedad.

Considerando tales argumentos, así como la alta frecuencia de pacientes con glaucoma evaluados diariamente en el Servicio de Oftalmología el Hospital Universitario de Maracaibo, se realizó esta investigación que permitió determinar la prevalencia del síndrome pseudoexfoliativo y su asociación con otras enfermedades oculares en pacientes de dicha consulta. La importancia de esta investigación radica en poder aportar estadísticas fidedignas de la asociación de enfermedades oculares presentes en el SPEX que pueden complicar a los pacientes con dicha patología al momento de realizar intervenciones quirúrgicas oculares.

1. Materiales y métodos

Se realizó un estudio descriptivo de corte transversal, sobre las características clínicas del material pseudoexfoliativo en la superficie de las estructuras del segmento anterior del ojo y su asociación con otras enfermedades oculares. Se incluyeron pacientes de la consulta del Servicio de Oftalmología del Hospital Universitario de Maracaibo. La muestra estuvo conformada por 200 pacientes de

ambos sexos que acudieron a dicha consulta de julio 2017 a julio 2018, con edades entre los 40 y 85 años. Se obtuvo el consentimiento informado de todos los participantes (Anexo 1). Dichos pacientes se sometieron a una evaluación oftalmológica completa, que incluyo: historia clínica, agudeza visual, biomicroscopia con lámpara de hendidura, tonometría de aplanación, gonioscopia con lente de Goldmann, fondo de ojo con lente de 90D (Anexo 2). Se excluyeron 21 pacientes, entre las razones destacan: pacientes que no quisieron participar en la investigación, pacientes con opacidad corneal que no permitía la evaluación del segmento anterior y posterior del ojo, pacientes con trauma ocular previo y pérdida de la anatomía estructural del segmento anterior.

El análisis de los datos obtenidos se realizó mediante la aplicación de la estadística descriptiva a las variables objeto de estudio (valores promedios, desviación estándar, porcentajes, expresados en tablas y gráficos). Para ello, se utilizó un computador personal (Laptop) HP Pavilon dv2927la Notebook y el programa estadístico computarizado Epi-Info 6.0.

2. Resultados y discusión

Los resultados obtenidos muestran una prevalencia general del síndrome pseudoexfoliativo de 31%, lo que quiere decir que, de 179 pacientes evaluados, solo 56 presentaron alguna manifestación clínica compatible con SPEX, tal como se presenta en el gráfico 1.

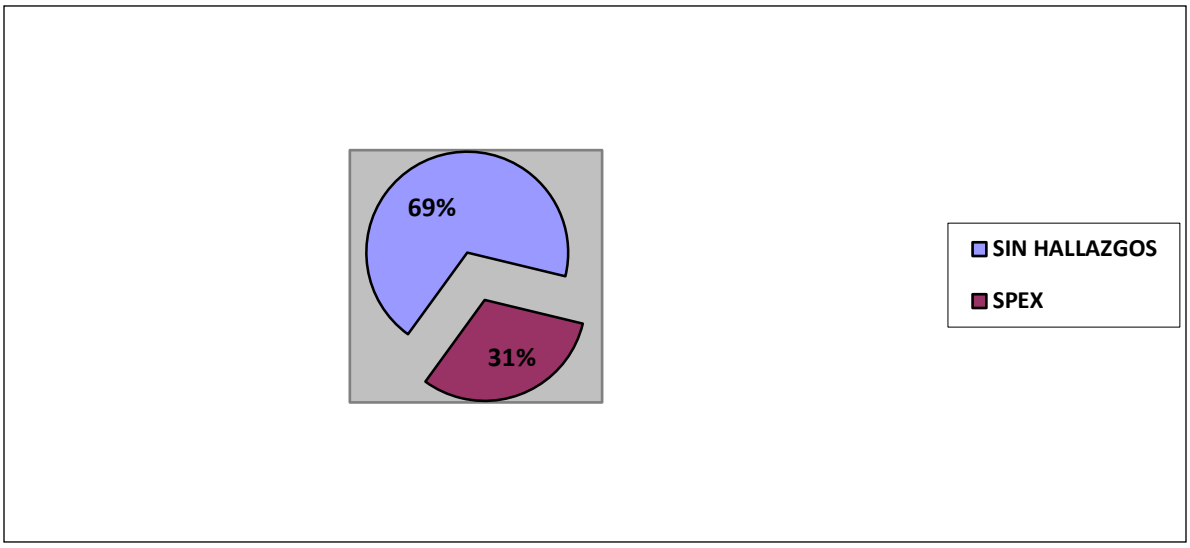

GRÁFICO 1: Prevalencia de Síndrome pseudoexfoliativo en pacientes de la consulta de Oftalmología del Hospital universitario de Maracaibo. Municipio Maracaibo. Estado Zulia, 2018.

En el estudio publicado por Muawyah y col., realizado en 1195 pacientes del Hospital de Jordan en 2008, estiman una prevalencia de 9,1% de SPEX. Por su parte Schweitzer (2018), describe en su trabajo que no hay datos epidemiológicos completos sobre la prevalencia del SPEX en el mundo, las metodologías de los estudios publicados difieren según la población y el procedimiento diagnóstico. Sin embargo, muchos estudios revelan una distribución global de este síndrome, pero a tasas muy bajas, según grupos étnicos, aéreas geográficas, también condiciones ambientales y este estudio no escapa de dichas consideraciones.

Tabla 1: Prevalencia del síndrome pseudoexfoliativo según edad y asociado a glaucoma pseudoexfoliativo. Consulta de Oftalmología Hospital Universitario de Maracaibo. Municipio Maracaibo. Estado Zulia, 2018.

EDAD	PEX		GPEX		TOTAL	
	N°	%	N°	%	N°	%
40 - 49 años	2	6,45	0	0,00	2	3,89
50 – 59 años	5	16,12	3	12,00	8	14,28
60 – 69 años	13	41,93	8	32,00	21	37,50
70 – 79 años	9	29,03	8	32,00	17	30,35
› 80 años	2	6,45	6	24,00	8	14,28
TOTAL	31	55,35	25	44,64	56	100

Según el estudio realizado por Muawyah y col., la edad promedio fue de 68.3 años compatible con la población de este estudio la cual fue de 65±4. La prevalencia tenía una tendencia a aumentar con la edad tal como lo demuestran los resultados del presente estudio, siendo mayor en mujeres que en hombres. Además, los resultados dejan ver la relación directa que existe entre el SPEX y el GPEX, se observa que del 100% de pacientes evaluados con síndrome pseudoexfoliativo solo 44,64% (25/56) presento características clínicas compatibles con GPEX (Ver tabla 1).

Tabla 2: Asociación del síndrome pseudoexfoliativo con otras enfermedades oculares. Consulta de Oftalmología del Hospital Universitario de Maracaibo. Municipio Maracaibo. Estado Zulia. 2018

EDAD	SPEX (31/56)		GPEX (25/56)		TOTAL	
	N°	%	N°	%	N°	%
Cataratas	9	29,03	5	20,00	14	25,00
Facodonesis	1	3,02	3	12,00	4	7,14
OVCR*	0		1	4,00	1	1,78
Sublujación de cristalino	0		1	4,00	1	1,78
Total	10	32,25	10	40,00	20	35.71

*OVCR: Oclusión de la vena central de la retina.

En la Tabla 2. Se aprecia que del 100% de pacientes con síndrome pseudoexfoliativo 35,7% presentaron enfermedades oculares asociadas. Siendo la catarata la que predomino con un 25% (14/56) del total. Resultados compatibles con el estudio publicado por Muawyah y col., el cual arrojo que el SPEX se asoció significativamente con la catarata, glaucoma y facodonesis., mostrando los siguientes resultados: de los ojos con PSEX, el 92.1% tenía catarata, el 33.1% tenía glaucoma y el 7.9% tenía facodenesis.

Conclusiones y Recomendaciones

En la actualidad, gracias a múltiples estudios se entiende que el SPEX es una patología común en todas las etnias y en diferentes países. Sin embargo, Young Al y col. (2004) determinaron que es una condición rara en los chinos. Su estudio epidemiológico basado en la población de un hospital de Hong Kong, identificó una tasa de prevalencia del 0,4% en pacientes de 60 años o más. Analizando dichos estudios, se puede concluir que la prevalencia varía según las poblaciones y para comparar dichos resultados hay que tomar en cuenta las bases metodológicas de dichos estudios, así como los diferentes criterios diagnósticos y la edad de cada población, dado que se puede interpretar de forma incorrecta al momento de realizar comparaciones.

En el presente estudio la prevalencia de pacientes con síndrome pseudoexfoliativo en la consulta del Hospital Universitario de Maracaibo fue de 31%. Observándose que tal como describe la literatura la prevalencia del SPEX aumenta con la edad. Sin embargo, Teshome T. y col (2004) determinaron en su estudio de prevalencia de SPEX en pacientes Etíopes que la edad de presentación es menor que en personas que sirvieron de muestra para otros estudios donde se pudo comparar.

Por otra parte, en este trabajo se evidencio que el glaucoma es la principal enfermedad asociada al SPEX, seguida de catarata y facodonesis en menor proporción. Hallazgo similar a lo planteado por Thomas R. y col (2005) es su estudio sobre SPEX en el Sur de la India, donde encontraron que la prevalencia de SPEX en pacientes con glaucoma fue de 4,2%. Por tal motivo se sugieren estudios con bases genéticas, étnicas y multicéntricos, para definir la estadística nacional del PSEX y GPEX.

Referencias

Benitez J., Morion M., Marco M., Parron T., (2015). Epidemiología del síndrome pseudoexfoliativo: desmitificando leyendas con la mirada en el futuro. *Archivos Sociedad Española de Oftalmología.* (10), 455–457.

Cook C., Foster P. (2012). Epidemiology of glaucoma: what's new? *Can J Ophthalmol*. 2012; 47(3):223-6. doi: 10.1016/j.jcjo.2012.02.003.

Forsman E., Cantor R., Eriksson A., Fellman J., Jarvela I., Forsius H. (2007). Prevalence and inheritance in a subisolate of the Finnish population. *Acta Ophthalmol Scand* 85: 500–507.

Kanski J. (2009). Oftalmología clínica. Barcelona – España. Editorial Elvesier. p.p 389-391.

Muawyah A., Maha I., Ghaida M., Khawla A. (2008). Pseudoexfoliation syndrome at Jordan University Hospital. *Acta Ophthalmologica*. 86: 755-757. doi: 10.1111/j.1755-3768.2008.01258.x

Ritch R., Schlotzer U. (2001). Exfoliation syndrome. *Survey of Ophthalmology. 45*: 176-7.

Schweitzer C. (2017). Syndrome pseudo-exfoliatif et glaucoma exfoliatif. *Journal français d'ophtalmologie.* 41: 78—90

Tham Y., Li X., Wong T., Quigley H., Aung T., Cheng C. (2014). Global prevalence of glaucoma and projections of glaucoma burden through 2040: a systematic review and meta-analysis. *Ophthalmology*. 121(11):2081-2090. doi: 10.1016/j.ophtha.2014.05.013.

Teshome T., Regassa K. (2004). Prevalence of pseudoexfoliation syndrome in Ethiopian patients scheduled for cataract surgery. *Acta Ophthalmol Scand*. Jun;82(3 Pt 1):254-8. Doi: 10.1111/j.1395-3907.2004.00263.x

Thomas R., Nirmalan P., Krishnaiah S. (2005). Pseudoexfoliation in southern India: the Andhra Pradesh Eye Disease Study. *Invest.Ophthalmol.* Apr;46(4):1170-6. doi: 10.1167/iovs.04-1062

Young AL., Tang WW., Lam Ds. (2004). The prevalence of pseudoexfoliation syndrome in Chinese people. Br. *J. Ophthalmol*. Feb;88(2):193-5. Doi: 10.1136/bjo.2003.021816

Síndrome metabólico como factor de riesgo para aumento de la presión intraocular

Nelson E. Sanguinetty M.*
Diógenes E. Solórzano G.* **

RESUMEN

Objetivo: Relacionar el síndrome metabólico (SM) como factor de riesgo para aumento de la presión intraocular (PIO). **Metodología:** Investigación correlacional, prospectiva. Incluyó 100 pacientes con diagnóstico de SM, evaluados de enero a septiembre de 2018. Se realizó examen oftalmológico, se midió la PIO. Los datos fueron expresados en cifras absolutas y porcentajes. Se aplicó análisis de correlación de Pearson, se determinó el factor de riesgo relativo. **Resultados:** Se observó asociación significativa entre HIO y triglicéridos altos (p= 0,000), así como con hiperglicemia (p= 0,030). La PIO mostró una correlación positiva y significativa con los triglicéridos (r = ,943**; p= 0,000) y con la glicemia (r = ,371*; p= 0,043). El riesgo de HIO en pacientes con triglicéridos altos es 4,5; IC: 2,3-8,8 y con hiperglicemia 4,2; IC: 2,1-8,2. **Conclusión:** Se demostró que los triglicéridos altos y la hiperglicemia son factores de riesgo independiente para aumentar la PIO, con una correlación directamente proporcional.

PALABRAS CLAVES: Síndrome metabólico, presión intraocular.

* Servicio de Oftalmología, Hospital Universitario de Maracaibo. Maracaibo – Venezuela, sanguinetty@gmail.com
** División de Estudios para Graduados. Facultad de Medicina. Universidad del Zulia. Maracaibo – Venezuela.

Recibido: 18/03/2019 Recibido: 02/05/2019

Metabolic syndrome as a risk factor for increasing intraocular pressure

ABSTRACT

Objective: To relate the metabolic syndrome (MS) as a risk factor for increased intraocular pressure (IOP). **Methodology:** Correlational, prospective research. It included 100 patients diagnosed with MS, evaluated from January to September 2018. An ophthalmological examination was performed, IOP was measured. The data were expressed in absolute figures and percentages. Pearson correlation analysis was applied, the relative risk factor was determined. **Results:** There was a significant association between HIO and high triglycerides (p = 0.000), as well as hyperglycemia (p = 0.030). The IOP showed a positive and significant correlation with triglycerides (r =, 943 **, p = 0.000) and with glycemia (r =, 371 *; p = 0.043). The risk of IOP in patients with high triglycerides is 4.5; CI: 2.3-8.8 and with hyperglycemia 4.2; IC: 2.1-8.2. **Conclusion:** It was demonstrated that high triglycerides and hyperglycemia are independent risk factors to increase IOP, with a directly proportional correlation.

KEY WORDS: Metabolic syndrome, intraocular pressure.

Introducción

El glaucoma es una neuropatía óptica progresiva que constituye la primera causa de ceguera irreversible en el mundo occidental. Actualmente, representa la segunda causa de ceguera en el mundo. La prevalencia del glaucoma primario de ángulo abierto en blancos europeos, estadounidenses y australianos es similar, pero en África, el Caribe y los Estados Unidos es mayor. Se estima que aumente con el crecimiento demográfico y el envejecimiento de la población; así mismo se espera que para el 2020 el número de personas afectadas haya aumentado a 76 millones, así lo expresan Cook et al. (2012).

En el año 2010 se estimó que existían 60.5 millones de pacientes afectados con glaucoma primario de ángulo abierto. Un metaanálisis de estudios epidemiológicos publicado por Tham et al. (2014) estimó la prevalencia de glaucoma primario de ángulo abierto y cerrado, para conocer el número aproximado de personas entre 40 y 80 años que pueden verse afectadas para el año 2020 y 2040. Las proyecciones revelaron que en el año 2013 vivían 64.3 millones de personas afectadas por glaucoma en el mundo.

Se considera que para el 2020 se incrementará a 76 millones para finalmente alcanzar 111.8 millones en el 2040 lo que representa el 3.54% de la población, Tham et al. (2014). El glaucoma es la segunda causa de ceguera prevenible en Venezuela, así lo expresan Siso et al. (2005). Esto sugiere un incremento desproporcionado, por lo que es necesario realizar estrategias de salud pública para garantizar la detección oportuna y tratamiento temprano con el objetivo de retrasar la pérdida visual.

La hipertensión ocular es el estado en el que la presión intraocular (PIO) es mayor a 21mmHg y el ángulo de la cámara anterior está abierto, y ambas anomalías más el defecto del campo visual no suelen ser detectables. Mientras tanto, el glaucoma es un tipo de neuropatía óptica, y los pacientes glaucomatosos sufren de una disminución en la calidad de la visión, provocando un defecto progresivo del campo visual, (Touboul et al. 2008:616-622). La hipertensión ocular es uno de los principales factores de riesgo del glaucoma primario de ángulo abierto, pero no es un agente determinante, existiendo otros factores implicados en la génesis y progresión de esta enfermedad (Brown et al. 2006, Doughty et al. 2002).

Es así como puede haber glaucoma en personas con PIO normal y no existir en personas con PIO elevada. Hay otros factores implicados en la generación de esta enfermedad, con variada influencia en la patogenia. Algunos de estos factores son el antecedente familiar de glaucoma, la edad mayor de 40 años, la raza y el grosor corneal

central (GCC) (Brown et al. 2006, Doughty et al. 2002). y algunos componentes que integran el síndrome metabólico (SM), entre ellos la diabetes mellitus e hipertensión arterial (HTA) K Imai et al. (2012).

El SM propuesto por Reaven la primera vez en 1988 (Cook et al. 2012), también llamado síndrome X ó síndrome de insulino-resistencia se refiere a una serie de factores asociados con alto riesgo de padecer enfermedad cardiovascular y/o diabetes mellitus tipo 2 (DM2) Tham et al. (2014). Este síndrome ha sido definido por diversas organizaciones relacionadas con la salud como la Organización Mundial de la Salud (OMS) Ford et al. (2002), el Adult Treatment Panel (ATP III) de los Estados Unidos de Norteamérica (Rubio et al. 2004, NIH Publication 01-3670; May 2001) y la Internacional Diabetes Federation (IDF) con sede en Europa, caracterizándose por agrupar obesidad abdominal, intolerancia a la glucosa, HTA y dislipidemia (hipertriacilgliceridemia y niveles bajos de HDL-C) (Consenso Brusells, Belgium, 2005).

Se ha demostrado que la PIO tiende a aumentar linealmente en función del número de factores de riesgo del síndrome metabólico. Tres de los cinco componentes del síndrome metabólico (glucosa plasmática en ayuna, presión arterial y triglicéridos) estuvieron asociados con la hipertensión ocular. Pero, la relación entre esta condición y la hipertensión ocular es desconocida (K Imai et al. 2012). Por otro lado, se describe que los medicamentos que controlan la HTA o la hipertrigliceridemia que a menudo acompaña al SM, podrían reducir la PIO (Oh Sw, Lee S. 2011). Sin embargo, esta posibilidad requiere una validación por parte de futuros estudios longitudinales, así como la necesidad de conocer la relación del referido síndrome con la hipertensión ocular, cuyos resultados podrían ser útiles para plantear nuevas alternativas terapéuticas para el control de la presión intraocular.

Considerando tales argumentos, así como la alta frecuencia de pacientes con hipertensión ocular evaluados diariamente en el Servicio de Oftalmología del Hospital Universitario de Maracaibo y la elevada incidencia de SM en la población zuliana cuya prevalencia en la región es de 42,7% (Bermúdez et al. 2013), se realizó el presente estudio para relacionar el SM como factor de riesgo para aumento de la presión intraocular en pacientes de la consulta de Medicina Interna y evaluados en la consulta de Oftalmología del Hospital Universitario de Maracaibo, en el lapso comprendido entre enero a septiembre de 2018.

1. Materiales y métodos

Investigación correlacional, prospectiva, transversal. La población objeto del estudio, quedó constituida por pacientes del Servicio de Medicina Interna con diagnóstico de síndrome metabólico y evaluados en el Servicio de Oftalmología del Hospital Universitario de Maracaibo, en el lapso comprendido entre enero a septiembre de 2018. La muestra fue calculada a través de un programa estadístico computarizado Epinfo y quedó representada por 100 pacientes quienes cumplieron con los criterios de inclusión.

Se incluyeron los pacientes que cumplieron con los siguientes parámetros: Pacientes masculinos o femeninos mayores de 18 de edad con diagnóstico de síndrome metabólico según el ATPIII (NIH Publication 01-3670; May 2001).

Se excluyeron del estudio los pacientes con glaucoma de ángulo abierto o cerrado, glaucoma neovascular o facomórfico, glaucoma congénito o infantil. Pacientes con enfermedades neurológicas, con cataratas maduras, cirugía ocular previa, o que utilicen medicamentos que afecten la presión intraocular y sensibilidad visual. Además, pacientes que no desearon participar en la investigación.

A cada paciente seleccionado, se le explicó el estudio y luego de su consentimiento se les realizó una historia clínica en donde se recogieron datos de identificación,

antecedentes personales, familiares, enfermedad actual y la evaluación oftalmológica que incluyó agudeza visual, valoración completa del segmento anterior con lámpara de hendidura, incluyendo tonometría, gonioscopia y paquimetría.

La medición de la PIO se efectuó con lámpara de hendidura con tonómetro de aplanación (Goldman), previa colocación de anestesia tópica (Alcaine) con fluoresceína 1 gota en ambos ojos antes la medición de la presión intraocular, la cual fue expresada en mmHg.

La paquimetría se realizó con el Speculary Microscopy EM-4000 Tomey.

Para la recolección de los datos se diseñó un instrumento tipo encuesta, validado por dos expertos en la materia y un experto metodológico, estructurado de la siguiente manera: número de historia, nombre, edad, sexo, resultados de la tonometría (Goldman), paquimetría y componentes del síndrome metabólico y se le aplicó una prueba de confiabilidad.

Los datos fueron analizados a través de medidas de tendencia central, mediante el uso de cifras absolutas y porcentajes. Se aplicó el análisis de correlación de Pearson en las variables cuantitativas y se determinó el factor de riesgo relativo (RR), en el sentido de medir el riesgo de los expuestos en relación con los no expuestos considerando cada uno de los componentes del SM. Se empleó el programa estadístico SPSS, versión 23. Posteriormente, se realizará el análisis e interpretación de los resultados que se expresaran en cuadros o figuras.

2. Resultados

Para relacionar el síndrome metabólico como factor de riesgo de hipertensión intraocular en pacientes de la Consulta de Medicina Interna y evaluados en la Consulta de Oftalmología del Hospital Universitario de Maracaibo, en el lapso comprendido entre enero a septiembre de 2018, se seleccionó una muestra de 100

pacientes con diagnóstico de SM, de ello 52 (52,0%) fueron de género masculino 52 (52,0%) y 48 (48,0%) femenino. La edad promedio en los masculinos fue 38±10,4 y en las femeninas 40±12,8, con edad promedio total 40±12,8. Figura 1 y 2

El promedio de la PIO en los ojos derechos fue 20,5±4,1 mmHg y en los izquierdos 20,2±4,5 mmHg. Figura 3.

La PIO estuvo entre el rango de normalidad en 55 (55,0%) y con hipertensión ocular 45 (45,0%). Figura 4

En relación con los componentes del SM evaluados, predominaron los triglicéridos altos con 70 pacientes, obesidad abdominal 65, hiperglicemia 61, hipertensión arterial 57 y HDLc bajo 44 pacientes. Se observa una asociación significativa entre hipertensión ocular y triglicéridos altos (p= 0,000), así como, con la hiperglicemia (p= 0,030). Los demás componentes, aunque porcentualmente prevalecieron en los pacientes con hipertensión ocular, mostraron diferencias no significativas en comparación con los pacientes con PIO normal. Tabla 1.

La presión intraocular mostró una correlación positiva y significativa con los triglicéridos (r = ,943**; p= 0,000) y con la glicemia (r = ,371*; p= 0,043). No se reporta correlación entre los demás parámetros del SM con la presión intraocular. Tabla 2.

El riesgo de hipertensión ocular en los pacientes con triglicéridos altos es 4,5; IC: 2,3-8,8 y con hiperglicemia 4,2; IC: 2,1-8,2. Tabla 3.

FIGURA 1

DISTRIBUCIÓN DE LOS PACIENTES CON SÍNDROME METABÓLICO SEGÚN EL SEXO.

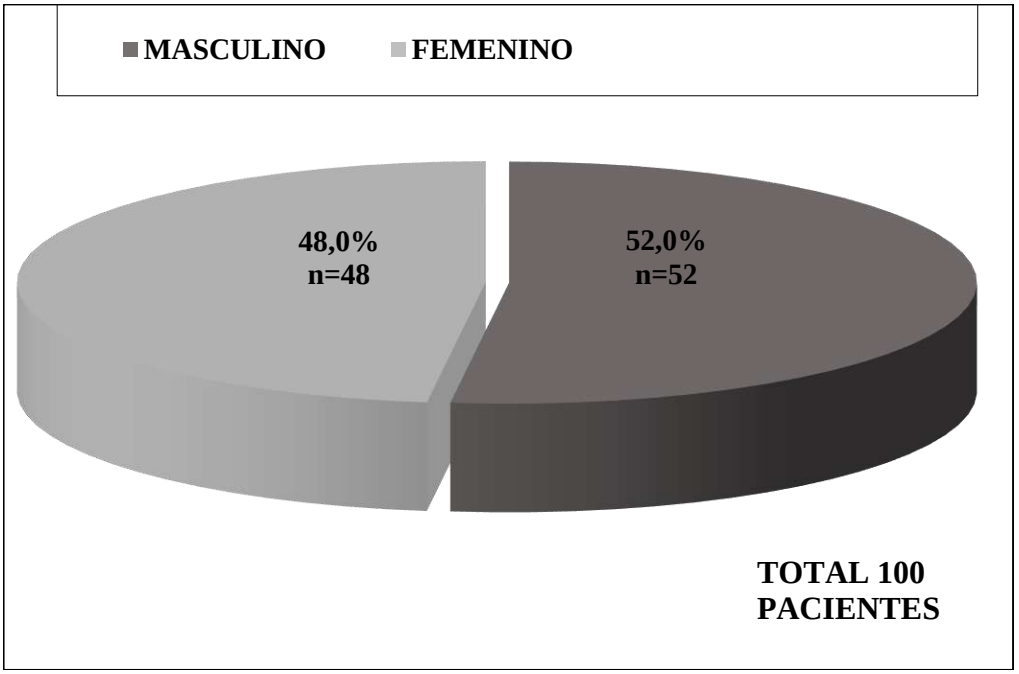

FIGURA 2. DISTRIBUCIÓN DE LOS PACIENTES CON SÍNDROME METABÓLICO SEGÚN LA EDAD PROMDIO.

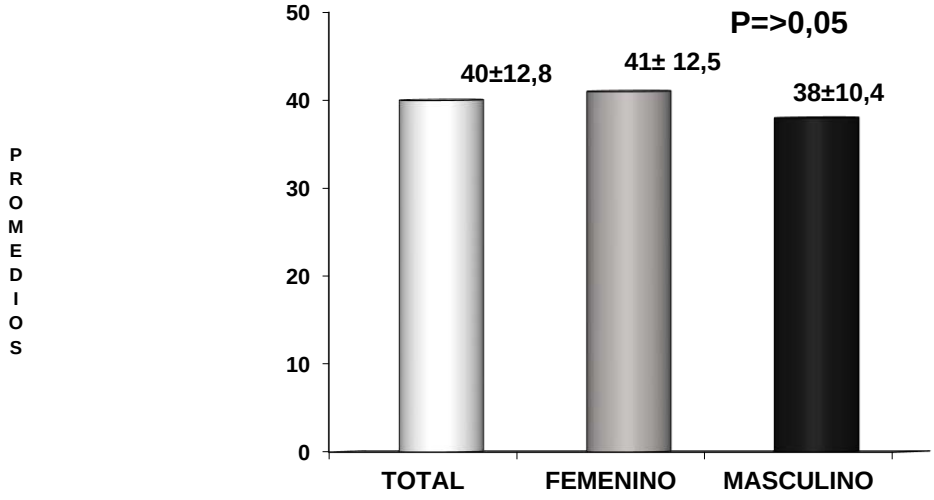

FIGURA 3. DISTRIBUCIÓN DE LOS PACIENTES CON SÍNDROME METABÓLICO SEGÚN LA PRESIÓN INTRAOCULAR.

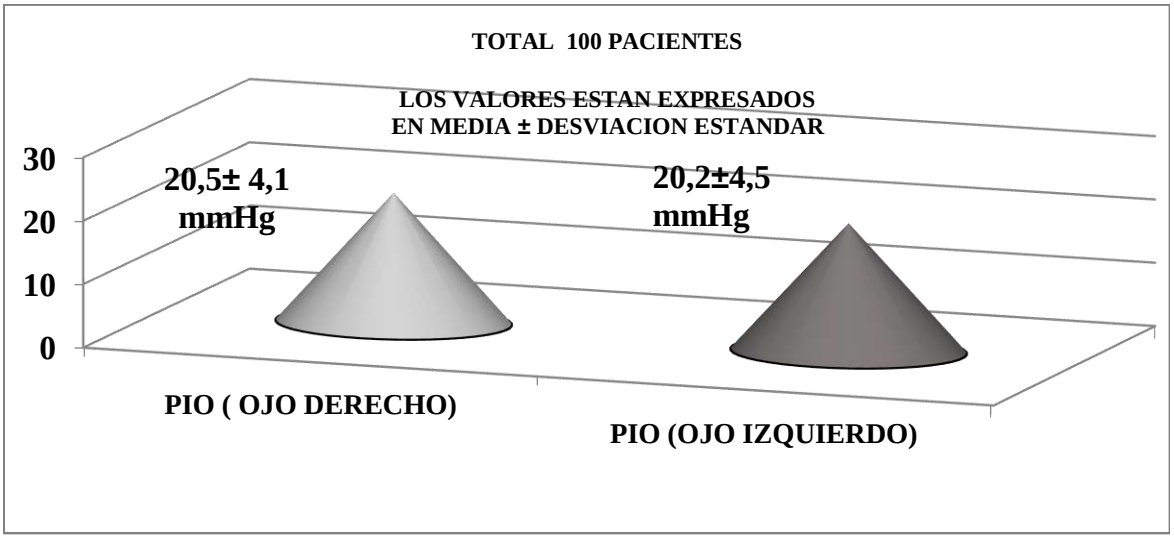

FIGURA 4. DISTRIBUCIÓN DE LOS PACIENTES CON SÍNDROME METABÓLICO SIN O CON HIPERTENSIÓN OCULAR.

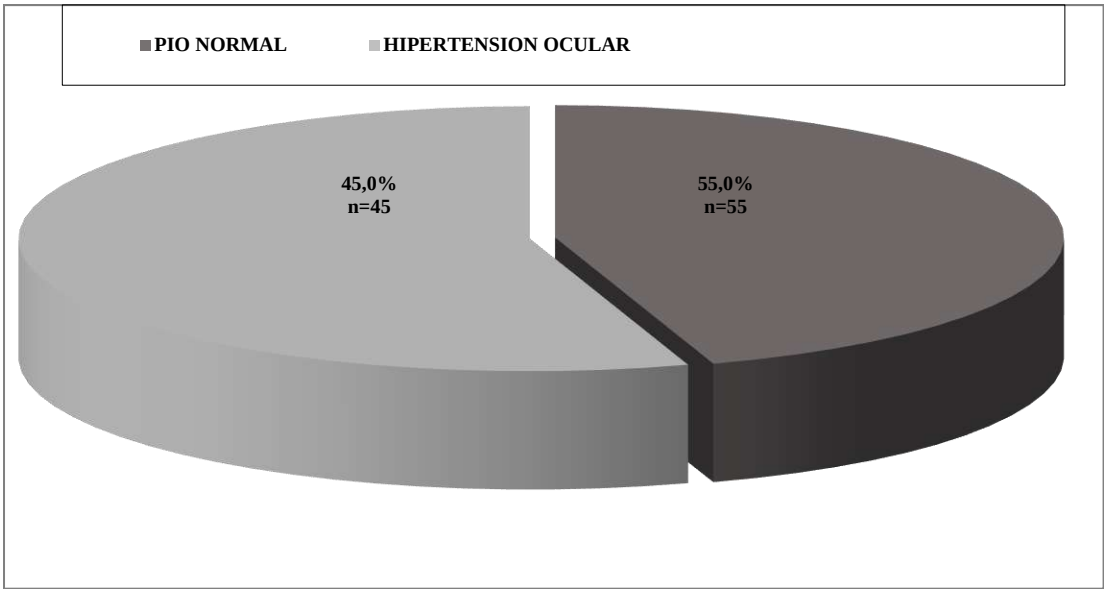

TABLA 1. RELACIÓN ENTRE LOS COMPONENTES DEL SÍNDROME METABÓLICO Y PRESIÓN INTRAOCULAR EN LA POBLACIÓN ESTUDIADA.

Componentes del Síndrome Metabólico	Hipertensión Ocular (n = 45)	PIO Normal (n = 55)	*P*
Triglicéridos Altos	41 (91,1%)	29 (52,7%)	**0,000***
Hiperglicemia	39 (86,7%)	22 (40,0%)	**0,030***
Obesidad Abdominal	33 (73,3%)	32 (58,2%)	0,257
Hipertensión arterial	29 (64,4%)	28 (50,9%)	0,895
HDL c bajo	24 (53,3%)	20 (36,4%)	0,376

***** Significativo

2. Discusión

El glaucoma es una patología frecuente, que si no se diagnóstica y se trata precozmente puede conducir a la ceguera, y esto compromete el desenvolvimiento social del individuo, trayendo como consecuencia problemas psicológicos, económicos que repercuten en el bienestar del paciente y se extiende a todos los integrantes del grupo familiar. Por ello surge la necesidad de profundizar más sobre este tema en busca de algún o algunos factores que pudieran estar influyendo en su desarrollo.

TABLA 2. COEFICIENTE DE CORRELACIÓN DE PEARSON PARA PRESIÓN INTRAOCULAR CON LAS VARIABLES CLÍNICAS Y BIOQUÍMICAS DEL SÍNDROME METABÓLICO.

		PIO	PAS	PAD	Glicemia ayuna	HDLC	TRIG	CA
PIO	Correlación de Pearson	1	-,063	,108	**,371***	-,086	**,943****	-,091
	Sig. (bilateral)		,741	,569	**,043**	,650	**,000**	,633
	N	100	100	100	100	100	100	100
PAS	Correlación de Pearson	-,063	1	,111	,046	-,099	-,273	-,236
	Sig. (bilateral)	,741		,560	,809	,604	,144	,208
	N	100	100	100	100	100	100	100
PAD	Correlación de Pearson	,108	,111	1	-,063	,055	-,042	,015
	Sig. (bilateral)	,569	,560		,741	,772	,824	,938
	N	100	100	100	100	100	100	100
Glicemia ayuna	Correlación de Pearson	**,371***	,046	-,063	1	-,023	,214	-,281
	Sig. (bilateral)	**,043**	,809	,741		,905	,255	,132
	N	100	100	100	100	100	100	100
HDLC	Correlación de Pearson	-,086	-,099	,055	-,023	1	-,352	,180
	Sig. (bilateral)	,650	,604	,772	,905		,056	,341
	N	100	100	100	100	100	100	100

TRIG	Correlación de Pearson	**,943****	-,273	-,042	,214	-,352	1	,085
	Sig. (bilateral)	**,000**	,144	,824	,255	,056		,656
	N	100	100	100	100	100	100	100
CA	Correlación de Pearson	-,091	-,236	,015	-,281	,180	,085	1
	Sig. (bilateral)	,633	,208	,938	,132	,341	,656	
	N	100	100	100	100	100	100	100

******. La correlación es significativa al nivel 0,01 (bilateral).

*****. La correlación es significante al nivel 0,05 (bilateral).

PIO= Presión Intraocular PAS: Presión arterial Sistólica PAD: Presión arterial Diastólica

TRIG: Triglicéridos CA: Circunferencia abdominal

TABLA 3. RIESGO DE HIPERTENSIÓN OCULAR EN PACIENTES CON TRIGLICERIDOS ALTO Y OBESIDAD ABDOMINAL.

	Hipertensión Ocular (n = 45)	PIO Normal (n = 55)	RR	IC. 95%
Triglicéridos Altos	41	29		
Triglicéridos normal	4	26	4,5	2,3- 8,8
Hiperglicemia	39	22		
Glicemia Normal	6	33	4,2	2,1- 8,2

El SM es una entidad compuesta por una serie de alteraciones metabólicas que actúan sinérgicamente, por lo que incrementan el riesgo de desarrollo de varias enfermedades, entre la más común se encuentran la enfermedad cardiovascular. Además, algunos de los componentes de este síndrome, como la diabetes, HTA, se asocian con enfermedades oftálmicas con daño en retina, si no son controladas adecuadamente.

La finalidad del presente estudio fue relacionar el SM como factor de riesgo de HIO, seleccionándose 100 pacientes con el referido síndrome, observándose predominio porcentual (52,0%) en los hombres, resultados similares al estudio publicado por Tielchs et al. (1994). La edad promedio de estos pacientes se ubicó dentro de la cuarta década de la vida.

El promedio de la PIO estuvo alrededor de los 20 mmHg, este hallazgo llama la atención ya que a pesar de que se encuentra dentro del límite de la normalidad, es evidente que está cerca del nivel superior. Esto significa que estos pacientes están en riesgo de desarrollar glaucoma. Este resultado pudiera atribuírsele a que el 45% de los pacientes presentaron HIO o la otra posibilidad sería que el conjunto del componente del SM, haya influido en el resultado. Dado a que existe un estudio publicado por Núñez (2014) en ese mismo centro en pacientes sanos y se reporta una PIO de 13,3 ±2,59 mmHg .

El 45% de los pacientes presentaron HIO, lo que representa que 45 de cada 100 pacientes con SM, presenta HIO. Los triglicéridos altos y la hiperglicemia fueron 2 factores que se asociaron significativamente con la HIO.

Si bien la PIO es el principal factor de riesgo para el desarrollo de glaucoma, otros factores de riesgo se han implicado en la patogénesis del glaucoma, incluyendo la enfermedad estructural, anomalías y desregulación funcional de la vasculatura que irriga al nervio óptico y el entorno del tejido retinal, como la disfunción vascular, pueden desempeñar un papel patógeno adicional como lo reportan Pertl et al. (2017).

La hipertrigliceridemia, que puede conducir a una disfunción vascular, se ha relacionado con el desarrollo de glaucoma. La presencia de disfunción vascular en pacientes con glaucoma se postuló recientemente en un estudio clínico, Leuven Eye Study, publicado por Abegão et al. (2016).

En el metaanálisis de Pertl et al. (2017), realizados para investigar la asociación de los niveles de triglicéridos con el riesgo de glaucoma en los estudios de casos y controles, se encontró que los pacientes con glaucoma presentaron niveles de triglicéridos más altos que los pacientes sin glaucoma. Este hallazgo es consistente con el concepto de que la hipertrigliceridemia representa un factor de riesgo adicional para el glaucoma. Si esta asociación es causal y / o podría ser modificada por los medicamentos para el glaucoma, queda por investigar.

Así mismo, en la investigación de K Imai et al. (2012), sobre la relación entre el síndrome metabólico y la presión intraocular (PIO)". Tres de cinco componentes del SM (glucosa plasmática en ayunas, presión arterial y triglicéridos) se relacionaron con la PIO alta y concluyeron que el SM es un factor de riesgo de PIO alta. Sin embargo, esto no se confirmó un estudio de Ko et al. (2016), e incluso encontraron una relación inversa significativa entre los niveles triglicéridos altos y glaucoma.

Al igual que los triglicéridos hubo una correlación entre la PIO y la hiperglucemia en nuestro estudio; sin embargo, el mecanismo detrás de cómo la hiperglucemia afecta a la PIO no está claro. El gradiente osmótico inducido por el aumento de la glucosa en sangre, con un consecuente cambio de líquido hacia el espacio intraocular, y la disfunción autonómica se ha propuesto como los factores que explican la asociación, tal como lo señala Abegão et al. (2016). Así mismo, en el estudio de K Imai et al. (2012) entre los factores del SM que se asociaron con PIO, se incluyó la glucosa plasmática en ayunas, mientras que Gilbert y col (2012) reportaron que la asociación entre diabetes mellitus y la mayor parte de los subtipos de glaucoma fue estadísticamente no significativa, excepto para el GNV.

En el estudio se evidencio que el paciente con triglicéridos alto tiene un riesgo de 4,5 veces más de desarrollar PIO que un sujeto con triglicéridos normales y con hiperglicemia el riesgo es de 4,2 veces más que el sujeto euglucemico.

Otros investigadores como Cohen et, al (2016) han reportado la relación entre obesidad y PIO, refieren que probablemente se deben al exceso de tejido graso intraorbital, a un aumento en la viscosidad de la sangre y a un aumento en la presión venosa episcleral, que en consecuencia, disminuye la facilidad de salida. De igual forma, Tenorio et. Al (2014) han encontrado relación entre hipertensión arterial - PIO y sugirieron que las causas de una PIO alta en la hipertensión sistémica son la producción excesiva de humor acuoso y el aumento de las presiones arteriales venosas y ciliares epiesclerales.

Tales resultados estimulan a seguir investigando sobre este tema ya que además de aporta datos sobre factores relacionados con la PIO, pudieran abrirse otras perspectivas terapéuticas para el control de la PIO.

Conclusiones

Luego del análisis de los resultados y de la discusión planteada, se concluye que:

Es alto el porcentaje de hipertensión ocular en pacientes con síndrome metabólico.

Entre los componentes del síndrome metabólico, los triglicéridos altos y la hiperglicemia se asociaron significativamente con la hipertensión ocular.

Así mismo, estos 2 factores mostraron una correlación directamente proporcional con la presión intraocular, es decir que en la medida que aumentan los niveles de dichos factores se incrementa la presión intraocular.

Los pacientes con triglicéridos altos tienen un riesgo de 4,5 y con hiperglicemia de 4,2 veces más de desarrollar hipertensión ocular que un sujeto con triglicéridos y glicemia normales.

Referencias

Abegão P., Willekens K., Van K., Shibesh A., Molenberghs G., Vandewalle E., Stalmans I. (2016). Ocular blood flow in glaucoma - the Leuven Eye Study. *Acta Ophthalmol. 2016;* 94, 592–598.

Bermúdez Valmore, Y. Luti, D. Aparício (2013). Prevalencia de Síndrome Metabólico en la población adulta del municipio Maracaibo, Estado Zulia. VIII Congreso Venezolano de Hipertensión. Revista Latinoamericana de Hipertensión, 2013; 4 (1): 2-4.

Brown K.E., Congdon N.G. (2006). Corneal structure and biomechanics: impact on the diagnosis and management of glaucoma. *Curr. Opin. Ophthalmol*. 2006; 17:338 -343.

Cohen E., Kramer M., Shochat T., Goldberg E., Garty M., Krause I. (2016). Relación entre el índice de masa corporal y la presión intraocular en hombres y mujeres: un estudio basado en la población. *J Glaucoma.* 2016 de mayo; 25 (5): e509-13. doi: 10.1097 / IJG.0000000000000374.

Cook C., Foster P. (2012). Epidemiology of glaucoma: what's new? *Can J Ophthalmol*. 2012; 47(3):223-6. doi: 10.1016/j.jcjo.2012.02.003.

Doughty M.J., Zaman M.L. (2002). Human corneal thickness and its impact on intraocular pressure measures: a review and metaanalysis approach. *Surv Ophthalmol* 2002; 44: 367408.

Ford E.S., Giles W.H., Dietz W.H. (2002). Prevalence of the metabolic syndrome among US adults: findings from the third National Health and Nutrition Examination Survey. *JAMA*. 2002; 287: 356-359.

Gilbert M., García M., Ruiz N., Gil Félix, García A., Casab Homero. (2012). Estudio epidemiológico de glaucoma en población mexicana. *Rev Mex Oftalmol*, 2012; 84(2):86-90.

K. Imai, M. Hamaguchi, K. Mori, N. Takeda, M. Fukui, T. Kato, Y. Kawahito, S. Kinoshita and T. Kojima. (2012). Metabolic syndrome as a risk factor for high-ocular tension, *International Journal of Obesity*, 2012; 34 (32): 1209–1217

Ko Fang, Michael Boland, Priya Gupta, Shekhar K., Susan Vitale, Eliseo Di Zhao, David S. Diabetes, Triglyceride Levels, and Other Risk (2016). Factors for Glaucoma in the National Health and Nutrition Examination Survey 2005-2008. *Invest. Ophthalmol. Vis. Sci. 2016*; 57, 2152–2157.

Núñez Javier (2014). "Presión intraocular y espesor corneal central en pacientes diabéticos del servicio de Oftalmología del Hospital Universitario de Maracaibo". Trabajo Especial de Grado Universidad del Zulia. Facultad de Medicina. División de Estudios para Graduados. Venezuela, 2014. 30 p.

Oh S.W., Lee S., Park C., Kim D.J. (2011). Elevated intraocular pressure is associated with insulin resistance and metabolic syndrome. *Diabetes Metab Res Rev* 2011; 21: 434–440.

Pertl L., Georg M., Andreas W., Martin W., Oliver K., Günther S., Florian P. (2017). Triglycerides and Open Angle Glaucoma – A Meta-analysis with meta-regression *Scientific Reports*; 2017 (7): *7829* | DOI:10.1038/s41598-017-08295-1

Rubio M., Moreno C., Cabrerizo L. (2004). Guías para el tratamiento de las dislipemias en el adulto: Adult Treatment Panel III (ATP-III) *Endocrinol Nutr* 2004;51:254-65

Siso F., Esche G., Limburg H., Grupo RACSS-Venezuela. (2005). Test Nacional de Catarata y Servi-cios Quirúrgicos "RACSS Rapid Assessmentof Cataract and Surgical Services": primera encuesta nacional. *Rev Oftalmol Venez.*2005;61(2):112–39

Tenorio G., Avila L., Ramírez J., .Henríquez C., Zamora D., García J., Izazola C. (2014). Cambios de la presión intraocular en pacientes con hipertensión arterial. *Revista Médica del Hospital General de México*, 2014; 77 (3): 101-107

Tham Y.C., Li X., Wong T.Y., Quigley H.A., Aung T., Cheng C.Y. (2014). Global prevalence of glaucoma and projections of glaucoma burden through 2040: a systematic review and meta-analysis. *Ophthalmology*. 2014; 121(11):2081-2090.

The IDF consensus worldwide definition of the metabolic syndrome. (2005). Brusells. Belgium. Disponible en: https://www.idf.org/.../consensus.../60-idfconsensus-worldwide-d.

Third report of the National Cholesterol Education Program (NCEP) Expert Panel on the detection, evaluation, and treatment of high blood cholesterol in adults (Adult Treatment panel III). Executive summary. NIH Publication 01-3670; May 2001.

Tielchs J.M., Katz J., Sommer A., Quigley H.A., Javitt J.C. (1994). Risk of open angle glaucoma. *Arch Ophthalmol*, 1994; 112:69-73.

Touboul D., Roberts .C, Kérautret J., Garra C., Maurice-Tison S., Saubusse E. (2008). Correlations between corneal hysteresis, intraocular pressure, and corneal central pachymetry. *J Cataract Refract Surg* 2008; 34:616 - 622.

The problem of eco-dependent states in the area of public health (on the example of dental health)

Anna Vladimirovna Gordeeva/ 0000-0001-6948-3950*
Irina Dmitrievna Sitdikova /0000-0002-3699-5359*
Irina Alexandrovna Galimova /0000-0003-4887-0358**
Olga Anatolievna Gurevskaia/ 0000-0003-3378-7973**
Irina Nikolaevna Usmanova/ 0000-0001-7876-6020**
Violetta Robertovna Detochkina /0000-0002-1886-6975***

ABSTRACT

An integrated approach to the examination, differentiated treatment and rehabilitation of patients with various forms of recurrent aphthae of the oral cavity (K12.0) allows increasing the effectiveness of treatment, restoring the microbial landscape characteristic of a healthy oral cavity, increasing the period of remission of the disease, and reducing the rate of relapses and the severity of clinical manifestations.The clinical manifestations of chronic recurrent aphthae of the oral cavity in residents of regions with adverse environmental factors, including those with a developed petrochemical industry, using the example of the city of Ufa, are characterized by certain manifestations, which contributes not only to a slowdown in the process of recovery and regenerative processes in the area of pathological elements on the oral mucosa. The microbiological method using modern test systems found an extremely diverse state of the microbiota of the oral cavity and its species diversity on the surface of aphthae in patients with gastrointestinal pathologies. Using the microbiological method, we determined the triggers and established the role of various microorganisms - enterococci, staphylococci, streptococci, yeast-like fungi of the genus *Candida* (*C. albicans*) and obligate anaerobes in exacerbating the clinical course of recurrent aphthae of the oral cavity. The data obtained can serve as an indication for the development of an integrated approach to examination, the development of differentiated treatment regimens and rehabilitation of patients with pathology of the gastrointestinal tract and various forms of recurrent aphthae of the oral cavity (K12.0), which will not only increase the effectiveness of local and general treatment but also restore the microbial landscape characteristic of a healthy oral cavity, increase the period of remission, reduce the rate of relapses and the severity of clinical manifestations in this category of people.

KEYWORDS: eco-dependent conditions, recurrent aphthae of the oral cavity, mucous membrane, microbial contamination, gastrointestinal pathology

** Kazan Federal University, 420008, Kazan, 18 Kremlyovskaya str.* annagordeeva92@mail.ru
*** Federal State Budgetary Establishment of Higher Education "Bashkir State Medical University" of the Ministry of Health of the Russian Federation, 450008, Republic of Bashkortostan, Ufa,.47 Zaki Validi str.*
**** Non-profit joint-stock company "Medical University of Astana", Nur-Sultan, Kazakhstan, Beibitshilik str., 49a.*

Recibido: 05/11/2019 Aceptado: 29/11/2019

El problema de los estados eco dependientes en el ámbito de la salud pública (sobre el caso de salud oral)

RESUMEN

Un enfoque integrado para el examen, el tratamiento diferenciado y la rehabilitación de pacientes con diversas formas de aftas recurrentes de la cavidad oral (K12.0) permite aumentar la efectividad del tratamiento, restaurando el paisaje microbiano característico de una cavidad oral sana, aumentando el período de remisión de la enfermedad y reducción de la tasa de recaídas y la gravedad de las manifestaciones clínicas. Las manifestaciones clínicas de aftas recurrentes crónicas de la cavidad oral en residentes de regiones con factores ambientales adversos, incluidos aquellos con una industria petroquímica desarrollada, utilizando el ejemplo de la ciudad de Ufa, se caracteriza por ciertas manifestaciones, lo que contribuye no solo a una desaceleración en el proceso de recuperación y procesos regenerativos en el área de elementos patológicos en la mucosa oral. El método microbiológico que utiliza sistemas de prueba modernos encontró un estado extremadamente diverso de la microbiota de la cavidad oral y su diversidad de especies en la superficie de las aftas en pacientes con patologías gastrointestinales. Utilizando el método microbiológico, determinamos los desencadenantes y establecimos el papel de varios microorganismos: enterococos, estafilococos, estreptococos, hongos similares a levaduras del género Candida (C. albicans) y anaerobios obligados a exacerbar el curso clínico de las aftas recurrentes de la boca. Los datos obtenidos pueden servir como una indicación para el desarrollo de un enfoque integrado para el examen, el desarrollo de regímenes de tratamiento diferenciados y la rehabilitación de pacientes con patología del tracto gastrointestinal y diversas formas de aftas recurrentes de la cavidad oral (K12.0), lo que no solo aumentará la efectividad del tratamiento local y general, sino que también restaurará el paisaje microbiano característico de una cavidad oral sana, aumentará el período de remisión, reducirá la tasa de recaídas y la gravedad de las manifestaciones clínicas en esta categoría de personas.

PALABRAS CLAVE: afecciones ecodependientes, aftas recurrentes de la cavidad oral, membrana mucosa, contaminación microbiana, patología gastrointestinal.

Introduction

Chronic diseases of the gastrointestinal tract in the modern aspect are a serious problem for modern medicine in general, due to their steady growth on average up to 65% of cases, as a number of authors state. Currently, many researchers pay great attention to studying the mechanisms of the onset and progression of diseases of the gastrointestinal tract with manifestations on the oral mucosa, due to the fact that the oral cavity is the initial part of the digestive tract and the pathological processes that occur in this case most often have

manifestations of a specific nature (Lesions of the oral mucosa, 2017; Usmanova, 2016; Clemente et al., 2012).

Manifestations of the pathology of the oral mucosa, regardless of the presence of somatic diseases, is one of the most difficult and important problems of modern dentistry, which requires a more thorough examination using additional research methods. The reasons for the development of the pathology of the mucous membrane also have their own characteristic features depending on the presence of a complex of influence of various etiological factors, the region of residence, as well as on the relationship of pathogenetic factors with somatic status and chronic stress (Usmanova et al., 2015; Chim, 2012). In this regard, patients with gastrointestinal pathologies and recurrent aphthae of the oral cavity who seek specialized help, actively need not only a thorough comprehensive somatic examination by related specialists - gastroenterologists, therapists, immunologists, as well as a set of examinations by dentists-physicians (Lesions of the oral mucosa, 2017; Round et Mazmanian, 2009).

The prevalence of recurrent aphthae of the oral cavity in the modern aspect does not depend on any age criteria and gender differences. Nevertheless, cases of manifestation of a severe course of recurrent aphthous stomatitis with certain clinical symptoms are very common in dental practice (Lesions of the oral mucosa, 2017; Usmanova et al., 2015; Round et Mazmanian, 2009).

The analysis of the data obtained by flow cytometry allowed many researchers to note the accumulation of IgM and IgG, an increase in the integral protein ICAM-1, as well as the development of macrophage-lymphocytic tissue infiltration. In samples of oral fluid and in blood serum, non-specific protection factors are violated in the form of changes in the composition of subpopulations and enzymatic activity of lymphocytes, an increase in the number of cytotoxic lymphocytes (CD8+), and a decrease in the number of T-helper cells (CD4+) in peripheral blood. In 10-12% of cases in patients, the clinical manifestations of recurrent aphthous stomatitis take on characteristic features in the form of a permanent course, which is typical for Setton aphids in Behcet's disease, while 40% of cases of analysis of the data of additional research methods have HLA - B51 system antigens found in the blood (Galizina, 2014; Jünemann et al., 2012; Clemente et. al., 2012).

The state of the microbial biocenosis of the oral cavity in patients with recurrent aphthae of the oral cavity is directly dependent on the influence of various negative factors,

which determines the interconnected triggers for the development and maintenance of the pathological process not only on the oral mucosa but also in the body in general (Lesions of the oral mucosa, 2017; Usmanova, 2016; Round et Mazmanian, 2009; Chim, 2012).

Thus, patients with recurring aphthae of the oral cavity on the background of chronic gastrointestinal diseases are recommended to use clinical and laboratory methods to plan common approaches to the management of local and general treatment, which determined the relevance and objective of our study.

1. Methods

To solve the tasks, a comprehensive examination of 250 young people (average age - 32.2±1.4 years) with diseases of the gastrointestinal tract was carried out. Using the open sampling method, we distinguished two clinical groups of patients comparable by sex and age. The main group included 90 patients with diseases of the gastrointestinal tract with chronic gastritis and duodenitis, chronic pancreatitis and cholecystitis with biliary dyskinesia with the presence of manifestations of recurrent aphthae of the oral cavity. The control group consisted of 35 patients with diseases of the gastrointestinal tract without pathology of the oral mucosa.

Dental examinations conducted in this category of persons included the recording of complaints, anamnesis vitae and anamnesis morbi, an assessment of the intensity of the manifestation of a pain symptom over time, as well as the severity and duration of local symptoms in the oral cavity. The diagnosis of the dental status of the examined patients used the STEPS approach that includes WHO recommendations, 2013.

The scheme of a comprehensive examination by gastroenterologists, therapists, and allergists consisted of a survey, analysis of data obtained by ultrasound of the internal organs, complete blood count and blood chemistry, and immunogram data (Vlasova et al, 2000).

To study the species composition of microbiota from the surface of the aphthous element (aphthous, ulcers) in patients, clinical material was collected from the surface of the lesion elements. Subsequently, to isolate facultative anaerobic microorganisms, the material was inoculated on special HiCrome differential diagnostic media for their further cultivation and subsequent identification of microorganisms. A part of the obtained clinical raw material from the surface of the aphthous element (plaque) was tested on a PCR analyzer. PCR testing

of the clinical material was carried out in real time using the Dentoscreen test system for 6 types of periodontopathogens: Porphyromonas gingivalis, Treponema denticola, Aggregatibacter actinomycetemcomitans, Tannerella forsythensis, P. endodentalis, Fusobacterium nucleatum, Prevotella intermedia. The advantage of using PCR diagnostics is the ability to detect not only viable bacteria but also the identification of DNA fragments of the studied microorganisms in the resulting clinical material. To determine the quantitative secretory immunoglobulin A, the IgA sector-IFA-BEST kit was used using the enzyme-linked immunosorbent assay. The concentration of lysozyme in the samples of the oral fluid was studied using the agar gel diffusion method (Vlasova, 2000; Usmanova et al., 2015; Clemente et al., 2012).

Statistical processing of the obtained data was carried out on a personal computer. The level of significance was $p \leq 0.05$.

2. Results

To achieve our goals, we carried out a comprehensive dental examination of 250 patients with diseases of the gastrointestinal tract of the therapeutic department of the Clinic of FSBEI HE BSMU in the city of Ufa, and in the course of a targeted sampling we selected 90 men and women, aged 24 to 45 years, with chronic gastritis and duodenitis (49 patients), with chronic pancreatitis and cholecystitis and with biliary dyskinesia (51 patients).

During a comprehensive dental examination of patients with diseases of the gastrointestinal tract, recurrent aphthae of the oral cavity were diagnosed in an average of 37% of cases.

Painful aphthae with a corolla of hyperemia and covered with dense yellowish fibrinous plaque irremovable during scraping were more often located on the mucous membrane of the transitional fold of the upper or lower jaw in 28.9% of cases; more round aphthae were located on the transitional fold of the mucous membrane of the upper or lower lip in 21.1%, on the lateral surface or on the tip of the tongue in 18.9%, on the mucous membrane of the cheeks in 5.5% and a mixed form in 25.6% of cases.

The mucous membrane of the oral cavity was brighter in color, the aphthae were oval in shape, up to 3 mm in size, with clear boundaries and a rim of hyperemia, covered with a fibrinous coating, with sharp pain on palpation. The duration of aft existence is no more than

10-14 days, the periods of remission are also different and can vary on average from 1-2 to 6-12 months.

When examining the organs of the oral cavity, we studied the condition of the vermilion border and the corners of the mouth with a focus on their color, size, and the presence of pathological elements. Most often, patients complained of dryness and non-aesthetic appearance of the vermilion border and corners of the mouth. 58.8±0.33% of the examined were diagnosed with meteorological cheilitis (dry vermilion border, flakes, and cracks), 29.6 ± 0.66% exfoliative cheilitis (dry form) - grayish flakes tightly attached in the center to red border and lagging along the edges, easily removable, with exposure of a bright red surface. Only 11.7±0.15% of patients with a clinical dental examination had no pathological changes in their vermilion border. Recurrent herpes was detected on average in 33.8±0.08% of cases. Desquamative glossitis was diagnosed in 54.4±1.4%, diamond-shaped glossitis was diagnosed in 33±1.2% of the examined individuals.

Patients with chronic gastritis were in normal condition, had their skin clean, regional lymph nodes not palpated, and the face configuration not changed. Clinical manifestations of recurrent aphthae of the oral cavity on the oral mucosa are characterized by the appearance of painful oval secondary elements - aphthae in the amount of 0.1 to 0.8 mm, covered with fibrinous yellowish-white bloom in an average amount of 1 to 3, surrounded by a clear periphery of the aphtha whisk of hyperemia, or inflammatory infiltration is observed. The main complaints during the survey of patients with chronic gastritis and duodenitis are heaviness and pain in the epigastric region, impaired taste perception in 69% of cases, respectively.

In the oral cavity, the mucous membrane is hyperemic in the area of aphthae in 37% of cases, with a whitish-gray plaque on the dorsal surface of the tongue - 100%, hypertrophic changes in the fungiform papillae of the tongue - 92%, as well as desquamative glossitis in 16.2% of cases.

Patients with chronic duodenitis, chronic pancreatitis, and cholecystitis with biliary dyskinesia were in satisfactory general condition. Most often, patients complain of burning and soreness in the tongue, aggravated in the evening, or bitterness in the mouth - 33% of cases. Objectively, atrophy of the filiform papilla and the presence of yellow plaque on the dorsal surface of the tongue, hyperemic mucous vestibule and the oral cavity proper are

determined in 83% of cases, tongue edema, dryness and taste disturbance are observed on average in 33% of examinations.

100% of patients with chronic recurrent aphthae had representatives of *Enterococcus spp.*, *Staphylococcus spp.*, *Streptococcus spp.* revealed. 45.6% of the examined patients had microorganisms not characteristic of the oral cavity, both aerobic and anaerobic - *Escherichia spp.*, *Klebsiella spp*, *Bacteroides spp*. In 20% of cases in individuals with recurrent aphthae, yeast-like fungi of the genus *Candida* (*C. albicans*) in the amount of 10^1-10^2 CFU/ml were detected, in 39.2% of cases a quantitative increase in yeast-like fungi of the genus *Candida* (*C. albicans*) from 10^3 to 10^4 CFU/ml was observed. In 40.8% of cases, an increase was from 10^3 to 10^5 CFU/ml ($p \leq 0.05$). The number of yeast-like fungi in the oral cavity among the young people with recurrent aphthae of the oral cavity examined by us ranged from lg 1.0 CFU/ml to lg 5.0 CFU/ml.

Microscopic examination of smears from various parts of the oral cavity most often found yeast-like fungi of the genus *Candida* (*C. albicans*) in smears from the tongue in 55% of cases, mucous membranes of the cheeks and gums in an average of 22% of cases.

The results of PCR diagnostics in patients with recurrent aphthae of the oral cavity in 64% of cases showed the average prevalence of obligate-anaerobic microorganisms in the affected areas - *Porphyromonas gingivalis*, *Treponema denticola*, *Aggregatibacter actinomycetemcomitans*, *Tannerella forsythensis*, *Fusobacterium nucleatum*, *Prevotella intermedia.*

3. Discussion

During the healing period of aphthae, a whitish, opalescent area remains on the mucous membrane in the area of their location, most often disappearing without a trace within 7-10 days, which indicates a fibrinous form according to the ICD-X classification – small aphthae, of moderate severity.

However, when interviewing patients, the most painful single or multiple aphthae were located in transitional folds and on the lateral surface of the tongue. In the oral cavity, this was clinically expressed in increased tissue infiltration, hyperemia in the area of aphtha location.

Patients with chronic gastritis were in normal condition, had their skin clean, regional lymph nodes not palpated, and the face configuration not changed. Clinical manifestations

of recurrent aphthae of the oral cavity on the oral mucosa are characterized by the appearance of painful oval secondary elements - aphthae in the amount of 0.1 to 0.8 mm, covered with fibrinous yellowish-white bloom in an average amount of 1 to 3, surrounded by a clear periphery of the aphtha whisk of hyperemia, or inflammatory infiltration is observed. The main complaints during the survey of patients with chronic gastritis and duodenitis are heaviness and pain in the epigastric region, impaired taste perception in 69% of cases, respectively.

The average concentrations of secretory immunoglobulin A and lysozyme in oral samples in the group of patients with chronic recurrent aphthae of the oral cavity against diseases of the gastrointestinal tract were 0.115 ± 0.001 g/l and 0.146 ± 0.001 μg/ml, respectively, which is significantly lower than normal values.

4. Summary

36% of patients with diagnosed somatic pathology have recurrent aphthae of the oral cavity detected.

Identification of individual characteristics of the state of the oral microbiome in chronic recurrent aphthae of the oral cavity includes a combination of microbiological studies and PCR diagnostics.

The results of an in-depth study of the state of the oral microbiome showed frequent detection of bacteria of the genus enterococci, streptococci and yeast-like fungi of the genus *Candida* (*C. albicans*), *Porphyromonas gingivalis, Treponema denticola, Aggregatibacter actinomycetemcomitans, Tannerella forsythensis, Fusobacterium nucleatum, Prevotella intermedia.*

Samples of the oral fluid showed a deficiency of humoral factors of local immunity.

Conclusions

Thus, 36% of patients with diagnosed somatic pathology have recurrent aphthae of the oral cavity detected, which requires the development of modern methods of therapeutic and preventive measures in this category of people.

Acknowledgments

The work is performed according to the Russian Government Program of Competitive Growth of Kazan Federal University.

References

Chim Y.J. (2012). Effect of sodium lauryl sulfate of recurrent aphthous stomatitis: a randomized controlled clinical trial / Y.J. Chim, J.H. Choi, H.J. Ahn, J.S. Kwon // OralDis. 2012 Oct. 18(7):655-609.

Clemente J.C., Ursell L.K., Parfrey L.W., Knight R. (2012). The Impact of the Gut microbiota on Human Health. An Integrative View. Cell. 2012; 148: 1258–1270.

Galizina O.A. (2014). The main aspects of the occurrence, clinical manifestation, treatment, and prevention of chronic recurrent aphthous stomatitis / O.A. Galizina // Russian Dental Journal. - 2014. - No. 6. - P. 39-42.

Jünemann S, Prior K, Szczepanowski R, Harks I, Ehmke B, Goesmann A, et al. (2012). Bacterial community shift in treated periodontitis patients revealed by ion torrent 16S rRNA gene amplicon sequencing. PloS One. 2012; 7 (8): e41606

Lesions of the oral mucosa in gastrointestinal diseases / Gerasimova L.P., Daurova F.Iu., Usmanova I.N., Kabirova M.F., Vaits S.V., Makeeva M.K. // Textbook / Moscow, 2017. P. 232.

Round J.L., Mazmanian S.K. (2009). The gut microbiota shapes intestinal immune responses during health and disease. Nat. Rev. Immunol. 2009; 9: 313–323

Usmanova I.N. (2016). Optimization of the diagnosis, treatment, and prevention of inflammatory diseases of periodontal and oral mucosa in young people / Author's abstract for the degree of Ph.D. Medicine / Bashkir State Medical University. Ufa, 2016. P. 47.

Usmanova I.N., Tuigunov M.M., Gerasimova L.P., Kabirova M.F., Gubaidullin A.G., Gerasimova A.A., Khusnarizanova R.F. (2015). Role of conditionally pathogenic and pathogenic microflora of oral cavity in the development of inflammatory diseases of the periodontal and oral mucosa (literature review) // Bulletin of the South Ural State University. Series: Education, healthcare, physical education. 2015. Vol. 15. No. 2. P. 37-44.

Vlasova L.F., Nepomniashchikh L.M., Reznikova E.O. (2000). Cytological analysis of the surface layers of the epithelium of the oral mucosa // Bull. expert. biology. - 2000. - No. 1. - P. 113-116.

Análisis de la velocidad de los plasmones en la interfaz dieléctrico – metal

Karina Silvana Gutiérrez Valverde *
Carlos AlbertoRíos Campos **
NemesioSantamaría Baldera ***
Ronald OmarEstela Urbina ****

RESUMEN

Se analizó la dependencia de la velocidad de los plasmones en la interface dieléctrico – metal. Se calculó la frecuencia espacial resonante para la interface dieléctrico -metal – dieléctrico con capa metálica de plata y oro de diferentes espesores desde 50 nm hasta 2 nm, obteniéndose que, el modo plasmónico simétrico débilmente cambia y el modo plasmónico anti simétrico cambia significativamente. La velocidad de fase de los plasmones superficiales en el modo antisimétrico depende fuertemente del espesor de la capa metálica.

PALABRAS CLAVE: Plasmones superficiales, interface dieléctrico – metal, frecuencia espacial

*Docente universitaria. Jefe del Laboratorio de Física y Termodinámica. Universidad Nacional de Frontera. Licenciada en Física. E-mail: kgutierrez@unfs.edu.pe
**Docente Investigador, Universidad Politécnica Amazónica. Dr. en Gestión Universitaria.
***Docente auxiliar. Jefe de Bienestar Universitario. Universidad Nacional Intercultural Fabiola Salazar Leguía de Bagua. Licenciado en Física.
****Docente Asociado. Jefe de Laboratorio de Física. Universidad Nacional Intercultural Fabiola Salazar Leguía de Bagua.

Recibido: 01/11/2019 Aceptado: 29/11/2019

Plasmon velocity analysis at the dielectric - metal interface

ABSTRACT

The speed dependence of plasmons on the dielectric-metal interface was analyzed. The resonant spatial frequency for the dielectric -metal-dielectric interface with silver and gold metallic layer of different thicknesses from 50 nm to 2 nm was calculated, obtaining that, the symmetrical plasmonic mode weakly changes and the anti-symmetrical plasmonic mode changes significantly. The phase velocity of the surface plasmons in the antisymmetric mode depends strongly on the thickness of the metal layer.
KEYWORDS: Surface plasmons, dielectric interface - metal, spatial frequency

Introducción

La nanoplasmónica se define como el estudio de las excitaciones en superficies metálicas localizadas en nanoestructuras (Rodríguez-Mijangos & García-Llamas, 2018).

La búsqueda de nuevos métodos de síntesis de nanopartículas metálicas es una necesidad reciente debido a que se espera mejorar la eficiencia de los ya existentes (Zea, Talavera, Arenas, Pacheco, Osorio & Vera, 2019).

Un plasmón es un cuanto de oscilación del plasma (estado de la materia). El plasmón es la cuasipartícula resultado de la cuantización de las oscilaciones del plasma, de la misma forma que un fotón o un fonón son cuantizaciones de ondas electromagnéticas y mecánicas. Por tanto, los plasmones son oscilaciones de la densidad del gas de Fermi (gas de electrones libres), usualmente a frecuencias ópticas. También pueden interactuar con un fotón para crear una tercera cuasipartícula llamada polaritón de plasma.

Como los plasmones son la cuantización clásica de las oscilaciones del plasma, la mayoría de sus propiedades pueden ser derivadas de las ecuaciones de Maxwell (Abrikosov, 1987) (Kittel, 1987).

Los plasmones son explicados clásicamente usando el modelo de Drude de los metales. El metal es tratado como un cristal tridimensional de iones positivos, junto a un gas de electrones deslocalizado que se mueve en esta red de iones que forman un potencial periódico.

En la mayoría de los metales, la frecuencia de plasma está en el ultravioleta, haciéndolos brillantes (reflectivos) en el rango de la luz visible. Algunos metales, como el cobre o el oro, presentan transiciones electrónicas de bandas en el rango visible, por lo cual algunas longitudes de onda del visible (colores) son absorbidas, emitiendo su color característico. En semiconductores, la frecuencia de plasma de los electrones en la banda de valencia está usualmente en lo profundo del ultravioleta (Zavitaev, 2003), razón por la cual son también materiales reflectivos.

Usualmente, la energía del pasmón puede ser estimada en el modelo del electrón libre como

$$E_p = \hbar \sqrt{\frac{n_e e^2}{m_e \varepsilon_0}}$$

Donde n_e es la densidad de electrones de conducción, e es la carga elemental del electrón, me es la masa del electrón y ε_o es la permitividad del espacio libre.

Los plasmones de superficie son aquellos plasmones que están confinados a las superficies y que forman un polaritón cuando interactúan con la luz. Ocurren en la interfaz entre un dieléctrico y un metal. Permiten explicar las anomalías en la difracción de una red de difracción metálica (Anomalía de Wood) y también son útiles en la espectroscopia Raman de superficie entre otras aplicaciones. La resonancia de plasmones superficiales es utilizado en bioquímica para el estudio de mecanismos y la cinética de los enlaces entre los ligados y los receptores (i.e. el enlace entre un sustrato y una enzima).

Los plasmones de superficie son ondas electromagnéticas a frecuencias ópticas ligadas al interfaz entre un dieléctrico y un metal que muestran un

confinamiento de campo en regiones sublambda con alta intensidad de campo eléctrico. Los plasmones superficiales se usan en sensores muy sensibles por la elevada concentración de campo eléctrico en el interfaz metal-dieléctrico (Camacho, 2018).

Los plasmones son considerados como medios de transmisión de información en microprocesadores y chips de computadoras ya que pueden alcanzar altas frecuencias (de hasta 100 THz, mientras que los cables convencionales alcanzan las decenas de GHz) (Lewotsky, 2007)

En el presente trabajo se hará un estudio detallado de la dependencia de la velocidad de los plasmones superficiales con el espesor de la película delgada metálica en la interfaz dieléctrico-metal.

1. Función dieléctrica en un gas de electrones libres

Al analizar las propiedades ópticas de los metales siguiendo el modelo de Drude, encontramos que este modelo describe la respuesta de un metal cuando está en presencia de la radiación electromagnética, y está basado en la aproximación del electrón libre. Para analizar las propiedades ópticas es necesario conocer la función dieléctrica. Sobre un gran rango del espectro electromagnético, las propiedades ópticas de los metales pueden ser explicadas por el modelo de plasma, tomando en cuenta que el plasma es una colección de partículas cargadas que presentan una dinámica colectiva, donde los electrones libres se comportan como un gas con un numero de electrones por unidad de volumen, presente sobre un fondo de núcleos positivos que crean carga neta cero desde el punto de vista macroscópico. Los electrones oscilan aleatoriamente en estado natural, pero cuando se aplica un campo eléctrico, los electrones en respuesta son estimulados por el campo externo y conducidos en el interior del material, creando una polarización interna dependiente de la dirección del campo que se está aplicando, y generando una reorganización de las cargas.

1.1. Plasmones en metales

La interacción de la luz visible con los electrones de conducción en los metales es de importancia fundamental. La excitación colectiva de este gas de electrones en relación con la red cristalina del metal se le denomina plasmón. Dependiendo de las condiciones de frontera el plasmón puede clasificar en tres tipos: Plasmón en bulto (o plasmón de volumen), plasmón de superficie (o plasmón superficial) y plasmón de nanopartícula (o plasmón localizado). Brevemente se explicará las características más resaltantes de estas clases de plasmones.

1.2. Modelo de Drude – Sommerfeld

Las propiedades ópticas de metales pueden ser descriptas por una función dieléctrica compleja que depende la frecuencia de la luz, y están determinadas principalmente por la gran movilidad que tienen los electrones de conducción dentro del material y por las transiciones interbanda que tienen lugar cuando la energía de los fotones supera el gap de energía del metal.

Lo importante de las ecuaciones (1.2) está en el significado de la parte real, y la parte imaginaria, de la función dieléctrica. La parte real y la parte imaginaria de la función dieléctrica no son independientes entre sí, sino que están conectadas por las relaciones integrales de Kramers-Kronig. Esta condición impone una restricción a los valores que pueden tomar, más aún, si se conoce una de ellas en un rango de frecuencias puede conocerse la otra por integración. Un valor no nulo de la parte imaginaria de se manifiesta por la absorción de energía electromagnética por parte del medio, y los valores de la parte real están relacionados con la velocidad de propagación de la onda en el medio.

1.3. Excitación de ondas de plasma

La energía de los plasmones es grande, por lo que éstos no se excitan al calentarse. La excitación de los plasmones la efectúan los electrones rápidos (del orden de varios kilovoltios) que pasan a través de películas delgadas. Cuando los electrones rápidos pasan a través de películas de berilio, magnesio o aluminio, pierden energía, según sea el número de plasmones que hayan excitado. La

frecuencia de plasma que se observa coincide bien con la calculada teniendo en cuenta los electrones de valencia (dos en el Be y Mg y tres en el Al). En algunos metales y no metales (C, Si, Ge, ...) los electrones excitan un plasmón cada uno. En el carbono, silicio y germanio la frecuencia de plasma también se determina por los electrones de valencia (cuatro en cada átomo). En los metales Cu, Ag, Au y otros muchos de transición, en las oscilaciones de plasma, además de los de valencia, participan otros electrones.

1.4. Plasmones superficiales en la interface metal – dieléctrico

Los plasmones superficiales fueron predichos en 1957 por Rufus Ritchie (Ritchie, 1957), y se originan a partir de la redistribución de carga electrónica en la superficie, producida por una perturbación externa, de un modo análogo al caso de los Plasmones de volumen. Como esta redistribución de carga se produce en la superficie, la onda se propaga sobre la misma, y por lo tanto se trata también de una onda longitudinal. En realidad, la carga superficial está distribuida en una región finita sobre y por debajo de la superficie. De acuerdo al modelo de electrones libres (Pines, 1963), para un mismo metal, la frecuencia de estos Plasmones está relacionada con la frecuencia de los plasmones de volumen, de la siguiente forma:

$$\omega_{PS} = \frac{\omega_{pl}}{\sqrt{2}}$$

Estas frecuencias generalmente están en el rango del visible y del infrarrojo próximo y pueden ser excitadas usando fotones, quienes se acoplan con los Plasmones de superficie dando origen a los llamados polaritones. La superficie se vuelve entonces una especie de canal donde viaja la onda lumínica de una forma muy similar a cómo funcionan las guías de ondas y fibras ópticas.

2. Metodología

2.1. Objeto de estudio

Interfaz dieléctrico -metal - dieléctrico

2.2. Métodos y Técnicas

Se realizó un estudio detallado de los plasmones de volumen en los conductores y de los plasmones superficiales en las interfaces metal – dieléctrico; se resolverá las ecuaciones de Maxwell para determinar las componentes del campo electromagnético en la interface dieléctrico – metal – dieléctrico; utilizando métodos computacionales (EES) se calculará las frecuencias espaciales resonantes para la interface dieléctrico – metal – dieléctrico con capa metálica de plata y oro de diferentes espesores y se examinará la dependencia de la velocidad de los plasmones superficiales con el espesor de la capa delgada metálica en la interface dieléctrico – metal– dieléctrico.

2.3. Procedimiento

a) Adquisición y revisión de literatura actual sobre física de los materiales electrónicos a través de revistas científicas – tecnológicas: técnica individualizada. b) Contacto con avances científicos y tecnológicos en materia de los plasmones superficiales en interfaces metal - dieléctrico, a través de internet: técnica individualizada. c) Selección y organización de la información, procurando abarcar, a través de los métodos analíticos e inductivo – deductivo y aplicando las técnicas individualizada e interactiva. d) Análisis y evaluación de los diferentes métodos de aproximación para determinar la dependencia de la velocidad de los plasmones superficiales en la interface metal - dieléctrico: métodos analítico e inductivo – deductivo con una técnica individualizada. e) Discusión de la información analizada, comparando con otras fuentes sobre el tema que permita interpretar y describir el comportamiento de las variables estudiadas, las mismas que son coherentes y concordantes con el estudio de los plasmones superficiales en interfaces metal - dieléctrico. Con ello, se podrá valorar los resultados obtenidos: métodos analógico e inductivo – deductivo con las técnicas individualizada e interactiva: Conclusiones, utilizando el método sintético – inductivo. f) Organización y revisión de la información resultante: método sintético y técnica

interactiva. g) Redacción y sustentación del informe final: método mixto y técnica tipo clase magistral.

3. Resultados

En los últimos 20 años, la atención de los investigadores y profesionales se ha centrado en la posibilidad de la supresión de la emisión espontánea de átomos (moléculas) en un espacio no homogéneo en el que no hay modos de campo electromagnético en la frecuencia de transición atómica. Tales medios se llaman cristales fotónicos.

Pero no la supresión, sino, por el contrario, el aumento en la probabilidad de radiación de transición en un átomo. Esta posibilidad surge en átomos cerca de los cuerpos de nanoescala. Este interés no es solo académico, sino también práctico. Sin lugar a dudas, la capacidad de un átomo para emitir espontáneamente pulsos ópticos de duración no de 10-8 s, y muchas veces más cortos pueden resultar útiles para las aplicaciones prácticas.

3.1. Ondas electromagnéticas propias de espacios no homogéneos

Consideramos la cuestión de espacios no homogéneos, espacios que contienen cuerpos materiales. Nos interesarán las ondas superficiales, los llamados polaritones y polaritones-plasmones, que surgen en la superficie de los cuerpos con $\varepsilon<0$. Tal propiedad es poseída por el zafiro a una longitud de onda de aproximadamente 12 μm (Failache, 2002) (Schubert, 2000) y metales que reflejan la luz a frecuencias ópticas, véase, por ejemplo, [30]. Polaritones y polariton-plasmones son las ondas propias de la ecuación de onda. Polaritones y polariton-plasmones generalmente se consideran ondas compuestas en el sentido de que son movimientos colectivos de la energía electromagnética y de las excitaciones elementales del medio, fonones en zafiro y electrones de conducción en metales. Esta idea de ondas surge de una consideración microscópica de los procesos en el medio ambiente. Con la introducción de ε, la característica macroscópica del medio, los polaritones y los plasmones aparecen como las ondas electromagnéticas intrínsecas de un espacio no homogéneo.

Las ondas superficiales se propagan a lo largo de la interfaz entre dos medios. Sus amplitudes disminuyen exponencialmente con la distancia desde la interfaz.

3.2. Ondas superficiales en interfaces planas

Comenzamos considerando un plasmón en una interfaz de plano único entre medios con ε1 ≥ 1 y ε2 ‹ 0, con | ε2 |›ε1 [30]. En una interfaz de este tipo (los ejes x e y se encuentran en el plano de la interfaz, el eje z es perpendicular a este límite y dirigido hacia el medio con ε2 , z = 0 en la interfaz) puede propagarse la onda $\vec{E} = \vec{E}0\ e^{-k_z z}\ e^{i(k_x x + k_y y)}$ con número de onda kpl ›ω/c , el cual es igual a :

$$k_{pl} = \sqrt{k_x^2 + k_y^2} = \frac{\omega}{c}\sqrt{\frac{\varepsilon_1\ \varepsilon_2}{\varepsilon_1 + \varepsilon_2}} \qquad (3.1)$$

El campo de esta onda decrece exponencialmente con respecto a z al alejarse de la interfaz con decrementos kz = (ω/c)$(\varepsilon_1^2/|\varepsilon_1 + \varepsilon_2|)1/2$, kz = - (ω/c)$(\varepsilon_2^2/|\varepsilon_1 + \varepsilon_2|)1/2$.

Para la frecuencia elegida en la superficie de separación pueden existir no solamente ondas con número de ondas kpl , sino que también ondas con número de onda arbitrario $k = \sqrt{k_x^2 + k_y^2}$. Sin embargo, mientras mayor sea la diferencia entre k y kpl, será menor la amplitud de la onda superficial. Cuando k se aproxima a kpl la amplitud de la onda superficial crece fuertemente. Si consideramos la pérdida la amplitud resulta ser finita.

Examinemos el espacio que está ocupado por tres capas como se muestra en la fig.3.1. Las capas 1 y 3 son muestras con ε1, μ1 ≥ 1 y ε3, μ3 ≥ 1, la capa 2 es un buen metal reflectivo con ε2 < 0 y μ2 ≥ 1. Todas las ondas que se van a describir más abajo tienen la forma

$$H_{iy}(\mathbf{r},t) = H_{iy} e^{ik_{iz}z} e^{i(k_{ix}x - \omega t)}$$

$$E_{ix}(\mathbf{r},t) = \left(\frac{ck_{iz}}{\omega\varepsilon_j}\right) H_{iy} e^{ik_{iz}z} e^{i(k_{ix}x-\omega t)}\ , \quad E_{iz}(\mathbf{r},t) = -\left(\frac{ck_{ix}}{\omega\varepsilon_j}\right) H_{iy} e^{ik_{iz}z} e^{i(k_{ix}x-\omega t)} \qquad (3.2)$$

$$\text{Con} \quad k_{ix}^2 + k_{iz}^2 = \left(\frac{\omega}{c}\right)^2 \varepsilon_i \mu_i$$

En la región 1 hay una onda plana no homogénea (evanescente), como, por ejemplo, detrás de la superficie de la hipotenusa del prisma en un experimento con reflexión interna total. Ella se describe mediante las fórmulas (3.2) con índices i = 0, j = 1. Además de la onda incidente en la capa 1, se tiene la onda reflejada. Ella se describe con la formula (3.2) con índices i = 1, j = 1. Supondremos que la onda reflejada no influye en la fuente de la onda incidente, ya que disminuye exponencialmente hacia el lado de la fuente (en la dirección negativa de z), y sus repetidas reflexiones pueden ser despreciadas. En la capa 2, que por el momento se considera infinitamente extendido, hay una onda que penetra en la capa del metal, que se describe por las fórmulas (3.2) con índices i = 2, j = 2. Aplicamos las condiciones de contorno y como resultado obtenemos (e2 = -ε2):

k0x = k1x = k2x (3.3)

$$H_{1y}(\mathbf{r},t) = \left[\frac{1+(\frac{k_{2z}\varepsilon_1}{k_{0z}e_2})}{1-(\frac{k_{2z}\varepsilon_1}{k_{0z}e_2}}\right] H_{0y} e^{k_{0z}(z-d_1)} e^{i(k_{ix}x-\omega t)} \quad (3.4)$$

$$H_{2y}(\mathbf{r},t) = \left[\frac{2}{1-(\frac{k_{2z}\varepsilon_1}{k_{0z}e_2}}\right] H_{0y} e^{-k_{2z}(z-d_1)} e^{i(k_{ix}x-\omega t)} \quad (3.5)$$

Para (k2zε1/k0ze2) = 1, las amplitudes de las ondas reflejadas y penetradas se vuelven infinitamente grandes. Esto del infinito desaparece cuando se tienen en cuenta las pérdidas en el medio 2. Se observa el fenómeno de resonancia. Si calculamos la resonante k0x con la última igualdad (k2zε1/k0ze2) = 1, obtenemos:

$$k_{0x}^2 = (\omega/c)^2 \varepsilon_1 \varepsilon_2 \frac{\varepsilon_1\mu_2 - \varepsilon_2\mu_1}{(\varepsilon_1-\varepsilon_2)(\varepsilon_1+\varepsilon_2)} \quad (3.6)$$

Para μ1 = μ2 recibimos la fórmula $k_{0x}^{pl} = \frac{\omega}{c}\sqrt{\frac{\varepsilon_1\ \varepsilon_2}{\varepsilon_1+\varepsilon_2}}$ para el número de onda del plasmón superficial. De esta manera la fórmula (3.4) y (3.5) demuestran la presencia de la resonancia del plasmón superficial. Ahora examinemos la onda amortiguada en el espacio con una placa metálica plana limitada en la dirección z. Como se hizo anteriormente, tendremos en cuenta un metal con una buena reflectividad con ε2 < 0 y μ2 ≥ 1. La estructura del espacio y las representaciones son las mismas que en la fig. 3.1.

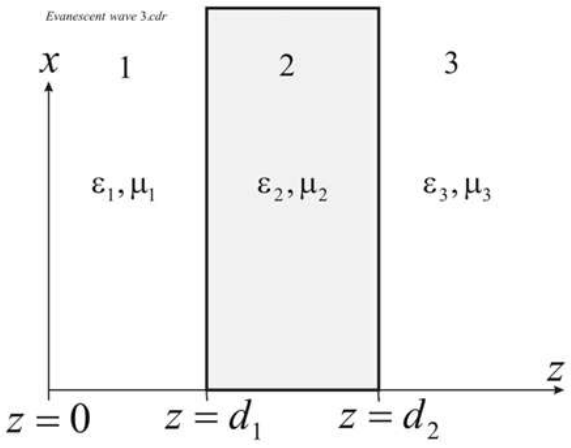

Figura 3.1

Ahora examinemos la onda amortiguada en el espacio con una placa metálica plana limitada en la dirección z. Como se hizo anteriormente, tendremos en cuenta un metal con una buena reflectividad con ε2 ‹ 0 y μ2 › 1. La estructura del espacio y las representaciones son las mismas que en la fig. 3.1. En este caso es necesario examinar las ondas del tipo (3.2): onda incidente con índice 0, onda reflejada en la frontera z= d1 con índice 1, onda transmitida en la capa de metal con índice 2, onda reflejada en la frontera z= d2 con índice r y onda transmitida en el espacio 3 con índice 3. Vamos a considerar que

$k_{0z}= i\kappa_{0z}$, $k_{1z}= -i\kappa_{0z}$, $k_{2z}= i\kappa_{2z}$, $k_{rz}=-i\kappa_{2z}$, $k_{3z}= i\kappa_{0z}$ (3.7)

Suponiendo que$\varepsilon_1 = \varepsilon_3$. Aplicando las condiciones de frontera en z= d1 y z= d2 y como resultado recibimos las ecuaciones:

$$-H_{1y}e^{\kappa_{0z}d_1} + H_{2y}e^{-k_{2z}d_1} + 0.H_{3y} + H_{ry}e^{k_{2z}d_1} = H_{0y}e^{-k_{0z}d_1}$$

$$H_{1y}e^{\kappa_{0z}d_1} - \frac{\kappa_{2z}\varepsilon_1}{\kappa_{0z}e_2}H_{2y}e^{-\kappa_{2z}d_1} + 0.H_{3y} + \frac{\kappa_{2z}\varepsilon_1}{\kappa_{0z}e_2}H_{ry}e^{\kappa_{2z}d_1} = H_{0y}e^{-\kappa_{0z}d_1}$$

$$0.H_{1y} + H_{2y}e^{-k_{2z}d_2} - H_{3y}e^{-k_{0z}d_2} + H_{ry}e^{k_{2z}d_2} = 0$$

$$0.H_{1y} - \frac{\kappa_{2z}\varepsilon_1}{\kappa_{0z}e_2}H_{2y}e^{-\kappa_{2z}d_2} - H_{3y}e^{-\kappa_{0z}d_2} + \frac{\kappa_{2z}\varepsilon_1}{\kappa_{0z}e_2}H_{ry}e^{\kappa_{2z}d_2} = 0$$

Los cálculos nos dan el siguiente resultado:

$$H_{1y} = -H_{0y}\frac{(K-1)(K+1)(1-{}^{e1}/_{e2})}{(K-1)^2-(K+1)^2({}^{e1}/_{e2})}\ ,\ H_{2y} = -2H_{0y}\frac{(K-1)}{(K-1)^2-(K+1)^2({}^{e1}/_{e2})}\ ,$$

$$H_{3y} = -4H_{0y}\frac{Ke_1}{(K-1)^2-(K+1)^2({}^{e1}/_{e2})}\ ,\ H_{ry} = -2H_{0y}\frac{(K+1)({}^{e1}/_{e2})}{(K-1)^2-(K+1)^2({}^{e1}/_{e2})}\ , \qquad (3.8)$$

Donde $e1 = e^{-(\kappa_{2z}-\kappa_{0z})d_2}$, $e2 = e^{(\kappa_{2z}+\kappa_{0z})d_2}$, $K = \left({}^{\kappa_{2z}\varepsilon_1}/_{\kappa_{0z}e_2}\right)$

Los denominadores en (3.8) se hacen igual a cero para dos valores de K:

$$K = \frac{1+e^{-\kappa_{2z}d_2}}{1-e^{-\kappa_{2z}d_2}} \ , \ K = \frac{1-e^{-\kappa_{2z}d_2}}{1+e^{-\kappa_{2z}d_2}} \qquad (3.9)$$

La división de la resonancia en la película se asocia con la existencia de un modo simétrico y antisemétrico. Para espesores grandes de la capa, cuando exp(-κ2zd2) ‹‹ 1, la división es pequeña, y el valor resonante de K es aproximadamente igual a 1, y para espesores pequeños de la capa metálica (1 + exp(-κ2zd2)) ›› (1 - exp(-κ2zd2)), y la división de la resonancia resulta ser grande. El efecto de la división de la resonancia superficial plasmonica en la capa metálica de espesor limitado se describe detalladamente en (Kovacs, 1977).

El campo en el espacio con capa metálica, en la cual interactúa la onda evanescente, contiene simultáneamente cinco ondas evanescentes. Estas son la onda incidente H0y, la onda reflejada en la primera frontera H1y, la onda transmitida en la capa metálica H2y, la onda reflejada en la segunda frontera Hry y la onda que atraviesa la capa metálica H3y. Se ha elegido para la discusión las ondas transversales magnéticas Hiy, es decir la onda TM. Las amplitudes de las ondas H1y, H2y Hry y H3y superan significativamente a H0y. En condiciones de resonancia superficial-plasmonica estas amplitudes tienden al infinito (en ausencia de pérdida), mientras que H0y permanece finita. Las condiciones de frontera de las componentes tangenciales del campo en la primera frontera se cumplen gracias a la igualdad aproximada entre H1y y H2y en esta frontera. En la segunda frontera el efecto se repite: la onda H2y, la cual será pequeña en la segunda frontera, genera unas ondas aproximadamente de igual y mayor amplitud Hry y H3y. Las ondas H1y, H2y y Hry, H3y forman ondas superficiales en pareja en la primera y segunda frontera del metal.
La presencia de ondas con amplitudes aumentadas en la capa metálica no contradice la ley de conservación de energía. El punto es que el problema planteado anteriormente no es un problema de propagación de la radiación electromagnética, sino que es un problema de búsqueda de las ondas propias Hn(r) de la ecuación de onda sin considerar la dependencia temporal $\Delta\mathbf{H}(\boldsymbol{r}) + \left(\frac{\omega}{c}\right)^2 \varepsilon\mu\mathbf{H}(\mathbf{r}) = 0$en un espacio no homogéneo, es decir con condiciones de frontera correspondientes. El

problema de propagación es la búsqueda de la solución de la ecuación$\boldsymbol{\Delta \mathbf{H}(r,t) - \frac{1}{v^2}\frac{\partial^2}{\partial t^2}\mathbf{H}(\mathbf{r},t) = 0}$en la forma$\mathbf{H}(\mathbf{r},t) = \sum[a_n(t)\mathbf{H}_n(\mathbf{r}) + a_n^*(t)\mathbf{H}_n^*(\mathbf{r})]$, donde Hn(r) es la solución de la ecuación de onda sin considerar el tiempo.

Partiendo de la igualdad (3.9) y considerando que$\kappa_{0z} = \sqrt{k_{0x}^2 - (\omega/c)^2\varepsilon_1\mu_1}$ se puede construir dos curvas $k_{0x} = \varphi_1(\kappa_{2z})$ y $k_{0x} = \varphi_2(\kappa_{2z})$:

$$k_{0x} = \varphi_1(\kappa_{2z}) = \sqrt{\left[\frac{\kappa_{2z}\varepsilon_1}{e_2}\frac{1+e^{-\kappa_{2z}d_2}}{1-e^{-\kappa_{2z}d_2}}\right]^2 + (\omega/c)^2\varepsilon_1\mu_1}$$

$$k_{0x} = \varphi_2(\kappa_{2z}) = \sqrt{\left[\frac{\kappa_{2z}\varepsilon_1}{e_2}\frac{1-e^{-\kappa_{2z}d_2}}{1+e^{-\kappa_{2z}d_2}}\right]^2 + (\omega/c)^2\varepsilon_1\mu_1} \qquad (3.10)$$

Para$\kappa_{2z}d \gg 1$las dos curvas coinciden, tomando la forma

$$\kappa_{0x} = \sqrt{\left(k_{2z}\varepsilon_1/e_2\right)^2 + (\omega/c)^2\varepsilon_1\mu_1} \qquad (3.11)$$

Donde ω siempre se considera constante.

Las curvas (3.10) es el lugar geométrico de los puntos, en donde para el par de valores de κ2z y κ0x hace cero el denominador en la expresión (3.8). Sin embargo, κ2z y κ0x están relacionados con la siguiente igualdad

$$\kappa_{2z} = \sqrt{\kappa_{0x}^2 + (\omega/c)^2 e_2\mu_2} \qquad (3.12)$$

Las intersecciones de las curvas (3.12) y (3.10) ó (3.11) nos dan el número de onda que corresponde al plasmón superficial.

Para grandes espesores de la capa metálica ($\kappa_{2z}d \gg 1$) de (3.11) y (3.12) se obtiene:

$$\kappa_{0x} = (\omega/c)\sqrt{\frac{\varepsilon_1\varepsilon_2}{\varepsilon_1+\varepsilon_2}} \qquad (3.13)$$

Que coincide con (3.6) para el numero de onda del plasmón superficial para la interfaz dieléctrico – metal para$\mu_1 = \mu_2 = 1$

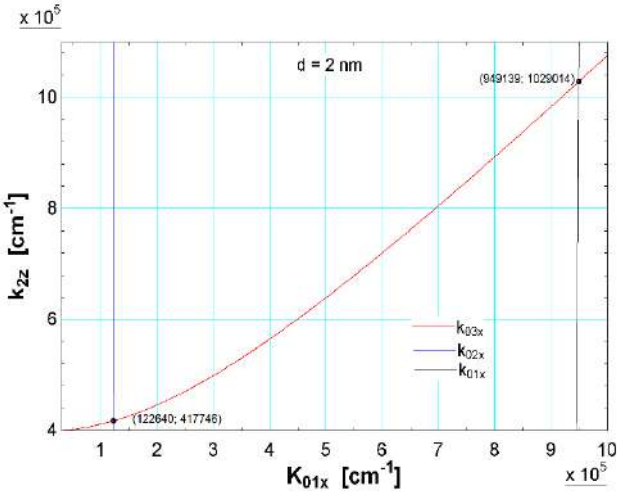

Figura 3.2. Intersección de las curvas (3.10) y (3.12) para una muestra de plata con espesor de 50 nm

Utilizando el método computacional EES, en la figura 3.2 se muestra el comportamiento de las curvas (3.10) y (3.12) para una muestra de plata con espesor de 50 nm y un k0 = ω/c = 1,22*105 cm-1. Las curvas de (3.10) son la azul y la morada. La de la izquierda está relacionado con el plasmón simétrico y el de la derecha con el plasmón antisimétrico. La curva roja se ha construido de acuerdo con la relación (3.12).

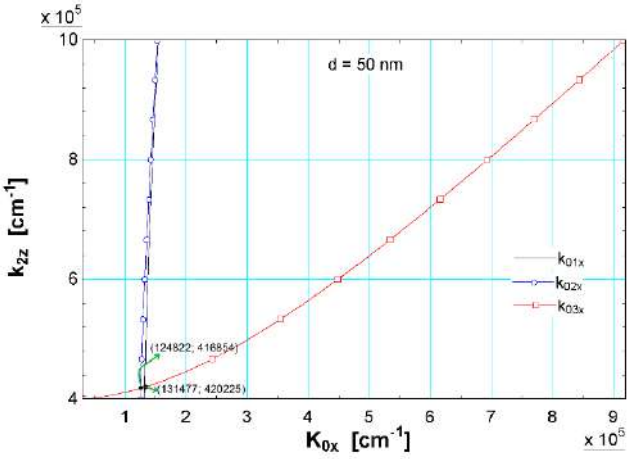

Figura 3.3. Intersección de las curvas (3.10) y (3.12) para la plata con espesor de 2 nm

Las curvas (3.10) y (3.12) se intersectan para valores de k0x igual a 1,25*105 cm-1 y 1,31*105 cm-1, que no se diferencia mucho del valor de ko. Las intersecciones corresponden a frecuencias espaciales de las resonancias plasmónicas.

En las cercanías de las resonancias plasmónicas las amplitudes de las ondas superficiales son aproximadamente 107 veces mayor que la amplitud de la onda incidente H0y. Lejos de las resonancias plasmónicas las amplitudes de las ondas superficiales son pequeñas.

En la figura 3.3 se muestra el comportamiento de las curvas (3.10) y (3.12) para una muestra de plata con espesor de 2 nm y un k0 = ω/c = 1,22*105 cm-1. Las curvas de (3.10) son la azul y la morada. La de la izquierda está relacionado con el plasmón simétrico y el de la derecha con el plasmón antisimétrico. La curva roja se ha construido de acuerdo con la relación (3.12). La división de los modos plasmónicos para la película metálica de 2 nm significativamente creció (ver fig. 3.8) en comparación con la división de los modos plasmónicos para una película metálica de 50 nm (ver fig. 3.2). La curva (3.12) en este caso se intersecta con la curva para el plasmón antisimétrico para k0x = 9,49*105 cm-1.

En la fig. 3.4 se muestra la frecuencia espacial de resonancia plasmónica en función del espesor de la capa metálica de plata para k0 = 1,22*105 cm-1 (los puntos rojos corresponden al plasmón simétrico y los puntos negros al plasmón antisimétrico). A medida que aumenta el espesor de la capa metálica, la división en plasmón simétrico y antisimétrico desaparece, y se tiene un solo plasmón superficial que de acuerdo con (3.13) para $\varepsilon_1 = 1$, $\varepsilon_2 = -10{,}67$ k0x = 1,28*105 cm-1 que no se diferencia mucho de k0 .

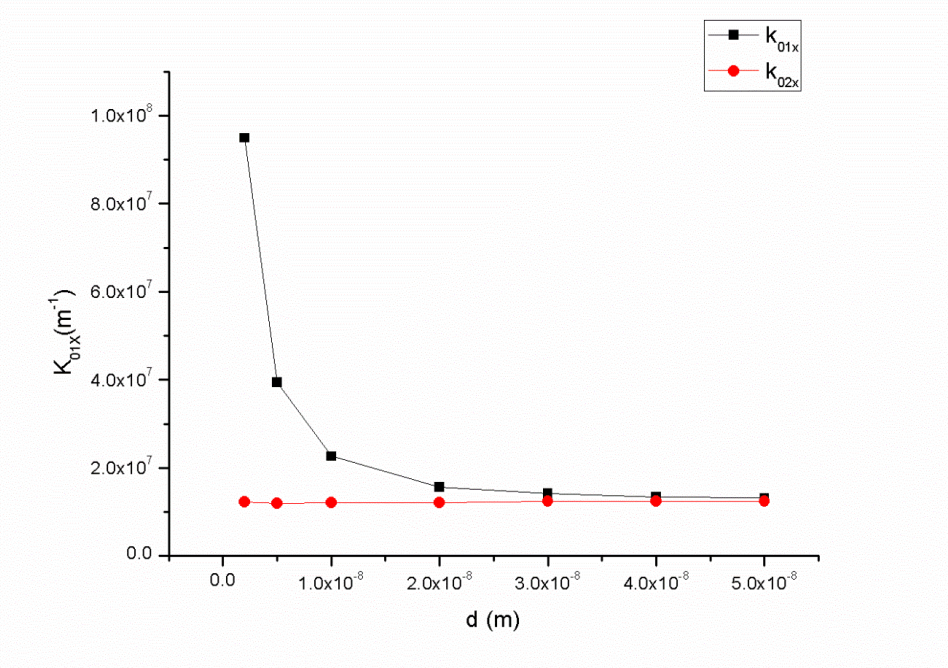

Figura 3.4. Frecuencia espacial de resonancia en función del espesor para la plata

Los plasmones superficiales en la capa delgada del metal son más lentos que la onda plana en el espacio adyacente. En mayor medida es más lento el plasmón antisimétrico como en el caso de la plata se puede observar de la tabla 3.1. Así por ejemplo en la película metálica con espesor d = 2 nm, su velocidad de fase vpla es 7,78 veces más lenta que la velocidad de la onda plana c en el espacio adyacente.

Tabla 3.1. Relación de la velocidad de la luz c y la velocidad de fase de los plasmones superficiales simétrico vpls y antisimétrico vpla para diferentes espesores de la plata

d(nm)	2	5	10	20	30	40	50
c/v_{pls}	1,01	0,98	1,00	1,00	1,02	1,02	1,02
c/v_{pla}	7,78	3,23	1,85	1,28	1,16	1,11	1,08

En las figuras del 3.5 al 3.11 se muestran el comportamiento de las curvas (3.10) y (3.12) para una muestra de oro con espesores desde 50 nm hasta 2 nm y un k0 = ω/c = 1,20*105 cm-1 y ε1 =ε3 =1, ε2 = -3,95 (Ver anexo B). Las curvas de (3.10) son la azul y la morada. La de la izquierda está relacionado con el plasmón simétrico y el de la

derecha con el plasmón antisimétrico. La curva roja se ha construido de acuerdo con la relación (3.12).

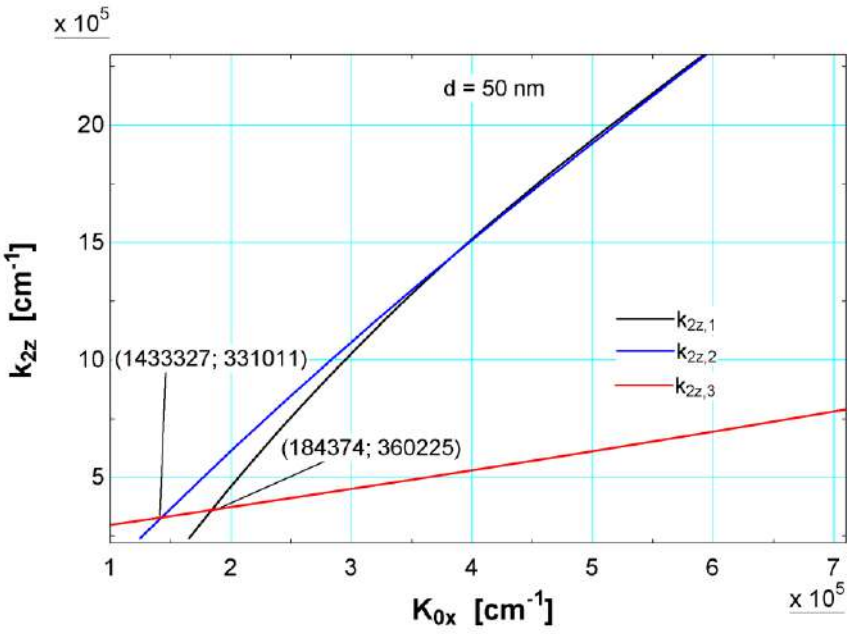

Figura 3.5. Intersección de las curvas (3.10) y (3.12) para el oro con espesor de 50 nm

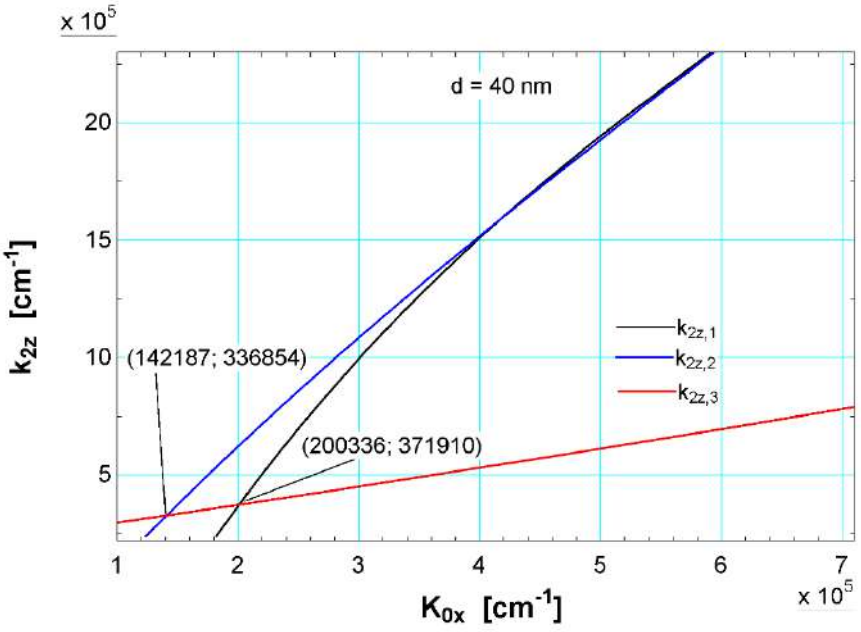

Figura 3.6. Intersección de las curvas (3.10) y (3.12) para el oro con espesor de 40 nm

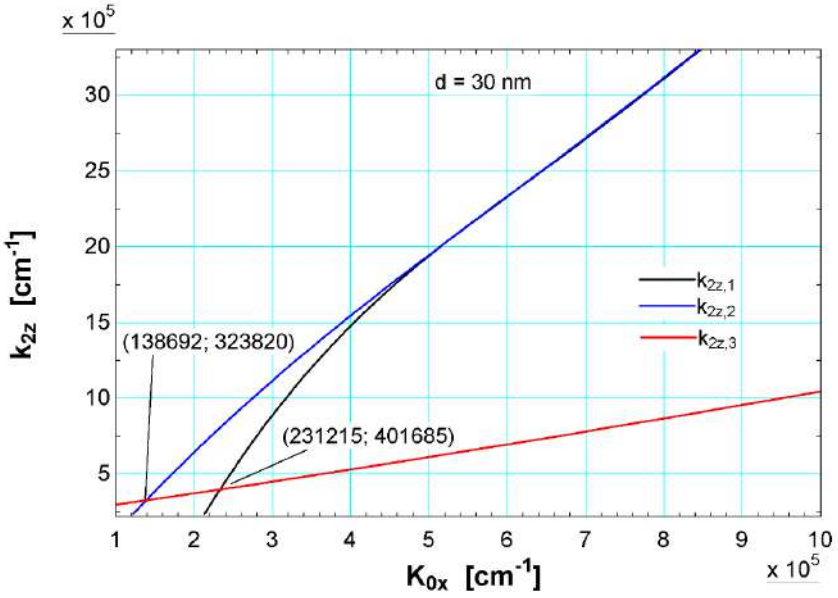

Figura 3.7. Intersección de las curvas (3.10) y (3.12) para el oro con espesor de 30 nm

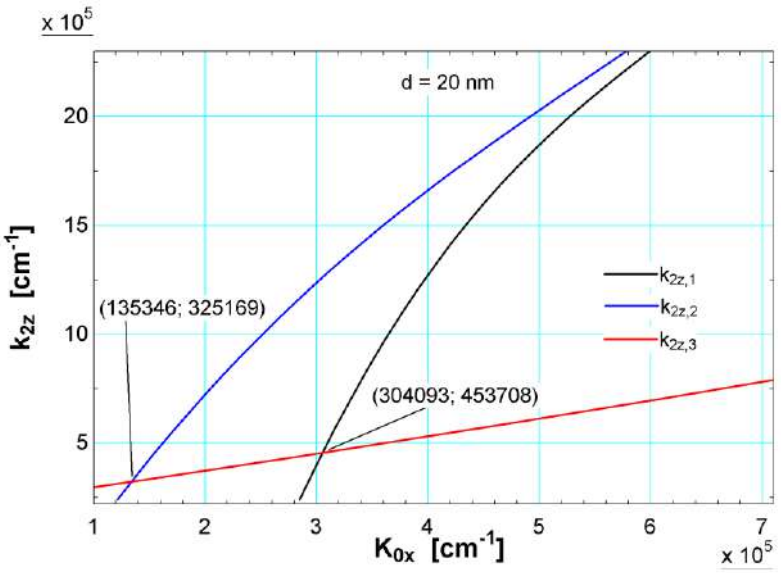

Figura 3.8. Intersección de las curvas (3.10) y (3.12) para el oro con espesor de 20 nm

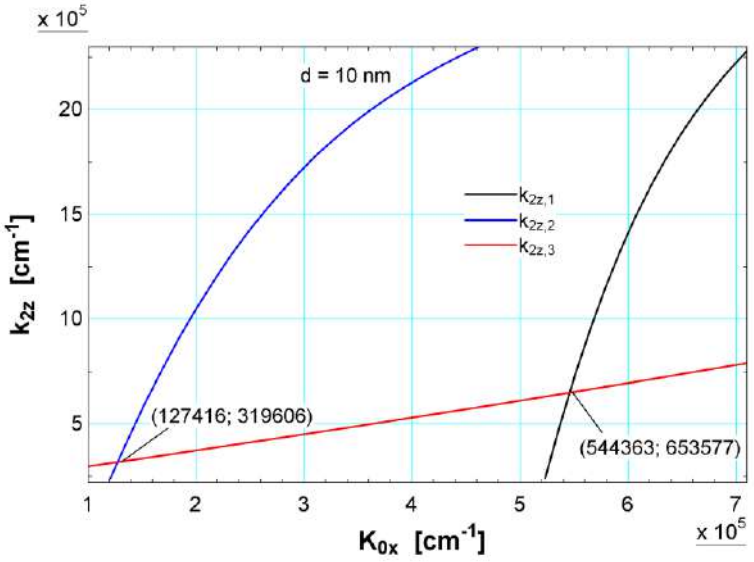

Figura 3.9. Intersección de las curvas (3.10) y (3.12) para el oro con espesor de 10 nm

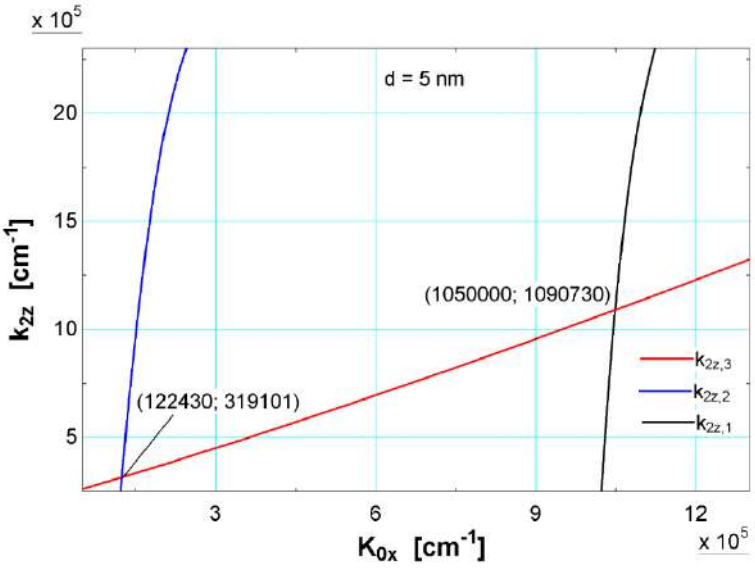

Figura 3.10. Intersección de las curvas (3.10) y (3.12) para el oro con espesor de 5 nm

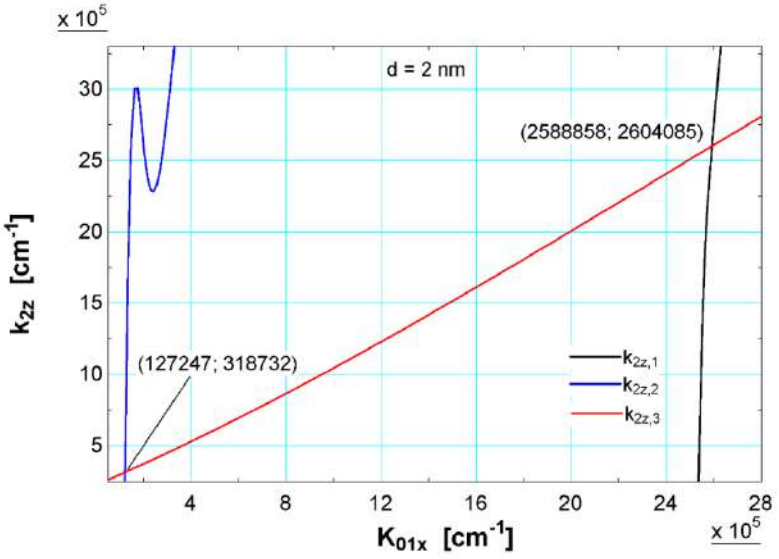

Figura 3.11. Intersección de las curvas (3.10) y (3.12) para el oro con espesor de 2 nm

En la fig. 3.12 se muestra la frecuencia espacial de resonancia plasmónica en función del espesor de la capa metálica de plata para k0 = 1,20*105 cm-1 (los puntos rojos corresponden al plasmón simétrico y los puntos negros al plasmón antisimétrico). A medida que aumenta el espesor de la capa metálica, la división en plasmón simétrico y antisimétrico desaparece, y se tiene un solo plasmón superficial que de acuerdo con (3.13) para $\varepsilon_1 = 1$, $\varepsilon_2 = -3{,}95$ k0x = 1,39*105 cm-1 que no se diferencia mucho de k0 .

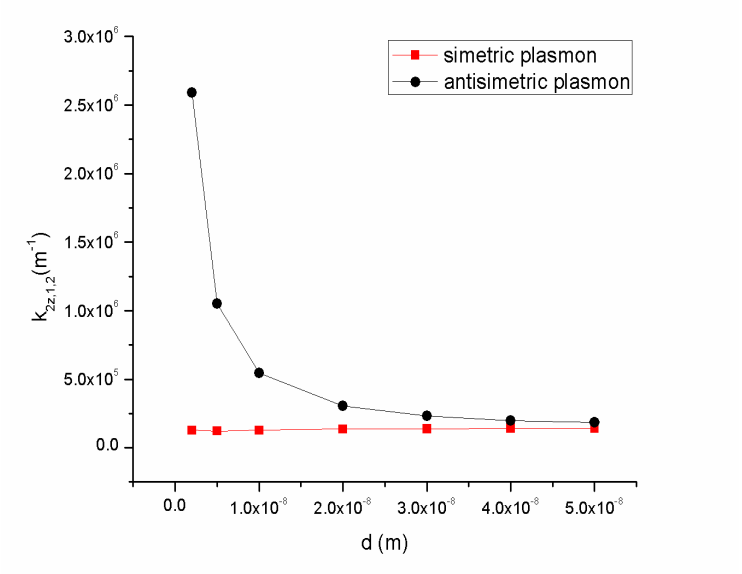

Figura 3.12. Frecuencia espacial de resonancia en función del espesor para el oro

Los plasmones superficiales en la capa delgada del metal son más lentos que la onda plana en el espacio adyacente. En mayor medida es más lento el plasmón antisimétrico como en el caso del oro se puede observar de la tabla 3.2. Así por ejemplo en la película metálica con espesor d = 2 nm, su velocidad de fase vpla es 21,57 veces más lenta que la velocidad de la onda plana c en el espacio adyacente.

Tabla 3.2. Relación de la velocidad de la luz c y la velocidad de fase de los plasmones superficiales simétrico vpls y antisimétrico vpla para diferentes espesores del oro

d(nm)	2	5	10	20	30	40	50
c/v_{pls}	1,06	1,02	1,06	1,12	1,16	1,18	1,19
c/v_{pla}	21,57	8,75	4,53	2,53	1,92	1,67	1,53

4. Discusión

En la interface dieléctrico – metal aparecen modos electromagnéticos (plasmones) de superficie. La amplitud del campo electromagnético del plasmón de superficie tiene un máximo en la interface y decae en el interior de ambos medios. De aquí se puede definir la longitud de propagación o penetración, L_p, como la distancia, desde la interface, a la cual la amplitud del campo ha decaído en un factor de 1/e . Esta longitud de propagación viene limitada por las pérdidas de absorción en el metal (muy altas). Esto significa que a mayor frecuencia se producirá mayor confinamiento (menor δ_d) en el dieléctrico y mayor penetración en el metal (δ_m), producirá mayores pérdidas.

En la interface dieléctrico – metal – dieléctrico aparecen dos modos electromagnéticos de superficie. La división de la resonancia en la película se asocia con la existencia de un modo simétrico y antisimétrico. Para espesores grandes de la capa, la división es pequeña y ambos modos tienden a un mismo valor como para el caso de una interface entre dos medios semi infinitos dieléctrico – metal.

Conclusiones

Cuando una onda electromagnética incide en la interface dieléctrico – metal se generan ondas superficiales (plasmones). Las ondas superficiales se propagan a lo largo de la interfaz entre los dos medios semi infinitos. Sus amplitudes disminuyen exponencialmente con la distancia desde la interfaz, y la frecuencia espacial resonante de los plasmones superficiales se expresa a través de (3.1).

Si la onda electromagnética incide en la interface dieléctrico – metal – dieléctrico con capa metálica delgada se generan plasmones superficiales en las dos fronteras, apareciendo dos modos electromagnéticos superficiales, uno simétrico y otro anti simétrico. Sus amplitudes disminuyen con la distancia desde la interfaz. La frecuencia espacial resonante depende del espesor de la capa metálica y para grandes espesores de la capa metálica tiende a la expresión (3.1) que corresponde a la interface dieléctrico – metal de medios semi infinitos.

Utilizando métodos computacionales se calculó las frecuencias espaciales resonantes para la interface dieléctrico – metal – dieléctrico con capa metálica delgada de plata y oro para diferentes espesores desde 50 nm hasta 2 nm para una onda electromagnética incidente con vector de onda para el caso de la plata k0 = 1,22*105 cm-5 ε1 =ε 3=1, ε2 = -10,67, y para el caso del oro k0 = 1,20*105 cm-5 ε1 =ε 3=1, ε2 = -3,95 obteniéndose en ambos casos que el modo plasmónico simétrico débilmente cambia, sin embargo el modo plasmónico anti simétrico cambia significativamente. Por lo tanto, la velocidad de fase de los plasmones superficiales en el modo anti simétrico depende fuertemente del espesor de la capa metálica como se muestran en la tabla 3.1 y 3.2.

Los resultados obtenidos para la interface dieléctrico – metal – dieléctrico con capa metálica delgada de plata y oro nos muestran que las propiedades ópticas de este sistema dependerían significativamente del espesor de la capa metálica.

Referencias

Abrikosov, A. (1987). *Fundamentos de la teoría de los metales*. Moscú: Nauka.

Camacho, A. (2018). ¿Cómo se pueden usar los nanoplasmones en la vida diaria?. *Revista de Física*, No. 56E, 14-21. Recuperado de https://revistas.unal.edu.co/index.php/momento/article/view/71616/65622

Failache, H. S. (2002). Phys. Rev. Lett., v.88, 243603.

Kittel, C. (1987). *Quantum Theory of Solid*. New York: Jhon Wiley &Sons.Inc.

Kovacs, G. J. (1977). Phys. Rev. B, v.16, 1297-1311.

Lewotsky, K. (2007). *The promise of plasmonics*. SPIE Professional.

Pines, D. (1963). *Elementary Excitation in Solids*. New York.

Ritchie, R. (1957). Phy. Rev., 106, 874.

Rodríguez-Mijangos, R. & García-Llamas, R. (2018). Modos electromagnéticos en esferas metálicas; plasmones en micro y nanopartículas. *Revista Mexicana de Física* E, 64(2), 154-161. Recuperado de http://www.scielo.org.mx/scielo.php?script=sci_arttext&pid=S1870-35422018000200154&lng=pt&tlng=pt.

Schubert, M. T. (2000). Phys. Rev. B, v.61, 8187-8201.

Zavitaev, E. V. (2003). JTF T.72.

Zea, J., Talavera, M., Arenas, C., Pacheco, D., Osorio, A., & Vera, C. (2019). Obtención y caracterización del nanocomposito: nanopartículas de plata y carboximetilquitosano (NPsAg-CMQ). *Revista de la Sociedad Química del Perú*, 85(1), 14-24. Recuperado de http://www.scielo.org.pe/scielo.php?script=sci_arttext&pid=S1810-634X2019000100003&lng=es&tlng=es.

Touch static analysis and dynamic exercises of insulated patients

B.I. Vakhitov *
I.S. Raginov
I. Kh. Vakhitov
T. L. Zefirov
R.E. Khisamutdinov

ABSTRACT
For the first time, studies were conducted on the study of the amplitude indices (C-EMG) and the frequency of the oscillations following (CSC-EMG) when performing dynamic and static exercises among patients with stroke and healthy people. It was revealed that in healthy individuals (control group) the amplitude of the EMG depends on the nature of the exercises. The largest EMG amplitude is registered when performing static exercises. It was found that patients who were hospitalized in the acute period of stroke when flexion and extension of the fingers were performed were mainly recorded low-amplitude movement stretched for the entire cycle without a clear peak of the extremum of EMG activity. When performing static exercises in these patients, a greater amplitude and an increase in the frequency of the EMG oscillations were revealed.

KEYWORDS: Electromyography, sick and healthy patients, average amplitude (SA-EMG), frequency of fluctuations following (CSK-EMG), dynamic and static exercises.

Análisis estático táctil y ejercicios dinámicos en pacientes aislados

RESUMEN
Por primera vez, se realizaron estudios sobre el estudio de los índices de amplitud (C-EMG) y la frecuencia de las oscilaciones posteriores (CSC-EMG) al realizar ejercicios dinámicos y estáticos entre pacientes con accidente cerebrovascular y personas sanas. Se reveló que en individuos sanos (grupo de control) la amplitud del EMG depende de la naturaleza de los ejercicios. La mayor amplitud EMG se registra al realizar ejercicios estáticos. Se encontró que los pacientes que fueron hospitalizados en el período agudo de accidente cerebrovascular, cuando se realizaron la flexión y la extensión de los dedos, se registraron principalmente movimientos de baja amplitud estirados durante todo el ciclo, sin un pico claro del extremo de la actividad EMG. Al realizar ejercicios estáticos en estos pacientes, se reveló una mayor amplitud y un aumento en la frecuencia de las oscilaciones EMG.

PALABRAS CLAVE: Electromiografía, pacientes enfermos y sanos, amplitud media (SA-EMG), frecuencia de fluctuaciones posteriores (CSK-EMG), ejercicios dinámicos y estáticos.

* Kazan Federal University, 420008, Kazan, Kremlyovskaya str., 18. vakhitov.1989@mail.ru

Recibido: 09/10/2019 Aceptado: 07/11/2019

Introduction

In cerebral strokes, the earliest possible and most comprehensive rehabilitation plays a significant role and can significantly improve the functional and social outcome of the disease. Rehabilitation measures are effective in about 80% of post-stroke patients, another 10% recover spontaneously, and 10% have no success in rehabilitation measures (Khitrov et al., 2012; Vakhitrov, 2017). At the same time, post-stroke motor disorders remain the leading cause of maladaptation in this category of patients (Kirilchenko, 2006; Iusevich, 1958). Cerebral stroke is the most common cause of disability. According to various sources, the level of disability in patients who survived after a stroke reaches 70–85% (Vakhitov, 2014).

Despite significant achievements in disclosing the etiology and pathogenesis of acute cerebrovascular accidents (ACVA), the outcome of this disease remains unfavorable so far, which indicates the need for further improvement of medical care for stroke patients, especially at an early stage of the disease (Vakhitov, 2014; Lukianov, 2013). The most common symptom of ischemic stroke is hemiparesis, however, this group of patients has a complex motor defect, different in nature and severity. Data on the effect of the affected side is contradictory. Some authors note that patients with right-sided damage have a worse prognosis in terms of recovery (Vakhitov, 2017; Kirtly, 2006; Petrilli et. al., 2002). Other researchers suggest that worse recovery is observed in damages of the left hemisphere (Lukianov, 2013; Vakhitov, 2017). One of the methods of objectifying post-stroke motor disorders is surface electromyography with a change in the amplitudes of the maximum bilateral arbitrary activation of the muscles of the forearm, hand, and shoulder and the calculation of the coefficients of adequacy (CA) and reciprocity (CR) (Skvorytsova, 2006; Khitrov et al., 2012; Vakhitov, 2017; Petrilli et al., 2002). The ratio of the amplitude of the muscle during its involuntary activation (with the active maximum tension of the antagonist) to the amplitude of the same muscle in the mode of maximum arbitrary tension is called CA. CR characterizes the interaction of muscle antagonists and is calculated for a muscle in antagonistic tension. It shows the degree of its activation as a percentage in relation to the activity of the agonist muscle. Under normal conditions, the extensor muscles have a higher coefficient of adequacy and reciprocity than in the flexor and are up to 20%.

Currently, various medical simulators of domestic and foreign manufacture are widely used for the rehabilitation of patients along with other activities. However, a common drawback of these simulators in our opinion is the lack of feedback. The simulators are not equipped with sensors to provide information from the patient in dynamics, and subsequently, to promptly make correction into the rehabilitation process. Adequate correction of motor impairment is impossible without considering and analyzing changes in the body without using a feedback system. Moreover, the existing medical simulators are largely aimed at performing only dynamic exercises, excluding practically static exercises. Although many researchers have recently substantially supported the role of the latter in the rehabilitation process.

The objective of this study was to quantify EMG recordings in healthy individuals and stroke patients. This article presents the first results of a comparative analysis of muscle activity profiles of healthy individuals and stroke patients when performing dynamic and static exercises.

Materials and methods. The study involved 20 healthy subjects - 9 men and 11 women aged 45–63 years (control group), and 26 patients - 14 men and 12 women aged 42–65 years, with cerebral stroke (main group). The control groups at the time of the examination did not have neurological, orthopedic, and severe somatic diseases. The main group consisted of patients with spastic hemiparesis in the acute period of ischemic stroke.

To study the biomechanics of movements, all subjects were asked to perform a series of motor exercises. Given the healthy and post-stroke motor capabilities of patients, the following movements were selected: 1) at rest; 2) flexion and extension of the hands; 3) maximum abduction of the hand and further retention in a static position, and) maximum adduction of the hand and its further retention in this position.

Surface electromyogram (EMG) was performed using an electromyograph developed on the basis of the Myoware Muscle Sensor (AT-04-001). Disposable cutaneous electrodes were applied in accordance with the standards for biomechanical studies. Поверхностная ЭМГ регистрировалась со следующих мышц: m. flexor carpi ulnaris, m. flexor carpi radialis, m. flexor digitorum superficialis, m. extensor carpi ulnaris, m. extensor digitorum,

m. extensor carpi radialis longus. The average amplitude (AA-EMG) and the oscillation repetition rate (ORR-EMG) were analyzed.

To assess the significance of differences, standard values of Student t-test were used.

1. Results and Discussion

EMG in healthy individuals. Most healthy subjects showed spontaneous activity in EMG. EMG of healthy subjects resembled a static pattern of the so-called segmental irritation according to the classification of Iu.S. Iusevich (Skvortsova et al., 2006) — rhythmic constant fibrillations or fasciculations, sometimes recorded in relaxed muscles (at rest) with segmental lesions. A similar EMG picture (spontaneous activity) was recorded at rest in the majority of examined healthy individuals (Table 1). Exercises in the form of flexion and extension of the fingers caused in examined healthy subjects the rhythmic potentials of EMG with increased amplitude. Static exercises caused slight changes in the EMG record. Holding the hand in a static adducted position caused a significant increase in the EMG potentials that reached up to 2,14 mV, which turned out to be significantly higher compared to the EMG values obtained with the dynamic exercise (flexion and extension of the fingers). Holding the hand in a static abducted position caused a significant increase in the EMG amplitude compared to all EMG values obtained during the previous exercises. Thus, in healthy individuals, the amplitude of EMG depends on the nature of the exercises performed. The largest amplitude of EMG was recorded during static exercises.

EMG of stroke patients. EMG of patients with hemiparesis in the studied motor activities differed from healthy ones in clear "uniformity". In the majority of stroke patients, the studied movements included more than necessary muscles, i.e. there was significant irradiation. A clear uniformity in patients with stroke also differed in the profiles of EMG curves (Table 2). All patients in the acute period of a stroke during flexion and extension of their fingers showed predominantly a low amplitude stretched over the entire cycle of movement, without a clear peak of the extremum of EMG activity. There was an almost complete absence of activity of this muscle in the studied movement. In our opinion, it could involve other, additional muscle groups to perform the motion. EMG of these patients was characterized by low amplitude and a lower frequency, tremor, excess conjugate activity of

antagonist muscles and the presence of so-called "gaps" - sections of bioelectric silence lasting 10-30 ms in the analyzed fragments of records. During static exercises in patients with an acute stroke, the EMG profiles were slightly different from previous records.

2. Key indicators of total EMG

During dynamic and static exercises in healthy people

Table 1

Muscles	Type of exercise		AA-EMG (mV)	ORR-EMG (per sec)
m.extesnor carpi ulnaris	dynamic	M ±m	1.01 0.08	243 24
	static	M ±m	2.14 0.07	296 26
m.flexor carpi radialis	dynamic	M ±m	1.08 0.09	267 14
	static	M ±m	2.18 0.20	294 25
m. flexor carpi ulnaris	dynamic	M ±m	1.07 0.06	249 29
	static	M ±m	2.04 0.08	298 23
m.flexor digitorum superficialis	dynamic	M ±m	1.06 0.07	251 20
	static	M ±m	2.09 0.09	297 26
m. extensor digitorum	dynamic	M ±m	1.01 0.06	245 26
	static	M ±m	2.17 0.09	294 18
m.extensor carpi radialis longus	dynamic	M ±m	1.03 0.08	261 28
	static	M ±m	2.15 0.07	295 13

3. Key indicators of total EMG

During dynamic and static exercises in patients

Table 2

Muscles	Type of exercise		AA-EMG (mV)	ORR-EMG (per sec)
m.extesnor carpi ulnaris	dynamic	M ±m	0.11 0.03	190 14
	static	M ±m	0.24 0.07	222 6
m.flexor carpi radialis	dynamic	M ±m	0.18 0.06	178 14
	static	M ±m	0.28 0.20	254 15
m. flexor carpi ulnaris	dynamic	M ±m	0.07 0.02	209 29
	static	M ±m	0.14 0.01	304 13
m.flexor digitorum superficialis	dynamic	M ±m	0.16 0.07	241 20
	static	M ±m	0.29 0.07	256 16
m. extensor digitorum	dynamic	M ±m	0.11 0.02	215 26
	static	M ±m	0.27 0.09	271 8
m.extensor carpi radialis longus	dynamic	M ±m	0.13 0.02	201 28
	static	M ±m	0.25 0.07	295 13

Conclusion

Adequate correction of motor impairment is impossible without considering and analyzing changes in the body without using a feedback system. The currently used medical simulators are largely aimed at performing only dynamic exercises, excluding practically static exercises. In our work, we for the first time analyzed the average amplitude (AA-EMG) and the oscillation repetition rate (ORR-EMG) in healthy and sick people during dynamic and static exercises. According to our data, in healthy individuals, the amplitude of EMG depends on the nature of the exercises performed. The largest amplitude of EMG was recorded during static exercises.

All patients in the acute period of a stroke during flexion and extension of their fingers showed predominantly a low amplitude stretched over the entire cycle of movement, without a clear peak of the extremum of EMG activity. During static exercises, the EMG amplitude

and the frequency of EMG fluctuations in these patients were slightly higher than during dynamic exercises.

Thus, both healthy and sick patients, when performing static exercises, show a significant increase in the amplitude and frequency of EMG. In our opinion, the use of dynamic exercises in combination with static exercises as part of rehabilitation measures would significantly reduce the time needed to restore the lost functions of the upper limbs.

The preliminary results obtained by us in the clinical settings are sufficiently strong evidence of the need for EMG for the dynamic analysis of the recovery process. The data obtained should be considered as an additional justification for the use of static exercises in the rehabilitation process.

Summary

- The analysis and operational correction of the rehabilitation process require using sensors, in particular, EMG recording. This will provide feedback and promptly adjust the recovery process.

- Static exercises in patients ensure significant positive changes in the average amplitude (AA-EMG) and oscillation repetition rates (ORR-EMG).

Acknowledgments

The work is performed according to the Russian Government Program of Competitive Growth of Kazan Federal University.

References

Iusevich Iu. S. (1958). Electromyography in a clinic of nervous diseases. M: Medicine 1958; 128.

Khitrov M.V., Subbotina T.I., Iashin A.A. (2012). Electromyography as a method of objectifying the results of physical rehabilitation of injuries of the musculoskeletal system of athletes // Bulletin of Tula State University - 2012.

Kirilchenko T.D. (2006). The formation of pathological postures in the acute period of hemispheric ischemic stroke and their correction methods: Author's abstract, Cand. Med. M 2006.

Kirtly C. (2006). Clinical gait analysis: theory and practice. Edinburgh [et al]: Elsevier Science Health Science 2006; 316.

Lukianov M.V. (2013). Clinical electromyography. History and prospects // Neurological Journal - 2013.

Petrilli S., Durufle A., Nicolas B. et al. (2002). Prognostic factors in the recovery of the ability to walk after stroke. J Stroke Cerebrovasc Dis 2002; 11: 330—335.

Skvortsova V.I., Chazova I.E., Stakhovskaia L.V. et al. (2006). The primary prevention of stroke. The quality of life. Medicine 2006; 2: 72–77.

Vakhitov I. Kh. (2014). Brain neural reactivity control system in Paralympic athletes / S.Iu. Myshliaev, I.Kh. Vakhitov, G.M. Zagorodnyi, G.V. Popova // Scientific works of the Research Institute of Physical Culture and Sports of the Republic of Belarus: Collection of scientific works / Scientific and Research Institute of Physical Culture and Sports, Republic of Belarus; Editorial: A.A. Mikheev (ch. Ed.) [and others]. - Minsk, 2014. - Issue. 14. - P. -224-230.

Vakhitov I. Kh. (2017). Peculiarities of heartbeat rate and stroke volume of blood, negative phase, manifestation among young sportsmen after muscular load / B. I. Vakhitov*, I. Kh. Vakhitov, A. H. Volkov, S. S. Chinkin // Journal of Pharmacy Research. -2017, -Vol. 11, -P. 1198 - 1200.

Methods for the synthesis of arsines and arsine dihalides

Farid Dgamaletdinovich Yambushev *

ABSTRACT

Arsenic is an essential biologically active element, and its compounds are used in various fields and areas of activity. Arsenic chemistry is widely used in agriculture, industry, and medicine. Many organic arsenic compounds have bactericidal and herbicidal properties necessary for practical use; some of them found its application in polymer chemistry. This necessitates the production of new substances with previously known properties. Therefore, the problem of studying methods for the synthesis of organic arsenic compounds is important and relevant.The present article is devoted to the analysis of methods for the synthesis of primary arsines and the corresponding arsine dihalides. Based on a study of literature containing a description of various methods for preparing compounds of this group, as well as on the basis of the results of own experimental studies, the author makes a choice in favor of the synthesis of primary aryl arsine dihalides by reduction of the corresponding arsonic acids. Subsequent substitution of halogen atoms can produce compounds of a specific structure. Thus, using aryl arsonic acids as starting products for the synthesis of subsequent classes of organic arsenic compounds, it is possible to obtain organic arsenic compounds of a given structure and complexity. A detailed description of the methods of conducting experiments is made, their comparative characteristics are given, and the physical properties of the obtained substances are described.

KEYWORDS: organic arsenic compounds, arsines, arsine dihalides, aryl arsonic acids, arsine oxide.

**Kazan Federal University, rosa_safina@mail.ru*

Recibido: 09/10/2019 Aceptado: 07/11/2019

Métodos para la síntesis de arsinas y dihaluros de arsina

RESUMEN

El arsénico es un elemento biológicamente esencial, y sus compuestos se utilizan en diversos campos y áreas de actividad. La química del arsénico se usa ampliamente en la agricultura, la industria y la medicina. Muchos compuestos orgánicos de arsénico tienen propiedades bactericidas y herbicidas necesarias para su uso práctico; algunos de ellos encontraron su aplicación en la química de polímeros. Esto requiere la producción de nuevas sustancias con propiedades previamente conocidas. Por lo tanto, el problema de estudiar métodos para la síntesis de compuestos de arsénico orgánico es importante y relevante. El presente artículo está dedicado al análisis de métodos para la síntesis de arsinas primarias y los correspondientes dihaluros de arsina. Basado en un estudio de literatura que contiene una descripción de varios métodos para preparar compuestos de este grupo, así como en base a los resultados de estudios experimentales propios, el autor toma una decisión a favor de la síntesis de dihaluros de aril arsina primaria por reducción de los correspondientes ácidos arsónicos. La posterior sustitución de átomos de halógeno puede producir compuestos de una estructura específica. Por lo tanto, utilizando ácidos aril arsónicos como productos de partida para la síntesis de clases subsiguientes de compuestos de arsénico orgánico, es posible obtener compuestos de arsénico orgánico de una estructura y complejidad dada. Se realiza una descripción detallada de los métodos para realizar experimentos, se dan sus características comparativas y se describen las propiedades físicas de las sustancias obtenidas.

PALABRAS CLAVE: compuestos orgánicos de arsénico, arsinas, dihaluros de arsina, ácidos aril arsónicos, óxido de arsina

Introduction

The subject of the work is relevant and important because many arsenic compounds are of interest for solving highly significant scientific and practical problems in various fields of life.

The objective of this work is to study, compare, and select the most effective way to obtain organic arsenic compounds of a given structure. Objects of research are arsines and arsine halides and methods for their synthesis.

1. Methods

Primary arsines $RAsH_2$, used for the synthesis of secondary and tertiary arsines, are usually obtained by reduction of the corresponding acids, their salts (Feltham et al., 1967; Cookson and Mann, 1949), arsine halides (Brooker et al., 1958; Abbers et al., 1952), arsenic

compounds containing the As=As bond, and oxides (Tzschach and Lange, 1964). The most effective reducing agents are zinc dust and hydrochloric acid (Feltham, 1967; Brooker et al., 1958; Newbery and Philips, 1928), zinc amalgam (Pabmer and Dehn, 1901; Tzschach and Lange, 1964; Rapoport and Iliinskaia, 1963), zinc copper (Wigren, 1930), and zinc platinum (Abbers et al., 1952). Depending on the nature of the reducing agent, the reaction does not always proceed with a good yield. For example, in (Cragoe et al., 1947) methylphenylchlorarsine was reduced to the corresponding arsine with zinc amalgam in methanol with a good yield, while the reduction of dialkylchlorarsines with $LiAlH_4$ did not give satisfactory results in (Issleib and Tzschach, 1961; Stone and Burg, 1954).

To reduce CF_3AsJ_2 and $(CF_3)_2As\text{-}As(CF_3)_2$, the researchers used $LiAlH_4$, hydrochloric acid, and copper-coated zinc (Emeleus et al., 1953). When phenyl and diphenylarsine chlorides were reduced with lithium aluminum hydride and borohydride, the corresponding arsines were obtained in high (81%) yield (Kockel, 1956; Cullen, 1961). The restoring effect of $LiAlH_4$ is not always effective because it is assumed to interact with the resulting arsine according to the following scheme:

$$C_6H_5AsH_2 + AlH_3 \rightarrow C_6H_5AsH_2 \cdot AlH_3 \rightarrow C_6H_5As(H)AlH_2 + H_2$$

For recovery under these conditions, both $C_6H_5AsCl_4$ and $C_6H_5AsCl_2$ can be used. The final reaction product in both cases will be $C_6H_5AsH_2$.

During the reduction of $(CF_3)_2AsCl$ with metallic mercury in hydrochloric acid, the formation of diarsine is supposed, which under the action of HCl is decomposed by the As-As bond:

$$2(CF_3)_2AsCl + Hg \rightarrow (CF_3)_2As - As(CF_3)_2 + HgCl_2$$
$$(CF_3)_2As - As(CF_3)_2 + HCl \rightarrow (CF_3)_2As\text{-}H + (CF_3)_2AsCl$$

According to the authors of (Cavell and Dobbil, 1967; Fichter and Elkind, 1916), the reduction of the corresponding arsiniodides with mercury in hydrochloric acid ensures more effective results. Thus, $(CF_3)_2AsJ$, $J_2(CF_3)_2As\text{-}As(CF_3)_2J_2$ and $(CF_3)_2AsJ_3$ are reduced. As a result, $(CF_3)_2AsH$ was obtained in high yield.

Primary and secondary arsines can be obtained through metal arsinides formed by the interaction of AsH_3 with active metals such as Na, K, or Ca in liquid ammonia. The reaction of the corresponding metal arsinides with alkyl or aryl halides leads to the formation of primary and secondary arsines (Johnson and Pechwkas, 1937; Tzschach and Pacholke, 1964):

$$NaAsH_2 + C_6H_5Cl \rightarrow C_6H_5 AsH_2 + NaCl$$

The reaction of calcium diarsinide $Ca(AsH_2)_2$ with methyl chloride forms a mixture of products consisting of methyl, dimethyl, and trimethylarsines. Secondary dialkyl or mixed alkylarylarsines can be prepared by heating triaryl and alkyl diarylarsines with potassium metal in dioxane. Hydrolysis of the resulting potassium arsinide with water leads to the synthesis of secondary arsine in high yield (Issleib and Tzschach, 1961; Tzschach and Lange, 1964).

$$R_3As + 2K \rightarrow KAsR_2 + RK$$
$$R_2AsK + HOH \rightarrow R_2AsH + KOH$$

Magnesium arsinides react similarly with water (Blicke and Oneto, 1935).

To obtain primary arsenic aryl dihalides, the reaction of arsenic trichloride with organometallic compounds is most often used. However, it should be emphasized that the use of organic magnesium reagents in this reaction is ineffective due to their interaction with arsenic trihalides with the simultaneous substitution of all halogen atoms (Freidlina, 1945).

$$3RMgBr + AsCl_3 \rightarrow R_3As + 3MgClBr$$

The reaction of aromatic organic mercury compounds with arsenic trichloride is mainly used to produce aryl arsine dichlorides. In this reaction, an excess of arsenic trichloride and an increase in the reaction temperature to 200–230 °C make it possible to obtain only aryl arsine dichlorides, in good yield.

$$R_2Hg + AsCl_3 \rightarrow RAsCl_2 + RHgCl$$

Monoaryl arsine dichlorides are also obtained by the reaction of arsenic trichloride with aromatic organic mercury salts (Michaelis, 1894). Secondary and tertiary arylarsines formed during this reaction are disproportionate under the action of the resulting mercuric chloride and improve the yield of arylarsindichlorides.

In addition to those considered, one of the most convenient methods for obtaining primary aromatic arsenic dihalides is the reaction of triarylarsines with arsenic trihalides (Michaelis and Reese, 1882).

$$(C_6H_5)_3As + AsCl_3 \rightarrow C_6H_5AsCl_2 + (C_6H_5)_2AsCl$$

The disproportionation reaction of tertiary arsines that have aryl radicals under the action of arsenic trichloride leads to the formation of the corresponding primary arylarsine dihalides. This reaction is carried out by prolonged heating of the mixture. The yield of primary arylarsine dihalides depends on the ratio of reagents and increases when excess arsenic trichloride is used.

The primary aromatic arsine dihalides in the product mixture are obtained by the interaction of aromatic hydrocarbons with arsenic trichloride.

$$(CH_3)_2NC_6H_5 + AsCl_3 \rightarrow (CH_3)_2NC_6H_4AsCl_2 + HCl$$

The presence of electron-donating substituents in the benzene ring increases the yield of the main products (Cullen, 1966).

Primary arylarsine dihalides can be synthesized from the corresponding arsenic hydrides by reacting with halogens, hydrogen halides and inorganic metal and phosphorus halides. According to this technique, arylarsine dichloride was obtained by the interaction of phenylarsine with chlorides of mercury, tin, phosphorus, arsenic, and antimony (Kamai and Gatilov, 1961):

$$C_6H_5AsH_2 + 2J_2 \rightarrow C_6H_5AsI_2 + 2HJ$$

Primarily substituted arylarsine dihalides can be obtained from the corresponding oxides, which easily react with hydrogen halides (Michaelis and Schulte, 1982):

$$RAsO + 2HCl \rightarrow RAsCl_2 + H_2O$$

Primary arylarsine difluorides are obtained by this reaction using hydrofluoric acid. However, as described by the authors of (Lang et al., 1946), the best method for producing fluorine derivatives is the exchange interaction of arylarsine dichloride with ammonium or silver fluorides.

$$C_6H_5AsCl_2 + 2NH_4F \rightarrow C_6H_5AsF_2 + 2NH_4Cl$$
$$C_6H_5AsCl_2 + 2AgF \rightarrow C_6H_5AsF_2 + 2AgCl$$

The considered methods for the preparation of primary arylarsine dihalides are much inferior to the method consisting in the reduction of arylarsonic acids in the presence of hydrogen halide:

$$RAsO(OH)_2 + SO_2 \xrightarrow{HCl} RAsCl_2 + H_2SO_4$$

Reducing agents in this reaction are sulfur dioxide, hypophosphorous acid, phosphorus trichloride, sodium hypophosphate, thionyl chloride, and other reducing agents. The reduction reaction is catalyzed by iodidanion and is usually carried out in concentrated hydrochloric acid.

The reduction of arylarsonic acids with sulfur dioxide in the presence of other HX acids (X= Br, J) leads to the production of bromine and iodarsines (Freidlina, 1945).

Primary arylarsine halides can be obtained from aryl diarsine halides. According to this method, Michaelis obtained phenylarsine diiodide by oxidation of phenylarsenic diiodide with oxygen in an aqueous medium:

$$C_6H_5(J)As - As(J)C_6H_5 + O_2 + H_2O \rightarrow C_6H_5AsJ_2 + C_6H_5AsO_3H_2$$

The authors of (Brooker and Nikiforova, 1958) proposed a method for the preparation of primary aryldiarsine halides by the interaction of phenylhydrazine with arsenic trichloride in the presence of copper chloride and oxygen.

$$C_6H_5{-}NH{-}NH_2 + AsCl_3 \xrightarrow{O_2CuCl_2} C_6H_5AsCl_2 + (C_6H_5)_2AsCl$$

2. Results and discussion

Arylarsine dichlorides were synthesized by us by reduction of arylarsonic acids with sulfur dioxide in a concentrated hydrochloric acid (Iambushev et al., 1983). The recovery process proceeds in two stages. In the first, as arylarsonic acid dissolves in hydrochloric acid, the hydroxyl groups associated with the arsenic atom are exchanged for chlorine atoms to form arsenic acid chlorides in a hydrochloric acid solution.

$$XC_6H_4AsO(OH)_2 + HCl \rightarrow XC_6H_4As(O)Cl_2 + H_2O.$$

At the second stage, when acting with sulfur dioxide, the acid chlorides are reduced to the corresponding aryl aromatic dichlorides:

$$XC_6H_4As(O)Cl_2 \xrightarrow{SO_2} XC_6H_4AsCl_2$$

X= o-, м-, п-H, Cl, Br, J, CH_3, OCH_3, NO_2

Some physical constants and analytical data on the obtained monosubstituted arylarsine dichlorides are given in Table 1.

Arylarsine dichlorides $XC_6H_4AsCl_2$, X=o-Cl, Br, CH_3O, o-, m-n-NO_2, n-J, CH_3 are crystalline substances with a low melting point. Compounds of O-H, CH3, m-CH3, m-, n-CH3O, Cl, Br - liquids that are well distilled in a vacuum, have a characteristic arsenic trichloride odor, dissolve well in both polar and non-polar solvents, and are quite stable during storage. However, water and other solvents with active hydrogen atoms, when heated, can start interaction:

$$XC_6H_4AsCl_2 \xrightarrow[-HCl]{ROH} XC_6H_4As(OR)_2$$

Phenylarsine dichloride (Los K. Synthetic poisons, 1963), which is part of the group of chemical warfare agents, as well as its synthesized derivatives, discussed in this section, have a pronounced skin-blistering effect.

The experimentally found and calculated values of the elemental analysis of arsenic, as well as the molecular refraction data of the synthesized arylarsine dichlorides, confirm their compliance with the accepted structures. The found data of atomic refraction to arsenic averaged 11.63 for these compounds, which is also within the normal range and complies with literature data.

Table 1

Arylarsindichlorides $XC_6H_4AsCI_2$

№	X	B. t., °C - p, mmHg	M.t. ,°C	d_4^{20}	n_d^{20}	MR_D		AR_D, As	Output %	As, %	
						found	calculated			found	calculated
I	p-H	112-13/2	-	1.6504	1.6371	38.49	37.14	11.35	68	33.17	33.63
II	p-CH_3	-	40	-	-	-	-	-	72	31.29	31.64
III	p-CI	112-23/1	-	1.7476	1.6491	53.67	42.00	11.67	84	28.97	29.12

IV	p-Br	143-44/2	33	1.9975	1.6741	56.73	44.90	11.63	73	24.65	24.83
V	p-OCH_3	140-41/1	-	1.6764	1.6695	56.33	43.40	12.93	62	29.17	29.64
VI	p-I	-	41	-	-	-	-	-	56	21.09	21.48
VII	p-NO_2	128/2	30	1.5640	1.6217	-	-	-	61	27.54	27.98
VIII	m-CH_3	128/2	-	1.5640	1.6217	53.34	41.76	11.53	74	31.17	31.64
IX	m-CI	128/2	-	1.7582	1.6443	53.04	42.00	11.04	76	29.05	29.22
X	m-Br	187/4	-	2.0079	1.6678	56.03	44.90	11.13	70	24.57	24.83
XI	m-OCH_3	135-36/1	-	1.6264	1.6300	55.34	43.40	11.94	69	29.31	29.64
XII	m-NO_2	-	51	-	-	-	-	-	77	27.79	27.98
XIII	o-CH_3	91-93/2	-	1.5840	1.6298	53.22	41.76	11.46	81	31.25	31.64
XIV	o-CI	156-57/2	44	1.7732	1.6413	52.39	42.00	11.39	80	2.029	29.12
XV	o-Br	-		-	-	-	-	-	66	24.35	24.83
XVI	o-OCH_3	-		-	-	-	-	-	75	29.29	29.64
XVII	o-NO_2	-		-	-	-	-	-	64	27.63	27.98

o-tolylarsine dichloride synthesis.

A hydrochloric acid solution of o-tolylarsonic acid was placed in a 2L round bottom flask equipped with a reflux condenser. A 10% alcohol solution of iodine was added. The reaction mixture was heated to a boil in a water bath and, maintaining this temperature, a strong stream of sulfur dioxide was applied. After the recovery process was completed, the aqueous layer was drained, the product was extracted with benzene. The resulting solution was filtered, the solvent was distilled off, and the residue was distilled in vacuum. 98g (96%) of the product were isolated. B.t. 93°C (1mm Hg); n_D^{20} 1.6298; d_4^{20} 1.5846 (gradually crystallizes, M.t. 41°C).

Arsenic content, %: Found As 31.44 $C_7H_7AsCl_2$. Calculated As 31.64. IR o-tolylarsine dichloride contains all the main absorption bands characteristic of the aromatic ring in the

region of 7 As–Ph 1070-1130; δ Ph - As 485 cm^{-1}. RS contains in the region of 360–395 cm^{-1} very strong bands characteristic of ν_{as} and ν_{s} $AsCl_2$ vibrations. PMR contains resonant signals of aromatic protons at δ 7.11-7.83, methyl group at δ 2.45 m.d. regarding TMS.

Using a similar technique, phenyl-o-, m-, p-tolyl-, anisyl-, chloro-, bromo-, nitrophenylarsine dichlorides (I-XVII) were obtained, some physical constants and analytical data of which are given in Table 1.

Summary

The chemistry of organic arsenic compounds has many methods developed to obtain organic arsenic derivatives of various classes. An analytical review of the synthesis of primary arsines and the corresponding arsine dihalides was carried out in the work, their negative and positive points were analyzed. The most effective method has been tested and recommended.

Conclusions

The intensive development of the chemistry of organic element compounds, including in the field of the study of derivatives of the fifth group, poses new challenges. The author expresses confidence that in choosing a research strategy for organic arsenic compounds, this work will serve as a major asset for chemists.

Acknowledgments

The work is performed according to the Russian Government Program of Competitive Growth of Kazan Federal University.

References

Abbers H., Kunzel W. und Schuler W. (1952). Zur Kenntnis der acylierten Arsenwasserstoff- und Phosphorwasserstoff-Derivate und der Isoarsile// Chem.Ber. - 1952. - v.85. - p.239-249.

Blicke F.F. and Oneto J.F. (1935). A Purther Study of Phenyl- and Diphenylarsines // J.Amer.Chem.Soc. - 1935. - v.57. - p. 749-753.

Brooker A.B. et al. (1958). Study of the reaction of tetrafluoroethylene with arsenic trichloride in the presence of aluminum chloride // ZhOKh. - 1958. - v.28. - p. 350-355.

Brooker A.B., Nikiforova N.M. (1958). A new method for producing arsenic-aromatic compounds by oxidation of air with a mixture of phenylhydrazine and arsenic trichloride in the presence of copper chloride // ZhOKh. - 1958. - v.28. - issue 9. - p. 2407-2412.

Cavell R.G., Dobbil R.C. (1967). A Convenient and Efficient Preparation of Trifluoromethyl-phosphorus and –arsenic Hidrides// J.Chem.Soc. - 1967. - A. - p.1308-1310.

Cookson R.C. and Mann F.G. (1949). The Cyanoethylation of Amines and Arsines // J.Chem.Soc. - 1949. - p. 67-72.

Cragoe E.I., Andres R.I., Coles R.F., Morgan I.F. and Hamilton C.S. (1947). Derivatives of Methylphenilarsine//J.Amer.Chem.Soc. - 1947. - v.69. - p. 925-926.

Cullen W.R. (1961). Improved Preparation of bistrifluoromethylaraine//Can.J.Chem. - 1961. - v.39. - p. 1855-1857.

Cullen W.R. (1966). Organoarsenic chemistry // Advances in organometallic chemistry.N.Y.:Academic Press, 1966. - p.198.

Emeleus H.J., Haszeldine R.N. (1953). Walaschewsky E.G. Organometallic and Organometalloidal Fluorine Compounds: Part VI. Trifluoromethyl Arsenicals// J.Chem.Soc. - 1953. - p. 1552-1564.

Feltham, R. D.; Kasenally, A.; Nyholm, R. S., (1967). A new synthesis of di- and tri-tertiary arsines // J.Organometal.Chem. - 1967. - v.7(2), p. 285-288.

Fichter F. and Elkind E. (1916). Elektrochemische Versuche mit organischen Arsen-Verbindungen. - Ber. - 1916. - 49. - P.239-251.

Freidlina R.Kh. (1945). Synthetic methods in the field of organometallic arsenic compounds. - M., L., Academy of Sciences of the USSR. - 1945. - 180 p.

Iambushev F.D., Kokorev G.I., Khalitov F.G. et al. (1983). Synthesis and properties of arylarsindichlorides // ZhOKh. - 1983. - v.53. - p. 2478-2482.

Issleib K. and Tzschach A. (1961). Uber Alkil-organoarsenide// Angrew.Chem. - 1961. - B.73. - p. 26.

Johnson W.S. and Pechwkas A. (1937). Hydrogen Compounds of Arsenic.II.Sodium and Dihydrogen Arsenides//J.Amer.Chem.Soc. - 1937. - v.59. - p.2068-2071.

Kamai G., Gatilov Iu.F. (1961). On asymmetric tertiary arsines: I. Phenylethylalkylarsines and their derivatives // ZhOKh. - 1961. - v.31. - p. 1844-1847.

Kockel B. (1956). Weitere Berechnung der Grundzustandes des H_2-Molekuls//Z.Naturforsch. - 1956. - B.11A. - p.736-751.

Lang L.H., Emeleus H.I., Briscoe H.V.A. (1946). The Difluoroarsines // J.Chem.Soc. - London. - 1946. - p. 1123-1126.

Los K. Synthetic poisons. - M.: I. L., 1963. - 258 p.

Michaelis A. (1894). Loesner Veber nitrirte Phenylarsenverbindungen. - Ber. - 1894. - v.24. - p. 263-272.

Michaelis A., Reese A. (1882). Uber aromatische Antimonverbindungen und eine neue Bildungsweise aromatischer Arsenverbindungen. - Ber. - 1882. - v.15. - N 27. - p.2876-2877.

Michaelis A., Schulte C. (1982). Uber arsenobensol, arsenonaphtalin, and phenilkakodyl. - Ber. - 1982. - v.15. - N 24. - p.1952-1955.

Newbery G. and Philips M.A. (1928). Gertain Aryl Arsenoxides and the Corresponding Dichloro- and Di-iodoarsines.-// Chem. Soc., - 1928. - p. 2375-2381.

Pabmer A.W., Dehn W.M. (1901). Ueber primare Arsine. - Ber. - 1901. - Jahrg.34. - p. 3594-3599.

Rapoport F.M., Iliinskaia A.A. (1963). Laboratory methods for producing pure gases. - M.: Goskhimizdat. - 1963. - 419 p.

Stone F.G. and Burg A.B. (1954). Chemistry of Arsenic-Borch Bonding Arsine Borines and Arsinoborine Polymers// J.Amer.Chem.Soc. - 1954. - v.76. - p. 386-389.

Tzschach A. and Pacholke G. (1964). Zur Darstellung der dieekunderen Arsine.//Chem.Ber. - 1964. - N97. - e. 419-425.

Tzschach A., Lange W. (1964). Zur Darstellung von Kaliumdiarylund- alkylarylarsiden aus tertiren Arsinen//Z.Anorg.Allg.Chem. - 1964. - v.330. - p. 317-323.

Wigren N. (1930). Mitteilung aus den Laboratorium fur Organ Chemie der Universitat Upsala (Prof.Dr.L.Ramberg)//J. Prakt.Chem. - 1930. - v.126. - p.223-233.

Decision-making supporting algorithm for choosing the duration of the audio communication session in a mobile ad-hoc network

Kostiantyn Polshchykov *
Sergej Lazarev
Elizaveta Kiseleva

ABSTRACT

The article presents the research results on the development of the decision-making support algorithm for choosing the duration of audio communication sessions, which allows transmission of audio streams with a given quality level in a mobile ad-hoc network.The recommended communication session duration depends on the limiting number of packets in the audio stream, which is calculated based on the mathematical models, which describes the average volume of a multimedia message which can be transmitted in the given network parameters with the required quality. The proposed algorithm implementation will allow the ad-hoc node to display a message about the recommended audio communication session length.
KEYWORDS: decision-making supporting algorithm, duration of the audio communication session, mobile ad-hoc network.

Algoritmo de soporte para la toma de decisiones al elegir la duración de la sesión de comunicación de audio en una red móvil ad-hoc

RESUMEN

El artículo presenta los resultados de la investigación sobre el desarrollo del algoritmo de soporte de toma de decisiones para elegir la duración de las sesiones de comunicación de audio, que permite la transmisión de secuencias de audio con un nivel de calidad dado en una red móvil ad-hoc. La duración recomendada de la sesión de comunicación depende del número límite de paquetes en la secuencia de audio, que se calcula en función de los modelos matemáticos, que describe el volumen promedio de un mensaje multimedia que se puede transmitir en los parámetros de red dados con la calidad requerida. La implementación del algoritmo propuesto permitirá que el nodo ad-hoc muestre un mensaje sobre la duración recomendada de la sesión de comunicación de audio.
PALABRAS CLAVE: algoritmo de soporte para la toma de decisiones, duración de la sesión de comunicación de audio, red móvil ad-hoc.

**Belgorod State University 85 Pobedy str., Belgorod, Russia.*

Recibido: 11/10/2019 Aceptado: 12/11/2019

Introduction

In the process of conducting search and rescue operations and emergency situations countermeasures, the great importance acquires the forces and means management organization through the provision of effective information exchange. At the same time, tasks are often carried out under the conditions of an inoperable (damaged) or missing telecommunications infrastructure and possible destructive external influences (Cheong et al., 2011; Polshchykov et al., 2017a). To transfer information in such situations, it is preferable to deploy a mobile ad-hoc network (MANET), which is capable of operating without base stations and has an arbitrary decentralized topology (Basagni et al., 2004; Polshchykov et al., 2018a).

MANET belongs to the class of packet data networks. With the packet transmission of audio streams, slight losses of individual packets are allowed. Lost voice information can be recovered using an approximation based on previous and subsequent data. However, significant packet loss cannot be recovered using this method. This leads to an unacceptable reduction in audio communication quality (Polshchykov et al., 2017b; Konstantinov et al., 2017).

The main causes of packet loss in MANET are network nodes random movement, their on and off switching, as well as the bit errors occur due to the low power of transmitting devices. Under conditions of significant packet loss, it is recommended to limit the length of transmitted messages or reduce the length of audio streaming sessions.

The purpose of the research presented in the article is to provide the choice of the audio communication sessions duration, with which it is possible to transfer an audio stream with a given quality level in a MANET. To achieve this goal, it is required to develop a decision-making supporting algorithm on the choice of audio streams transmission duration in a mobile ad-hoc network.

1. Task assessment

Assume that the audio stream consisting of α packets is transmitted with acceptable quality if no packets were lost in the delivery process or the data of all lost packets were successfully restored. In this case, to recover the loss of one packet at the

receiving node, you need to get at least βprevious packets and at leastβsubsequent packets. Also, are given the following values:

*P*isthe required probability of audio stream transmitting with acceptable quality;

*L*ispacket bit length;

*C*isinformation bit rate;

t is required to develop an algorithm for choosing the valueτisthe duration of the audio stream transmission.

2. Algorithm Development

The audio stream transmission duration depends on the value α – the number of packets in a stream. The following expression can be used to calculate the valueτ:

$$\tau = \frac{\alpha L}{C}. \tag{1}$$

There commended value o fα can be obtained based on the mathematical models, which describes the average volume of a multimedia message which can be transmitted with the required quality with the specified operation characteristics of the MANET (Polshchykov et al., 2018b):

$$P = \sum_{b=0}^{c} k_{\alpha,b} \cdot p^{\alpha-\beta} \cdot q^{b}, \tag{2}$$

where q – is the packet loss probability in the process of an audio stream transmitting; $\alpha = \beta \ldots \infty; \alpha \in N; \quad \beta \in N$;

$$p = 1 - q; \tag{3}$$

$$c = \left\lceil \frac{\alpha - 2\beta}{\beta + 1} \right\rceil; \tag{4}$$

$$k_{\alpha,0} = 1; \tag{5}$$

$$k_{\alpha,1} = \begin{cases} 0, & \alpha \le 2\beta; \\ \alpha - 2\beta, & \alpha > 2\beta; \end{cases} \tag{6}$$

$$k_{\alpha,2} = \begin{cases} 0, & \alpha \le 3\beta + 1; \\ \sum\limits_{i=2\beta+1}^{\alpha-(b+1)} k_{i,b-1}, & \alpha > 3\beta + 1. \end{cases} \tag{7}$$

By performing calculations using expressions (2) – (7), it is possible to create a relational database containing the recommended values of $\alpha$for different values of β, $q$and$P$.Table 1 presents an example of the fragment of the specified database.

Table1 – Values of αat β=2

q	P				
	...	0,85	0,86	0,87	...
...	...	...	...	...	...
0,028	...	38	30	22	...
...	...	...	...	...	...
0,030	...	30	22	16	...
...	...	...	...	...	...
0,032	...	22	16	10	...
...	...	...	...	...	...

The value of the packet loss probability can be calculated by the formula:

$$q = \frac{K_{loss}}{K_{sum}}, \tag{8}$$

where K_{loss} is the number of packets lost during the specified observation period; K_{sum} – the total number of packets received by the node during the specified observation period.

3. Algorithm scheme

Fig. 1 shows a scheme of the desicion-making supporting algorithm for choosing the duration of an audio communication session in a MANET (Verma and Chauhan, 2015).

The following notation is used in the algorithm scheme:

$i$isthe received packet sequence number;

n_i isnumber in the stream of i-th received packet.

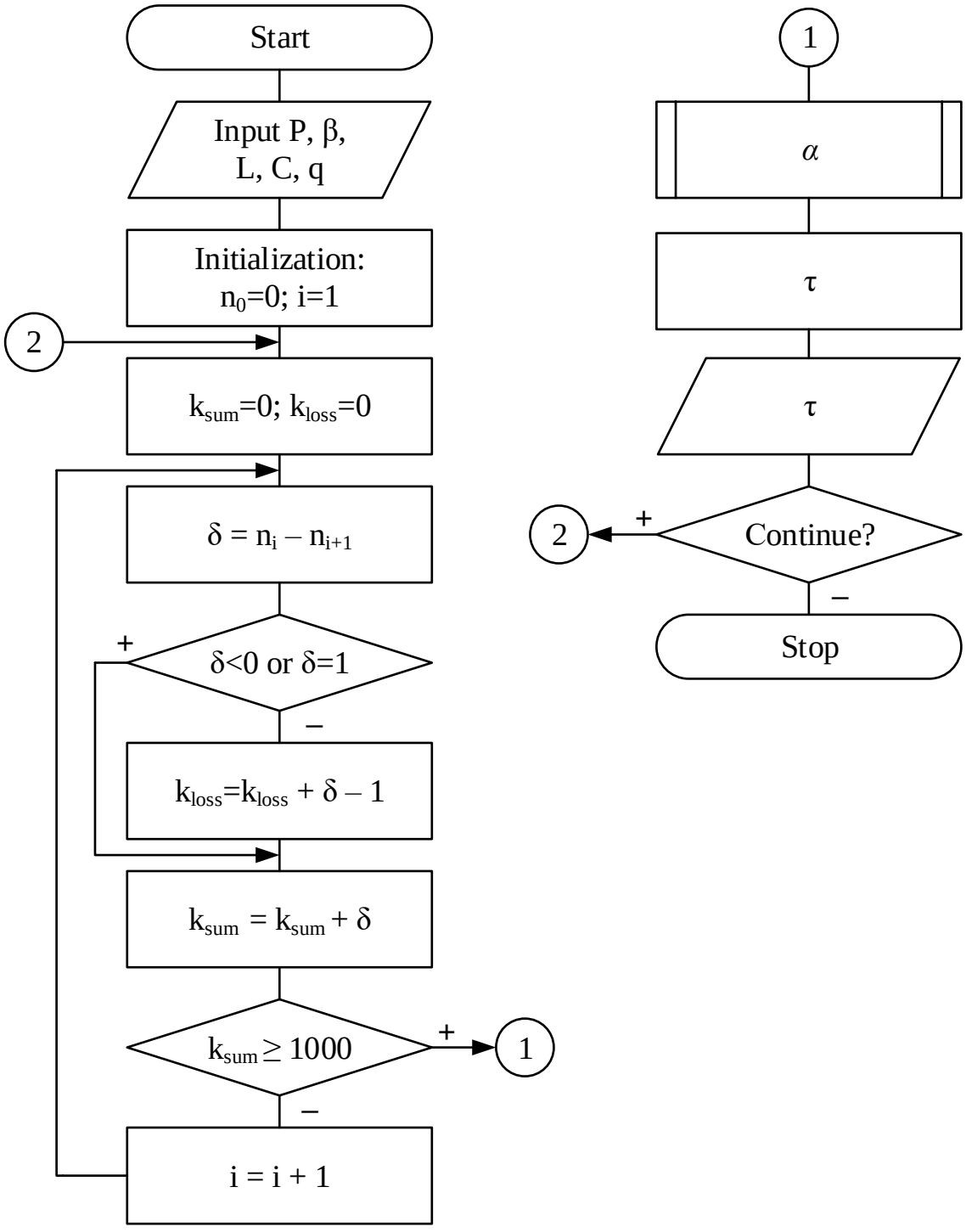

Fig. 1 – Scheme of the algorithm

As a result of the algorithm execution, the message with the recommended length of the audio communication session will be displayed on the ad-hoc node screen.

Conclusion

Thus, in the article was developed an algorithm for estimating the recommended duration of audio stream transmission in a MANET.The calculation of this value is based on mathematical models, which allow obtaining the value of packets number with which the audio communication session will be carried out with acceptable quality.

The direction of further research will be the development of software for implementing the proposed algorithm and obtaining experimental results.

Acknowledgments

The research is carried out with the financial support of the Ministries of Education and Science of the Russian Federation, project: 2.5681.2017/BP.

References

Cheong S.H., Lee K.I., Si Y.W., U L.H., (2011). Lifeline: Emergency Ad Hoc Network. Proc. of 7th International Conference "Computational Intelligence and Security (CIS)". Hainan: 283–289.

Basagni S., Conti M., Giordano S., Stojmenovic I., (2004). Mobile Ad Hoc Networking. IEEE Press, 461.

Konstantinov I.S., Polshchykov K.O., Lazarev S.A., Zdorovtsov A.D., (2017). Mathematical Models for Estimating Radio Channels Utilization When Transmitting Real-Time Flows in Mobile Ad Hoc Network. Journal of Fundamental and Applied Sciences, 9(2S): 1510–1517.

Polshchykov K., Lazarev S., Zdorovtsov A., (2017 b). Multimedia Messages Transmission Modeling in a Mobile Ad Hoc Network. Proc. of the 11th International Conference on Application of Information and Communication Technologies (AICT). Moscow: 24–27.

Polshchykov K.O., Lazarev S.A., Zdorovtsov A.D., (2017 a). Neuro-fuzzy control of data sending in a mobile ad hoc network. Journal of Fundamental and Applied Sciences, 9(2S), 1494–1501.

Polshchykov K.A., Lazarev S.A., Zdorovtsov A.D., (2018 a). Evaluation of channel accessibility waiting period prediction channel to transmit real-time streams in mobile ad hoc network. Journal of Advanced Research in Dynamical and Control Systems, 10 (4): 1460–1467.

Polshchykov K.O., Lazarev S.A., Kiseleva E.D., (2018 b). Mathematical Model of Multimedia Information Exchange in Real Time Within a Mobile Ad Hoc Network. International Journal of Computer Science and Network Security, 18 (6): 20–24.

Verma H., Chauhan N., (2015). MANET based emergency communication system for natural disasters. Proc. of International Conference "Computing, Communications & Automation (ICCCA)". Noida: 480–485.

Software complex for measuring operating systems' main functions performance

Alexey I. Martyshkin *

ABSTRACT

This paper describes the software package created by the author for measuring the performance of operating system functions. This work aims to synthesize a software package designed to analyse the execution time of software functions of uniprocessor and multiprocessor operating systems. The package analyses a number of functions of operating systems: mutexes, semaphores, read-write locks, FIFO and PIPE channels, TCP and UDP sockets, context switching, system calls. Unlike analogues, this package is represented by a convenient graphical user interface; the Qt and Qwt libraries are used for its implementation, they have a rich set of widgets, i.e. programs that facilitate access to information. The libraries used are cross-platform, which allows us to make a simpler procedure for transferring applications to different operating systems; smoothing the test results curves is used. In conclusion, the results of test measurements are presented.

KEYWORDS: Linux, performance measurement, operating system functions, QT and QWT libraries, C ++ language.

Paquete de software para medir el rendimiento de las funciones principales de los sistemas operativos

RESUMEN

Este documento describe el paquete de software creado por el autor para medir el rendimiento de las funciones del sistema operativo. Este trabajo tiene como objetivo sintetizar un paquete de software diseñado para analizar el tiempo de ejecución de las funciones de software de los sistemas operativos uniprocesador y multiprocesador. El paquete analiza una serie de funciones de los sistemas operativos: mutexes, semáforos, bloqueos de lectura y escritura, canales FIFO y PIPE, zócalos TCP y UDP, cambio de contexto, llamadas al sistema. A diferencia de los análogos, este paquete está representado por una conveniente interfaz gráfica de usuario; las bibliotecas Qt y Qwt se utilizan para su implementación, tienen un amplio conjunto de widgets, es decir, programas que facilitan el acceso a la información. Las bibliotecas utilizadas son multiplataforma, lo que nos permite hacer un procedimiento más simple para transferir aplicaciones a diferentes sistemas operativos; se utiliza el suavizado de las curvas de resultados de la prueba. En conclusión, se presentan los resultados de las mediciones de prueba.

PALABRAS CLAVE: Linux, medición de rendimiento, funciones del sistema operativo, bibliotecas QT y QWT, lenguaje C ++.

*Candidate of Technical Sciences, Associate Professor, Computational Machines and Systems Department, Penza State Technological University (440039, Russia, Penza, 1/11 Baydukova passage / Gagarina st., 1/11 e-mail: alexey314@yandex.ru)

Recibido: 30/07/2019 Aceptado: 11/09/2019

Introduction

The goal was set to develop a software package designed to analyse the execution times for software functions of uniprocessor and multiprocessor operating systems. The performance measurement for various functions of an operating system is necessary not only for the operating system developers to evaluate the effectiveness of the implementation of a particular function and to compare the performance of its implementation in other operating systems, but also for application programmers (Biktashev and Martyshkin, 2013), who need to measure the performance of the operating system functions to select the most suitable implementation for their projects (especially for large software systems projects) (Ivanov et al., 2017; Skvortsov and Pyurova, 2016). Implementations of the same operating system functions can significantly differ in different operating systems both in performance and in the ways of working with them (Duplenko, 2013 a,b). For this reason, a developer can select the most preferred tools for development in a specific operating system, or vice versa - choose an operating system in which the implementation of these functions most optimally meets the requirements of the designed software.

1. Formulation of the problem

The software package should perform testing of operating system functions, such as:

- Means for synchronizing processes (threads): mutual exceptions (mutexes), semaphores, read-write locks;
- Means of interprocess exchange: named FIFO channels, unnamed PIPE channels, TCP and UDP sockets;
- Context switching;
- System calls (read, write, open, close).

Currently, the software package Lmbench is widely used, which allows testing nix-compatible systems, incorporating a wide range of tests for various operating system subsystems (Stevens, 2003, 2007). The Lmbench composition includes tests for determining the following characteristics:

a) interprocess exchange means; b) means for synchronizing processes (threads); c) system calls; d) context switching.

This package allows its user to get a fairly holistic view of the tested operating system, to identify the strengths and weaknesses of the implementation of specific functions. But, on the other hand, the Lmbench package does not have a graphical interface and each type of testing is presented by a separate program that must be launched from the command line with some arguments passed.

From the foregoing, it is clear that the LMbench package has a number of drawbacks that make working with it inconvenient, requiring repeated repetition of the same actions and additional calculations to obtain results. Repeatedly invoking the testing program also makes the testing procedure with Lmbench a cumbersome, time-consuming procedure.
Thus, the software package developed for testing the operating systems' functions makes the testing work more convenient, more productive, and affordable than the LMbench software package.

For the development of a software package, tasks that are supposed to be solved with its help are specified: 1) Selection of the tested functions; 2) Collection of test results; 3) Processing the results; 4) Displaying the received statistics in the form of graphs; 5) Displaying the results in a separate window; 6) Colour settings for displaying data; 7) Smoothing charts. Analysing the set tasks, we conclude about the input and output data of the developed software package. Input data are: a) name of the tested function; b) a colour palette for displaying results; Output data are: a) Graphs of the results obtained; b) Display of results that do not require presentation in the form of graphs.

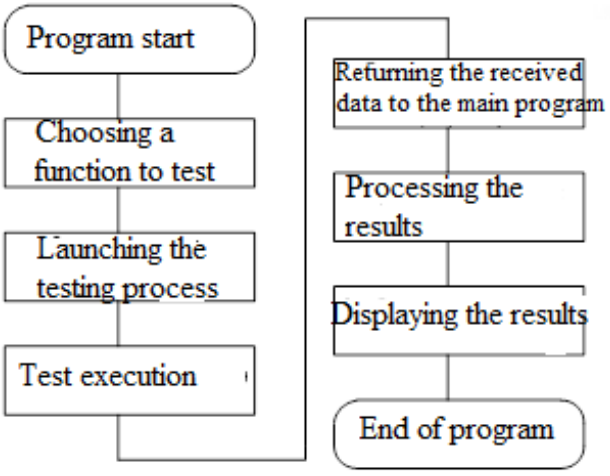

Fig. 1. The operation algorithm of the developed software package

The objectives of the study are:

- to determine the composition of U-functions (the software function of the operating system

kernel associated with any system call) that implement the network and transport levels;

- to measure the execution time of each U-function in the process of transmitting data blocks;

- to determine the probabilistic characteristics of the call and processing of U-functions;

- to determine the dependences of the probability-time characteristics that determine the computation system performance depending on the traffic parameters and the characteristics of network devices.

Network protocols are implemented programmatically in the operating system kernel as a set of U-functions.

Since these protocols are implemented in software, the performance of the network and transport layers of the OSI network model can be measured using software tools. To do this, we can use software monitors (Martyshkin, 2016a; Martyshkin et al, 2018a).

Monitors of the tracer type (tracers) are programs that record the specified parameters of the computing process at specific points. Each such point corresponds to a specific event in the work of the computation system, and when it passes, a transmission is organized to the measurement monitor programs that collect, accumulate and display measurement information.

2. Mathematical model of work with semaphores

Semaphores are used to coordinate the use of single or fixed sets of resources by several computational processes. The semaphore performance problem is that when processes interact, there are requirements for access to shared resources that lead to a collision of transactions, as they conflict with each other. Conflicts lead to loss of operating system

performance (Martyshkin, 2018, 2016b). This is most characteristic in parallel and multiprogram systems when interacting processes are implemented in independent processors which may require a common resource at the same time. If the resource is required by too many processes, then they are queued. At the same time, requests are satisfied on the basis of: "first in, first out" principle (FIFO) (Martyshkin et al, 2018b; Tanenbaum and Bos, 2015).

We assume that a computer system comprises a common resource available to the set of processes executed in the nodes and n –processor nodes protected by a semaphore S. An analytical model of an n-processor system with a single shared resource for evaluating performance losses due to conflicts over access to the semaphore, using such scheduling concept as FIFO, is shown in Fig. 2 a. The model is presented as an open stochastic queuing network consisting of n (S_1,. .., S_n) queuing systems simulating processor nodes and a single-channel queuing system (S_n +1) which simulates a semaphore. A thread of requests for the execution of processes with intensity $\lambda_0 = 1/T$ arrives at the input of the n-processor system where T is the average duration of the interval between incoming requests (Martyshkin, et al., 2018a).

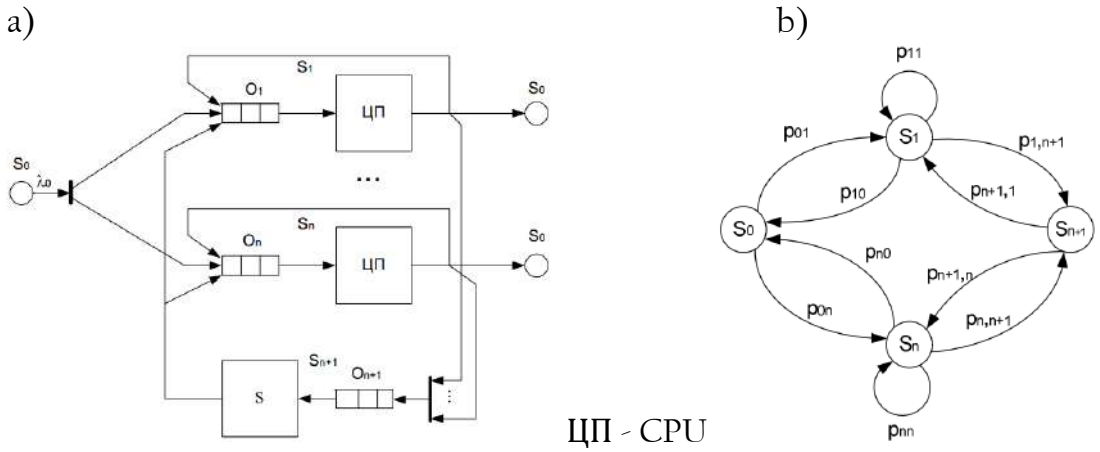

Fig. 2. Diagram of the analytical model of the n-processor system (a) and its flow graph (b)

The request flow is distributed by the preliminary scheduler to the processor nodes with probabilities p_{01},. .., p_{on}, presented in the form of a probability flow graph for the stochastic network shown in Fig. 2, b. We suppose that the flows of requests for the execution of processes at the input of a multiprocessor system are distributed equally

between processor nodes, i.e. $p_{01} = \ldots = p_{on} = 1 / n$. Requests that have been served in the semaphore are an equally likely return to the processor nodes for continued service, therefore, $p_{n+1,1} = \ldots = p_{n+1,n} = 1 / n$.

The waiting time for a request in the network is estimated by

$$T_w = \alpha_1 t_{w1} + \alpha_2 t_{w2} + \ldots + \alpha_n t_{wn} + \alpha_{n+1} t_{wn+1}, \quad (1)$$

Where $\alpha_i = \lambda_i / \lambda_0$ is the network transmission coefficient (i = 1,. .., n +1); t_{wi} is the waiting time in the i-th queuing system. The intensity of request flows is determined by the system of equations: $\lambda_i = \sum_{i=0}^{n} p_{ij} \lambda_j$, where p_{ij} is the probability of transmission from the queuing system S_i in the queuing system S_j ; i, j = 0,1,. .., n + 1

Priority-based scheduling yields almost twice advantage as to waiting time in a queue for a semaphore than using a FIFO- based strategy. The obtained models allow us to make quantitative estimates of the waiting time of processes accessing a shared resource through a semaphore. The models can be used in the designing of parallel operating systems, where the execution time of processes is critical (Martyshkin, 2018).

3. Architecture of the software and hardware package

Work with software package was carried out on a computer running an operating system of the Linux family. To ensure the operability of the program, a nix-compatible operating system with installed Qt and Qwt libraries is required. Having analysed the data on the advantages and disadvantages of modern programming languages, we can conclude that it is most advisable to use the C ++ language to solve the problems posed for a number of the following reasons: support for the paradigm of object-oriented programming, high performance of final programs, etc.

The data structure of the developed software package is shown in Fig. 3. The scheme of the main program algorithm is shown in Fig.4.

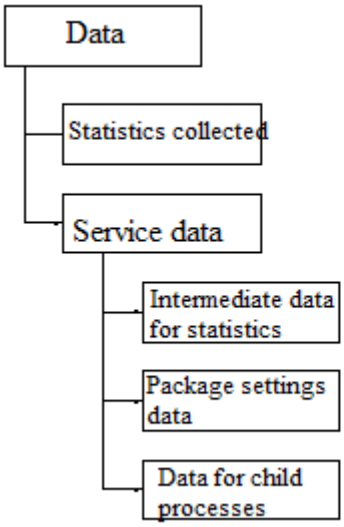

Fig. 3. Data structure of the *software package* under development

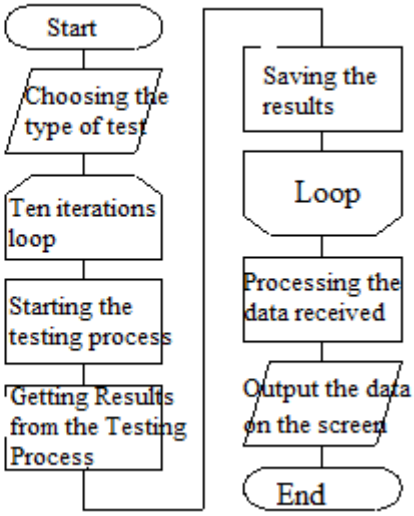

Fig. 4. The scheme of the main program algorithm

4. Program development

In accordance with RAD technology, we outline three stages in the development of the software package:

1) development of a graphical interface for user interaction with the program; 2) the
2) development of functional modules that solve the tasks specified in the Development Task;
3) binding the implementation of the functional part to the graphical interface.

The basis of the future user interface is a multi-window interface. Separate windows are created for various problems to be solved, providing an unloaded interface that is necessary for their solution (Rodríguez et al., 2007; Williams, 2014; Hughes and Hughes, 2004).

In the developed software package, the curve smoothing (filtering) is used. Smoothing is a technology used to eliminate the "jagged" effect that occurs at the edges of a multitude of 2D or 3D images that are displayed separately from one another at the same time. Almost all normal graphics are offered in two forms: raw and smooth. A graph can be built in a straightforward manner from message to message, why it will have angular outlines. But if smoothing is selected, then the graph will have a smoother outline. The

smoothing level and algorithm are the same for all graphs. Smoothing is performed using several consecutive data, and their number is usually selected experimentally.

Figs. 5-6 show the graphs of test results (semaphore and context switching).

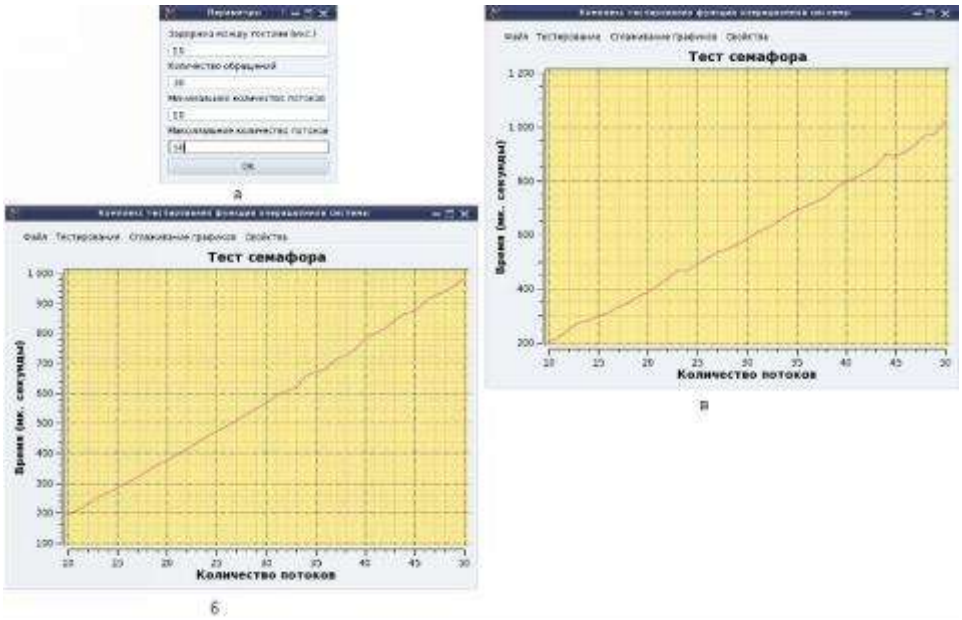

Fig. 5. Semaphore test: setting parameters (a), without smoothing (b), and using the most probable smoothing (c). Fig. 6. Context switching time test: setting parameters (a) without smoothing (b) and using the most probable smoothing (c)

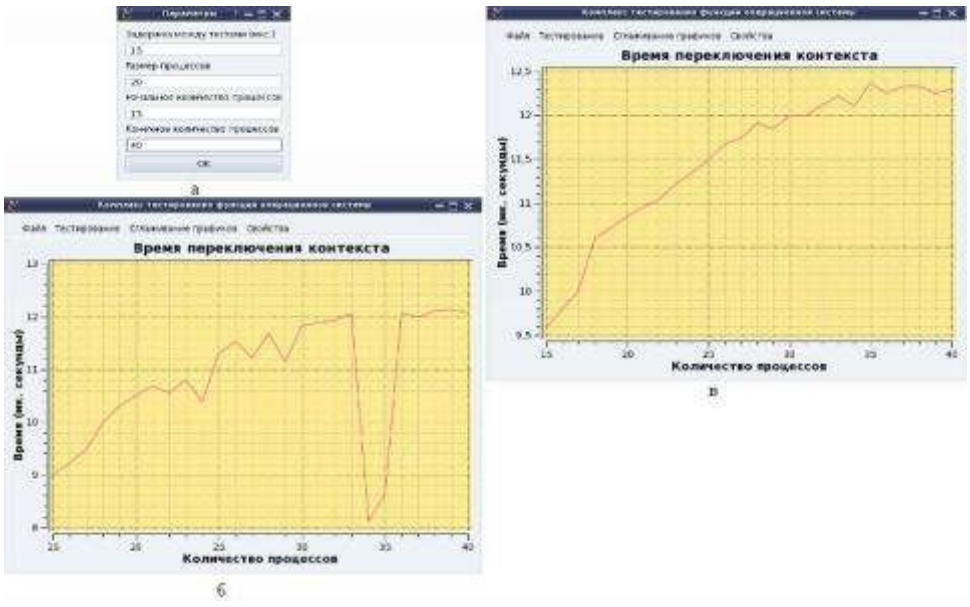

The software package developed is registered with the Federal Service for Intellectual Property.

Conclusions

The software package was developed to test the operating system functions: mutexes, semaphores, read-write locks, FIFO and PIPE channels, TCP and UDP sockets, context switching, system calls (read, write, open, close). After selecting the type of testing, the software package allows us to automatically collect the necessary statistics, process it and display the processing results in a user-friendly form.

Unlike analogues, this package is represented by a convenient graphical user interface, for the implementation of which the Qt and Qwt libraries are used. These libraries have a rich set of widgets, i.e. programs that facilitate access to information, with which we can create a complex graphical interface. The libraries used are cross-platform, which makes it easier to transfer requests to different operating systems.

Acknowledgements

The paper is published with the support of the scholarship granted by the President of the Russian Federation to young scientists and graduate students for 2018-2020. (SP-68.2018.5).

References

Biktashev R.A., Martyshkin A.I. (2013). A set of programs for measuring the performance of operating system functions // XXI Century: Results of the past and problems of the present plus. 2013. No. 10 (14). Pp. 190–197.

Duplenko A.G. (2013a). Comparative analysis of data sorting algorithms in arrays // Young scientist. 2013. No. 8. Pp. 50-53.

Duplenko A.G. (2013b). Evolution of methods and algorithms for sorting data in arrays // Young Scientist. 2013. No. 9. Pp. 17-19.

Hughes C., Hughes T. (2004). Parallel and distributed programming using C ++. 2004.672 p.

Ivanov K.K., Razdobudko S.A., Kovalev R.I. (2017). Parallel sorting methods // Young scientist. 2017. Number 7. Pp. 15-16.

Martyshkin A. I. (2016a). Modern methods of measuring the performance of multicore computing systems // New Information Technologies and Systems: Collection of scientific papers of the XIII International Scientific and Technical Conference. 2016. Pp. 128 - 131.

Martyshkin A. I. (2016b). Semaphore performance problems in parallel systems // Collection of papers of the International scientific-practical conference: in 3 parts. 2016. Pp. 81-83.

Martyshkin A. I. (2018). Mathematical models of semaphores for coordinating access to shared resources of multiprocessor systems // Colloquium-journal.No. 8 (19). part 1. 2018. Pp. 36-39.

Martyshkin A.I., Markin E.I., Tereshkin D.O., Razdobudov S.A. (2018a). Analytical models for evaluating the performance of semaphores of multiprocessor systems // Collection of papers of the XII International Scientific and Practical Conference: in 2 parts. 2018. Pp. 78-81.

Martyshkin A.I., Markin E.I., Zotkina A.A., Razdobudov S.A. (2018b). Modern methods of measuring the performance of multi-core systems with HT technology // collection of papers of the XXV International scientific and practical conference.2018. Pp. 50-52.

Razdobudov S. A., Salnikov I. I. (2018). Research and analysis of the possibility of multithreading when developing software in C ++ // International Student Scientific Herald.2018. No. 3-2. Pp. 334-337.

Rodriguez C.Z., Fisher G., Smolsky S. (2007). Linux. ABC core. - Kudits Press, Moscow, 2007.584 p.

Skvortsov S.V., Pyurova T.A. (2016). Parallel data sorting algorithms and their implementation on the CUDA platform // Vestnik RGRTU. 2016. No. 58. Pp.42-48.

Stevens U.R. (2007). UNIX : developing network requests. Peter, 2007.1039 p .

Stevens U.R. (2003). UNIX : process interconnection. Peter, 2003.576p.

Tanenbaum E., Bos H. (2015). Modern Operating Systems. 4th ed. SPb. : Peter, 2015.1120 p. : ill. (Series "Classic computer science").

Williams E. (2014). Parallel programming in C ++ in action. The practice of developing multi-threaded programs. DMK Press, 2014, 672 p.

Tellurides and native elements in copper-zinc ores of manifestations «Zapadnoe» (Subpolar Urals, Russia)

Konstantin Yu. Kudrin*
Andrey I. Starikov *
Yuriy V. Korzshov *

ABSTRACT

Background: Previously conducted mineralogical and geochemical studies of copper-zinc ores manifestations «Zapadnoe» showed that the feature of pyrrhotite, pyrite, chalcopyrite and sphalerite is an increased content of Ag and industrially significant Au content, as well as the appearance of silver-containing sphalerite. The purpose of this study is to establish the mineralogical form of noble metals in ores. **Methods**: Mineralogical studies were conducted using an electronic scanning microscope JSM-6510LV (Jeol Ltd). 13 samples taken from the core of the wells were studied: 954 determinations of the ore-forming minerals were made, 140 of them recorded the presence of precious metals. **Results**: Precious metals – gold and silver – tellurides are mainly: hessite, stutzite, volynskite, matildite, cervelleite, petzite and sylvanite; rarely native gold. The host mineral matrix is most often sulfides: sphalerite, pyrrhotite, chalcopyrite, pyrite; rarely – galena. **Conclusion**: The angular, xenomorphic form of separation of aggregates and the consistency of the mineral composition of telluride mineralization can be the result of crystallization of a relatively low-temperature melt among thermally more stable silicate and sulfide phases

KEYWORDS: Subpolar Urals, copper-zinc ores, tellurides, native elements

*Yugra State University University, Khanty-Mansiysk, Russia: kudringeo@inbox.ru

Recibido: 11/09/2019 Aceptado: 13/10/2019

Telururos y elementos nativos en minerales de cobre-zinc de manifestaciones «Zapadnoe» (Urales subpolares, Rusia)

RESUMEN

Antecedentes: estudios mineralógicos y geoquímicos realizados previamente sobre manifestaciones de minerales de cobre y zinc «Zapadnoe» mostraron que la característica de pirrotita, pirita, calcopirita y esfalerita es un mayor contenido de Ag y contenido de Au industrialmente significativo, así como la aparición de plata que contiene Esfalerita. El propósito de este estudio es establecer la forma mineralógica de los metales nobles en los minerales. Métodos: se realizaron estudios mineralógicos utilizando un microscopio electrónico de barrido JSM-6510LV (Jeol Ltd). Se estudiaron 13 muestras tomadas del núcleo de los pozos: se hicieron 954 determinaciones de los minerales formadores de mineral, 140 de ellas registraron la presencia de metales preciosos. Resultados: Los metales preciosos - oro y plata - telururos son principalmente: hessita, stutzita, volynskita, matildita, cervelleita, petzita y silvanita; raramente oro nativo. La matriz mineral del huésped suele ser sulfuros: esfalerita, pirrotita, calcopirita, pirita; raramente - galena. Conclusión: La forma angular y xenomórfica de separación de agregados y la consistencia de la composición mineral de la mineralización de telururo pueden ser el resultado de la cristalización de una masa fundida de temperatura relativamente baja entre las fases de silicato y sulfuro térmicamente más estables.
PALABRA CLAVE: Urales subpolares, minerales de cobre-zinc, telururos, elementos nativos.

Introduction

The manifestation «Zapadnoe» was revealed during the prospecting for iron ore in 1988 in the south-eastern exocontact zone of the Khorasur massif (Fig. 1) on the Eastern slope of the Subpolar Urals (Komaritsky S.I. «Preparation of geophysical bases for searches (forward operation) iron ore skarn-magnetite formation on Usininskyarea in 1988-90», JSC «Sosvapromgeologiya», 2001). Assay analysis of copper-zinc ores showed a constant presence of a significant impurity of gold (up to 3.19 g/t, average – 0.36-0.46 g/t) and silver (up to 19.95 g/t, average – 4.39 g/t). The author's resources (the sum of categories P_2 and P_3) were: gold – 8.9 t, silver – 361.1 t.

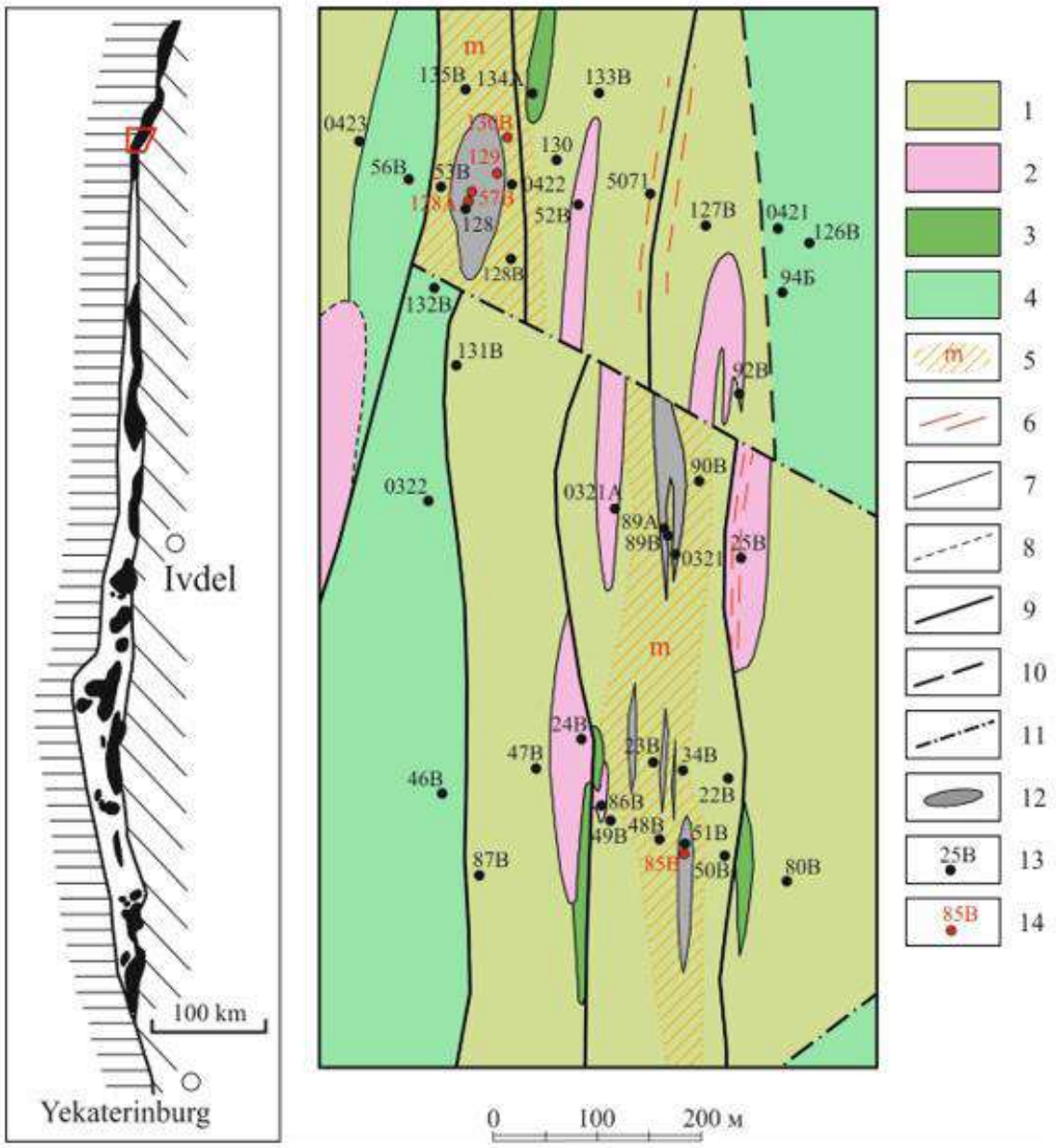

Fig. 1. Schematic geological map of the Zapadnaya area
(byBaturin S.Y., JSC «UGSE», 2009)

1 – tectonic-injection-metasomatic ore-hosting complex. Hornfels on the gabbroids, dike rocks and presumably volcanogenic-sedimentary formations of Shemur suite (O_3-S_1šm), metasomatic rocks undifferentiated; 2 – quartz diorite of the second phase Severorudnichniy complex ($q\delta S_2s_2$); 3 – microgabbro of the second phase of tagilokitlimskiy complex ($\mu\upsilon\delta S_1t_2$); 4 – amphibole and amphibolization gabbro of the second phase of tagilokitlimskiy complex (υS_1t_2); 5 – metasomaticalbite-quartz-chlorite, quartz-epidote-chlorite, epidote-prenite undifferentiated; 6 – blastokataclasite and blastomylonite; 7-8 – geological boundaries: 7 – established; 8 – alleged; 9-11 – tectonic disturbances: 9 – established; 10 – alleged; 11 – by geophysical data; 12 – contours of ore bodies; 13 – exploration wells and their numbers; 14 – exploration wells, the core of which studied noble metal mineralization.

In 2006-2009 on the area «Zapadnaya» was made prospecting for copper (JSC «Ural geological surveying expedition», Yekaterinburg, Baturin S.Y.): there are two complex-structured ore deposits (Zapadnaya and Novaya) (Fig. 1); author's resources of gold of categories P_1+P_2 amounted to 26 tons, silver resources were not estimated. The gold content reaches 24.1 g/t (the average in the ore deposit «Zapadnaya» 0.53 g/t, in the ore deposit «Novaya» – 0.73 g/t); the silver content – up to 69.6 g/t.

Mineralogical and geochemical studies of copper-zinc ores, performed at the Institute of Mineralogy of UrO RAS (Miass), showed that the feature of pyrrhotite, pyrite, chalcopyrite and sphalerite manifestations «Zapadnoe» is an increased content of Ag and industrially significant Au content, as well as the appearance of silver-containing sphalerite. Sphalerite-silver-galena and chalcopyrite-gold-silver-telluride associations are distinguished, «...obviously represented by thin scattered invisible mineralization in chalcopyrite and sphalerite». According to the results of these studies, the manifestation «Zapadnoe» is presumably attributed to the gold-silver-copper-zinc sulfide scarn type. Analogues of the symptoms of copper-zinc ores «Zapadnoe» proposed Tarnierskoedeposit (chalcopyrite) and Sarbaisky (mineralization occurs in) in the North and Middle Urals: the range of available mineralogical characteristics it is recognized as the intermediate between them (Safina et al., 2010).

Thus, the analysis of the results of previous work on the manifestation «Zapadnoe» shows that the question of the form of gold and silver in copper-zinc ores remains open.

1. Materials and methods

Mineralogical studies were conducted on the electronic scanning microscope JSM-6510LV (Jeol Ltd) with energy-dispersive spectrometer INCAEnergy 350 with the detector X-Max 80 (Oxford Instruments Analytical Ltd) at an accelerating voltage of 20 kV, electron beam current of 0.3-0.5 on the time when the set of 10 spectra with (Novosibirsk, Institute of Geology and Mineralogy SB RAS, analyst Karmanov N.S.). Studied 13 samples taken from the core of wells 85B (ore deposit «Novaya») and 57B, 128A, 129, 130B (ore deposit «Zapadnaya») (Fig. 2). A total of 954 definitions of the

composition of ore-forming minerals were performed, of which 140 recorded the presence of precious metals. The nomenclature of noble-metal minerals is determined in accordance with (Zelenov, 1989).

Since the size of the analyzed grains often turned out to be equal to (or slightly less than) the cross section of the analyzer beam, the analysis results also included figures relating to the host mineral matrix. Therefore, when determining the composition of the mineral, an adjustment to the composition of the host mineral was introduced.

1. Results

Gold and silver mineralogy of ores of manifestations «Zapadnoe»

In the composition of manifestations «Zapadnoe» oresthe presence of the following mineral species, in which the noble metals play a major role: hessite, stutzite, volynskite, matildite, cervelleite, petzite and sylvanite; rarely native gold.

Hessite(Ag_2Te) was found in all studied samples in the form of tiny secretions, occasionally reaching 10, extremely rarely – 30 microns. The mineral forms both independent grains and participates in coalescence with other tellurides (rarely with native gold). Most often hessite was observed in sulfides – sphalerite, chalcopyrite, pyrite, pyrrhotite and galena, less often – in silicates (chlorite, biotite, plagioclase, epidote and garnet).

In this regard, it should be noted some features. First, hessite (often together with other tellurides) forms a chain of linearly elongated grains, indicating control of their location by microcracks or intergranular space; this feature is observed only when it is placed in sulfides. Second, the mineral (and intergrowths with other tellurides) occurs, as isometric inclusions does not detect connection with the fracture: in sulfides (with hessite has a rectilinear shape) or silicates (mineral or has wavy and bay border or forms a very thin rash of grains, the nature of the constraint for which an estimate is very difficult).

Willing hessite forms intergrowths (up to gradual mutual transitions) with other tellurides – volynskite, petzite, tellurobismuthite, melonite and altait. Features of the hessite composition according to the results of electron probe studies are given in table 1, the forms of hessite in the ores of the manifestation «Zapadnoe» are shown in figure 3.

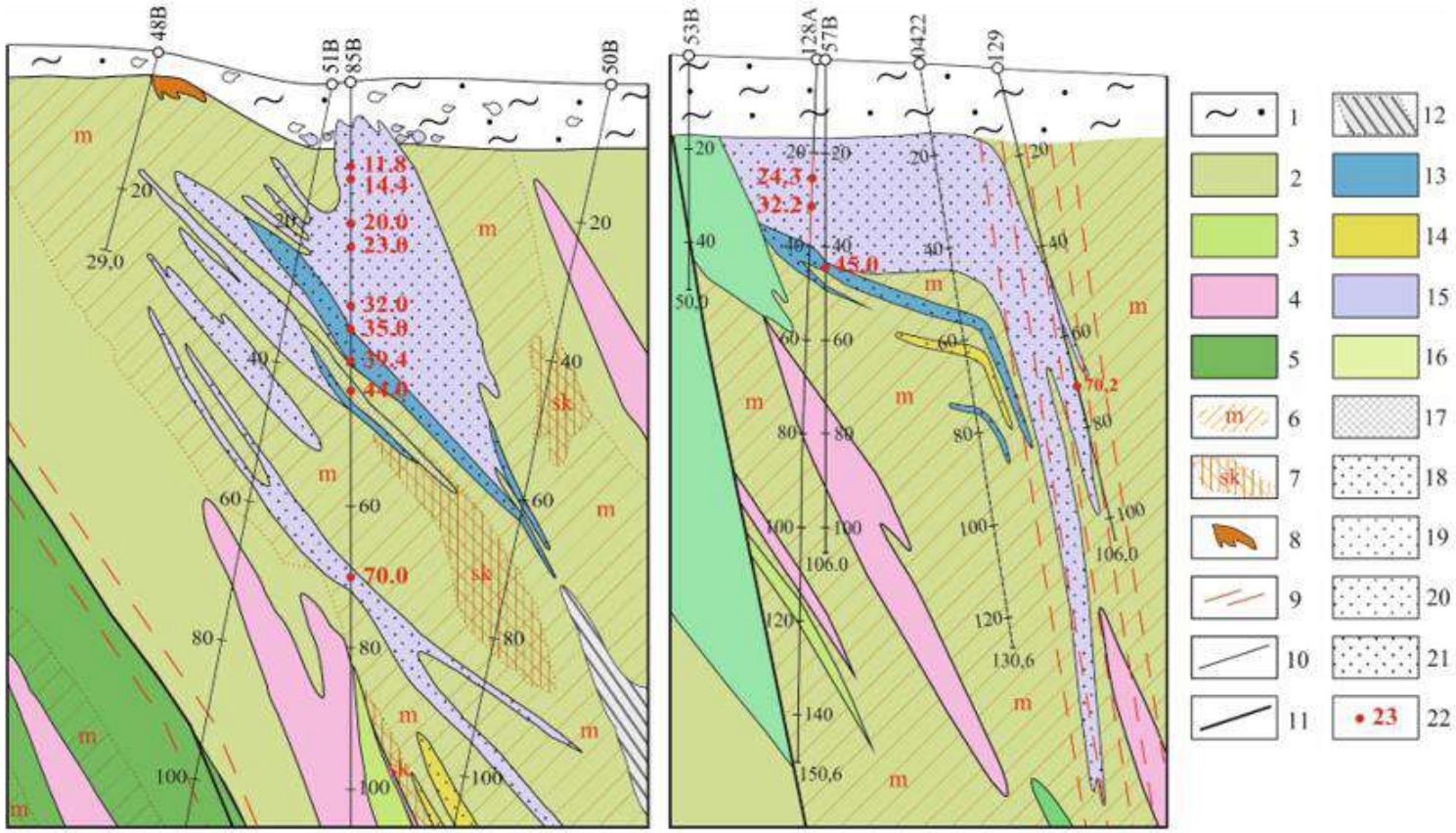

Fig. 2.The manifestation «Zapadnoe». Ore deposit «Novaya» (left) and ore deposit «Zapadnaya» (right) Geological sections (by Baturin S.Y., JSC «UGSE», 2009) and sampling scheme for mineralogical studies 1 – unconsolidated Quaternary sediments; 2 – dykes of spessartites; 3 – tectonic-injection-metasomatic ore-bearing complex; 4 – quartz diorites of the second phase Severorudnichniy complex ($q\delta S_2s_2$); 5 – microgabbro of second phase Tagilokitlimskiy complex ($\mu\upsilon\delta S_1t_2$); 6 – metasomatites; 7 – skarns; 8 – iron hat; 9 – blastomylonite and blastokataclasite; 10 – geological boundary; 11 – tectonic faults; 12 – prospective ore body; 13-16 – pyrite ores: 13 – copper (Cu›0,7%); 14 – zinc (Zn›1%); 15 – copper-zinc (Cu›0,7%; Zn›1%); 16 – sulfur (S›35%); 17-21 – grades of ores (krap by the corresponding color): 17 – solid massive; 18 – impregnated copper; 19 – impregnated zinc; 20 – impregnated copper-zinc; 21 – substandard (Cu‹0.7%; Zn‹1%; S‹35%); 22 – points of material selection for electron probe studies.

Native gold (Fig. 4) recorded in six samples, in all mineralogical types of ore deposits «Novaya» and «Zapadnaya» throughout the vertical scale of mineralization; forms a fine selection, occasionally reaching 12 microns. Usually found alone, rarely observed intergrowths with hessite and petzite. The features of propagation – forms of separation or cracks in the intergranular space of sulphides (sphalerite, chalcopyrite, galena); in the development of secondary minerals (chlorite, epidote, amphibole) have wavy contacts and califoornia. In the composition (table 2) there is always a significant admixture of silver until the appearance of electrum (only in copper-zinc ores). With the depth of the probity of native gold increases.

Table 1. Composition of hessite(%) and characteristics of the host mineral matrix

n	Composition				Host mineral matrix
	Ag		Te		
	min	max	min	max	
Well 85B, depth 11.8 m					
18	54,51	63,52	36,48	42,44	Sphalerite, pyrrhotite
Well 85B, depth 14.4 m					
5	58,23	62,87	37,13	41,77	Sphalerite, plagioclase, chlorite
Well 85B, depth 20.0 m					
10	61,70	63,33	36,67	38,30	Chalcopyrite, chlorite, pyrite, sphalerite, epidote
Well 85B, depth 23.0 m					
5	59,27	62,44	37,56	40,73	Sphalerite, chalcopyrite, pyrite
Well 85B, depth 32.0 m					
1		62,84		37,16	Sphalerite
Well 85B, depth 35.0 m					
7	60,86	63,36	36,64	39,14	Sphalerite, altaite, pyrite, pyrrhotite, chlorite, plagioclase
Well 85B, depth 39.4 m					
5	57,86	64,34	35,66	42,14	Chalcopyrite, chlorite, pyrite, garnet
Well 85B, depth 44.0 m					
15	55,94	63,84	33,15	44,06	Chlorite
Well 85B, depth 70.0 m					
11	61,36	63,70	36,30	38,64	Pyrite, sphalerite, chlorite
Well 57B, depth 45.0 m					
5	62,28	65,06	34,94	37,72	
Well 128A, depth 24.3 m					
1		62,42		37,58	Chalcopyrite
Well 130B, depth 64.6 m					
5	62,44	63,22	36,78	37,56	Sphalerite, pyrrhotite, pyrite

Note: n – number of tests

Petzite (Au_3AgTe_2) rare material recorded in three samples taken from core wells 85B (the deposit «Novaya»), dedicated to the sphalerite (as a rule, the cleavage

cracks), is always present together with the other precious-metal tellurides (hessite, cervelleite), forming small inclusions of irregular shape with size less than 5 microns in all mineralogical types of ores. Features of petzite the results of electron-probe studies is shown in table 3, forms of petzite in ores of «Zapadnoe» manifestations is presented in figure 4.

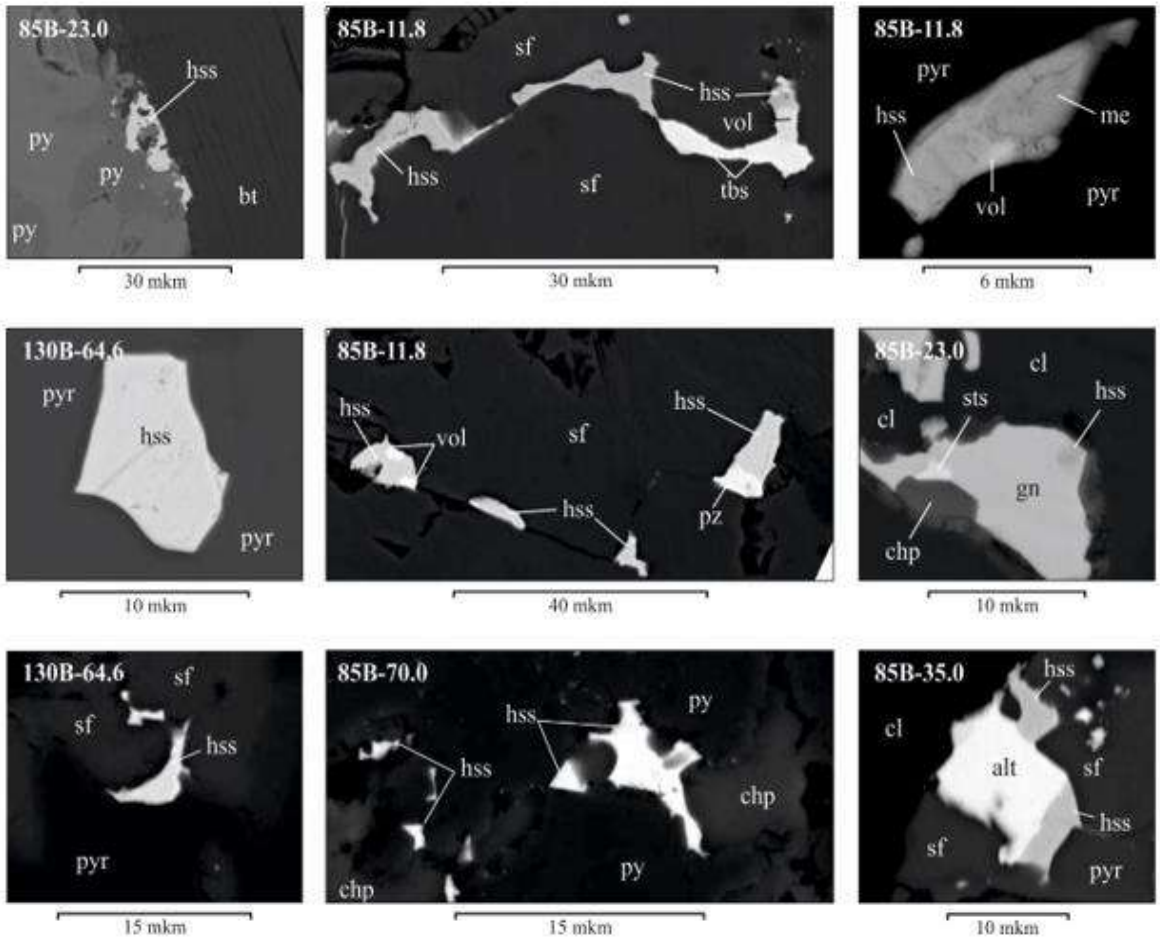

Fig. 3. Forms of hessite in ores of manifestations «Zapadnoe» hss – hessite; me – melonite; pz – petzite; vol – volynskite; tbs – tellurobismuthite; sts – stutzite; alt – altait; py – pyrite; pyr – pyrrhotite; sf – sphalerite; chp – chalcopyrite; gn –galena; bt – biotite; cl – chlorite. In the upper left corner – well number and sampling depth.

Volynskite ($AgBiTe_2$) was observed in two samples of disseminated copper-zinc ores that have been taken from the core bore 85B (the deposit «Novaya»), dated for sphalerite and pyrrhotite, is typically present in the form of intergrowths with

hessite, meloniteand tellurobismuthite, rarely forms pure grain, sometimes having hypidiomorphicsubprismaticshape, reaching up to 15 μm. On contact with chlorite volynskite acquires shapeless lumpy shape. The features of the composition of volynskite according to the results of electron probe studies are given in table 3, the forms of volynskite in the ores of the «Zapadnoe» manifestation are shown in figure 4.

Stutzite (Ag_5Te_3) was observed in three samples of disseminated copper-zinc ores that have been taken from the core bore 85B (the deposit «Novaya»), timed to coincide with pyrrhotite and galena and silicate minerals (epidote and andradite), forming independent grains of isometric shape with a size of up to 7 microns and has a clear sharp limits. Features of stutzitethe results of electron-probe studies is shown in table 3, forms of stutzitein the ore of manifestations «Zapadnoe» shown in figures 3 and 4.

Table 2. Composition of native gold (%) and characteristics of the host mineral matrix

n	Composition				Host mineral matrix
	Au		Ag		
	min	max	min	max	
Well 85B, depth 20.0 m					
4	61,62	65,94	34,06	38,38	Chlorite, plagioclase, sphalerite, chalcopyrite
Well 85B, depth 35.0 m					
1		70,74		15,48	Sphalerite
Well 85B, depth 44.0 m					
2	69,51	69,87	30,13	30,49	Chlorite
Well 85B, depth 39.4 m					
7	67,77	76,23	23,77	32,23	Amphibole, chlorite, chalcopyrite, galena, petzite, plagioclase
Well 85B, depth 70.0 m					
5	60,27	78,02	21,98	39,73	Sphalerite, hessite
Well 128A, depth 24.3 m					
2	47,54	48,93	51,07	52,46	Chalcopyrite

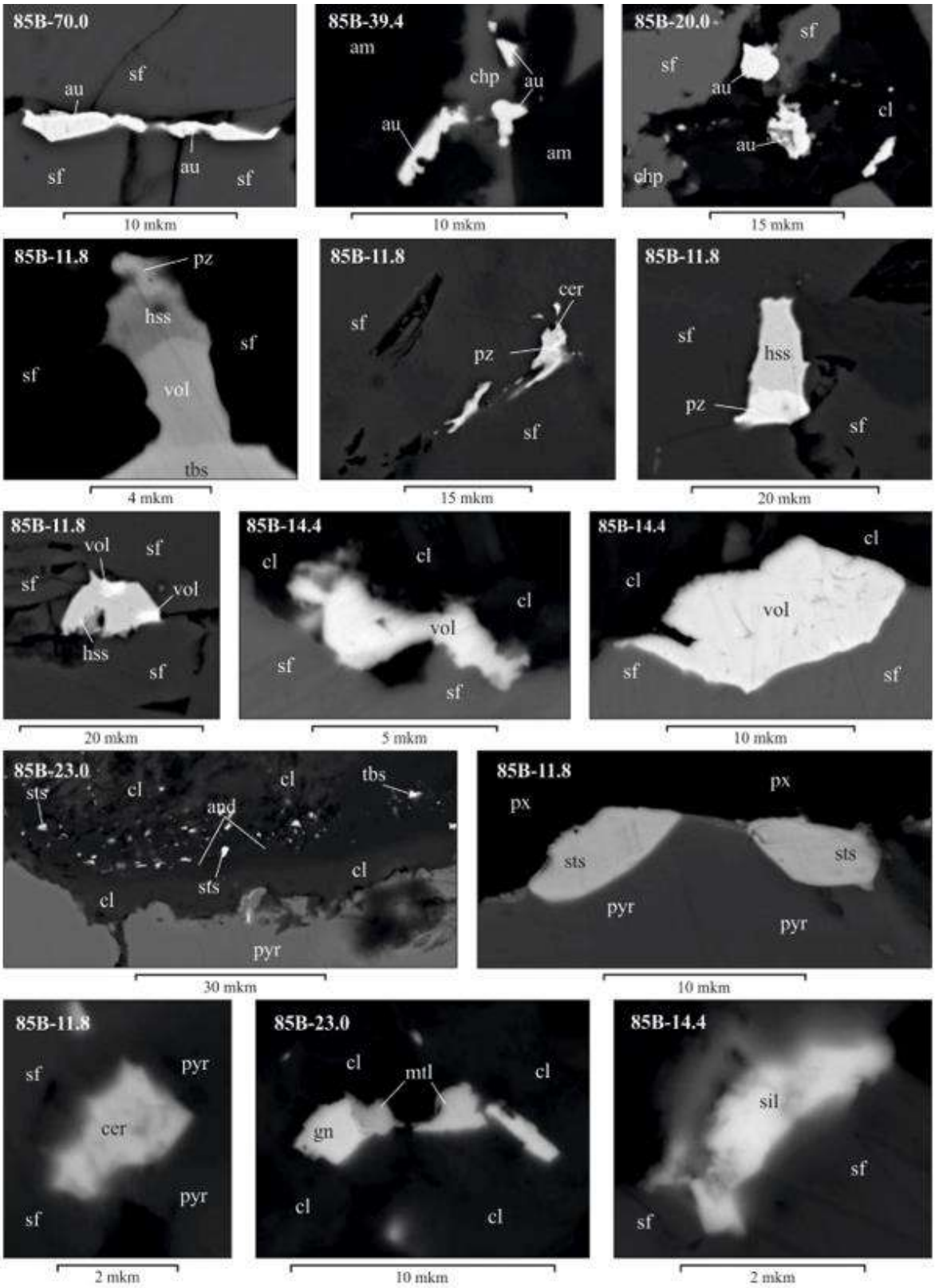

Fig. 4. Forms of native gold (top row), petzite (second row), volynskite (third row), stutzite(fourth row), matildite, cervelleiteand sylvanite(bottom row) in the ores of manifestations «Zapadnoe» au – native gold; am – amphibole; cer – cervelleite; pl – plagioclase; and – andradite; px – pyroxene; mtd – matildite; sil – sylvanite; other abbreviations and symbols see Fig. 3

Table 3. Composition of (%)petzite, volynskite, stutzite, cervelleite, sylvanite andmatildite and characteristics of the host mineral matrix

n	Composition										Host mineral matrix
	Au		Ag		Bi		S		Te		
	min	max	min	max	min	max	min	max	min	max	
Petzite											
Well 85B, depth 11.8 m											
4	23,2	41,7	38,2	44,0					20,1	34,0	Sphalerite
Well 85B, depth 39.4 m											
1		34,6		41,9						23,6	Amphibole, chlorite
Well 85B, depth 44.0 m											
1		24,8		51,0						24,3	Chlorite
Volynskite											
Well 85B, depth 11.8 m											
3			18,2	22,8	35,6	35,9			41,3	46,1	Sphalerite, hessite
Well 85B, depth 14.4 m											
3			18,5	18,7	35,7	36,6			44,6	45,9	Chlorite, sphalerite
Stutzite											
Well 85B, depth 11.8 m											
2			57,7	58,0					42,0	42,3	Pyrrhotite
Well 85B, depth 20.0 m											
1				53,4						40,2	Epidote
Well 85B, depth 23.0 m											
3			59,0	62,6					37,4	41,0	Garnet, galena
Cervelleite											
Well 85B, depth 11.8 m											
3	2,87	4,43	55,6	59,9			2,14	4,88	32,0	39,2	Sphalerite, pyrrhotite
Well 128A, глубина 24.3 m											
1				58,81				5,98		35,2	Sphalerite
Sylvanite											
Well 85B, depth 14.4 m											
1		21,07		23,31						55,6	Sphalerite
Matildite											
Well 85B, depth 23.0 m											
2			21,8	23,0	56,6	58,5	18,4	18,6			Galena, chlorite

Cervelleite (Ag_4TeS), **matildite** ($AgBiS_2$) and **sylvanite** ($(Au,Ag)_2Te_4$) as single grains were found in four samples taken from the core of interspersed copper-zinc ores in wells 85B (deposit «Novaya») and 128A (deposit «Zapadnaya»). Find a close

association with pyrrhotite, sphalerite (cervelleiteand sylvanite) and chlorite (matildite) (Fig. 4). Mineral compositions are given in table 3.

2. Discussion of results and conclusions

These data suggest that:

1. The greatest mineralogical diversity of tellurides and native elements is typical for ores of the deposit «Novaya», in the ore deposit «Zapadnaya» the set of minerals of the considered types is sharply limited.

2. Silver and gold mineralization is represented mainly by tellurides, much less – sulfides and native elements. Minerals often have complex relationships with each other, and there are no signs of substitution of some minerals with others.

Silver forms 5 independent mineral forms (in descending order of importance): hessite (Ag_2Te), stutzite(Ag_5Te_3), volynskite ($AgBiTe_2$), matildite ($AgBiS_2$), cervelleite(Ag_4TeS). Silver in high concentrations (up to 15%) is present in other tellurides: melonite ($NiTe_2$) and tellurobismuthite (Bi_2Te_3).Hessit is a through mineral – fixed in both ore bodies, in all mineralogical types of ores, at all depths. Gold forms 3 independent mineral forms – petzite (Au_3AgTe_2), electrum and native gold. As a permanent and significant impurities present in gold cervelleite(to 3.6%), occasionally in hessite (up 2.5%).

Angular, xenomorphic form of aggregates and consistency of mineral composition of telluride mineralization can be the result of crystallization of relatively low-temperature melt among thermally more stable silicate and sulfide phases (Ciobanu et al., 2006; Tomkins, 2007).

The presence of noble metal telluride mineralization in copper-zinc ores is fixed in many deposits (Bortnikov et al., 1988; Moloshag et al., 2004). Telluriana form of gold and silver in ores may reflect the upper level of the epithermal mineralization similar to deposits Birgildinsko-Tominskiy ore node (Plotinskaya and Trubkin, 2010).

3. Noble metal mineralization is confined mainly to the main ore-forming minerals – sphalerite and pyrrhotite, rarely – galena. The association of gold-silver mineralization with zinc sulfides (sphalerite) demonstrates the proximity of the

manifestation «Zapadnoe» to the modern pyrite constructions Mir and TAG of the Mid-Atlantic ridge (Mozgova et al., 2000).

There is a close spatial and possibly paragenetic relationship with secondary minerals – epidote and chlorite.

4. The features of the geological position of the manifestation «Zapadnoe» and mineralogy of precious metals practically correspond to the Tarnier copper deposit (Belogub et al., 2010). A distinctive feature is the absence of telluride-bismuth mineralization (Belogub et al., 2010) and the confinement of noble metal mineralization to all types of ores.

Conflict of interest

The author confirms that the submitted data does not contain conflict of interest.

Acknowledgement

The work was published with the financial support of the Russian Foundation for basic research and the Government of the Khanty-Mansiysk Autonomous Okrug – Ugra (the contract № 18-45-860008\18) and Russian Geographical Society (the contract № 05-2019-P).

References

Belogub EV, Moloshag VP, Novoselov KA, Kotlyarov VA (2010) Native bismuth, tsumoite and lead-bearing variety of tsumoite of Tarnierskoye copper-zinc massive sulfide deposit (the North Urals). ZapiskiRossiyskogoMineralogicheskogoObschestva, 6: 108–119.

Belogub EV, Novoselov KA, Moloshag VP, et al. (2010) Mineralogy of precious metals in the ores of the Tarnier copper deposit (North Ural). Native gold: typomorphism of mineral associations, conditions of formation of deposits, problems of applied research, vol. 1, Moscow, IGEM RAS.

Bortnikov NS, Kramer H, Genkin AD, KrapivaLYa, Santa-Krus M. (1988). Parageneses of tellurides of gold and silver in the gold Deposit of Florence (Republic of Cuba). Geology of ore deposits, 2: 49–61.

Ciobanu CL, Cook NJ, Damian F, Damian G (2006). Gold scavenged by bismuth melts: An example from Alpine shear-remobilizates in the Highiş Massif, Romania. Mineralogy and Petrology, 87: 351–384.

Mozgova NN, BorodaevYuS, Stepanova TV, et al (2000) Precious metals in sulfide associations of deep parts of the active construction of the TAG (Mid-Atlantic ridge. 26º08' n.l.). Lithology and mineral resources, 1: 5–24.

Plotinskaya OYu, Trubkin NV (2010) Mineral associations and forms of gold location in the fields of the Birgildinsko-Tominsky ore node (Ural). Native gold: typomorphism of mineral associations, conditions of formation of deposits, problems of applied research, vol. 1, Moscow, IGEM RAS.

Safina N.P, Maslennikov V.V, Maslennikova S.P (2010) Mineralogical and geochemical features of sulfide ore deposits of the manifestation «Zapadnoe», Subpolar Urals. Ways of realization of oil and gas and ore potential of Khanty-Mansiysk Autonomous Okrug–Yugra,Khanty-Mansiysk, Izdatnaukaservis, book 2: 492–500.

Tomkins AG (2007). Three mechanisms of ore re-mobilisation during amphibolitesfacies metamorphism at the Montauban Zn-Pb-Au-Ag deposit. Mineralium Deposita, V. 42: 627–637.

Zelenov VI (1989). Method of research of gold and silver ores, Moscow, Nedra, pp. 302.

The relationship of correct option location, distractor efficiency, difficulty and discrimination indices in analysis of high-stakes multiple-choice questions exam of medical students

Madjid Shafiayan *

Balal Izanloo **

ABSTRACT

Background: Analysis of Multiple-Choice Questions (MCQs) is the psychometric **Objective:** This study was method pertains to validity and reliability of the exam. conducted to identify psychometric properties of high-stakes MCQ exam of under-graduate Medical Students' assessment. With this in mind we tried to investigate the effect of correct option location on difficulty index (DIF I) and discrimination index (DI) regarding distractor efficiency (DE) in the context of Medical Education. **Materials and Methods:** National high –stake MCQ exam was conducted to senior medical students belonging to universities of Medical Sciences to assess knowledge of Basic and Clinical sciences. Data were analyzed using Classical Test Theory to investigate effect of correct – option position on DIF I and DI and DE. Microsoft Excel spread sheet; SPSS version 23; R Psych Package softwars were used. Descriptive statistics; Point biserial correlation; Fisher's Exact Test; ANOVA test and Pearson correlation were performed. **Results:** The mean score was 107.30±19.10 ranging from 40 – 174.Mean DIF I and DI were 0.54 ± 0.20 and 0.20 ± 0.10, respectively. Fourthly three and half percent MCQs were of average DIF I (0.30< P< 0.70) and DI >0.2. Overall 127/600 (21.16%) were null distractors (< 5%) and DE was 78.84%. Mean DIF I and SD key option 1; 2; 3; 4 were 0.50±0.20; 0.59 ± 0.18; 0.54 ± 0.23; 0.50 ± 0.17, respectively. **Conclusion:** Our data suggest that correct option location remarkably affect DIF I of item. We believe our study provides considerable insight into validating MCQs of Medical students' assessment to optimizing question bank.

KEY WORDS: Difficulty index; Discrimination index; Distractor efficiency; Correct option position; Multiple – Choice Questions; Medical Education

*Ph.D Candidate Of Medical Education, Department of Medical Education,School of Medicine,Tehran University of Medical Sciences, Tehran, Iran.

**Assistant Professor of Curriculum Planning, Department of Curriculum Planning, Faculty of Psychology and Education, Kharazmi University, Tehran, Iran.

Recibido: 11/09/2019 Aceptado: 14/10/2019

La relación de la ubicación correcta de las opciones, la eficiencia del distractor, los índices de dificultad y discriminación en el análisis de preguntas de opción múltiple de alto riesgo en el examen de estudiantes de medicina

Antecedentes: el análisis de las preguntas de opción múltiple (MCQ) es el método psicométrico relacionado con la validez y confiabilidad del examen. Objetivo: Este estudio se realizó para identificar las propiedades psicométricas del examen MCQ de alto riesgo de la evaluación de estudiantes de medicina de pregrado. Con esto en mente, tratamos de investigar el efecto de la ubicación correcta de las opciones en el índice de dificultad (DIF I) y el índice de discriminación (DI) con respecto a la eficiencia del distractor (DE) en el contexto de la educación médica. Materiales y métodos: se realizó un examen nacional MCQ de alto nivel a estudiantes de medicina de alto nivel pertenecientes a universidades de ciencias médicas para evaluar el conocimiento de las ciencias básicas y clínicas. Los datos se analizaron utilizando la teoría de prueba clásica para investigar el efecto de la posición de opción correcta en DIF I y DI y DE. Hoja de cálculo de Microsoft Excel; SPSS versión 23; Se utilizaron softwares R Psych Package. Estadísticas descriptivas; Punto de correlación biserial; Prueba exacta de Fisher; Se realizó la prueba ANOVA y la correlación de Pearson. Resultados: El puntaje promedio fue de 107.30 ± 19.10, que varió de 40 a 174.El promedio de DIF I y DI fue 0.54 ± 0.20 y 0.20 ± 0.10, respectivamente. Cuarto, el tres y medio por ciento de MCQ fue de DIF I promedio (0.30< P< 0.70) y DI >0.2. En general, 127/600 (21.16%) fueron distractores nulos (< 5%) y DE fue de 78.84%. Promedio DIF I y SD clave opción 1; 2; 3; 4 fueron 0,50 ± 0,20; 0,59 ± 0,18; 0,54 ± 0,23; 0.50 ± 0.17, respectivamente. Conclusión: Nuestros datos sugieren que la ubicación correcta de la opción afecta notablemente el DIF I del artículo. Creemos que nuestro estudio proporciona una visión considerable sobre la validación de MCQ de la evaluación de los estudiantes de medicina para optimizar el banco de preguntas.

PALABRAS CLAVE: índice de dificultad; Índice de discriminación; Eficiencia del distractor; Posición correcta de la opción; Preguntas de selección múltiple; Educación médica

Introduction

Assessment in Medical Education is generally accepted to be a critical component in both the teaching and learning process of Medicine. Certification procedure to pass/fail decision in high stakes exam and evaluative action are two

constructs of assessment (Swanwick, 2013). MCQs are one of the assessment methods that enable assessors to measure two initial competency levels of Miller Assessment Pyramid called Knows and Knows How in clinical skills with the adoption of Bloom Taxonomy of Educational Objectives (Miller, 1990). In addition, quality assurance of the assessment method requires psychometric techniques which are applied to internal structure of test to identify flawed items in order to optimize them (Tavakol, 2016; Downing, 2003).

Item analysis typically includes computing DIF I and DI to accurately measure the examinee's abilities through developing best assessment tool. DIF I in MCQs that is dichotomously scored items is proportion of examinee who correctly responds the test item. DI that is point-biserial coefficient typically corresponds between test item response and total test score. DE reflects the number of functioning distractors (De Champlain, 2010).

This cross-sectional study aims to identify psychometric properties of high-stakes MCQ pre-internship exam of under-graduate Medical Students' assessment in Iran. Classical test theory is used to test and item analysis. With this in mind we tried to investigate the effect of key option position on DIF I and DI regarding DE in the context of Medical Education.

What we know is largely based on validating the studies that have been extensively applied to investigate psychometric properties of MCQ exam in Medical students' assessment. However, very little research to date has focused on DE relationship to DIF I and DI in high-stakes MCQ exam of Medical student's assessment. Moreover, not much is known about the association of key option position to DIF I and DI considering DE.

MCQ test and item analysis have most often been investigated in terms of psychometric properties. Soler (2002) found a schema to be useful for distractor analysis. He reported that item difficulty is related to distractors and revision of whole test and modification of distractors were needed. This left the test designer to obtain optimal approach in MCQ analysis by applying a Classical Test Theory framework (Soler and Arias, 2002).

Rodriguez (2005) furthered this idea in his Meta-analysis on empirical research and theoretical reviews by considering optimal number of multiple–choice options. Three options were found optimal for MCQ test in most settings. He also emphasized that researchers needed to study the role of more effective plausible distractors (Rodríguez, 2005).

These studies hinted that DIF I and DI may be predicted based on DE. A later experiment concluded that there was little probability of designing more than two functional distractors. As such, three-option MCQ were optimal (Tarrant et al., 2009).

A study of quality assurance of MCQ exam in high-stakes of Medical student assessment reported that the number of functional distractor in addition to DIF I and DI should be included as the criteria of MCQ exam quality (Ware, 2009).

A greater level of relationship between item difficulty and discrimination indices was found on psychometric characteristics of MCQ test in undergraduate Medical student's assessment in Malaysia (Barman et al, 2010).

Rogausch and co-workers (2010) analyzed rarely the selected distractors in high-stakes MCQ test of Medical student's assessment based on the Swiss Federal Graduation Examination since 2005 to 2007. They reported just 30% of MCQs had DE of 100%.

Another study was performed in Dental College, Karachi to find the effects of non-functioning distractors on ideal questions. They concluded that items with acceptable DIF I and DI range are those items which include at least two functional distracters (Gajjar et al, 2014).

Gajjar and co-workers (2014) analyzed MCQs of Medical student's assessment in Ahmedabad, Gujarat. They stated that MCQ item would be optimal when it has the maximum DE, high D I (DI › 0.25) and average DIF I (DIF between 31% and 60%).

Other researchers (2015) investigated the impact of low functioning distracters on MCQ test in preclinical assessment of Medical Education. Substituting the nonfunctioning distractors with functioning distractors have been demonstrated that will improve discrimination ability of the exam (Ali et al, 2015).

Another MCQ test analysis was conducted in teaching Prosthodontic to Dental students focusing on distractor analysis and item difficulty and discrimination indices. Their results highlighted that item analysis must be used to determine DIF I and DI and DE (Madhav, 2015).

Patil et al (2016) analyzed MCQ test of first year medical student assessment in India. Their results indicated that just 65% and 75% items had acceptable range of DIF I and DI.

MCQ analysis of Medical student's assessment has shown that the range of DIF I between 31% - 60%; DI (DI › 0.25) and DE of 100% are characteristics of optimal MCQ (Rao et al, 2016).

Ferdousi (2017) analyzed MCQ test of Anatomy, Biochemistry and Physiology in Bangladesh. He stressed the omission or replacement of nonfunctioning distractors.

A recent comprehensive review on MCQ analysis states that the Achilles' heels of MCQ questions has generally been DE. There have been little or no researches pertaining to key option position regarding DE (Gierl et al, 2017).

Garg and co-workers (2018) analyzed the MCQ test of Medical student assessment in India to validate DIF I and DI and DE. An association between DIF I; DI and DE was reported (Garg et al, 2018).

Kheyami and co-workers (2018) investigated the MCQ test of the Department of Pediatrics in Bahrain to assess relationship between DIF I; DI and DE. They confirmed the conclusion of previous study that the development of three-option is easier than four or five-option. Additionally, this decreased the number of nonfunctioning distractors.

A recent investigation on final summative MCQ test for the graduates of Pharmacy students in Qatar highlighted that DIF I of the exam was in an acceptable range, but DI require improvement. A high percentage of nonfunctioning distractor was obvious as a result of difficulty of faculty members to construct plausible distractors (Pawluk et al. 2018).

These studies have only dealt with psychometric properties of MCQs of Medical Student's exam, whereas our study focuses on the relationship of key option position with DIF I and DI by considering the DE of items.

The aim of the present work is a comprehensive investigation of the effect of key option location on DIF I and DI of MCQs in high-stakes pre-internship exam of undergraduate Medical Students.

The results of the present study are encouraging and have gone some way toward enhancing our understanding of the internal structure of MCQ exam in the context of Medical Education.

We hope that our research will be constructive in solving the difficulty of test construction in high-stakes MCQs Pre-Internship Exam. Furthermore, we believe that our results may improve knowledge about psychometric properties of MCQs in the field of Medical Student's assessment.

1. Method

We performed psychometric test and item analysis to investigate item and test characteristics of MCQ Pre-Internship Exam. This National high-stakes exam is carried-out to assess the competency level of Knows and Knows How category of Miller assessment Pyramid pertaining to Senior undergraduate medical students (Miller, 1990). The Exam content was blueprinted according to proportionated 17 sub-tests of clinical sciences designated to undergraduate medical education curriculum in Iran.

A total of 2758 undergraduate medical students from 43 universities of medical sciences participated in the Exam on March 6th , 2014. All examinees had to mark the correct answer out of four options on the answer sheet based on 200 MCQ randomized in two booklets in 200 minutes. There was one mark for the correct answer and no negative marking for incorrect answer.

In order not to have any direct involvement of human subjects, the examinee's identity was concealed. As such, the study was exempted from ethical oversight.

Microsoft Excel spread sheet was used to enter data that were obtained for examinees' selected response for each item from the Assessment Center of Ministry of Health and Medical Education in Iran. Data screening was executed by using SPSS version 23 software (Green et al, 2016).

In order to validate the exam, we first had to obtain descriptive statistics which include central tendency indices for example, Mean; Median; Mode, and the Range of total scores of examinees by using SPSS version 23 software (Green et al, 2016).

Our preliminary aim was to get the general picture of psychometric properties of Exam and item. The next step was consequently to investigate DIF I; DI, and DE. Classical Test Theory Model was applied using R Psych Package software to identify item parameters regarding key option position and distractors efficiency (De Champlain, 2010; Team, 2014). The percentage of the correct answer that was chosen by the examinees was considered as item difficulty. Point biserial correlation between item score and total test score was applied as item discrimination. Functional distractor option was identified if it was selected by › 5% examinees. Existence of at least 1;2, and 3 functional distractor in an MCQ item is representative of DE of 33.3%;66.6%, and 100% (De Champlain, 2010; Patil et al, 2016; Ferdousi et al, 2017; Garg, 2018; DeVellis, 2006; Team, 2014).

To provide a way of evaluating the association between DIF I and DI of exam adaptation of scatter plot was selected. This method was chosen in that it is one of the most practical ways to assess the relation between DIF I and DI of the exam. Fisher's Exact Test was used to see the associations among DIF I and DI and DE (Raymond and Rousset, 1995).

Finally, ANOVA test was used to compare the mean of DIF I, DI, and key option position. Kuder Richardson 20 was obtained for the reliability of the exam. In this study, the p values less than 0.05 were considered statistically significant (González-Rodríguez, 2012; Feldt, 1965).

2. Results

A total of 2758 undergraduate medical students fulfilled the exam. Female examinees were 1701(61.70%), whereas male students were 1057(38. 30%). Examinees' marks ranged from 40 to 174 (out of 200). The mean marks and SD were 107.30 and 19.10, respectively. Normal distribution of scores was observed. All three reliability coefficients including alpha Cronbach; alpha if item deleted, and kuder Richardson 20 were 0.89.

DIF I and DI ranged from 0.07 to 0.95 and -0.09 to 0.40, respectively. The mean DIF I and SD were 0.54 and 0.20; 95% confidence interval for the difference = 0.14 – 0.93, respectively. The mean DI and SD were 0.20 and 0.10; 95% confidence interval for the difference = 0.00 – 0.41, respectively.

Pearson correlation of the whole test, between DIF I and DI was 0.42; 95% confidence interval for the difference = 0.30 – 0.53. The correlation was significant at $p \leq 0.001$. At first, the DI rose along the DIF I. Maximum DI 0.40 occurred in acceptable DIF I range between 0.35 – 0.55 at plateau and then decreased slightly with further development in DIFI (figure 1).

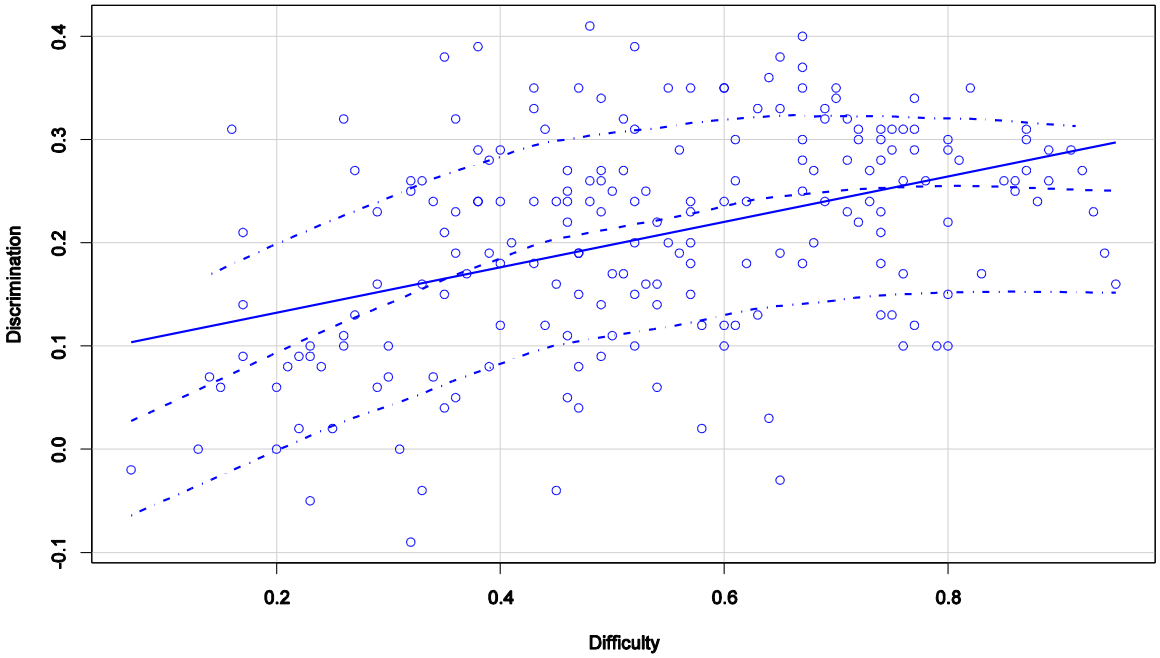

Figure 1: An approximate dome shaped regression line is not evident between DIF I and DI as illustrated on scatter plot. (N= 200)

Considering key option 1, The mean and SD for DIF I were 0.50 and 0.20, respectively. The mean and SD for DI were 0.22 and 0.09, respectively. The Fisher's Exact Test highlighted the more difficult MCQs (DI ≤ 70), the higher DE (81.81% Vs. 4.54% P = 0.01), thus association was found statistically significant. Additionally, approximately two- thirds of MCQs with key option 1 with higher DI (DIC ≥ 0.20) were having higher DE (61.36% Vs. 4.54% P = 0.31) therefore, association was found statistically insignificant (Table 1).

The mean and SD for DIF I were 0.59 and 0.18, respectively regarding key option 2. The mean and SD for DI were 0.19 and 0.10, respectively. The Fisher's Exact Test highlighted the more difficult MCQs (DI ≤ 70), the higher DE (56.85% Vs. 5.88% P = 0.01), thus association was found statistically significant. Additionally, over two-thirds of MCQs with key option 2 with higher DI (DIC ≥ 0.20) were having higher DE (35.29% Vs. 13.72% P = 0.32) therefore, association was found statistically insignificant (Table 1).

Table 1: Association among DIF I, DI and DE key 1 and key 2. (N=95)

Indices Key1 of	DE ≥ 66%	DE ≤ 33%	TOTAL	Test of Significance
DIF I ≤ 0.70	36(81.81%)	2(4.54%)	38(86.36%)	The Fisher exact test statistic value is 0.0135. The result is significant at p < .05.
DIF I > 0.70	3(6.81%)	3(6.81%)	6(13.63%)	
TOTAL	39	5	44	
DI < 0.20	12(27.27%)	3(6.81%)	15(34.09%)	The Fisher exact test statistic value is 0.3187. The result is not significant at p < .05.
DI ≥ 0.20	27(61.36%)	2(4.54%)	29(65.90%)	
TOTAL	39	5	44	
Indices Key2 of	DE ≥ 66%	DE ≤ 33%	TOTAL	
DIF I ≤ 0.70	29(56.86%)	3(5.88%)	32(62.74%)	The Fisher exact test statistic value is 0.0116. The result is significant at p < .05.
DIF I > 0.70	11(21.56%)	8(15.68%)	19(37.25%)	
TOTAL	40	11	51	
DI < 0.20	22(43.13%)	4(7.84%)	26(50.98%)	The Fisher exact test statistic value is 0.3238. The result is not significant at p < .05.
DI ≥ 0.20	18(35.29%)	7(13.72%)	25(49.01%)	
TOTAL	40	11	51	

DE = distractor efficiency; DIF I= difficulty index; DI = discrimination index

Considering key option 3, the mean and SD for DIF I were 0.54 and 0.23, respectively. The mean and SD for DI were 0.18 and 0.12, respectively. The Fisher's Exact Test highlighted almost over four-fifths of MCQs with key option 3 with lower DIF I(DIF I≤0.70) were having higher DE (65.00% Vs. 5.00% P = 0.00), thus association was found statistically significant. Additionally, half of MCQs with key option 3 with higher D I (D I ≥ 0.20) were having higher DE (40.00% Vs. 10.00% P = 1.00) therefore, association was found statistically insignificant (Table 2).

The mean DIF I and SD were 0.50 and 0.17, respectively regarding key option 4. The mean DI and SD were 0.23 and 0.09, respectively. The Fisher's Exact Test

highlighted almost over four-fifths of MCQs with key option 4 with lower DIF I(DIF I≤0.70) were having higher DE (82.00% Vs. 0.00% P = 0.02), thus association was found statistically significant. Additionally, over two-third of MCQs with key option 4 with higher D I (DIC ≥ 0.20) were having higher DE (62.22% Vs. 2.22% P = 1.00) therefore, association was found statistically insignificant (Table 2).

Table 2: Association among DIF I , DI and DE key 3 and key 4. (N=105)

Indices of key 3	DE ≥ 66%	DE ≤ 33%	TOTAL	Test of Significance
DIF I ≤ 0.70	39 (65.00%)	3(5.00%)	42(70.00%)	The Fisher exact test statistic value is 0.0004. The result is significant at p < .05.
DIF I > 0.70	9(15.00%)	9(15.00%)	18(30.00%)	
TOTAL	48	12	60	
DI < 0.20	24(40.00%)	6(10.00%)	30(50.00%)	The Fisher exact test statistic value is 1. The result is not significant at p < .05.
DI ≥ 0.20	24(40.00%)	6(10.00%)	30(50.00%)	
TOTAL	48	12	60	
Indices of key 4	DE ≥ 66%	DE ≤ 33%	TOTAL	
DIF I ≤ 0.70	37 (82.22%)	0(0.00%)	37(82.22%)	The Fisher exact test statistic value is 0.0283. The result is significant at p < .05.
DIF I > 0.70	6 (13.33%)	2 (4.44%)	8(17.77%)	
TOTAL	43	2	45	
DI < 0.20	15 (33.33%)	1 (2.22%)	16(35.55%)	The Fisher exact test statistic value is 1. The result is not significant at p < .05.
DI ≥ 0.20	28 (62.22%)	1 (2.22%)	29(64.44%)	
TOTAL	43	2	45	

DE = distractor efficiency; DIF I= difficulty index; DI = discrimination index

Considering key option 1 position, Pearson correlation between DIF I and DI was 0.37; 95% confidence interval for the difference = 0.60 – 0.08. The correlation was significant at p ≤ 0. 01. Initially, DI rose along with difficulty index. Maximum DI 0.35

occurred in acceptable DIF I range between 0.40 – 0.60 at plateau and then decreased slightly with further development in DIF I (figure 2).

Pearson correlation between DIF I and DI was 0.57; 95% confidence interval for the difference = 0.73 – 0.35, regarding key option 2 position. The correlation was significant at p ≤ 0. 0001. There is an approximately linear relationship between DIF I and DI. As such, the most difficult items pertained to low discriminant ones, higher discrimination for difficulties ranged 0.30 – 0.70, and then increased slightly for the easiest items (figure 2).

Considering key option 3 position, Pearson correlation between DIF I and DI was 0.51; 95% confidence interval for the difference = 0.68 – 0.29. The correlation was significant at p ≤ 0. 0001. Discriminants were somewhat linearly associated with difficult components. Firstly, the less discriminants, the less difficult items were observed, until difficulty range between 0.70- 0.80 at plateau discrimination increased and then rose slightly for the less difficult items (figure 2).

Pearson correlation between DIF I and DI was 0.30; 95% confidence interval for the difference = 0.55 – 0.04, regarding key option 4 position. The correlation was significant at p ≤ 0. 01. First, D I increased with rise of DIF I. Maximum DI 0.35 occurred in acceptable DIF I range between 0.40 – 0.60 at plateau and then decreased slightly with further development in DIF I (figure 2).

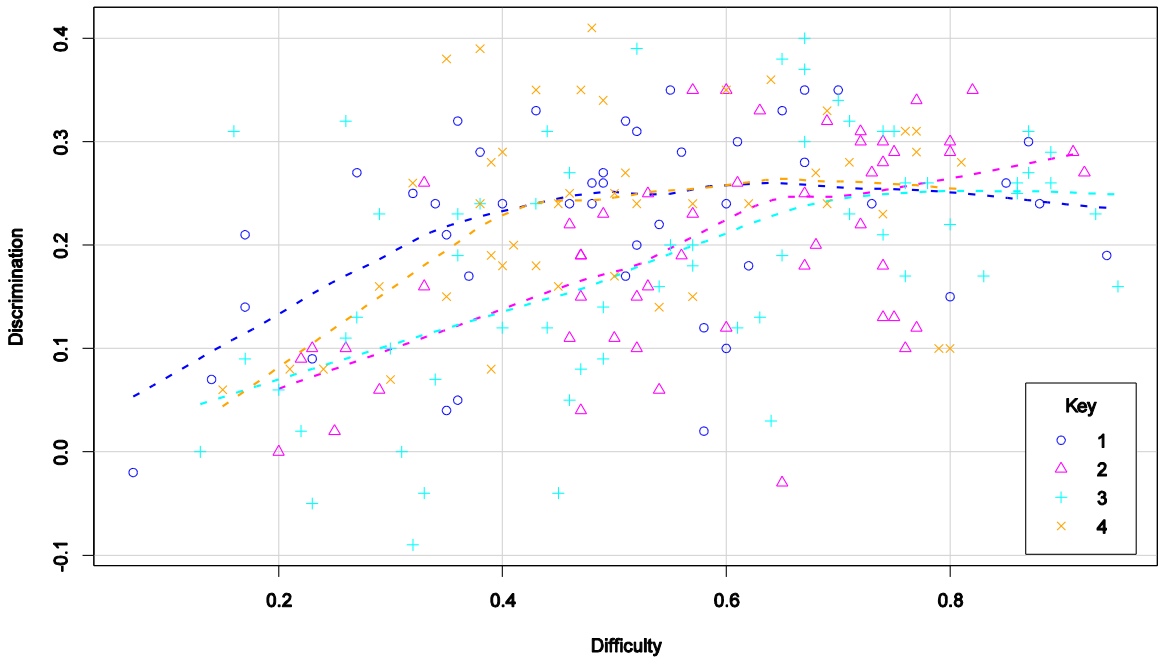

Figure 2: An approximate dome shaped regression line is not evident between difficulty and discrimination indices, regarding key option 1;2;3, and 4 as illustrated on scatter plot. (N=200)

There was not statistically significant relationship between DIF I and key option1;2;3, and 4, using ANOVA test (figure 3).

F = (3;196) = 1.857; p = 0.138

SOURCE OF VARIATION	Sum Sq	Df	Mean Sq	F value	Pr(>F)
KEY	0.223	3	0.07422	1.857	0.138
Residuals	7.832	196	0.03996		

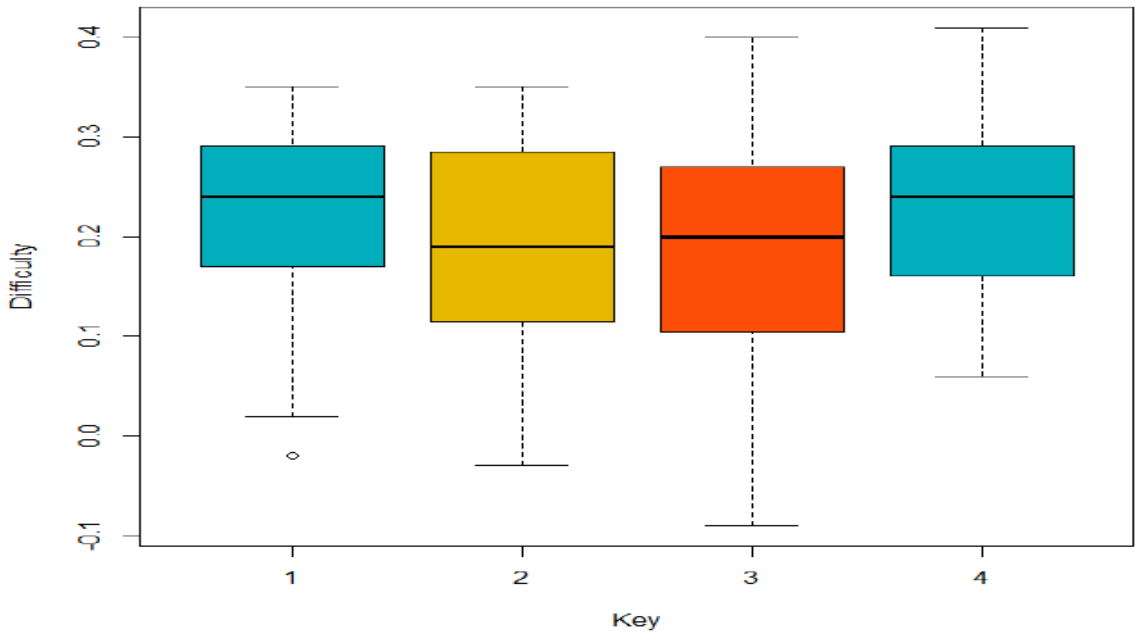

Figure 3: Relation between key option position and DIF I as reflected on Box plot illustration (n= 200) .

There was not statistically significant relationship between DI and key option1;2;3, and 4, using ANOVA test (figure 4).

F= (3;196) = 2.214; p = 0.087

SOURCE OF VARIATION	Sum Sq	Df	Mean Sq	F value	Pr(>F)
KEY	0.0721	3	0.02403	2.214	0.0878 .
Residuals	2.1267	196	0.01085		

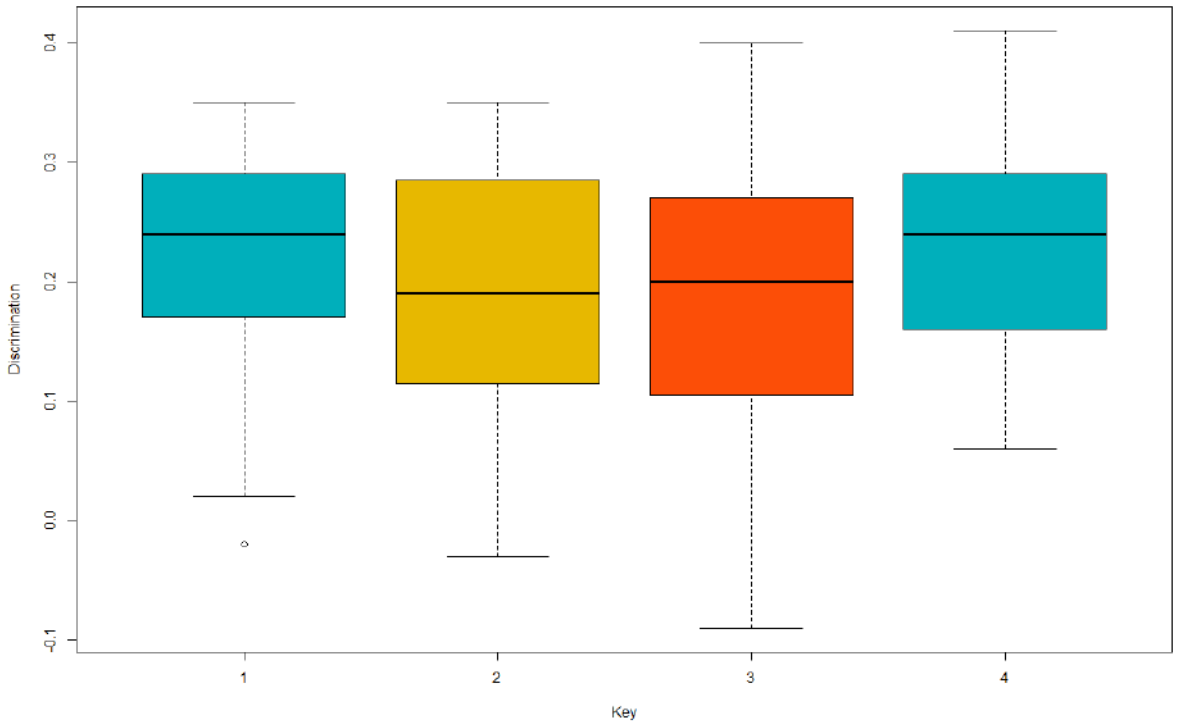

Figure 4: Relation between key option position and DI as reflected on Box plot illustration (n=200).

3. Discussion

The main goal of this study was to analyze psychometric properties of high-stakes MCQ pre-internship exam of undergraduate Medical students' assessment based on classical test theory. In addition, the present study seeks to investigate the effect of key option position on item indices regarding DE.

In our study, 123/200 items (61.5%) were within acceptable range of DIF I (0.30 – 0.70). Just 25/200 items (12.5%) were with DIF I($p<0.30$). Previous studies nearly correspond with the data presented in the Results. Ferdousi (2017) reported about preclinical assessment in Bangladesh. In his analysis 43.5% and 18.67% of items had DIF I> 0.9 and 0.66-0.80, respectively (Ferdousi et al, 2017). Furthermore, similar results were obtained from another study which was conducted on summative exam of patho-physiology (Caballero et al., 2014). Gajjar (2014) found mean DIF I of 39.4 ± 21.4% in the assessment of Medical students in Pakistan. Unlike the aforementioned citation, Rao (2017) reported mean DIF I of 75.0 ± 23.7% in psychometric analysis of assessment

of medical students in department of pathology. Similarly, another recent study by Garg (2019) mean DIF I of 71.6± 19.4% was reported in his analysis of formative assessment of Medical students in Delhi, India.

The mean DI and SD in our study was 0.2±0.1.However, Ferdousi (2017) concluded mean DI of 0.13. Like our research, another conducted one has reported the mean DI of case-based items was more than standard items and overall DI of 0.24 was reported (Caballero et al, 2014). In another analysis aligned with Ferdousi, Gajjar (2014) asserted mean DI of 0.14 in result of end of course exam of community medicine. Moreover, in Rao's analysis the mean DI which was more than 0.2 in 75% of items and 65% of them ≥0.4 resembles our findings. There were not any items with negative DI (Rao, et al, 2016). Likewise, mean DI and SD of 0.3±0.17 had been reported in other study by Garge (2018). According to what has been mentioned so far, the results indicate the mean DI of medical students' MCQs ranges 0.2 and 0.3.

In this study, even approximate dome shape regression line between DIF I and DI was not obvious. However, in other study by Ferdousi an illustration of dome shape regression line was obvious between DIF I and DI demonstrating the adaptability of items with maximum difficulty indices around 0.6 and DI up to 0.68. In another study, researchers reported the correlation of 60% between DIF I and DI with presence of difficult items which were not discriminating due to the very fact that difficulty level was beyond the comprehension of the class (Caballero et al, 2014). Meanwhile, Gajjar (2014) concluded in his analysis items with acceptable DIF I were not good at differentiating higher and lower ability examinees. As such, the relationship between DIF I and DI was not dome shaped. Like Ferdousi, Rao reported correlation of 0.56 between DI and DIF I indicating a reciprocal relationship. It means dome shape regression line was evident between these two indices meaning maximum discrimination power occuring in acceptable difficult items (Rao et al, 2016). Unlike the findings of the aforementioned studies, Garge in his analysis reported items with DIF I ≤ 0.7 were having higher DI, but the association were statistically insignificant (Garg, 2018). In fact, the achieved results does do not provide us with the opportunity to come up with a final decision on maximum DI occurring in acceptable DIF I range.

Ferdousi reported 15.74%; 21.31%; 12.5% as ineffective distractors in discipline of anatomy biochemistry ,physiology, respectively. Furthermore, 9.7% of distractors were with efficacy of more than 50%.(18)Gajjar reported mean DE of 88.6% ± 18.6% and 11.4% ineffective distractors.In his study , fifteen items with ineffective distractors had mean DIF I and mean DI of 53.5% ; 18% , respectively (Gajjar, 2014).(13)Rao elucidated that mean DE of 89.99% ± 24.42% with 5% ineffective distractor in his study. Thus, he observed compatibility of items including one ineffective distractor and DE 85.15% with difficulty indices (0.30 – 0.70) and discrimination indices (D > 0.24).(17)Garge stated mean distractor effectiveness 63.4% ± 33.3% indicating compatibility of lower difficulty indices (p ≤ 0.70) ; higher discrimination indices (D≥ 0.15) with higher DE, respectively.(20)In our study, 127/600 (21.16%) were null distractors (< 5%) and distractor efficacy was 78.84%.Finally,in terms of what has been studied so far, we come up with the conclusion that in the context of Medical Student Assessment a MCQ requires at least two effective distractors to have acceptable DIF I ranging 0.3 – 0.7 and DI ≥ 0.2.

To date in the context of Medical Student Assessment, no work has been published on the role of key option position on item characteristics considering DE. Our data suggest that key option position remarkably affects DIF I of item. Furthermore, there is not noticeable relationship between key option position and discriminative index. It seems that placing key option as first and last alternative in MCQ of medical student exam can produce more slightly difficult and more discriminant items in comparing middle alternative.

The elaborated results in our analysis may have been defined as key option position characteristics in internal structure of MCQ exam, and may propose some hypotheses for research in relation to reliability and validity in this contextual Medical Student Assessment for future. We only analyzed one high–stake exam in Medical Education field. Different number of samples could lead to higher generalization of our results in the domain of assessment.

The importance of our results generality and their relative ease of application can be used in other Medical Student Assessment method, such as Objective Structured Clinical Exam (OSCE).

Reference

Swanwick TJUMEE, Theory, Practice. Understanding medical education2013. 1-6 p.

Miller GEJAm. The assessment of clinical skills/competence/performance. 1990;65(9):S63-7.

Tavakol M, Dennick RJAM. Postexamination analysis: a means of improving the exam cycle. 2016;91(9):1324.

Downing SM. Validity: on the meaningful interpretation of assessment data. Medical education. 2003;37(9):830-7.

De Champlain AF. A primer on classical test theory and item response theory for assessments in medical education. Medical education. 2010;44(1):109-17.

Soler HH, ARIAS RMJEIdlUC. A new insight into examinee behaviour in a multiple-choice test: a quantitative approach. 2002;10(2002):113-37.

Rodriguez MCJEMI, Practice. Three options are optimal for multiple-choice items: A meta-analysis of 80 years of research. 2005;24(2):3-13.

Tarrant M, Ware J, Mohammed AMJBME. An assessment of functioning and non-functioning distractors in multiple-choice questions: a descriptive analysis. 2009;9(1):40.

Ware J, Vik T. Quality assurance of item writing: during the introduction of multiple choice questions in medicine for high stakes examinations. Medical teacher. 2009;31(3):238-43.

Barman A, Ja'afar R, Rahim F, Noor AJTomej. Psychometric Characteristics of MCQs used in Assessing Phase-II Undergraduate Medical Students of Universiti Sains Malaysia. 2010;3:1-4.

Rogausch A, Hofer R, Krebs R. Rarely selected distractors in high stakes medical multiple-choice examinations and their recognition by item authors: a simulation and survey. BMC Med Educ. 2010;10(1):85.

Hingorjo MR, Jaleel F. Analysis of one-best MCQs: the difficulty index, D I and DE. JPMA The Journal of the Pakistan Medical Association. 2012;62(2):142-7.

Gajjar S, Sharma R, Kumar P, Rana M. Item and test analysis to identify quality multiple choice questions (MCQs) from an assessment of medical students of Ahmedabad, Gujarat. Indian journal of community medicine: official publication of Indian Association of Preventive & Social Medicine. 2014;39(1):17.

Ali SH, Ruit KG. The Impact of item flaws, testing at low cognitive level, and low distractor functioning on multiple-choice question quality. Perspectives on medical education. 2015;4(5):244-51.

Madhav V. Item Analysis of Multiple-Choice Questions in Teaching Prosthodontics. Journal of dental education. 2015;79(11):1314-9.

Patil PS, Dhobale MR, Mudiraj NR. ITEM ANALYSIS OF MCQS'-MYTHS AND REALITIES WHEN APPLYING THEM AS AN ASSESSMENT TOOL FOR MEDICAL STUDENTS. International Journal of Current Research and Review. 2016;8(13):12.

Rao C, Kishan Prasad H, Sajitha K, Permi H, Shetty J. Item analysis of multiple choice questions: Assessing an assessment tool in medical students. 2016;2(4):201-4.

Ferdousi S, Rahman MM, Talukder HK, Habib MA. Post-application Quality Analysis of MCQs of Preclinical Examination Using Item Analysis. Bangladesh Journal of Medical Education. 2017;7(1):2-7.

Gierl MJ, Bulut O, Guo Q, Zhang XJRoER. Developing, analyzing, and using distractors for multiple-choice tests in education: a comprehensive review. 2017;87(6):1082-116.

Garg R, Kumar V, Maria J. Analysis of multiple choice questions from a formative assessment of medical students of a medical college in Delhi, India. International Journal of Research in Medical Sciences. 2018;7(1):4.

Kheyami D, Jaradat A, Al-Shibani T, Ali FA. Item Analysis of Multiple Choice Questions at the Department of Paediatrics, Arabian Gulf University, Manama, Bahrain. Sultan Qaboos University Medical Journal. 2018;18(1):e68.

Pawluk SA, Shah K, Minhas R, Rainkie D, Wilby KJ. A psychometric analysis of a newly developed summative, multiple choice question assessment adapted from Canada to a Middle Eastern context. Currents in Pharmacy Teaching and Learning. 2018.

Veney JE. Statistics for health policy and administration using Microsoft Excel: Jossey-Bass San Francisco; 2003.

Green SB, Salkind NJ. Using SPSS for Windows and Macintosh, Books a la Carte: Pearson; 2016.

Team RC. R: A language and environment for statistical computing. R Foundation for Statistical Computing, Vienna, Austria. 2013. 2014.

DeVellis RFJMc. Classical test theory. 2006:S50-S9.

Raymond M, Rousset FJE. An exact test for population differentiation. 1995;49(6):1280-3.

González-Rodríguez G, Colubi A, Gil MÁJCS, Analysis D. Fuzzy data treated as functional data: A one-way ANOVA test approach. 2012;56(4):943-55.

Feldt LSJP. The approximate sampling distribution of Kuder-Richardson reliability coefficient twenty. 1965;30(3):357-70.

Caballero J, Wolowich WR, Benavides S, Marino J. Difficulty and discrimination indices of multiple-choice examination items in a college of pharmacy therapeutics and pathophysiology course sequence. Int J Pharm Pract. 2014;22(1):76-83.

Mathematical models for evaluating efficiency and quality of means for synchronization of interacting processes in reconfigurable computer systems

Alexey I. Martyshkin *

ABSTRACT

In this paper, the modelling method is applied to evaluate the performance characteristics of various methods for synchronization of parallel processes in order to determine which way to use to implement them: software or hardware. Comparative characteristics of process synchronization by the spin lock method and the core lock method are presented. Charts have been constructed that display the obtained characteristics.

KEYWORDS: reconfigurable system, operating system, shared resource, process synchronization, task manager, model, stochastic network

Modelos matemáticos para evaluar la eficiencia y la calidad de los medios para la sincronización de procesos interactivos en sistemas informáticos reconfigurables.

RESUMEN

Se aplica el método de modelado para evaluar las características de rendimiento de varios métodos para la sincronización de procesos paralelos con el fin de determinar qué forma utilizar para implementarlos: software o hardware. Se presentan las características comparativas de la sincronización de procesos mediante el método de bloqueo de giro y el método de bloqueo de núcleo. Se han construido gráficos que muestran las características obtenidas.

PALABRAS CLAVE: sistema reconfigurable, sistema operativo, recurso compartido, sincronización de procesos, administrador de tareas, modelo, red estocástica.

*Candidate of Technical Sciences, Associate Professor, Computational Machines and Systems Department Penza State Technological University (440039, Russia, Penza, 1/11 Baydukovapassage / Gagarina str., 1/11 . e-mail: alexey314@yandex.ru)

Recibido: 14/09/2019 Aceptado: 19/11/2019

Introduction

The performance and reliability of an operating system largely depend on how the functions of computing process control are implemented: in the user space or the kernel of the operating system and how are they performed: in software or hardware. Traditionally, most of the operating system functions, including those for reconfigurable systems, are implemented in software and only part of the functions, such as interrupt control, calculating the executive address in virtual memory systems, providing cache coherence, and some others are implemented in hardware. Currently, reconfigurability is used both in universal computing systems, for example, based on multi-core processors, and in specialized ones implemented, for example, in systems based on a chip (Martyshkin, 2018a). The traditional approach to the implementation of an operating system acts as a brake for obtaining high performance and reliability, therefore, the current trend in the development of the operating system is associated with the expansion of the set of functions implemented in hardware. These include the synchronization functions for interacting parallel processes associated with access to shareable resources.

To implement synchronization, there are used mutual exclusion methods which are implemented through the critical sections mechanism (variable locks, mutexes, semaphores) and the monitor mechanism (Kreutzler, 1986; Tenembaum and Bos, 2015). The critical sections mechanism is that if a process trying to access shareable resources finds it busy, then it must wait for it to be released. This waiting can be organized in two ways: either being in a state of active waiting, i.e. occupying a certain processor, continuously try to access its critical sections, or, having released the processor, switch to the locked state until critical sections and some processor are simultaneously free. The first strategy is implemented in user space and is called spin lock or spinning. The second strategy is implemented by the operating system and is called as locking in the kernel.

Obviously, there are disadvantages in each of these strategies. When spinning is used, the processor performing the corresponding process stays in unproductive idle time waiting for access to shareable resources. Blocking a process in the kernel leads to switching of a current process and, consequently, to a possible reload of the cache memory of the corresponding processor, which, firstly, requires certain time costs and, secondly, increases the likelihood of a cache miss. With respect to the performance of the respective

processor, it is believed that the blocking procedure is equivalent to the loss of t_{cw} clock cycles required to switch the process.

The monitor is an intermediate strategy between spinning and blocking, in which the spin lock time is determined by some random value t_s until the process reaches the monitor entry. Upon reaching the monitor entry, the process either is serviced or leaves the monitor if it is found that the shareable resource is occupied by another process and is set by the kernel in a special queue of blocked processes (Martyshkin, 2018 b; Martyshkin, 2016a; Martyshkin, 2019).

Shareable resources can be characterized as lively or unlively. The shareable resources that are often accessed, that is, the interval between requests is small (Martyshkin, 2016b; Tenenbaum and Bos, 2015) or otherwise with high-intensity request flows, are lively. If the request intensity is high, then a queue will form before the shareable resource, leading to delays in the execution of processes. The shareable resources which are unlively do not create queues and, therefore, delays when accessing the critical section of the corresponding process. We consider the impact of lively and unlively shareable resources on the performance of a reconfigurable computation system by estimating the average process time through using stochastic queuing networks and compare the performance of a reconfigurable computation system for process synchronization strategies based on the critical section mechanism.

1. Mathematical configurable computer system using process synchronization by the spin locking method

The proposed model includes P statistically identical processes (flows), execution of each of them can be considered as an alternation of the computing phase of the processor (all N processors are also the same) with access to one of M statistically identical shareable resources, each of which is selected with a probability of 1 / M, i.e., there is an equally probable choice of shareable resources (Martyshkin, 2016e; Martyshkin and Yasarevskaya, 2015). Each process at the end of the calculation phase (the average time of which is t_p) with probability σ requires access to the i-th shareable resource. At the same time, the process is not blocked, but remains in standby mode (cyclically polls the bit semaphore) and uses the shareable resource during the average residence time (t_s) of the application in

the i-th queuing network (i = 1... M). Thus, the process does not leave the processor, and the duration of one stage of execution increases for the time the application stays in the access and use phase of the shareable resource ($t_p + t_s$). After using the shareable resource (the average time of which is t_{ks}), a new service phase starts, and the process continues the phase of calculations on the same processor.

The process execution ends with the processor release phase (S_0) with probability (1-σ), after which the process leaves the processor node. Then the task manager selects another task from the ready process queue by loading its context into a free processor, after which a new phase of calculations starts for it. Assuming the exponential nature of the time distributions of all the indicated phases of the process, we come to the reconfigurable computation system network model with the set of shareable resources shown in Fig. 1, where the processor node model is represented by a multi-channel queuing network, and the service models in critical sections are represented as a single-channel queueing network. Requests are selected in FIFO order of receipt.

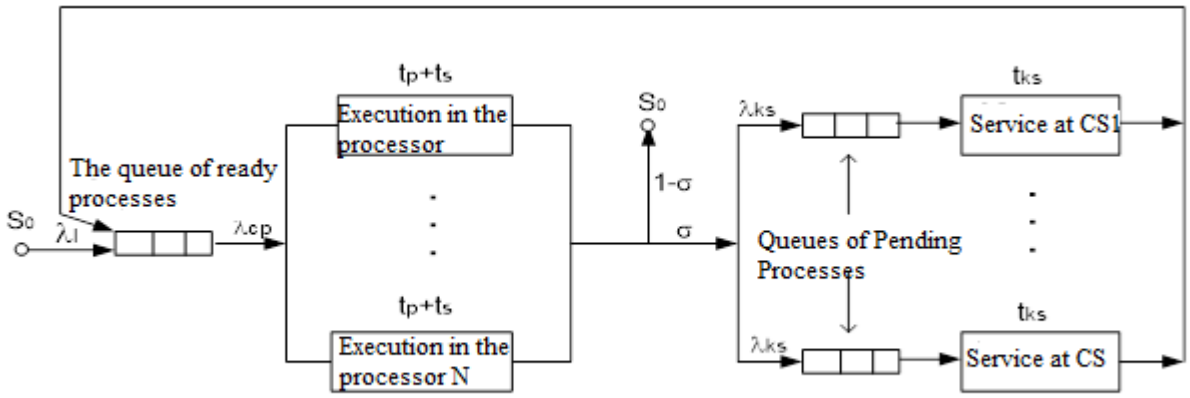

Figure 1 – The network model of a reconfigurable computation system with process synchronization by the spin lock method

We suppose that each process creates a simple flow of requests for the use of shareable resources, and their service times are exponentially distributed. Then the average residence time for one request in the critical section will be [10]

$$t_s = t_{ks} / 1 - \rho \quad , \qquad (1)$$

Where $\rho = \lambda_{ks} t_{ks}$ is loading of a critical section by a process requiring access to a shared resource; λ_{ks} is the intensity of the request flow at the input of the queuing

network simulating the procedure for accessing and using shareable resources $\lambda_{ks} = \lambda_{cp} \sigma / M$; λ_{cp} is the request flow rate at the input of the processor node $\lambda_{cp} = \lambda_I /(1-\sigma)$.

The execution time of one unit process in the processor node presented in the network model as a multi-channel queuing network will be.

$$t_{cp} = \frac{(t_p + t_s)\beta^N}{N!N(1-\beta/N)^2}\pi_0 + (t_p + t_s), \qquad (2)$$

Where $\beta = \lambda_{cp} t_p$ is the average number of busy channels in the queuing network in the calculation phase; π_0 is the probability of the absence of requests in a multi-channel queuing network (Martyshkin, 2016a).

If during the run time, the process would access the shareable resource n times, then the number of calculation steps in the processor node will be (n +1) [8]. The probability of the process moving from the calculation phase to the phase of access to the shareable resource and its use is $\sigma = n / n + 1$. The probability of the process moving into the processor release phase will be equal to 1 / n + 1, respectively. Then the execution time of a single process T in the reconfigurable computation system would be

$$T = t_{cp}(n+1) = t_{cp} /(1-\sigma), \qquad (3)$$

Figure 2 shows the diagram of the reconfigurable computation system analytical model with synchronization of processes by the spin lock method for a single shared resource, and Figure 3 shows the diagram for a set of shareable resources (Andrews, 2003).

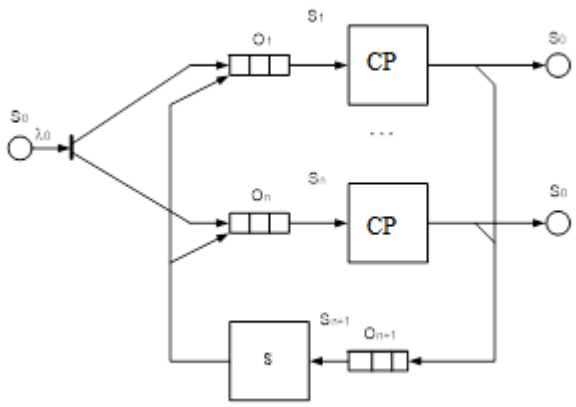

Figure 2 - Diagram of the reconfigurable computation system analytical model with the synchronization of processes by the spin lock method for a single shared resource

Here
- Sl-Sn - processor nodes;
- Sn + 1 - shareable resources (semaphore).

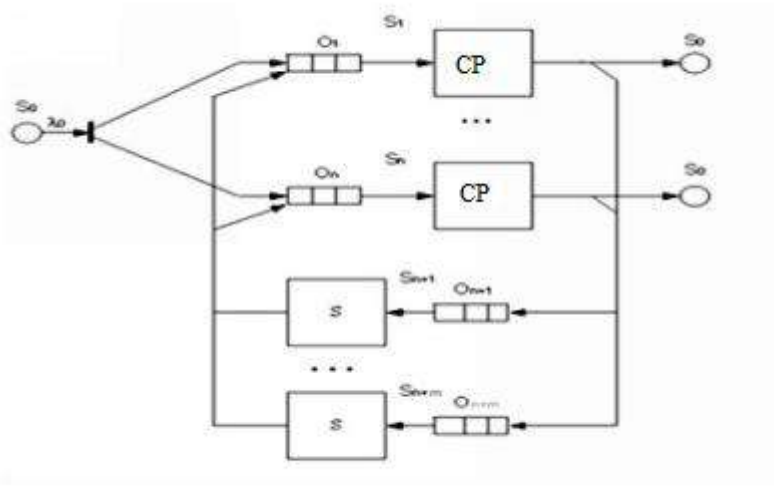

Figure 3 - Diagram of the reconfigurable computation system analytical model with the synchronization of processes by the spin lock method for many shareable resources

Here:
- Sl-Sn - processor nodes;
- Sn + 1, Sn + m - semaphores.

2. Mathematical model of a reconfigurable computation system using synchronization of processes with blocking in the kernel

This process synchronization strategy uses immediate blocking. At the end of the calculation phase, a process with probability σ requiring access to i-th shareable resource and finding the shareable resource busy, cannot enter its critical section, therefore it is blocked by the operating system, freeing the processor where it was running. The duration of the calculation phase is t_p. Then the task manager selects a new task from the ready-made process queue by loading its context into the freed processor. After using the shareable resource (the average time of which is t_{ks}), a new stage of servicing a previously blocked process starts, and the process continues the calculation phase mainly in another processor, which will lead to additional time losses due to a cache reboot. It is believed that the duration of the scheduling phase is determined by the time of switching the context and reloading the cache and is equal to the time value t_{cw} (Martyshkin, 2016c; Martyshkin,

2016d). Process execution with probability (1- σ) ends with the processor release phase (S_0), after which the process leaves the processor node.

The network model is shown in Figure 4. The average time of using a shared resource (staying one request in the critical section) will be

$$t_{ks} = \frac{t_{ks} + t_{cw}}{1 - \lambda_{ks}(t_{ks} + t_{cw})} = \frac{(t_{ks} + t_{cw})M(1-\sigma)}{M(1-\sigma) - \sigma\lambda_1(t_{ks} + t_{cw})} \quad (4)$$

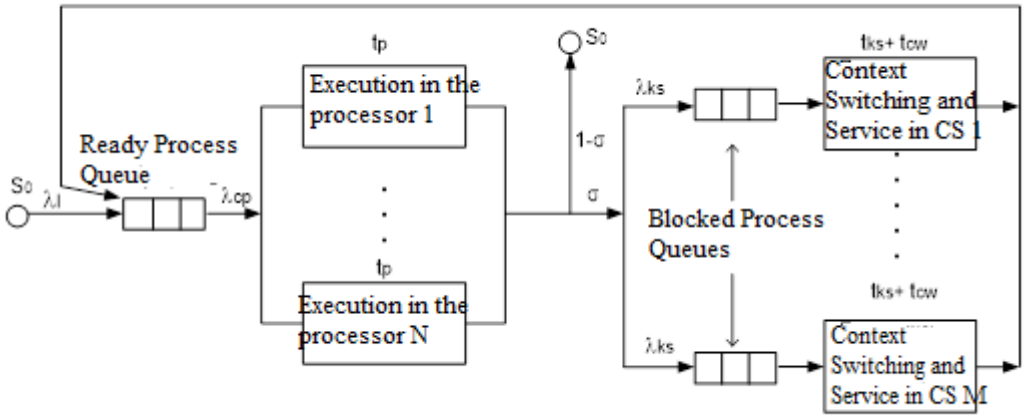

Figure 4 - Network model of a reconfigurable computation system with process synchronization by a method of blocking in the kernel

The execution time of a single process in the computational phase is

$$t_{cp} = \frac{t_p \beta^N}{N!N(1-\beta/N)^2}\pi_0 + t_p \quad (5)$$

The execution time of a single process taking into account the synchronization of parallel processes is determined as

$$T = (n+1)t_{cp} + \frac{nt_s}{M} = \frac{t_{cp}}{1-\sigma} + \frac{\sigma t_s}{M(1-\sigma)}. \quad (6)$$

Figure 5 shows a diagram representing a reconfigurable computation system analytical model with process synchronization using the method of locking in the kernel (monitor method) for a single shared resource. Figure 6 shows a diagram of n-processor reconfigurable computation system based on access to multiple shareable resources using the monitor method.

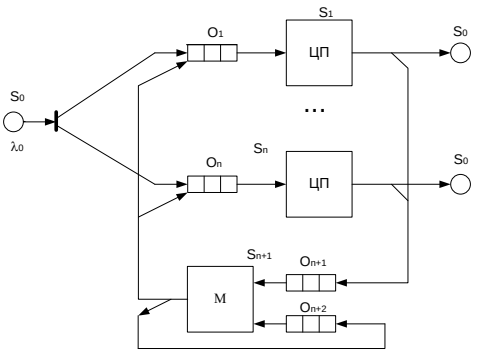

Figure 5 - Diagram of the reconfigurable computation system analytical model with process synchronization by the method of locking in the kernel for a single shared resource

Here:
- Sl-Sn - processor nodes;
- Sn + 1 - monitor;
- On + 2 - the queue of blocked processes

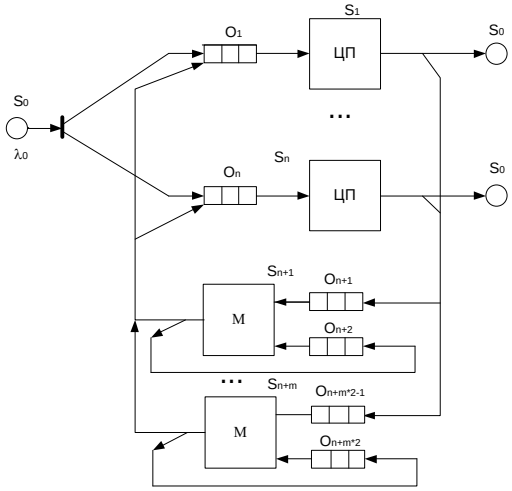

Figure 6 - Diagram of the analytical model of the n-processor reconfigurable computation system based on access to multiple shareable resources through the monitor method

Here:
- CPU $_{n}$ - n processor nodes;
-M - monitor;
- On $_{n+2}$ - the queue of blocked processes.

3. Study of the mathematical models considered

To evaluate performance losses due to conflicts over access to a shared resource (semaphore), an analytical model of n-processor reconfigurable computation system with a single shareable resource is considered (Fig.2). A model of n-processor reconfigurable computation system with a monitor-based access method is shown in Figure 5.

These models are presented in the form of an open stochastic queuing network consisting of n (Sl,..., Sn) single-channel queuing networks simulating processor nodes and a single-channel queuing network (Sn + 1), which simulates one of the access methods to the resource (Aliev, 2009). Moreover, the queuing network S0 acts as an external source of requests (requests for the execution of processes), which can be formed, for example, by user terminals (Kleinrock, 1979a; Kleinrock, 1979b). The queuing network S0 also acts as an absorber of requests served by a stochastic network. We assume that the request execution time vi in each processor node is exponentially distributed (Fundamentals of computational system, 1978).

The graph of the n-processor reconfigurable computation system transitions is shown in Figure 7.

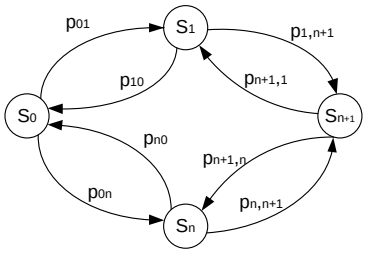

Figure 7 - Transition graph of the n-processor reconfigurable computation system analytic model with multiple shareable resources

Here:

- S0 - source of requests (terminals generating requests);

- Sl-Sn - n processor nodes;

- Sn + 1 - semaphores.

It is believed that applications form the simplest flows of requests, and service times follow exponential law. This distribution will make it possible to obtain results that are obviously worse than real values, which, in turn, will make it possible to upper-bound estimate the obtained results (Martyshkin et al, 2011).

4. Definition of initial data for modelling

The initial data are formed on the basis of architectural features in which the temporal characteristics are different.

The initial data was formed as follows:

- based on theoretical data;

- based on data obtained as a result of using programs that measure the context switching time and semaphore speed.

Thus, we get that the semaphore access time in user space is 50 μs, the access time to the monitor in the kernel space is 250 μs.

The service time in the processor node is taken from the following calculation: from a value commensurate with the minimum semaphore access time to a number much larger than the maximum resource access time. In numerical value, we get: from 50 μs to 600 μs.

In the reconfigurable computation system, when waiting for access to a shared resource, the processing time in the processor node increases by an amount equal to the latency of the critical resource. Upon that, an unproductive idling of the processor node for more than one cycle is likely. To analyse this behaviour of the system, an access control model with a single shareable resource was studied, where the service time of the processor node increases in each cycle (1)

$$V_{cp_n} = V_{cp_{n-1}} + W_{S_{n-1}} \qquad (7)$$

Initial data:

- the number of processor nodes in the queuing network K = 4;
- service time for requests by one processor node ν = 50; 600 μs;
- time for servicing requests with a critical resource ν = 50; 250 μs.

The simulation results are presented in Table 1.

Table 1 - The simulation results

Ps	Pcp	Vs, μs	Vcp, μs	Ws, μs	Wcp, μs
0.25	0.76	50	600	16.6	336.3
0.25	0.77	50	616.6	16.6	366.3
0.25	0.79	50	633.2	16.6	441.3
0.25	0.81	50	649.8	16.6	535.3
0.25	0.83	50	666.4	16.6	655.5
0.25	0.85	50	683	16.6	813
0.375	0.225	250	600	150	2,8
0.375	0.28	250	750	150	7.8
0.375	0.34	250	900	150	18.3
0.375	0.4	250	1050	150	37.5
0.375	0.45	250	1200	150	70.1
0.375	0.5	250	1350	150	123.1
0.375	0.225	250	600	150	2,8
0.375	0.28	250	750	150	7.8

0.375	0.34	250	900	150	18.3
0.375	0.4	250	1050	150	37.5
0.375	0.45	250	1200	150	70.1
0.375	0.5	250	1350	150	123.1
0.5	0.125	50	50	50	0,026
0.5	0.25	50	100	50	0.68
0.5	0.375	50	150	50	4.48
0.5	0.5	50	200	50	17.4
0.5	0.625	50	250	50	53.3
0.5	0.75	50	300	50	152.8
0.6	0,03	200	50	299.2	0,0002
0.6	0.26	200	349.2	299.2	2,8
0.6	0.49	200	648.4	299.2	50.7
0.6	0.71	200	947.6	299.2	364.7
0.6	0.94	200	1246.8	299.2	4130.4
0.6	› 1	200	1546	299.2	

The calculation results of the models showed that the waiting time for the release of the monitor is much higher than the waiting time for the semaphore, which increases the response time of the reconfigurable computation system; spin lock is the least time-consuming over the entire range of load changes.

At the same time, the simulation results confirm that it is most expedient to use spin-locking for processes that often turn to a common resource, the processing time of which on processor nodes is small. The disadvantage of this method is the cost of pre-programming, which greatly complicates its use.

When using a monitor, it takes a longer time to wait for it to be released, however, this method is simpler to use and can be used for processes that have a long processing time in the processor node.

Also, to develop a criterion for choosing the optimal method of access to a single shared resource, a study was made of various service times in the processor node and in the semaphore. In this case, the ratio of the loading coefficient of the semaphore Ps to the loading coefficient of the processor node Pcp was calculated as follows

$$Z = P_s / P_{cp} \quad (8)$$

If we analyse the 4-processor reconfigurable computation system with different service times in the processor node and semaphore, and also take into account the

conclusions made above, we find that in order to determine the optimal method for accessing data, it is necessary that the coefficient Z lie within the limits of

$$0{,}4 * K > Z > 1 * K \quad (9)$$

For the 4-processor reconfigurable computation system, 1.6› Z› 4; for the 8-processor reconfigurable computation system, 3.2› Z› 8.

To evaluate performance losses due to conflicts over access to the semaphore, an analytical model of n-processor reconfigurable computation system with many shareable resources (Fig.3) is considered. The model of n-processor reconfigurable computation system with a monitor-based access method is shown in Figure 2.

The studies were conducted on models with 2 and 4 shareable resources in the reconfigurable computation system.

Initial data:

- the number of processor nodes in the queuing network K = 2... 12
- the time for servicing requests by one processor node ν = 600 μs;
- the time for servicing requests with a critical resource ν = 150 μs.

The intensity of the request flow during modelling changed as follows:

0.0000005% * (number of processor nodes).

The bottleneck in a reconfigurable computation system with 4 shareable resources is a critical resource. With a request flow of 65 * 10^{-7} requests / μs (the number of processor nodes K = 13), the semaphore in the reconfigurable computation system with two critical resources does not cope with the number of calls - Ps› 1, the waiting time of the semaphore increases sharply. In a reconfigurable computation system with 4 critical resources, the load on the semaphore is 2 times lower.

When the access time to the semaphore is increased from 50 μs to 250 μs, the waiting time for the reconfigurable computation system with 2 shareable resources increased many times. The load factor also increases, reaching 1 at 8 processor nodes in a reconfigurable computation system with Vs = 250 μs, while in a reconfigurable computation system with Vs = 50 μs at 8 processor node Ps = 0.2 in a reconfigurable computation system with 2 critical resources.

In general, the simulation results show that the choice of the most optimal method for controlling access to a critical resource, which affects the access time, affects the performance of the entire system.

Formula (9) was obtained above for a model with a single shareable resource. For systems with multiple shareable resources, additional analysis is required. To do this, we studied the access control model with the single shareable resource, where in each cycle the service time of the processor node increases, formula (7) above.

Initial data:

- the number of processor nodes in the queuing network K= 4;
- the service time of requests by one processor node ν| = 50; 600 microseconds;
- the time for servicing requests with a critical resource ν = 50; 250 μs.

The calculation results for the models showed that the waiting time for the release of the monitor is much higher than the waiting time for the semaphore that increases the response time of the reconfigurable computation system; spin lock is the least time-consuming over the entire range of load changes.

At the same time, the simulation results confirm that it is most expedient to use spin-locking for processes that often access to shareable resources, the processing time of which on processor nodes is small. The disadvantage of this method is the cost of pre-programming, which greatly complicates its use.

When using a monitor, it takes a longer time to wait for it to be released, however, this method is simpler to use and can be used for processes that have a long processing time in the processor node.

A study of various service times in the processor node and in the semaphore was also made to develop a criterion for choosing the optimal access method for a single shareable resource. In this case, the ratio of the loading coefficient of the semaphore Ps to the loading coefficient of the processor node Pcp (8) was calculated.

If to analyse the 4-processor reconfigurable computation systems with different service times in the processor node and semaphore, and also take into account the conclusions made above, we find that in order to choose the optimal method of accessing data, it is necessary that the coefficient Z would lie within the limit

$$0{,}4 * K / n \leq Z \leq 1 * K / n, \qquad (10)$$

Where n is the number of critical resources.

For a 4-processor system with 2 shareable resources $0.8 \leq Z \leq 2$; for a 4-processor reconfigurable computation system with 4 resources $0.2 \leq Z \leq 1$.

Previously, data were obtained for the system (Biktashev and Martyshkin, 2013), based on which the graphs depicted in Figures 8 and 9 were constructed.

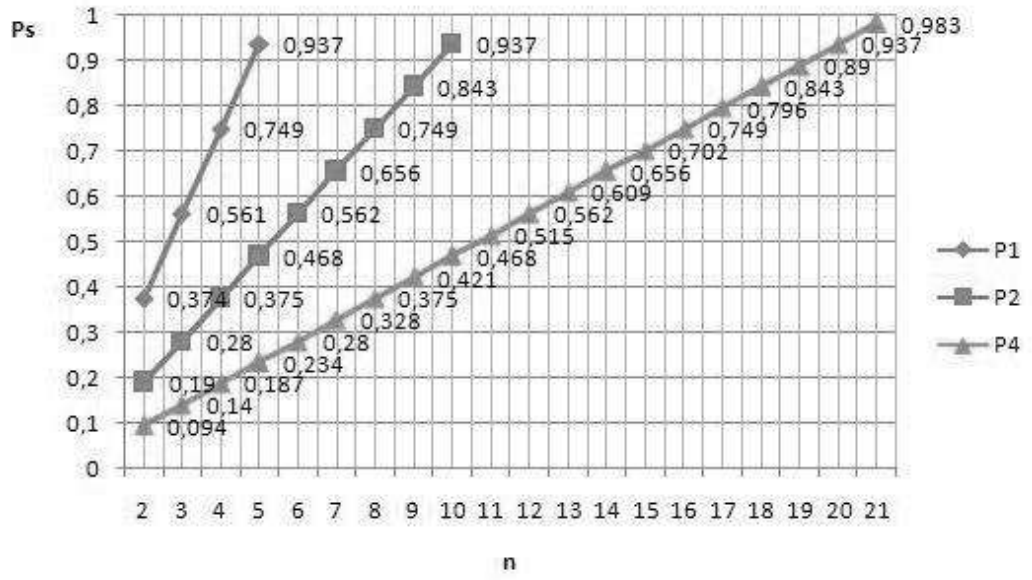

Figure 8 - Dependence of the semaphore load factor in the n-processor reconfigurable computation system on the number of processor node

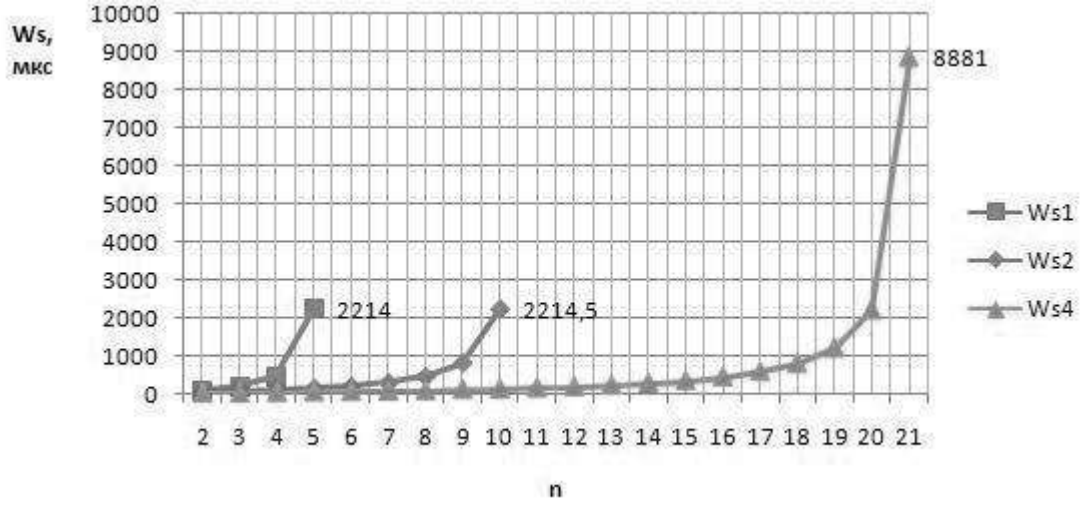

Figure 9 - Dependence of the semaphore latency in the n-processor reconfigurable computation system on the number of processor node

The graphs show that if there is one semaphore, the maximum number of executed processes is no more than 4, since the probability of accessing the semaphore is high, which

affects the increase in the wait time for this resource, while this probability decreases with the increase in the number of semaphores in the reconfigurable computation system.

Conclusions

The calculation for the models showed that spin lock method is the least time-consuming over the entire range of load changes for fixed values of t_{ks}, t_{cw}, σ, and t_p. The method based on locking in the kernel creates a higher complexity and significantly increases the response time (reduces performance) of the reconfigurable computation system.

It is known that the reliability of computing process control functions is higher if they are implemented in the kernel. However, such an implementation reduces the performance of the reconfigurable computation system. To remove the inconsistency and ensure high reliability in combination with high performance, a hardware implementation of the function for controlling the synchronization of parallel processes in the reconfigurable computation system is required.

Acknowledgements

Research was supported by the RFBR Grant for Best Projects of Basic Research, Grant No. 19-07-00516 A.

References

Aliev T.I. (2009). Fundamentals of modelling discrete systems. St. Petersburg: St. Petersburg State University ITMO, 2009.363 p.

Andrews G.R. (2003). Basics of multi-threaded parallel and distributed programming. Transl. from English M. : Williams, 2003.512 p.

Biktashev R.A., Martyshkin A.I. (2013). A set of programs for measuring the performance of operating system functions.// XXI century: results of the past and problems of the present plus. 2013. No. 10 (14). Pp. 190-197.

Fundamentals of computational system theory (1978). Edited by S.A. Mayorov. M.: Higher School, 1978.408p.

Kleinrock L. (1979a). Computing systems with queues: Publishing House Mir - M. : 1979. 600 p.

Kleinrock L. (1979b). Queuing Theory. - M.: Mechanical Engineering, 1979. 432 p.

Kreutzler S. (1986). Designing operating systems for small computers: Translated from English.- M.: Mir, 1986. 680 p

Martyshkin A.I. (2016a). Mathematical modelling and performance evaluation of process synchronization tools in multiprocessor systems. Scientific notes of the International Humanitarian University. Papers of participants of the Second International Multidisciplinary Conference. 2016. P. 151-157.

Martyshkin A.I. (2016b). Semaphore performance issues in parallel systems. The evolution of modern science: Collection of papers of the International scientific-practical conference: in 3 parts. Executive Editor: Asatur Albertovich Sukiasyan.2016. P. 81-83.

Martyshkin A.I. (2016c). Modern methods for measuring the performance of multicore computing systems. New information technologies and systems; collection of scientific papers at the XIII International scientific and technical conference.2016. P. 128-131.

Martyshkin A.I. (2017). Performance evaluation of high-performance systems, taking into account failures and recoveries of computing nodes // Modern innovative technologies for training engineering personnel for mining and transport.2017. Number 4. P. 425-429.

Martyshkin A.I. (2018a). Possible structural organization and performance assessment of reconfigurable computing systems based on a common bus // Models, systems, networks in economics, technology, nature and society.2018. No. 1 (25). Pp. 141-150.

Martyshkin A.I. (2018b). Mathematical models of semaphores for coordinating access to shared resources of multiprocessor systems // Colloquium-journal.2018. No. 8-1 (19). Pp. 36-39.

Martyshkin, A.I. (2016d). Development and research of open-loop models the subsystem "processor-memory" of multiprocessor systems architectures UMA, NUMA and SUMA. ARPN Journal of Engineering and Applied Sciences. 2016. Volume 11. Issue 23. PP. 13526-13535

Martyshkin, A.I. (2016e). Mathematical modelling of Tasks Managers with the strategy in space with a homogeneous and heterogeneous input flow and finite queue. ARPN Journal of Engineering and Applied Sciences. 2016. Vol. 11. Issue 19 PP. 11325-11332.

Martyshkin, A.I., Yasarevskaya, O.N. (2015). Mathematical modelling of Task Managers for Multiprocessor systems on the basis of open-loop queuing networks. ARPN Journal of Engineering and Applied Sciences. 2015. Vol. 10. Issue 16 PP. 6744-6749.

Matalytsky M.A., Tikhonenko O.M., Koluzaeva E.V. (2011). Queuing systems and networks: analysis and requests: Monograph. Grodno: GrSU, 2011.816 p.

Tanenbaum E., Bos H. (2015). Modern Operating Systems. 4th ed. SPb. : Peter, 2015.1120 p.: ill. (Series "Classic computer science").

Combined electric accumulation unit for air heating

Dmitry Tikhomirov *
Stepan Dudin *
Stanislav Trunov *
Sergey Rastimeshin **
Anatoly Tikhomirov *
Alexey Kuzmichov *

ABSTRACT
The article describes the functional-technological scheme of an energy-efficient combined electric accumulation heating system for agricultural production facilities. A distinctive feature and novelty is the use of direct and accumulative heating. They presented the main provisions of the heat power and aerodynamic calculation for the standard size range of such plants. Based on the results of experimental studies, a number of functional dependencies were obtained that characterize the operating modes of the plant. They determined the value of the heat transfer coefficient from the heat accumulating core to the circulating air depending on the coolant flow rate $\alpha = f(G)$. They presented the technical characteristic of the combined electrical unit current sample.
KEYWORDS: heat accumulation, convector, combined electrical unit, heat transfer, electrical heating, agriculture

Unidad combinada de acumulación eléctrica para calentamiento de aire

RESUMEN
El artículo describe el esquema funcional-tecnológico de un sistema de calefacción de acumulación eléctrica combinada de eficiencia energética para instalaciones de producción agrícola. Una característica distintiva y novedosa es el uso de calentamiento directo y acumulativo. Presentamos las principales previsiones de la potencia térmica y el cálculo aerodinámico para el rango de tamaño estándar de tales plantas. Con base en los resultados de los estudios experimentales, se obtuvieron una serie de dependencias funcionales que caracterizan los modos de funcionamiento de la planta. Determinamos el valor del coeficiente de transferencia de calor desde el núcleo acumulador de calor hasta el aire circulante dependiente del caudal de refrigerante $\alpha = f(G)$. Presentamos la característica técnica de la muestra de corriente de la unidad eléctrica combinada.
PALABRAS CLAVE: acumulación de calor, convector, unidad eléctrica combinada, transferencia de calor, calefacción eléctrica, agricultura.

* Federal Scientific Agroengineering Center VIM.
**Russian State Agrarian University - Moscow Timiryazev Agricultural Academy; Moscow, Russian Federation.

Recibido: 05/09/2019 Aceptado: 15/10/2019

Introduction

Agriculture is a large consumer of thermal energy (Tikhomirov et al., 2017). With the introduction of heat accumulators and electricity metering differentiated during the day, the efficiency of its use in technological processes of heat supply to various agricultural production facilities can be increased significantly (Tikhomirov et al., 2019). This ensures the alignment of daily schedules of electrical loads in networks; the reduction of costs to maintain the indicators of electricity quality among consumers; the reduction of the need for the energy system to reserve additional capacity; the possibility of a tangible increase in the power supply of the economy without a significant increase of electric network and distribution substation load; the reduction of electrical equipment set capacity by 40 ... 60%; the reduction of current annual electricity costs for consumers (Kagan et al., 1980).

The results of patent document analysis on the subject under consideration in the World Intellectual Property Organization (WIPO) database confirmed the research relevance. Over the past five years, they received more than 182 patent documents in the field of thermal energy accumulation. The leaders are the UK, China, Russia, the USA and Germany. Various materials and methods of thermal energy accumulation are considered and studied: by solids through their internal energy increase, by phase transition heat use, in saturated liquids, by the means of compressed gas, etc. (Dincer and Ezan, 2018).

The review of latent thermal energy storage devices for material stability increase and efficient load control is presented in (Rathod and Banerjee, 2013; Pielichowska and Pielichowski, 2014). The energy efficiency of heat storage device use with single-phase heat-accumulating materials was substantiated in (Kukolev and Kukelev, 2004).

The aim of the study is to develop an energy-efficient heat accumulating heating system and the methods for its operation calculation in agricultural production.

1. Design diagram of combined electrical unit

Two types of heating devices with heating elements — direct (convector) and accumulative heating (Fig. 1), are located in one thermally insulated casing of our electric unit for air heating (Patent 2638696), in contrast to the known designs.

Depending on the operating mode, these devices can operate simultaneously or separately. The mixing chamber 5 (Fig. 1) is located in the upper part of the electrical unit general case to combine air flows from the heat accumulator 2 and the convector 7, which significantly increases the heater efficiency (Trunov et al., 2016).

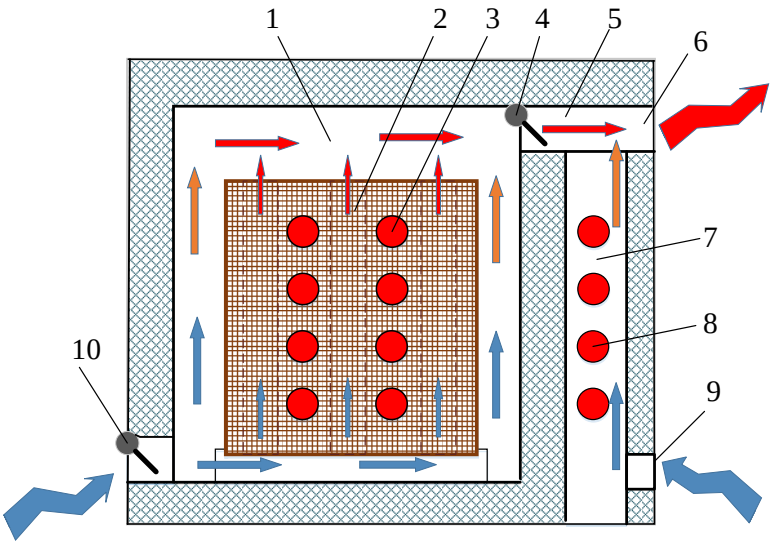

Figure 1 - The accumulation unit scheme:

1– heat accumulator chamber; 2 – heat accumulator core; 3 – accumulator core electric heaters; 4 – adjustable air damper; 5 – mixing chamber; 6 – heated air outlet; 7 – convector; 8 – convector electric heaters; 9 – air inlet; 10 – air damper.

The single-phase heat-accumulating core is enclosed in a protective heat-insulating casing, which has two openings: the inlet bottom and the outlet top with an adjustable air damper 4, which automatically or manually controls the flow of heated air and, accordingly, the heat transfer of the unit (Trunov et al., 2016).

2. Calculation method of electrical accumulation device

The methodology for electric storage device calculation to heat air includes thermal, structural, electrical and aerodynamic calculations. The technique is intended to justify the heat, power and structural parameters at a given power of the heating device for energy-efficient provision of the established operating modes.

2.1. Heat calculation

In general, the process of charging and discharging heat storage devices was solved in (Kukolev and Kukelev, 2003); however, particular solutions are required to calculate specific structures. One of the main parameters of a heater is the volume of the heat-accumulating core V_c, which is determined from the condition of the heat balance, and the following temperature values (average over the thickness of the accumulating core) are taken: when the "charging" process is completed, t_{max} = 500 - 600 ºC, when the "discharge" process is completed t_{min} = 100 - 120 ºC.

$$V_c = P_u \tau_d / \rho_c c_c (t_{max} - t_{min}) \quad (1)$$

Where P_u is the useful (given) power of the storage heater, W; τ_d — core discharge time, h; ρ_c is the density of the core material, kg/m^3; c_c - specific heat of the core material, J/kg°C.

Based on the existing experience in the design of storage electric heating plants, the volume of the device V is determined from the relation (Trunov and Rastimesin, 2015):

$$V = (1{,}8 - 2{,}0)\, V_c \quad (2)$$

Using the obtained value of V, they choose the relationship between the heater length, width and height for structural reasons. The height of the heater is determined by the results of aerodynamic calculation. The selected structural parameters of the unit make it possible to determine the outer surface area F_{ext} of the device.

The maximum temperature of the outer surface at the completion of the "charging" process is t_{ext} max = 40 ° C; upon completion of the "discharge" process - t_{ext} min = 20 ºC.

At the beginning of the heating cycle, there are practically no heat losses and the average value of the heat power loss P_{los} from the heating device during the charging process into the surrounding space is calculated for the outdoor temperature of the device surface:

$$t_{ext} = (t_{ext\,max} + t_{ext\,min})/2, \quad (3)$$

where $t_{ext\,max}$ and $t_{ext\,min}$ – the maximum and the minimum temperature of the heater outer surface, °C.

$$P_{los}=k_r\,\alpha_{ext}\,F_{ext}\,(t_{ext}-t_0), \qquad (4)$$

where α_{ext} is the heat transfer coefficient from the outer surfaces of the heater to the surrounding space (room), W/m^2 °C; t_0 is the temperature of the surrounding space, °C; k_r - the safety factor.

Heat losses associated with the radiation of the heat-transfer surface are not taken into account. For our calculations we can take the following according to the source (Trunov and Rastimesin, 2015) with sufficient accuracy:

$$\alpha_{ext} = 8\ \text{W/(m}^2\,^\circ\text{C)};\ k_r = 1{,}2;\ t_0 = 15\text{–}20\ ^\circ\text{C}$$

The main structural parameters of the storage heater include the thickness of the insulation layer δ_{ti}.

To determine δ_{ti}, one should proceed from the general principles of thermal conductivity theory, considering the lining as a single-layer flat wall. The required wall thickness of the heat-insulating layer (lining), at which the heat loss of the device will correspond to Plos, is determined from the following equation:

$$\delta_{ti} = [\lambda_l F_{av}(t_1 - t_{ext\,max})] / P_{los} \qquad (5)$$

where: λ_l – the coefficient of the lining material thermal conductivity, W/m°C; t_1 - the temperature of the lining inner layer makes 450-500 °C by the end of the charging process.

$$F_{av} = (F_{int}+F_{ext})/2, \qquad (6)$$

where F_{int} is the internal surface area of the lining.

At the first stage of the calculation, F_{av} value is taken equal to the F_{ext} area (Kagan et al., 1980). The accepted values are specified after the calculation the heat accumulating core heating.

After the loss power and thermal insulation thickness are determined, they determine installed (connected) power P_{inst} of the heat accumulator electric heating elements.

$$P_{inst} = \kappa_r P_u\ \tau_d/\tau_{ch} + P_{los}, \qquad (7)$$

where: κ_r = 1,1–1,2 – power reserve factor taking into account the aging of heating elements, the possibility of supply voltage reduction, etc.; τ_{ch} - the duration of the heat accumulator charging period, h.

The power spent on heat accumulating core heating is determined by the following formula:

$$P_c = P_{inst} / \kappa_r - P_{los}. \quad (8)$$

The calculation of the core heating process is reduced to the calculation of plate one-sided heating in constant heat flow mode. The temperature on the surface of the core t_c (from the lining side) is determined by the following expression (Sweenchanski, 1975).

$$t_c = t_{c1} + \frac{P_c \delta_c}{f_c \lambda_c}(2Fo + 2/3), \quad (9)$$

where: t_{c1} – the initial temperature (average) of the core by the end of the discharge process (taken at 100 °C and specified at the stage of discharge process calculation); λ_c - the coefficient of the core material thermal conductivity, W/m°C; δ_w - the wall thickness between the air channel and the lining, m; f_c - the surface area of the air channels of the core, m^2; $F_o = a_c \tau_{ch}/\delta_c^2$ – Fourier number; a_c – the thermal conductivity ratio of the core material, m^2/s.

The number of channels, the geometric dimensions of their cross section are selected for structural reasons (Fig. 1). They take the wall thickness δ_w roughly between the air channel and the lining equal to 0.065-0.1 m.

Based on the obtained value of the volume of the heat accumulator core V_c and thermal insulation ($\Delta V = V - V_c$), as well as the selected material from which the named structural elements are made, it is possible to determine the amount of accumulated heat by the following expression:

$$Q_{ak} = c_m \gamma_m V_c \Delta t; \quad (10)$$

where: c_m – the heat capacity of the core material, J/kg°C; γ_m – the specific gravity of the core material, N/m^3; Δt is the temperature difference, °C.

The amount of heat accumulated by the heater allows you to determine the time of its heating τ_h:

$$\tau_h = Q_{ak} / (0{,}8P_{inst} - 0{,}5P_{los}) \quad (11)$$

where: P_{los} – heat loss by the device, W.

The resulting heating device heating time must not exceed the time of the reduced tariff in the power system.

2.2. Aerodynamic calculation

The purpose of aerodynamic calculation is to determine the height of the instrument housing H_c, the interaxial distance H and the area of the inlet F_1 and outlet F_2 hole in the instrument housing (Fig. 2).

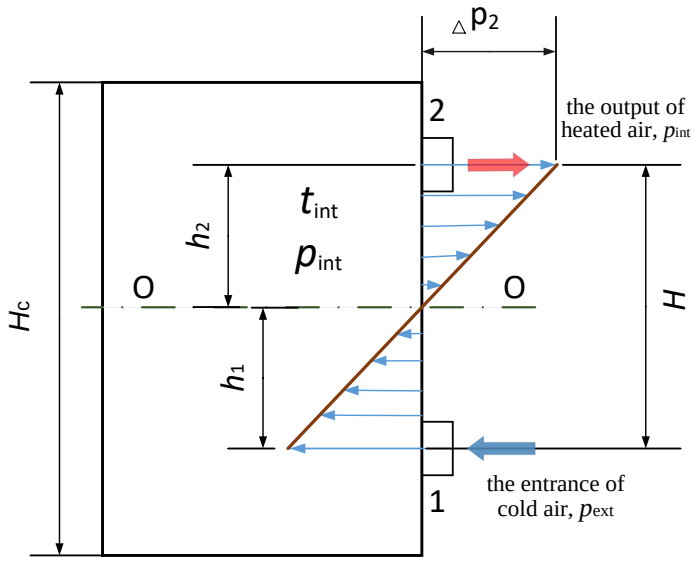

Figure 2 - The scheme of the accumulation unit aerodynamic calculation

The natural air flow in the heater is created due to the difference in air temperatures and, accordingly, the densities of air heated in the heat accumulating core of the heater and the air in the heated room (Rastimesin and Trunov, 2016).

Within the height H, which mainly affects the height of the heater unit H_c, there is a neutral plane 0-0, in which the pressure p inside the device will be the same as outside, i.e. the pressure difference is zero (Basta and Rudnev, 2010). The pressure of the external and internal air in the plane of the hole 1:

$$p_{1ext} = p + h_1 \rho_{ext} g, \quad (12)$$

$$p_{1int} = p + h_1 \rho_{int} g, \quad (13)$$

where p is the air pressure in the plane O-O, Pa; h1 is the distance from the center from hole 1 to the neutral plane, m; ρext is the density of outdoor air, kg/m^3; ρint is the density of internal air at t_{cmin}, kg/m^3; t_{cmin} is the minimum core temperature, i.e. at the end of discharge, °C; g is the acceleration of gravity, m/s^2.

According to the thermophysical properties, $\rho_{ext} > \rho_{int}$; therefore, $p_{1ext} > p_{1int}$. It follows that the outside air enters hole 1.

The pressure difference in the plane of the hole 1 is equal to:

$$\Delta p_1 = p_{1ext} - p_{1int} = (p + h_1 \rho_{ext} g) - (p + h_1 \rho_{int} g) = h_1 (\rho_{ext} - \rho_{int}) g, \quad (14)$$

Similarly, the pressure of the external and internal air in the plane of the hole 2 make the following: $p_{2ext} = p - h_2 \rho_{ext} g$, $p_{2int} = p - h_2 \rho_{int} g$.

Since $h_2 \rho_{ext} g > h_2 \rho_{int} g$, then $p_{2ext} > p_{2int}$. Internal warm air will go out of the hole 2 of the heater to the outside and the pressure difference in the plane of the hole 2 will be the following:

$$\Delta p_2 = p_{2int} - p_{2ext} = (p - h_2 \rho_{int} g) - (p - h_2 \rho_{ext} g) = h_2 (\rho_{ext} - \rho_{int}) g, \quad (15)$$

The total pressure required for air to move through the opening 1 and 2:

$$\Delta p = \Delta p_1 + \Delta p_2 = h_1(\rho_{ext} - \rho_{int})g + h_2(\rho_{ext} - \rho_{int})g = H(\rho_{ext} - \rho_{int})g. \quad (16)$$

According to a well-known expression in hydraulics:

$$\Delta p = U^2\rho/2g \quad (17)$$

and after its conversion relative to the air velocity U in the hole 1 and 2 respectively we get the following:

$$U_1 = \sqrt{2gh_1(p_{ext} - p_{int})/p_{ext}};\ U_2 = \sqrt{2gh_2(p_{ext} - p_{int})/p_{int}}. \quad (18)$$

The values of the air velocity at the inlet and outlet are taken for structural reasons at the level of 4–7 m/s [13]. Then

$$h_1 = \frac{U_1^2 p_{ext}}{2g(p_{ext} - p_{int})},\ h_2 = \frac{U_2^2 p_{int}}{2g(p_{ext} - p_{int})}, \quad (19)$$

Using the found value $H = h_1 + h_2$ and taking into account the design features of the heater with heat accumulation, the height of the heater body H_c is determined. The found value of the interaxial distance H determines the gravitational air pressure in the device Δp. At this pressure, air flows through the device with the speed U_1 and U_2 set at the inlet and outlet.

Inlet and outlet areas F_1 and F_2:

$$F_1 = G_1/(3600\mu U_1) = G_1/(3600\mu\sqrt{2gh_1(\rho_{ext} - \rho_{int})/\rho_{ext}}; \quad (20)$$

$$F_2 = G_2/(3600\mu U_2) = G_2/(3600\mu\sqrt{2gh_2(\rho_{ext} - \rho_{int})/\rho_{int}}; \quad (21)$$

where $G_{1,2}$ - the air flow through the holes of the device, m^3/h; μ is the flow coefficient that takes into account the pressure loss during the jet compression when it passes through the hole. Thus, the flow occupies the cross section smaller than the hole dimension (μ = 0.65).

Assuming that $G_1 = G_2$, the air flow is determined from the following expression:

$$G_{1,2} = 3600P_u/c\rho_{out}\Delta t_{ov}, \quad (22)$$

where P_u is the useful (given) device power, W; , °C; Δt_{ov} - the temperature of air overheating in the heating device, °C; ρout is the density of the air leaving the device at overheating temperature, kg/m^3.

2.3. Main provisions of electrical calculation

The tubular heating elements (THE) or spirals in ceramic tubes are used, as a rule, as the heating elements in such heating devices.

The calculation of electric heating elements includes the selection of the specific surface power of the heater at which the temperature on the heater surface does not exceed the permissible value. At that, the power released in the heating elements is transferred to the core during charging with thermal conductivity.

Tubular heating elements (THE) are used as the heating elements in the developed heating device, that are tightly installed in the heat accumulator core and located symmetrically.

Heat transfer through a cylindrical wall should be taken as an ideal design scheme for the specific surface power determination of a heating element.

The calculation includes the determination of the specific surface power of the heater at which the temperature on the heater surface does not exceed the allowable value.

For tubular spiral heaters, heat transfer through a uniform cylindrical wall, the thermal field of which will be one-dimensional, and isothermal surfaces are concentric cylinders whose axis coincides with the axis of the heater can be an ideal design scheme.

The actual specific surface power of the heating element working surface has the following form (Sweenchanski, 1975):

$$W_2 = k\frac{2{,}32\pi 10^{-2}\lambda}{H\ln D_2/D_1}(t_1 - t_2), \qquad (23)$$

where k is the coefficient of the heating element configuration; λ is the coefficient of the heat accumulator material thermal conductivity; H is the step of the heaters (the distance between the heaters; D_1 is the outer diameter of the tubular heating element; the equivalent

diameter $D_2 = 2/\pi(A + B)$; the values of A and B are the geometric dimensions of the heat storage core (A is the height and B is the thickness).

At that the specific surface power of the heater (TEH) will be equal to:

$$W_1 = k\frac{2{,}3210^{-2}\lambda(t_1 - t_2)H}{\pi d D_1 \ln D_2 / D_1}, \qquad (24)$$

d – the inner diameter of the heating element tube, mm.

The configuration coefficient k of tubular heating elements can be determined from known curves for wire frame heaters.

The obtained value of the specific surface power of the heater W_1 must be less than or equal to the allowable specific surface power of the heater W_v.

$$W_1 \leq W_v. \qquad (25)$$

They developed and tested the generalized calculation method, which allows one to determine the structural, heat-energy and electrical parameters of energy-efficient combined heat-storage electrical devices of a standard size range for air heating in agricultural premises.

3. Device main modes and experimental research

The main operating modes of the combined electric accumulating unit for air heating (Rastimesin and Trunov, 2016): the heat accumulator charging during the period of the reduced electricity tariff; the heat accumulator charging during the period of the reduced electricity tariff + operation of a direct electric heater - electric convector; the heat accumulator discharge during the period of the high tariff for electricity; the heat accumulator discharge

during the period of the high electricity tariff + the operation of a direct electric heater - electric convector; independent operation of the electric convector according to a given program.

Based on the calculation results, they developed the operational experimental model of a combined electrical device with heat storage and the set power of 7.2 kW (Fig. 3, Table 1).

The graph of charging and uncontrolled discharge of the heat storage unit is shown on Figure 4. During unregulated discharge of the device, the temperature of the heat accumulator t_c and the heat flux Q (kW) are changed exponentially from the heat storage core to the circulating air:

$$t_c=545,3e^{-0,3\tau}, \quad (26)$$

$$Q=16,6e^{-0,41\tau}. \quad (27)$$

Figure 3 - Combined electrical device with heat accumulation

Table 1 – Device Specifications

Power voltage, V	380/220
Heat storage power, W	4,8
Electric convector power, W	2,4
Heat accumulator charging time, h	4
Heat storage discharge time, h	4-8
Device weight, kg	200

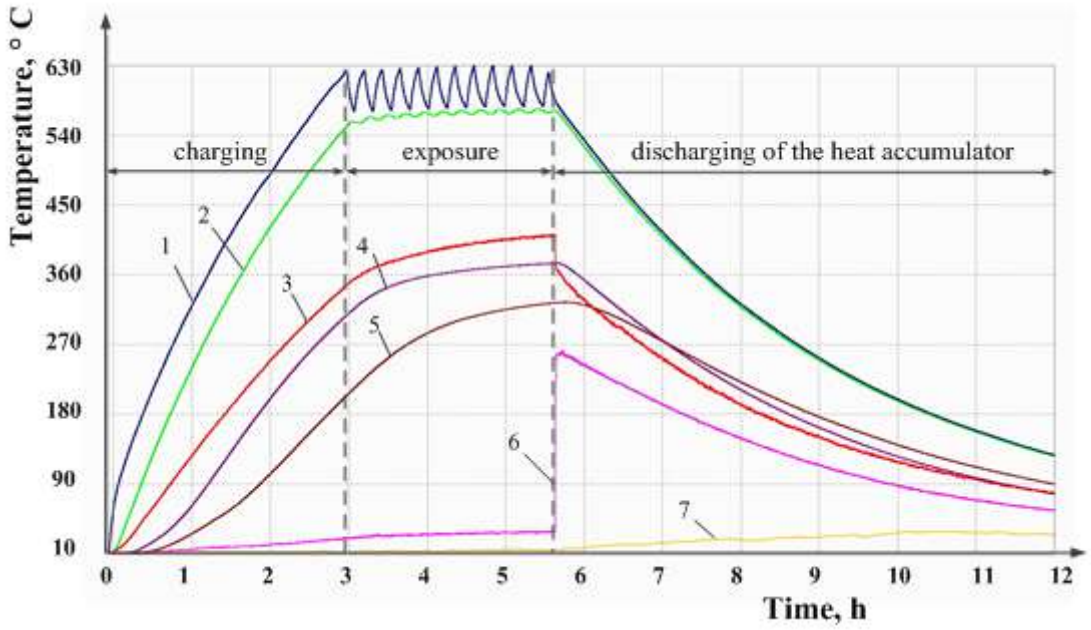

Figure 4 - Schedule of charging and unregulated discharge of the combined heat storage unit:

1 – the electric heater temperature; 2 – the heat accumulator temperature; 3, 4, 5 - the inner layer temperature of thermal insulation; 6 – the temperature of the outgoing heated air; 7 – indoor temperature.

The value of the heat transfer coefficient α (W/m^{2}K) from the heat-accumulating core to the circulating air is determined depending on the flow rate of the coolant G (m^3/h): α = 0.51G - 18.77. This parameter is decisive for heat flux calculation during the regulated and unregulated discharge of the device heat accumulator.

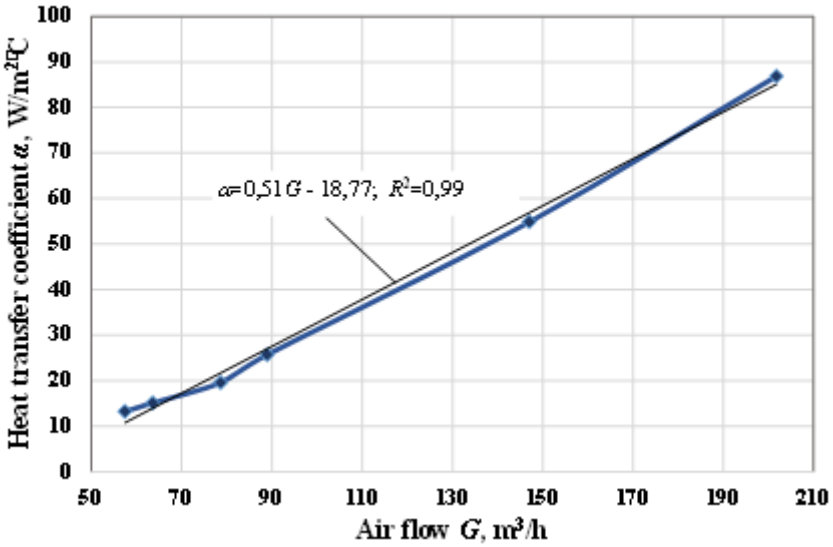

Figure 5 - The dependence of the heat transfer coefficient from the heat storage core to circulating air

4. Summary

They developed the functional diagram of an energy-efficient combined electric storage heating system for agricultural facilities. A distinctive feature is the use of direct and accumulation heating in one device. The accumulation of heat is carried out by a solid body made of chromomagnesite by its internal energy increase. The novelty of the design is protected by the Russian Federation patent (Patent 2638696).

They developed and presented the main provisions of the methodology for air heating electric storage device calculation, which includes the thermal, electrical and aerodynamic calculations necessary to justify the heat and power and structural parameters of the device at a given power and established operating modes.

Based on the calculation results, they developed the working model of an energy-efficient heating system for agricultural facilities with the power of 7.2 kW. The power of the heat accumulator makes 4.8 kW.

According to the results of experimental studies, they obtained a number of functional dependencies characterizing the device operating modes. The value of the heat transfer coefficient α (W/m^2K) from the heat-accumulating core to the circulating air is determined depending on the flow rate of the coolant G(m^3/h): $\alpha = 0.51G - 18.77$.

The current device sample has been introduced into production at the dairy farm. The annual economic effect amounted to 124 thousand rubles as compared to the electric heating plant without heat storage.

Conflict of interests

The author confirms that the presented data do not contain a conflict of interest.

References

Basta, T. M., Rudnev S. S. & Nekrasov, B. B. and others (2010). Hydraulics, hydraulic machines and hydraulic drives. M.: Alliance. 424 p.

Dincer I., Ezan M.A. (2018) *Thermal Energy Storage Methods. In: Heat Storage:* A Unique Solution For Energy Systems. Green Energy and Technology. Springer, Cham https://doi.org/10.1007/978-3-319-91893-8_3

Kagan, N. B., Kaufman, V. G., Pronko, M. B. & Yanevsky, G. D. (1980) *Electrothermal equipment for agricultural production.*– M.: Energy. 192 p.

Kukolev, M. I. & Kukelev, Y. K. (2003). *The calculation process of charge and discharge in thermal energy storage* (Part II) // Proceedings of the forest engineering faculty of PetrSU. Issue. 4. – Petrozavodsk: publishing House of PetrSU. – P. 68 – 72.

Kukolev, M. I. & Kukelev, Y. K. (2004). *The Energy efficiency of thermal drives with single-phase thermal storage materials* / Fundamental research in technical universities: materials of the VIII All-Russian conference on problems of science and higher education. – SPb: Izd-vo SPbSPU, p. 175-176.

Patent 2638696 RF. *Combined heat storage electric heating device with step heating of the heat storage core* / S.N. Dudin, D.A. Tikhomirov, S.S. Trunov, N.G. Lamonov, D.N. Dudina. Application No. 2016138606; declare 29.09.2016; publ. 15.12.2017. Bul. No. 35. - 7 p.

Pielichowska, K., & Pielichowski, K. (2014). *Phase change materials for thermal energy storage.* Progress in Materials Science, 65, 67–123.

Rastimesin, S. A., & Trunov, S. S. (2016). *Energy Saving system and technical means of heating and ventilation of livestock buildings*. Moscow: GNU vieskh, LTD. "Sam poligrafist". 180 p.

Rathod, M. K., & Banerjee, J. (2013). *Thermal stability of phase change materials used in latent heat energy storage systems*: A review. Renewable and Sustainable Energy Reviews, 18, 246–258.

Swenchanski A. D. (1975). *Electric furnace. Electric resistance furnaces.* Ed. 2-e, Rev., M., "Energy", 384 p.

Tikhomirov, A.V., Markelova, E. K. & Tikhomirov, D. A. (2017). *The main directions for the improvement of systems and means of energy supply of agricultural facilities* / Agricultural machinery and energy supply. 3 (16). 34–42.

Tikhomirov, D.A., Vasiliev, A.N., Budnikov D.A. & Vasiliev A.N. (2019). *Energy-saving device for microclimate maintenance with utilization of low-grade heat*: Innovative Computing Trends and Applications Сер. "EAI/Springer Innovations in Communication and Computing" Cham. 31-38.

Trunov, S. S., & Rastimesin, S. A. (2015). *The basis of the calculation of electroheating device* // Bulletin of viesh. 2(19). 57-63.

Trunov, S. S., Tikhomirov, D. A., Dudin, S. N. (2016). *Electric heating device with heat accumulation for agricultural premises* / Innovations in agriculture. № 4 (19). P. 146-152.

Effects of density dependent migration on the spread of infectious diseases: A Mathematical Model

S. k. Sharma *
J.B. Shukla **
Jitendra Singh ***
Shikha Singh ***

ABSTRACT

In this paper, an SIS Mathematical model is proposed and analyzed by considering population density dependent migration. It is assumed that the disease is transmitted by direct contact of susceptibles and infectives with immigration and emigration dependent contact rate. The equilibrium analysis of the model is conducted by using the stability theory of ordinary differential equation and simulation. The model analysis shows that the spread of infectious disease increases as therate of immigration increasesbut its spread decreases as emigration rate increases and also if non-emigrating population density increases then infective population increases. The simulation study also confirms these analytical results.

KEW WORDS: Epidemiology, mathematical modelling, Density dependent migration, stability.

*College of computer and Information Sciences, Majmaah University, Majmaah 11952, Saudi Arabia, jite_math@yahoo.co.in
**Innovative internet University for research (A think tank), Kanpur, (UP), India.
***Department of Mathematics PPN College, CSJM University, Kanpur (UP), India.
***Department of Mathematics PPN College, CSJM University, Kanpur (UP), India.

Recibido: 04/09/2019 Aceptado: 03/10/2019

Efectos de la migración dependiente de la densidad en la propagación de enfermedades infecciosas: un modelo matemático

RESUMEN

En este artículo se propone y analiza un modelo matemático SIS considerando la migración dependiente de la densidad de población. Se supone que la enfermedad se transmite por contacto directo de susceptibles e infecciosos con la tasa de contacto dependiente de inmigración y emigración. El análisis de equilibrio del modelo se realiza utilizando la teoría de la estabilidad de la ecuación diferencial común y la simulación. El análisis del modelo muestra que la propagación de enfermedades infecciosas aumenta a medida que aumenta la tasa de inmigración, pero su propagación disminuye a medida que aumenta la tasa de emigración y también si aumenta la densidad de población no emigrante, entonces aumenta la población infecciosa. El estudio de simulación también confirma estos resultados analíticos.

PALABRAS CLAVE: Epidemiología, modelación matemática, migración dependiente de la densidad, estabilidad.

Introduction

Epidemiology is the study of patterns, causes, and effects of health and disease conditions in a population. It provides critical support for publiche alth by identifying risk factors for disease and targets for preventive medicine. Epidemiology has helped develop methodology used in clinical research and public health studies. Major areas of epidemiological study include disease etiology, disease break, disease surveillance, and comparison of treatment effects such as in clinical trials. Epidemiologists gather data and apply a broad range of biomedical and psychosocial theories to generate theory, test hypotheses, and make educated, informed assertions as to which relationships are causal and in which way. For example, many epidemiological studies are aimed at revealing unbiased relationships between exposure to smoking, biological agents, stress, or chemicals to mortality and morbidity. In the identification of causal relationship between these exposures and outcome epidemiologists use statistical and mathematical tools.

In the age of globalization due to emigration from one geographic location to another location, the spread of infectious disease is measure concern for the human or animal

living. The density dependent dispersal movements play a key factor in the fate of epidemic outbreaks occurring within spatially distributed populations.

It is well established that the immigration is a very important factor to bring in a new disease or to spread of old disease that is present in community therefore in most of countries, apart from other disease related factors, the immigration is restricted and whenever it is allowed then lot of immunization process is applied. It is well known that migration effect the spread of disease but the number of people living in the habitat (non-emigrating population density) must also play a very important role in the spread of disease. The spread of infectious diseases in human population depend upon various factors including densities of susceptibles and infectives, their variable contact rate (Greenhalgh & Das, 1992), density population migration Linda (Q Gao & Herbert H W(1992), human carrying capacity of habitat and non-emigrating population of the habitat etc. Many infectious diseases transmit through the direct contact of susceptibles and infectives such as H1N1, tuberculosis, influenza, conjunctivitis, AIDS, Hepatitis and typhoid fever (Zhou & Hethcote, 1994; May & Anderson,1979). The most of the research related to the spread of infectious diseases is a constant immigration dependent (Last, 2001; Hsu & Zee, 2004) but density dependent migration (variable immigration and emigration) [Linda Q Gao & Herbert H W(1992] is also plays very important role in the spreading of infectious diseases. There are two aspect of migration process as immigration and emigration. The following two important aspects has been found missing.

(i) Thepopulation density of community under consideration (non-emigrating population) where the disease is spreading.
(ii) Human carrying capacity of habitat.

In the past, mathematical models have been used to study the spread of infectious diseases by taking the rate of contact between susceptible and infective as a constant (Hethcote,1979 & 1991; May & Anderson,1988; Singh et al,2003 &2015; Shukla et al,

2004). But population density dependent rate of contact plays an important role in the spread of infectious diseases (Greenhalgh,1990; Lee & Maa, 2002; Linda & Herbert, 1992).

The contribution of variable rate of migration (immigration and emigration) as well as density dependent rate of contact for the spread of infectious diseases are equally important but have not been studied so far.

In this paper, therefore, it is proposed to model and analyze the effect of density dependent migration as well as the non-emigrating population on the spread of infectious diseases by considering the density (immigration and emigration) dependent contact rate. The migration function $f(N)$ of human population density N with constant immigration rate A is assumed as follows.

$$f(N) = A + \mu_1(K - N) - \mu_0(N - N_0);\ A > 0, K \geq N, N \geq N_0 \geq 0. \quad (1.1)$$

In (1.1), K is the carrying capacity of the habitat, N_0 is the population density of non-emigrating population, μ_1 is the rate coefficient of immigration and μ_0 is the rate coefficient of emigration. It is noted from (1.1) that when K increases, immigration increases(i.e.when $K \to \infty$, immigration is allowed forever) .When $N = N_0$, the variable emigration is zero i.e. $f(N) = A + \mu_1(K - N)$(i.e. people are not allowed to leave the habitat).

In this paper, we also assume that the rate of contact between susceptibles and infectives is immigration and emigration dependent. Thus the variable rate of contact $\beta_c(N)$ is assumed non-negative function of N as follows:

$$\beta_c(N) = \beta + \beta_1(K - N) - \beta_0(N - N_0). \quad (1.2)$$

Where β is a constant rate of contact, β_1 is the coefficient of rate of immigration and β_0 is the coefficient of rate of emigration. It is noted that as K increases $\beta_c(N)$ increases.

1. SIS Model

In classical epidemiological models postulate that a population is divided into two class of epidemiological significance and homogeneously mixed. The spread of infectious diseases traditionally follows the principle of mass action and associated with incidence (Korobeinikiv & Maini, 2005).We consider that in the region under consideration, the total population density N which divided into two classes, the susceptibles with density X and infectives with density$Y$. If $\beta_c(N)$ is variable (density dependent) contact rate then there are $\beta_c(N)Y$ infective contacts. Then by using Equations (1.1) and (1.2), an SIS model is proposed as follows:

$$\frac{dX}{dt} = A + \mu_1(K-N) - \mu_0(N-N_0) - \big(\beta + \beta_1(K-N) - \beta_0(N-N_0)\big)XY - dX + \mu Y$$

$$\frac{dY}{dt} = \big(\beta + \beta_1(K-N) - \beta_0(N-N_0)\big)XY - (\mu + \alpha + d)Y \qquad (\mathbf{2.1})$$

$X(0) > 0, Y(0) \geq 0 \; and \; N(0) > 0$

In the model system (2.1), d is natural death rate of human population, α is death rate coefficient of infective human population due to disease related factors, $\mu$is the rate of recovery of infective human population density.

2. Equilibrium analysis

In the following, we analyze the model system (2.1). For this we consider the reduced form of model system (2.1) by using $N = X + Y, A_2 = A + \mu_1.K + \mu_0.N_0,\ d_2 = d + \mu_1 + \mu_0$

$$\frac{dY}{dt} = \Big(\big(\beta + \beta_1(K-N) - \beta_0(N-N_0)\big)\Big)(N-Y)Y - (\mu + \alpha + d)Y$$

$$\frac{dN}{dt} = A_2 - d_2N - \alpha Y \quad (3.1)$$

$$Y(0) \geq 0 \; and \; N(0) > 0$$

We need the following lemma for further analysis.

Lemma 3.1. The region of attraction of model system (3.1) is given by the set

$$\Omega = \{(Y,N) \in R^2 \; ; \; 0 \leq Y \leq N_{max} \; and \; N_{min} = \frac{A_2}{\alpha + d_2} \leq N \leq \frac{A_2}{d_2} = N_{max}\}$$

Which attracts all the solution of model system (3.1)initiating in the interior of the positive quadrant of the region**Ω.**

Theorem 3.2. The model system(3.1) has following two non-negative equilibria in **Ω**.

(i) $E_0(0, \quad \frac{A_2}{d_2})$, Thedisease free equilibrium.

(ii) $E_1 = E_1(Y^*, N^*)$is the endemic equilibrium state whichexists if$R_0 = \frac{(\beta+\beta_1 K+\beta_0.N_0)A_2}{((\alpha+\mu+d).d_2)+(\beta_1+\beta_0)\frac{{A_2}^2}{d_2}} > 1$.Here R_0 is the basic reproduction number.

Proof: The existence of the equilibrium point $E_0(0, \quad \frac{A_2}{d_2})$ is obvious. Now In the following we prove the existence of $E_1(Y^*, N^*)$.From model system (3.1),let $Y \neq 0$ then Y^* and N^* are given from the following equations.

$$\big(\beta + \beta_1(K-N) - \beta_0(N-N_0)\big)(N-Y) - (\mu + \alpha + d) = 0 (3.2)$$

$$A_2 - \; d_2 N - \alpha Y = 0 (3.3)$$

By using Equations (3.2) and (3.3) we define the following function,

$$F(Y) = \left\{\left(\beta + \beta_1 K + \beta_0.N_0 - (\beta_1+\beta_0).\frac{A_2}{d_2}\right)\frac{A_2}{d_2} - \; (\mu + \alpha + d)\right\}$$

$$+\left\{(\beta_1+\beta_0).\frac{\alpha A_2}{{d_2}^2} - \frac{(\alpha+d_2)}{d_2}\left(\beta + \beta_1 K + \beta_0.N_0 - (\beta_1+\beta_0).\frac{A_2}{d_2}\right)\right\}Y$$

$$-\left\{\frac{\alpha(\alpha+d_2)}{{d_2}^2}.(\beta_1+\beta_0)\right\}Y^2 = 0 (3.4)$$

From Equation (3.4) we note the following

(i) $F(0) = \left\{\left(\beta + \beta_1 K + \beta_0 . N_0 - (\beta_1 + \beta_0).\frac{A_2}{d_2}\right)\frac{A_2}{d_2} - (\mu + \alpha + d)\right\}$

which is positive provided $R_0 = \frac{(\beta+\beta_1 K+\beta_0 . N_0)A_2}{((\alpha+\mu+d).d_2)+(\beta_1+\beta_0)\frac{{A_2}^2}{d_2}} > 1$.

(ii) $F\left(\frac{A_2}{\alpha+d_2}\right) = -(\mu + \alpha + d) < 0$

Hence by intermediate value theorem at least one root of $F(Y) = 0$ lies in the interval

$$0 < Y < \frac{A_2}{\alpha + d_2}$$

To show the root is unique, we have to prove $F'(Y)$ is negative. To see this, by differentiating equation(3.4) with respect to Y, we get

$$F'(Y) = \left\{(\beta_1 + \beta_0).\frac{\alpha A_2}{{d_2}^2} - \frac{(\alpha + d_2)}{d_2}\left(\beta + \beta_1 K + \beta_0 . N_0 - (\beta_1 + \beta_0).\frac{A_2}{d_2}\right)\right\}$$

$$-\left\{\frac{\alpha(\alpha+d_2)}{{d_2}^2}.(\beta_1 + \beta_0)\right\}2Y. \qquad (3.5)$$

Then by using Equation (3.4) again, we have

$$YF'(Y) = -\left\{\left(\beta + \beta_1 K + \beta_0 . N_0 - (\beta_1 + \beta_0).\frac{A_2}{d_2}\right)\frac{A_2}{d_2} - (\mu + \alpha + d)\right\}$$

$$-\left\{\frac{\alpha(\alpha+d_2)}{{d_2}^2}.(\beta_1 + \beta_0)\right\}Y^2 \quad (3.6)$$

Which is negative for $R_0 > 1$. Since $Y > 0$ and $YF'(Y) < 0$ then $F'(Y) < 0$. Thus $F(Y) = 0$ has unique root in the interval $0 < Y < \frac{A_2}{\alpha+d_2}$.

Now by knowing the value of Y^*, the value of N^* can be uniquely determined from equation (3.3).

Hence $E_1(Y^*, N^*)$ exists if $R_0 > 1$.

Remark: From equations. (3.2) and (3.3), it is easy to note that $dY/d\mu_0 < 0$ and $dY/d\beta_0 < 0$. This implies that, as the μ_0 and β_0 increases, infected population density decreases.

3. Stability analysis

The mathematical model (3.1) is nonlinear in Y and N thus it may not possible to find the exact analytical solution of system of differential equaiton. Thus we have to examine the long term behavior of the system by using the stability theory of differential equation. The local stability behavior of the equilibria are stated in the following theorem.

Theorem4.1. The equilibrium$E_0(0, \frac{A_2}{d_2})$ is unstable if $R_0 > 1$ and the equilibrium$E_1(Y^*, N^*)$islocally asymptotically stable provided the following condition is satisfied.

$$\alpha\left(\{\beta_1 + \beta_0\}(N^* - Y^*)\right)^2 \langle 4d_2\left(\beta_c(N^*)\right)^2 \textbf{(4.1)}$$

Proof: The local stability behavior of each two equilibrium points E_0 and E_1 is studied by computing Jacobian Matrix at point.

Let $f_1 = \left(\beta + \beta_1(K - N) - \beta_0(N - N_0)\right)(N - Y)Y - (d + \alpha + \mu)Y$

$f_2 = A_2 - d_2N - \alpha Y$

Thus Jacobian matrix at E_0 as

$$J(E_0) = \begin{bmatrix} \left\{\left(\beta + \beta_1 K + \beta_0 . N_0 - (\beta_1 + \beta_0).\frac{A_2}{d_2}\right)\frac{A_2}{d_2} - (\mu + \alpha + d)\right\} & 0 \\ -\alpha & -d_2 \end{bmatrix}$$

Since R_0›1, one of Eigen value

$$\lambda_1 = \left\{\left(\beta + \beta_1 K + \beta_0 . N_0 - (\beta_1 + \beta_0).\frac{A_2}{d_2}\right)\frac{A_2}{d_2} - (\mu + \alpha + d)\right\} > 0$$

Hence E_0 is Unstable

Now we check the **local stability** of $E_1(Y^*, N^*)$by using the Lyapunov's method, for this the following positive definite function is used.

$$V(y,n) = \frac{1}{2}y^2 + \frac{k_1}{2}n^2 \quad (4.2)$$

By differentiating equation (4.2), we get

$$\dot{V}(y,n) = y\dot{y} + k_1 n\dot{n} \quad (4.3)$$

Now using linearization of the model system (3.1) about $E_1(Y^*, N^*)$by taking $y = Y - Y^*$, $n = N - N^*$, we get

$$\dot{V}(y,n) = -Y^*\big(\beta + \beta_1(K - N^*) - \beta_0(N^* - N_0)\big)y^2$$

$$-\big(\{\beta_1 + \beta_0\}(N^* - Y^*)Y^* + \big(\beta + \beta_1(K - N^*) - \beta_0(N^* - N_0)\big)Y^* - \alpha k_1\big)ny - k_1 d_2 n^2 \quad (4.4)$$

By choosing K_1such that $\Longrightarrow k_1 = \frac{Y^*\big(\beta+\beta_1(K-N^*)-\beta_0(N^*-N_0)\big)}{\alpha}$ then

$$\dot{V}(y,n) = -Y^*\big(\beta + \beta_1(K - N^*) - \beta_0(N^* - N_0)\big)y^2 - (\{\beta_1 + \beta_0\}(N^* - Y^*)Y^*)ny - k_1 d_2 n^2 \quad (4.5)$$

Now $\dot{V}(y,n) < 0$, provided ,

$$(\{\beta_1 + \beta_0\}(N^* - Y^*)Y^*)^2 < 4k_1 d_2 Y^*\big(\beta + \beta_1(K - N^*) - \beta_0(N^* - N_0)\big)$$

$$i.e \quad \alpha\big(\{\beta_1 + \beta_0\}(N^* - Y^*)\big)^2 < 4d_2\big(\beta_c(N^*)\big)^2 \quad (4.6)$$

$E_1(Y^*, N^*)$is locally stable providing equation (4.6) is satisfied.

Remark: It is pointed out here the inequality (4.6) is automatically satisfied if $\beta_1 = 0$and $\beta_0 = 0$. It also shows that the local stability of system increases if immigration increases but it decreases with emigration.

Theorem 4.2. The equilibrium $E_1(Y^*, N^*)$is globally asymptotically stable in Ω provided the following inequality is satisfied.

$$\alpha\left(\left\{\frac{\beta_1}{(p+K)} + \frac{\beta_0}{(q+N_0)}\right\}\frac{A_2}{d_2}\right)^2 < 4d_2\big(\beta_c(N^*)\big)^2 \quad (4.7)$$

Proof. To prove this theorem, we consider the following positive definite function

$$U = (Y - Y^* - Y^* ln\frac{Y}{Y^*}) + \frac{k_2(N-N^*)^2}{2} \quad (4.8)$$

By differentiating equation (4.8), we get,

$$\dot{U} = \left(\frac{Y-Y^*}{Y}\right)\dot{Y} + k_2(N-N^*)\dot{N} \qquad (4.9)$$

Now after using model (3.1) and equation (3.2) and (3.3) we get

$$\dot{U} = \left(\beta + \beta_1(K-N^*) - \beta_0(N^*-N_0) - \alpha k_2 - \frac{\beta_1}{p+K}(N-Y)\right)(N-N^*)(Y-Y^*)$$

$$-k_2 d_2(N-N^*)^2 - \left(\beta + \beta_1(K-N^*) - \beta_0(N^*-N_0)\right)(Y-Y^*)^2 \qquad (4.10)$$

By choosing $k_2 \quad s.t \quad k_2 = \frac{\left(\beta+\beta_1(K-N^*)-\beta_0(N^*-N_0)\right)}{\alpha}$ then

$$\dot{U} = -\left(\beta + \beta_1(K-N^*) - \beta_0(N^*-N_0)\right)(Y-Y^*)^2$$

$$- \{\beta_1 + \beta_0\}(N-Y)(N-N^*)(Y-Y^*) - k_2 d_2(N-N^*)^2 \qquad (4.11)$$

$\dot{U} < 0$, provided $(\{\beta_1 + \beta_0\}N_{max})^2 < 4k_2 d_2\left(\beta + \beta_1(K-N^*) - \beta_0(N^*-N_0)\right)$

$$i.e. \quad \alpha\left(\{\beta_1 + \beta_0\}\frac{A_2}{d_2}\right)^2 < 4d_2\left(\beta_c(N^*)\right)^2 \qquad (4.12)$$

$E_1(Y^*, N^*)$ is globally asymptotically stable Providing equation **(4.12)** satisfied.

4. Numerical simulation and discussion

Here we discuss the existence and stability of the nontrivial equilibrium point E^* by taking the following set of parameter values from table1 and using the software MAPLE.

$$A \sim 500,\ K \sim 25000,\ N_0 \sim 10000,\ d \sim 0.03,\ \alpha \sim 0.060,\ \beta \sim 0.000012,$$

$$\mu \sim 0.030,\ \mu_0 \sim 200,\ \mu_1 \sim 50,\ \beta_0 \sim 0.000002,\ \beta_1 \sim 0.0000001,$$
$$q \sim 200,\ p \sim 100$$

For these values of parameters the nontrivial equilibrium point E^* corresponding to equations. (3.2) and (3.3) is obtained as.

$$\boldsymbol{N^* = 12237.7 \cong 12238,\quad Y^* = 1899.65 \cong 1900.}$$

Further, It should be noted that for these parameter values as defined above, $R_0 > 1$, and local and global stability condition are satisfied.

The Jacobian Matrix of the model system (3.1) for above values of parameters at (1900,12238) is

$$M^* = \begin{bmatrix} -0.02205 & 0.01808 \\ -0.06 & -0.05179 \end{bmatrix}$$

The Eigen values of the Jacobian Matrix corresponding to the equilibrium point E^* for the model system(3.1) are:

$$-0.0369 + 0.02939i\,, \quad -0.0369 - 0.02939i$$

We note that both the Eigenvalues having negative real part. Hence the endemic equilibrium point E^* is asymptotically stable.

The numerical simulation of model system (3.1) are also conducted and the results are shown in figures [1-9]

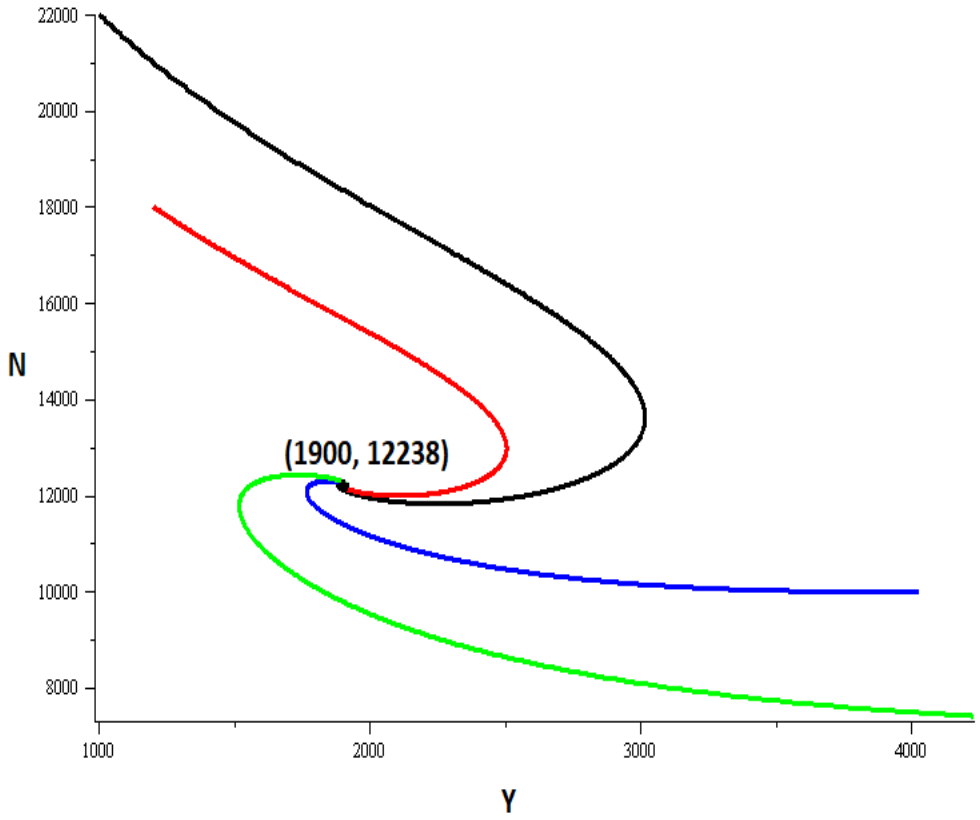

Figure1. Stability diagram for *Y* and *N*

From Fig.1 it can be seen that all trajectories goes tow ardsa single point (1900,12238) i.e. this point become locally stable point.

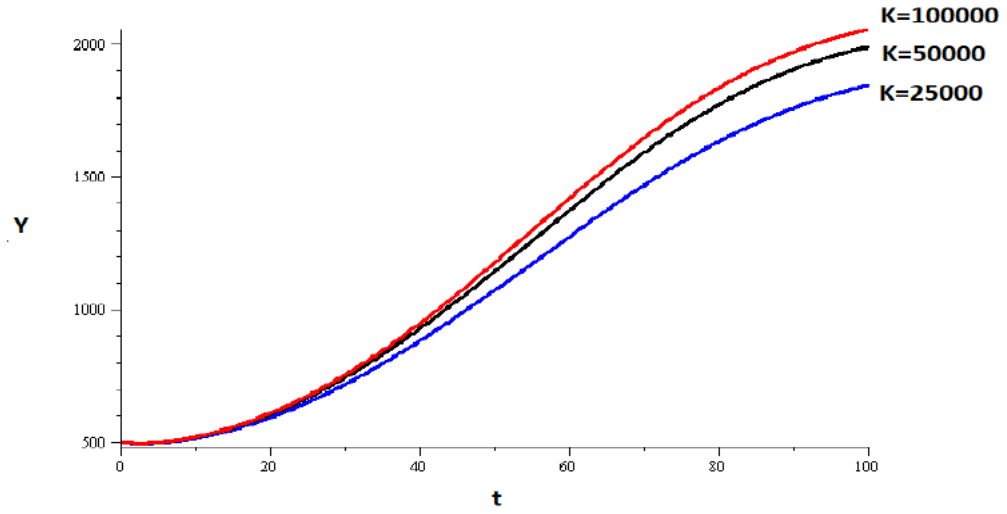

Figure2: Variation of infective population with time for different value of$K$.

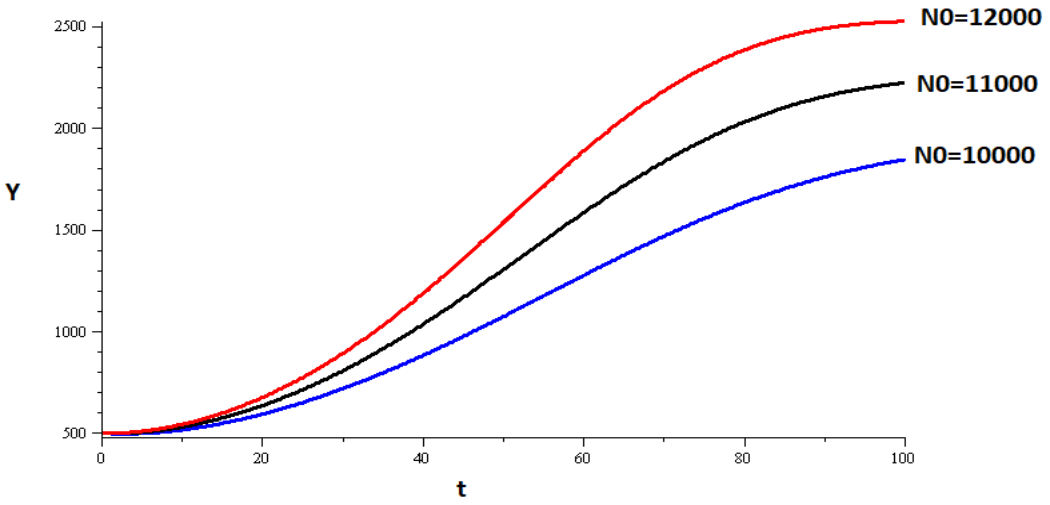

Figure3: Variation of infective population with time for different value ofN_0.

From Fig.2, it can be seen that as carrying capacity K of habitat increases (more people are allowed to immigrate in habitat) then the number of contact between

susceptible and infective increases, the infective population density (spread of disease) increases. From Fig.3, the non-emigrating population density N_0 increases i.e. population of habitat increases, the spread of disease increases.

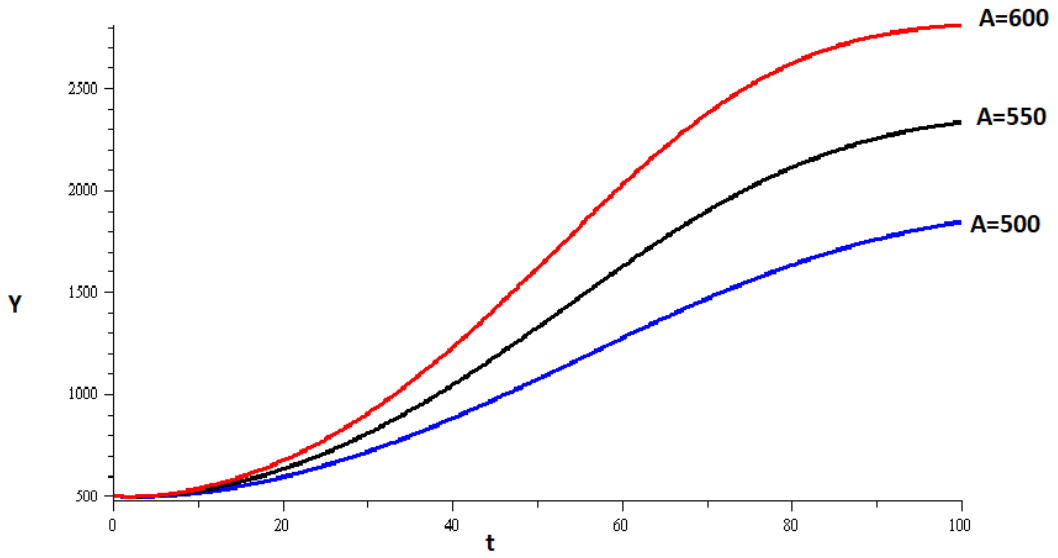

Figure4: Variation of infective population with time for different value of A.

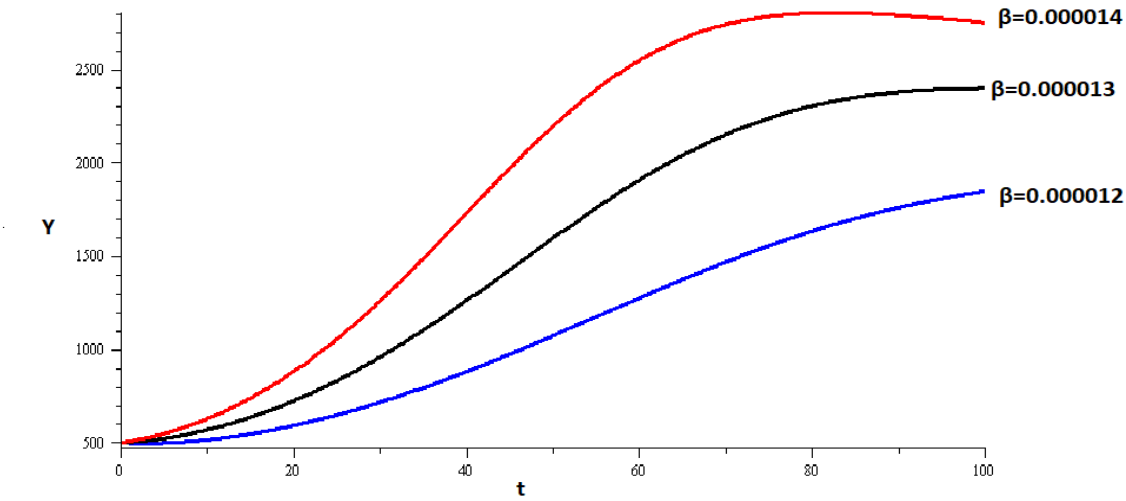

Figure 5: Variation of infective population with time for different value of β

From Fig.4, it can be seen that as the constant immigration rate A increases i.e. total population density N of habitat will increases, the infective population density Y increases. From Fig.5, as the constant contact rate β increases, the infective population density Y increases.

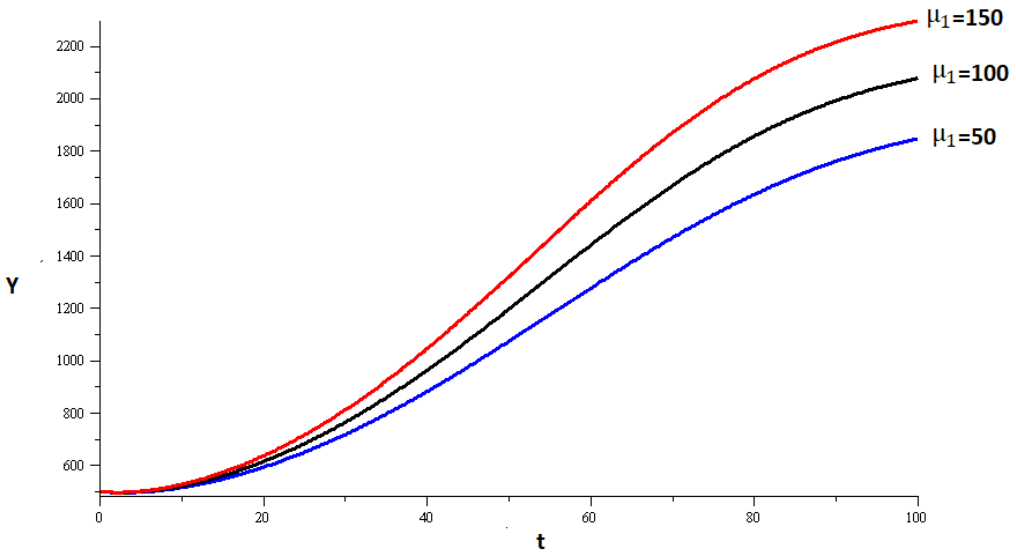

Figure 6: Variation of infective population with time for different value of μ_1.

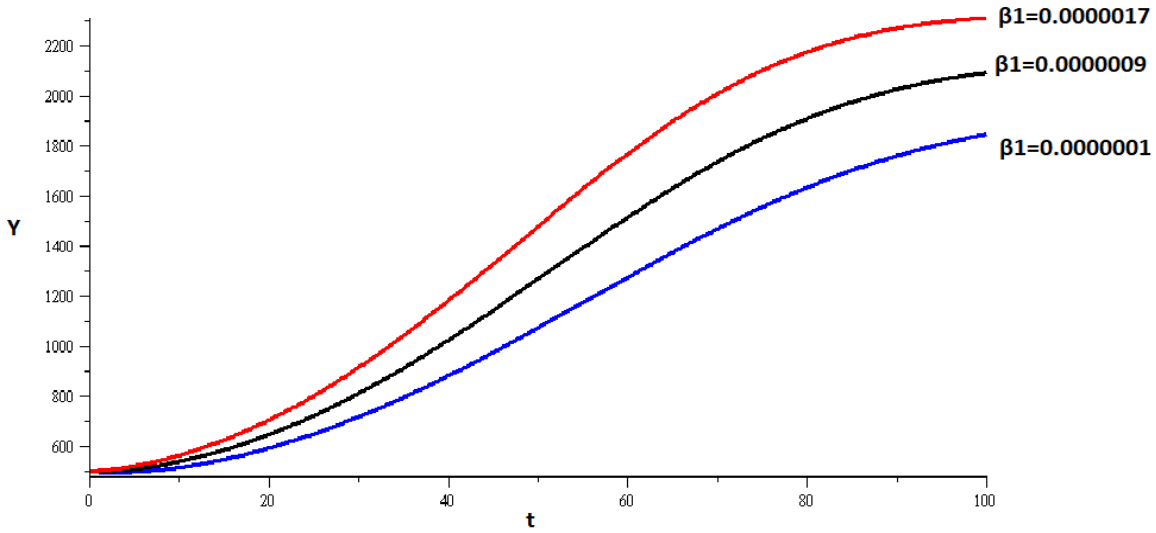

Figure 7: Variation of infective population with time for different value of β_1.

From Fig.6, as the variable immigration rate μ_1 increases i.e. total population density of habitat will increases, the infective population density Y increases. From Fig.7, as the variable contact rate β_1 increases, the infective population density Y increases

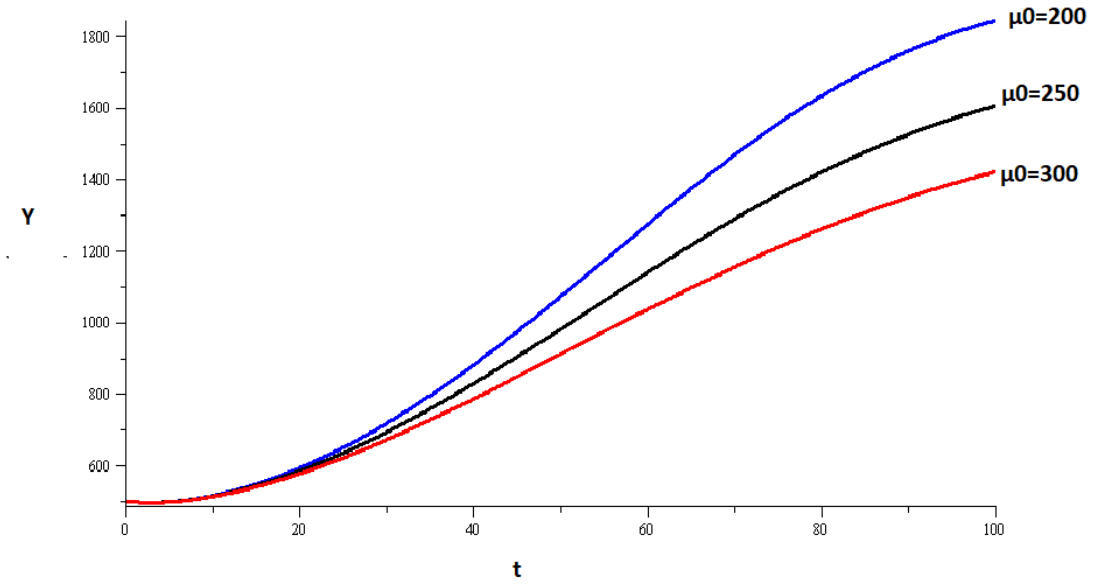

Figure 8: Variation of infective population with time for different value of μ_0.

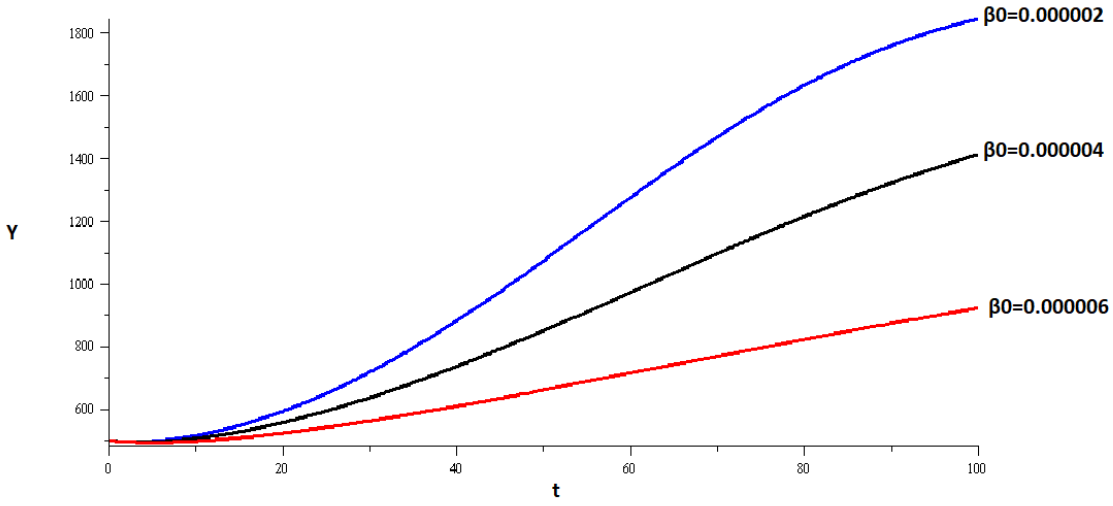

Figure 9: Variation of infective population with time for different value of β_0.

From Fig.8, it can be seen that as the variable emigration rate μ_0 increases i.e. total population density of habitat decreases, the number of infective contacts decreases in habitat i.e. infective population density Y decreases. From Fig.9, it can be seen that as the variable contact rate β_0 increases, the infective population density Y decreases.

Conclusions

In this paper, an SIS epidemic non-linear model have been proposed and analyzed to study the effects of density dependent migration as well asnon-emigrating population of the habitaton spread of infectious diseases. In the modeling process, the two variables have been considered namely, the susceptible population density and the infective population density. The rate of contact between susceptibles and infectives have been assumed to be density (immigration and emigration) dependent. The model has been analyzed by using the stability theory of differential equation and computer simulations. The model analysis has shown that if the variable carrying capacity of habitat or constant immigration rate increases, the infective population density increases. It has also been found that as the population density of non-emigrating population increases, the infective population density increases. Further, as variable immigration increases, not only the contact rate increases but the spread of infectious disease increases. But as variable emigration increases, not only the contact rate decreases but infected population density decreases. These results have been confirmed by numerical simulation of the model.

Acknowledgment

The second Author (Jitendra Singh) is thankful to P.P.N(PG) College, Kanpur India and Innovative internet University for research (A think tank) , Kanpur India for the help and support.

References

Greenhalgh D & Das R(1992), Modelling epidemic with variable contact rates: Theor

Pop Bio **47**: 129-179.

Greenhalgh D. (1990),Some threshold and stability results for epidemic models with a density dependent death rate:Theor Pop Bio **42**: 130-151.

Hethcote H. W & Driessche P(1991), Some epidemiological models with nonlinear incidence: J Math Biology**29**: 271-287.

Hethcote H. W(1979), qualitative analysis of communicable disease models: J Math Biology **8**: 301-302.

Hsu S &Zee A(2004), Global spread of infectious diseases, JBiol System**12**: 289-300.

Kermack W.O. & Mc KendrickA. G.(1927), A contribution to the mathematical theory of epidemics: Proc. R. Soc. Lond, 115, 700-721.

Last J M (2001), A dictionary of epidemiology: Oxford University press.

Lee L & Ma Z(2002), Qualitative analysis of SIS epidemic model with vaccination and varying total population size:Mathematical and computer modelling, **35**:1235-1243.

Linda Q Gao &Herbert H W(1992), Disease transmission models with density dependent demographic: J Math Biol **30**:717-731.

May R M & Anderson R M(1979),Population biology of infectious diseases II Nature **280**: 455-461,.

May R M &Anderson R M(1988), Possible demographic consequences of AIDS in developing countries:Nature**332**: 228-234.

Shukla J B, Goyal A &Singh S,Chandra P(2004), Effect of habitat characteristics on the growth of carrier population leading to increased spread of typhoid fever: Journal of epidemiology and global health**4(2):**107-114.

Singh S(2011), Mathematical modelling of the spread of carrier dependent infectious disease with ecological effects: SIRS model, Indian J of industrial and applied

mathematics **3(1):**96-106.

Singh S, Shukla J B & ChandraP(2005), Modelling and analysis of the spread of malaria: Environmental and ecological effects: J Biol Sys**13(1):**1-11.

Singh S,Shukla J B &Chandra, P(2003), Modeling and analysis of spread of carrier dependent infectious diseases with environmental effects: J Biological Systems**11(3)**: 325-335.

Zhou J & Hethcote H W(1994), Population size dependent incidence in models for diseases without immunity: J Math Biol **32**: 809-834.

Normas para la presentación de trabajos

1. Principios de la Revista

La REVISTA DE LA UNIVERSIDAD DEL ZULIA es un órgano científico de difusión de trabajos parciales o definitivos de investigadores y/o equipos de investigación nacionales y extranjeros. Su naturaleza es multidisciplinaria e interdisciplinaria, por ello su temática se divide en tres grandes ejes: a. *ciencias sociales y arte*; b. *ciencias del agro, ingeniería y tecnología*; c. *ciencias exactas, naturales y de la salud*. Su publicación es cuatrimestral. Cada número, de los tres del año, se corresponde con uno de los tres ejes temáticos. La *Revista de la Universidad del Zulia*, por su carácter histórico y patrimonial, está adscrita a la CÁTEDRA LIBRE HISTORIA DE LA UNIVERSIDAD DEL ZULIA.

2. Métodos de Envío y de Evaluación de los Trabajos

Los autores interesados en publicar su trabajo en la *Revista de la Universidad del Zulia* deberán remitir tres copias del mismo sin identificación en sobre cerrado a la siguiente dirección: Avenida Guajira, Fundadesarrollo, planta baja de la Sede Rectoral de La Universidad del Zulia. Este sobre debe estar acompañado de otro, el cual contendrá el original del trabajo con la identificación del autor o autores, indicando: nombre, apellido, institución que representa (universidad, instituto, centro de investigación, fundación), correo electrónico. Así mismo en este sobre se presentará una comunicación escrita firmada por todos los autores y dirigida al Director de la Revista. En esta comunicación se manifestará el interés de los autores de proponer su trabajo para la publicación en la *Revista de la Universidad del Zulia*, previa evaluación del Comité de Arbitraje. Se agregará también a este sobre una síntesis curricular de cada autor con una extensión no mayor de diez (10) líneas. Los artículos pueden agregarse a la plataforma OJS de la revista. También se podrá presentar el trabajo dirigiéndolo al siguiente correo electrónico: revistadeluz@gmail.com. El currículo de los autores se enviará en archivo adjunto, distinto al que contendrá el trabajo. Los artículos propuestos para esta revista deben ser inéditos y no deben haber sido propuestos simultáneamente a otras publicaciones. Todos los trabajos serán evaluados por parte de un Comité de Árbitros-Especialistas de reconocido prestigio, seleccionado por el Comité Editorial de la Revista. La evaluación de los Árbitros se realizará mediante el procedimiento conocido como par de ciegos: los árbitros y los autores no conocerán sus identidades respectivas. Los criterios de Evaluación son los siguientes: a. Criterios formales o de presentación: 1) originalidad, pertinencia y adecuada extensión del título; 2) claridad y coherencia del discurso; 3) adecuada elaboración del resumen; 4) organización interna del texto; 5) todos los demás criterios establecidos en la presente normativa. b. Criterios de contenido: 1) dominio de conocimiento evidenciado; 2) rigurosidad científica; 3) fundamentación teórica y metodológica; 4) actualidad y relevancia de las fuentes consultadas; 5) aportes al conocimiento

existente. Al recibirse la respuesta del Comité de Árbitros designado se informará a los autores por correo electrónico la decisión correspondiente; en caso de ser aceptado el trabajo deberá remitirse por correo electrónico la versión digital del mismo.

3. Presentación de los trabajos

Los trabajos deben presentar un resumen de 150 palabras como máximo y hasta cinco palabras claves; tanto el resumen como las palabras claves estarán en español e inglés. Igualmente el título y el subtítulo del trabajo serán presentados también en español e inglés. La extensión máxima del trabajo será de veinte (20) páginas, y diez (10) como extensión mínima (salvo excepciones plenamente justificadas). Todos los trabajos serán presentados en hoja tipo carta, impresos por una sola cara, con numeración continua y con márgenes de tres (3) centímetros a cada lado. El texto se presentará a espacio y medio, en fuente Times New Roman, tamaño 12.

4. Cuerpo del artículo

Se dividirá en Introducción, Desarrollo y Conclusiones (o Consideraciones Finales, según sea el caso). La introducción incluirá el propósito u objetivo general perseguido. El Desarrollo se organizará en secciones y subsecciones debidamente identificadas con subtítulos numerados completamente en arábigos de acuerdo al sistema decimal, respondiendo a una sucesión continua y utilizando un punto para separar los niveles de división. La Introducción y Conclusión están exceptuadas de esta numeración. Las fechas y horas se expresarán numéricamente. En caso de existir ilustraciones (gráficos, mapas, fotos) debe hacerse referencia a los mismos en el texto. Estas ilustraciones serán contadas dentro de la extensión máxima del artículo. Las notas explicativas o aclaratorias deben reducirse al mínimo necesario y colocarse al pie de páginas debidamente señalizadas. Los materiales complementarios se recogerán en anexos, los cuales se identificarán con una letra y un título y se colocarán después de la bibliografía. Los anexos serán contados también dentro de la extensión máxima del artículo.

5. Citado

El citado se realizará en el texto utilizando la modalidad autor-fecha, establecido en el *Reglamento para la presentación de trabajos en la Universidad del Zulia*, indicando, en caso de ser cita textual, apellido(s) del autor, seguido de coma, año de publicación de la obra, seguido de dos puntos y el (los) número(s) de la(s) página(s), por ejemplo: de acuerdo a Rincón (1998: 45) o (Rincón, 1998: 45); si no es cita textual sino una paráfrasis no se indicará el número de página, ejemplo: de acuerdo a Rincón (1998) o (Rincón, 1998). Si hay varias obras del mismo autor publicadas en el mismo año, se ordenarán literalmente en orden alfabético; por ejemplo, (Rincón, 2008a: 12), (Rincón, 2008b: 24). Si son dos autores, se colocarán solamente el primer apellido de cada uno, por ejemplo: Según Morales y Fleires (2008: 90) o (Morales y Fleires, 2008: 90), siguiendo el mismo criterio explicado anteriormente para las citas textuales y las paráfrasis. En caso de ser tres autores o más se colocará el apellido del autor principal

seguido de "et al", ejemplo: (Rincón *et al.*, 2008: 45). Deben evitarse, en lo posible, citas de trabajos no publicados o en imprenta, también referencias a comunicaciones y documentos privados de difusión limitada, a no ser que sea estrictamente necesario. En caso de fuentes documentales, electrónicas u otras que por su naturaleza resulten inviables o complejas para la adopción del citado autor-fecha, sugerido en estas normas, puede recurrirse u optarse por el citado al pie de página.

6. Referencias bibliográficas

Las referencias (bibliográficas, hemerográficas, orales y/o documentales) se presentarán al final del texto, según lo establecido en el *Reglamento para la presentación de trabajos en la Universidad del Zulia*. El orden de las referencias es alfabético por apellido. Las diferentes obras de un mismo autor se organizarán cronológicamente, en orden ascendente, y si son dos obras o más de un mismo autor y año, se mantendrá el estricto orden alfabético por título.

Fecha de evaluación_____

Instrumento de Evaluación del Árbitro

I.- Criterios formales o de presentación

CRITERIOS DE EVALUACIÓN	EXCELENTE	MUY BUENO	BUENO	REGULAR	DEFICIENTE OBSERVACIONES
Originalidad, pertinencia y adecuada					
Extensión del título					
Claridad y coherencia del discurso					
Adecuada elaboración del resumen					
Contiene abstract y palabras claves					
Objetivo, metodología y resultados.					
Organización interna del texto					

II. - Criterios de contenido

CRITERIOS DE EVALUACIÓN	EXCELENTE	MUY BUENO	BUENO	REGULAR	DEFICIENTE OBSERVACIONES
Dominio de conocimiento evidenciado					
Rigurosidad científica					
Fundamentación teórica y metodológica					
Actualidad y relevancia de las fuentes consultadas					
Aportes al conocimiento existente					

III. – Sugerencia de publicación

De acuerdo a la información obtenida usted recomendaría (favor marcar con una X):

Publicar sin modificaciones: _____ Publicar con ligeras modificaciones_____
Publicar con modificaciones sustanciales_____ No publicar_____

Fundamentación de la decisión:

REVISTA DE LA UNIVERSIDAD DEL ZULIA

FUNDADA EN 1947

PATRIMONIO DE LA

UNIVERSIDAD DEL ZULIA

FUNDADA EN 1891

MARACAIBO-VENEZUELA

REVISTA DE LA UNIVERSIDAD DEL ZULIA
CIENCIAS EXACTAS, NATURALES Y DE LA SALUD///
AÑO 10 N° 27, Mayo-Agosto 2019
ISSN 0041-8811

Contenido